

ESKOM

NUCLEAR SITES
SITE SAFETY REPORTS

NUMERICAL MODELLING OF
COASTAL PROCESSES

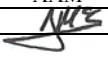
THYSPUNT

Report No. 1010/2/101

OCTOBER 2009



PRESTEDGE RETIEF DRESNER WIJNBERG (PTY) LTD
CONSULTING PORT AND COASTAL ENGINEERS

Numerical Modelling of Coastal Processes - Thyspunt					
Report 1010/2/101					
Revision	Date	Author	Checked	Status	Approved
00	March 2008	SAL	AAM/GKP	Draft for Comment	AAM
01	March 2008	SAL	AAM/GKP	For Use	AAM
02	March 2008	SAL	AAM/GKP	For Use	AAM
03	December 2008	SAL	AAM/GKP	For Use	AAM
04	October 2009	SAL	AAM/GKP	For Use	

Keywords: Numerical modelling, waves, water levels, currents, thermal plume, sediment transport, tsunamis, Thyspunt

ESKOM**NUCLEAR SITES
SITE SAFETY REPORTS****NUMERICAL MODELLING OF COASTAL PROCESSES
THYSPUNT****TABLE OF CONTENTS**

	PAGE NO.
1. INTRODUCTION	1
1.1 Background	1
1.2 Scope of work	1
1.3 Limitations	2
1.4 Conventions and terminology	2
2. DESCRIPTION OF NUMERICAL MODELS USED	4
2.1 Introduction	4
2.2 Wave refraction model	4
2.3 Cross-shore hydrodynamic model	5
2.4 Two-dimensional hydrodynamic model	6
2.5 Three-dimensional hydrodynamic model	6
2.6 Two-dimensional sediment transport model	7
2.7 Suspended sediment model	7
2.8 Extreme value analysis	8
3. WATER LEVELS	9
3.1 Tides	9
3.2 Water levels measured at the site	9
3.3 Extraction of tidal residuals	9
3.4 Extreme value analysis of tidal residuals	10
4. TSUNAMI FLOODING	12
4.1 Background	12
4.2 Distant tsunamis	12
4.2.1 Sources	12
4.2.2 Model setup	15
4.2.3 Model calibration	15
4.2.4 Results	16
4.3 Local tsunamis	17
4.3.1 Sources	17
4.3.2 Modelling approach	18
4.3.3 Model setup	18

4.3.4	Slumps modelled	19
4.3.5	Results	20
4.3.6	Discussion	21
4.4	Conclusions	21
4.5	Recommendations.....	22
5.	WAVES	23
5.1	Waves measured at the site.....	23
5.2	Offshore hindcast data	23
5.3	Model setup.....	23
5.4	Model calibration.....	24
5.5	Extreme value analysis of wave height	25
5.6	Wave transformation across surf-zone	26
6.	SEA TEMPERATURE	27
6.1	Temperature measured at site.....	27
6.2	Long-term data	27
6.3	Extreme value analysis of temperature	28
7.	CURRENTS AND THERMAL PLUME DISPERSION	29
7.1	Background.....	29
7.2	Currents measured at site.....	29
7.3	Hydrodynamic modelling.....	29
7.3.1	Model setup	29
7.3.2	Model calibration.....	30
7.3.3	Selection of wind and wave forcing	31
7.3.4	Discharge characteristics	32
7.4	Intake and outfall layouts tested	33
7.4.1	Layout 1: Offshore tunnel intake and nearshore pipeline outfall.....	34
7.4.2	Layout 2: Offshore tunnel intake and nearshore channel outfall	34
7.5	Results.....	35
7.5.1	Currents	35
7.5.2	Temperature and dilution.....	35
7.5.3	Recirculation.....	36
8.	SEDIMENT TRANSPORT	37
8.1	Background.....	37
8.2	Sediment grain size.....	37
8.3	Sediment transport rates.....	39
8.3.1	Model setup	39
8.3.2	Schematisation of wave and wind climate.....	39
8.3.3	Model calibration.....	39
8.3.4	Results	40
8.3.5	Conclusions	41
8.4	Suspended sediment concentrations	41

8.4.1	Background	41
8.4.2	Measured suspended sediment concentrations	41
8.4.3	Model setup	42
8.4.4	Conditions modelled.....	42
8.4.5	Results	42
8.4.6	Conclusions	44
9.	CONCLUSIONS AND RECOMMENDATIONS.....	45

REFERENCES

FIGURES

APPENDIX A: Reference list of DHI applications of the MIKE model to power plants and marine outfalls

APPENDIX B: Report on calibration of wave hindcast data by Fugro Oceanor

APPENDIX C: Council for Geoscience Report: A Probabilistic Tsunami Hazard Assessment for Coastal South Africa from Distant Tsunamogenic areas

APPENDIX D: Council for Geoscience Report: Potential Sources of Tsunami Along the South African Coast

APPENDIX E: Data Reports on Oceanographic Measurements by Lwandle

LIST OF TABLES

Table 3.1	:	Predicted tidal levels for Port Elizabeth
Table 3.2	:	Extreme tidal residuals at Port Elizabeth
Table 4.1	:	Distant tsunami sources modelled
Table 4.2	:	Fault parameters and vertical seabed displacement
Table 4.3	:	Modelled water levels at Thyspunt due to distant tsunamis
Table 4.4	:	Slump parameters modelled
Table 4.5	:	Modelled water levels at Thyspunt due to a theoretical 80 km ³ slump
Table 5.1	:	Extreme wave climate at -30 m CD
Table 6.1	:	Summary statistics of water temperatures measured at the Thyspunt site
Table 6.2	:	Summary statistics of measured surf-zone temperatures at three locations
Table 6.3	:	Extreme sea temperatures at three locations
Table 7.1	:	Summary statistics of current speeds measured at the Thyspunt site
Table 7.2	:	Seawater cooling requirements
Table 7.3	:	Recirculation results: increase in temperature at intake
Table 8.1	:	Sediment grain size analysis for Thyspunt
Table 8.2	:	Preliminary estimate of sand volume drawn into cooling water intake in 30 m depth

LIST OF FIGURES

Figure 1.1	:	Locality map for Thyspunt site.
Figure 1.2	:	Detailed locality map for Thyspunt site.
Figure 1.3	:	Multi-beam bathymetry showing location of the reef at Thyspunt.
Figure 3.1	:	Location of instruments deployed at Thyspunt.
Figure 3.2	:	Water levels measured at Thyspunt.
Figure 3.3	:	Analysis of water level residuals: Measured tide, predicted tide and residual at Port Elizabeth. Full 34 year dataset.
Figure 3.4	:	Analysis of water level residuals: Measured tide, predicted tide and residual at Port Elizabeth. Fourteen days including the May 1984 storm event.
Figure 3.5	:	Extreme value analysis of negative tidal residuals at Port Elizabeth.
Figure 3.6	:	Extreme value analysis of positive tidal residuals at Port Elizabeth.
Figure 4.1	:	Model bathymetry used for tsunami modelling of Sumatra and Karachi earthquake events.
Figure 4.2	:	Calibration of tsunami model: Measured and modelled water levels in the port of Port Elizabeth for the 26 December 2004 Sumatra tsunami event.
Figure 4.3	:	Maximum water levels predicted during tsunami event. Source is Sumatra A: 26 December 2004 earthquake, $M_w = 9.2$.
Figure 4.4	:	Minimum water levels predicted during tsunami event. Source is Sumatra A: 26 December 2004 earthquake, $M_w = 9.2$.

- Figure 4.5 : Maximum water levels predicted during tsunami event. Source is Sumatra B: maximum credible earthquake determined by the Council for Geoscience, $M_w = 9.2$.
- Figure 4.6 : Minimum water levels predicted during tsunami event. Source is Sumatra B: maximum credible earthquake determined by the Council for Geoscience, $M_w = 9.2$.
- Figure 4.7 : Maximum water levels predicted during tsunami event. Source is a Sumatra C: maximum plausible event from Borrero *et al* (2006), $M_w = 9.3$.
- Figure 4.8 : Minimum water levels predicted during tsunami event. Source is a Sumatra C: maximum plausible event from Borrero *et al* (2006), $M_w = 9.3$.
- Figure 4.9 : Maximum water levels predicted during tsunami event. Source is Karachi A: maximum credible earthquake determined by the Council for Geoscience, $M_w = 8.4$.
- Figure 4.10 : Minimum water levels predicted during tsunami event. Source is Karachi A: maximum credible earthquake determined by the Council for Geoscience, $M_w = 8.4$.
- Figure 4.11 : Model bathymetry used for tsunami modelling of the South Sandwich Islands earthquake events.
- Figure 4.12 : Maximum water levels predicted during tsunami event. Source is South Sandwich Islands A: maximum credible earthquake determined by the Council for Geoscience, $M_w = 7.6$.
- Figure 4.13 : Minimum water levels predicted during tsunami event. Source is South Sandwich Islands A: maximum credible earthquake determined by the Council for Geoscience, $M_w = 7.6$.
- Figure 4.14 : Maximum water levels predicted during tsunami event. Source is South Sandwich Islands B: magnitude increased to $M_w = 8.0$.
- Figure 4.15 : Minimum water levels predicted during tsunami event. Source is South Sandwich Islands B: magnitude increased to $M_w = 8.0$.
- Figure 4.16 : Main morphological and structural features of submarine slumps. Parameters defining slump model.
- Figure 4.17 : Location of slump zones around Southern Africa.
- Figure 4.18 : Model bathymetry used for tsunami modelling due to slumps on the South African shelf margin. Locations of the three slumps modelled are indicated.
- Figure 4.19 : Details of the Agulhas Slump.
- Figure 4.20 : Maximum water levels predicted during tsunami event. Source is theoretical Agulhas Slump with volume of slumped sediment = 80 km^3 .
- Figure 4.21 : Minimum water levels predicted during tsunami event. Source is theoretical Agulhas Slump with volume of slumped sediment = 80 km^3 .
- Figure 4.22 : Maximum water levels predicted during tsunami event. Source is theoretical Cape Town Slump (South) with volume of slumped sediment = 80 km^3 .
- Figure 4.23 : Minimum water levels predicted during tsunami event. Source is theoretical Cape Town Slump (South) with volume of slumped sediment = 80 km^3 .
- Figure 4.24 : Maximum water levels predicted during tsunami event. Source is theoretical Cape Town Slump (North) with volume of slumped sediment = 80 km^3 .
- Figure 4.25 : Minimum water levels predicted during tsunami event. Source is theoretical Cape Town Slump (North) with volume of slumped sediment = 80 km^3 .

- Figure 5.1 : Wave measurements at Thyspunt Sites A and B. Time-series of wave parameters.
- Figure 5.2 : Wave measurements at Thyspunt Site A. Wave rose and histogram of wave heights.
- Figure 5.3 : Wave measurements at Thyspunt Site B. Wave rose and histogram of wave heights.
- Figure 5.4 : Time-series of offshore wave hindcast parameters. Position is E 24.5°E, S 35.0° in 900 m depth.
- Figure 5.5 : Rose and histogram of offshore wave hindcast data. Position is E 24.5°, S 35.0° in 900 m depth.
- Figure 5.6 : Numerical mesh used for wave refraction modelling.
- Figure 5.7 : Calibration of wave model. Measured and modelled time-series of wave parameters at Site A.
- Figure 5.8 : Calibration of wave model. Measured and modelled time-series of wave parameters at Site B.
- Figure 5.9 : Example of wave refraction from offshore to Thyspunt site.
- Figure 5.10 : Example of wave refraction from offshore to Thyspunt site.
- Figure 5.11 : Characterisation of storm waves refracted to -30 m CD depth at Thyspunt site.
- Figure 5.12 : Extreme value analysis of waves at -30 m CD depth at Point 1.
- Figure 5.13 : Example of cross-shore wave transformation modelling from -30 m CD depth to shoreline.
- Figure 6.1 : Measured water temperatures at Thyspunt.
- Figure 6.2 : Time-series of measured sea temperatures (in surf-zone) at Tsitsikamma and Storms River Mouth.
- Figure 6.3 : Histograms of measured sea temperatures (in surf-zone) at Tsitsikamma and Storms River Mouth.
- Figure 6.4 : Extreme Value Analysis of measured sea temperatures (in surf-zone) at Tsitsikamma (morning).
- Figure 6.5 : Extreme Value Analysis of measured sea temperatures (in surf-zone) at Tsitsikamma (evening).
- Figure 6.6 : Extreme Value Analysis of measured sea temperatures (in surf-zone) at Storms River Mouth.
- Figure 7.1 : Current measurements at Site A. Time-series of surface and bottom currents.
- Figure 7.2 : Current measurements at Site B. Time-series of surface and bottom currents.
- Figure 7.3 : Current measurements at Sites A and B. Surface and seabed rose plots.
- Figure 7.4 : Numerical mesh and bathymetry used for hydrodynamic modelling.
- Figure 7.5 : Detail of numerical mesh and bathymetry used for hydrodynamic modelling.
- Figure 7.6 : Calibration of hydrodynamic model. Measured and modelled time-series of currents at Site A for period February to March 2008.
- Figure 7.7 : Calibration of hydrodynamic model. Measured and modelled time-series of currents at Site A for period April 2008.
- Figure 7.8 : Calibration of hydrodynamic model. Measured and modelled time-series of currents at Site A for period July 2008.
- Figure 7.9 : Calibration of hydrodynamic model. Measured and modelled time-series of currents at Site B for period July 2008.
- Figure 7.10 : Wave and wind time-series used in hydrodynamic and plume modelling. 14 day summer simulation period.

- Figure 7.11 : Wave and wind time-series used in hydrodynamic and plume modelling. 14 day winter simulation period.
- Figure 7.12 : Wave and wind time-series used in hydrodynamic and plume modelling. 14 day calm simulation period.
- Figure 7.13 : Layout 1: Offshore tunnel intake and nearshore pipeline outfall.
- Figure 7.14 : Layout 2: Offshore tunnel intake and nearshore channel outfall.
- Figure 7.15 : Example of modelled currents and thermal plume near water surface at a time when the currents are predominantly wave-driven.
- Figure 7.16 : Example of modelled currents and thermal plume near water surface at a time when the currents are predominantly wind-driven.
- Figure 7.17 : Thermal plume for Layout 1. Mean increase in temperature near water surface. Power output: 4 000 MWe.
- Figure 7.18 : Thermal plume for Layout 1. Mean increase in temperature near seabed. Power output: 4 000 MWe.
- Figure 7.19 : Thermal plume for Layout 1. Maximum increase in temperature near surface. Power output: 4 000 MWe.
- Figure 7.20 : Thermal plume for Layout 1. Maximum increase in temperature near seabed. Power output: 4 000 MWe.
- Figure 7.21 : Thermal plume for Layout 1. Mean increase in temperature near water surface. Power output: 10 000 MWe.
- Figure 7.22 : Thermal plume for Layout 1. Mean increase in temperature near seabed. Power output: 10 000 MWe.
- Figure 7.23 : Thermal plume for Layout 1. Maximum increase in temperature near surface. Power output: 10 000 MWe.
- Figure 7.24 : Thermal plume for Layout 1. Maximum increase in temperature near seabed. Power output: 10 000 MWe.
- Figure 7.25 : Thermal plume for Layout 2. Mean increase in temperature near water surface. Power output: 10 000 MWe.
- Figure 7.26 : Thermal plume for Layout 2. Mean increase in temperature near seabed. Power output: 10 000 MWe.
- Figure 7.27 : Thermal plume for Layout 2. Maximum increase in temperature near surface. Power output: 10 000 MWe.
- Figure 7.28 : Thermal plume for Layout 2. Maximum increase in temperature near seabed. Power output: 10 000 MWe.
- Figure 7.29 : Thermal plume for Layout 1. Mean increase in temperature near water surface. Sensitivity to climate change. Power output: 10 000 MWe.
- Figure 7.30 : Recirculation for Layout 1. Power output: 10 000 MWe.
- Figure 7.31 : Recirculation for Layout 2. Power output: 10 000 MWe.
- Figure 7.32 : Recirculation for Layout 1. Sensitivity to climate change. Power output: 10 000 MWe.
- Figure 8.1 : Sediment transport modelling. Measured D₅₀ grain size.

- Figure 8.2 : Sediment transport modelling. Testing of wave and current modules.
- Figure 8.3 : Sediment transport modelling. Testing of the coupled wave, current and sediment transport model.
- Figure 8.4 : Sediment transport modelling. Calibration of model based on sediment volume entering the existing Koeberg intake basin.
- Figure 8.5 : Sediment transport modelling. Potential net sediment transport to the west of Thyspunt.
- Figure 8.6 : Sediment transport modelling. Potential net sediment transport at Thyspunt.
- Figure 8.7 : Sediment transport modelling. Potential net sediment transport to the east of Thyspunt.
- Figure 8.8 : Sediment transport modelling. Alongshore transport rates.
- Figure 8.9 : Sediment transport modelling. Influence of grain size on net alongshore transport rates.
- Figure 8.10 : Sediment transport modelling. Maximum daily accretion rate.
- Figure 8.11 : Sediment transport modelling. Maximum daily erosion rate.
- Figure 8.12 : Example of modelled vertical profile of suspended sand concentration.

1. INTRODUCTION

1.1 Background

Eskom have embarked on a Nuclear Sites Programme as part of their overall Nuclear Programme. The purpose of the programme is to identify the most suitable nuclear sites to meet the requirements of sufficiency for a “Strategic reserve of banked potential sites” through a Nuclear Siting Investigation Programme implemented to internationally accepted standards, according to best practice and in line with authority requirements (e.g. the National Nuclear Regulator) as appropriate.

To this end, Eskom have embarked on a programme to prepare licenceable Site Safety Reports (SSR’s) for three sites, namely Duynefontein, Bantamsklip and Thyspunt. SSR’s are licensing documents that are submitted to the national nuclear regulatory authority in support of obtaining a site licence. The data incorporated into the SSR’s contain site-related information spanning the site life-cycle phases from Nuclear Siting Investigations through construction, commissioning, operation, decommissioning, to site reuse and thereafter.

Prestedge Retief Dresner Wijnberg (Pty) Ltd (PRDW), as part of a multi-disciplinary team preparing the SSR’s, are responsible for the Oceanography and Coastal Engineering Chapters of the Site Safety Report, which are required to be prepared in accordance with Eskom’s Technical Specification for this work. This report on the Numerical Modelling of Coastal Processes, along with the Coastal Engineering Investigations Report (PRDW, 2009a), detail the studies undertaken in support of the SSR Chapter on Oceanography and Coastal Engineering. Due to space constraints the SSR contains a summary of the methodology and results, whilst these two supporting reports provide additional details on the studies undertaken. This report describes the Thyspunt site (see Figures 1.1 and 1.2 for location), whilst similar reports have been prepared for the Duynefontein and Bantamsklip sites.

1.2 Scope of work

The scope of work is to characterise the following parameters at the Thyspunt site:

- Water levels
- Tsunami flooding
- Wave height, period and direction
- Sea temperatures
- Currents
- Thermal plume dispersion for typical intake and outfall configurations
- Sediment transport
- Suspended sediment concentrations.

1.3 Limitations

A comprehensive data collection programme is underway at the Thyspunt site comprising continuous wave, current, water level, water temperature, salinity and turbidity measurements, as well as water sampling, sediment sampling and beach profiling. The objective is to provide baseline data as well as data for calibrating the numerical models. The data collection programme commenced in January 2008 and is scheduled to run until August 2010 (31 months of data). The data measured up to September 2008 has been used to calibrate the numerical models and is presented in this report. This report will be updated to include all available measured data prior to finalising the SSR.

As required by Eskom's Technical Specification for this work, this study analyses return periods up to $1:10^6$ years for water levels, waves and sea temperatures. Since these predictions are based on the available measured or hindcast datasets covering only the last 15 to 30 years, the predictions for return periods longer than 50 to 100 years need to be interpreted with caution.

1.4 Conventions and terminology

The following conventions and terminology are used in this report:

- Wave direction is the direction from which the wave is coming, measured clockwise from true north.
- Wind direction is the direction from which the wind is coming, measured clockwise from true north.
- Current direction is the direction towards which the current is flowing, measured clockwise from true north.
- H_{m0} is the significant wave height, determined from the zeroth moment of the wave energy spectrum. It is approximately equal to the average of the highest one-third of the waves in a given sea state.
- T_p is the peak wave period, defined as the wave period with maximum wave energy density in the wave energy spectrum.
- Mean wave direction is defined as the mean direction calculated from the full two-dimensional wave spectrum by weighting the energy at each frequency.
- D_N is the diameter for which N% of the sediment, by mass, has a smaller diameter, e.g. D_{50} is the median grain diameter.
- Time is South African Standard Time (Time Zone -2).
- Seabed and water levels are measured relative to Chart Datum, which corresponds to Lowest Astronomical Tide (LAT) for Port Elizabeth. Chart Datum is 0.836 m below Mean Sea Level or Land Levelling Datum (South African Tide Tables, 2008).

- The map projection system is as follows:

Map projection:	Gauss Conformal
Datum:	Hartebeesthoek 94
Spheroid:	WGS84
Scale factor:	1
Central meridian:	25 °E
Reference system:	WG25
Co-ordinates:	Eastings (X, increasing eastwards) Northings (Y, increasing northwards)
Distance units:	International metre

2. DESCRIPTION OF NUMERICAL MODELS USED

2.1 Introduction

The numerical modelling has been undertaken using the MIKE suite of models developed by Danish Hydraulics Institute (DHI). The MIKE suite of models is the most comprehensive professional coastal engineering software suite currently available. This means that all the modelling for this project is being conducted using the same suite of integrated models, thus employing the same pre- and post-processing tools, numerical grids, data structures, and allowing direct coupling of the output of one model with the input to the next model. This increases the reliability of the results by minimising any errors associated with interfacing models and data structures from different sources.

The software is under continual development, testing and application by Danish Hydraulic Institute's more than 750 employees based in more than 25 countries worldwide. Major software updates occur annually and minor updates occur quarterly on average. The latest version is Release 2008 Service Pack 3, which is being used for the modelling described below. The software has been employed by DHI alone on more than 80 power, desalination and industrial plants worldwide.

A reference list of DHI applications of the MIKE model to power plants and marine outfalls is included in Appendix A. Validation documents, user manuals and scientific documentation for each model is available on request.

2.2 Wave refraction model

The MIKE 21 Spectral Waves Flexible Mesh model (DHI, 2008a) was used for wave refraction modelling. The model simulates the growth, decay and transformation of wind-generated waves and swell in offshore and coastal areas using unstructured meshes.

MIKE 21 SW includes two different formulations:

- Directional decoupled parametric formulation
- Fully spectral formulation.

The directional decoupled parametric formulation is based on a parameterization of the wave action conservation equation. The parameterization is made in the frequency domain by introducing the zeroth and first moment of the wave action spectrum as dependent variables.

The fully spectral formulation is based on the wave action conservation equation, where the directional-frequency wave action spectrum is the dependent variable.

MIKE 21 SW includes the following physical phenomena:

- Wave growth by action of wind
- Non-linear wave-wave interaction
- Dissipation due to white-capping
- Dissipation due to bottom friction
- Dissipation due to depth-induced wave breaking
- Refraction and shoaling due to depth variations
- Wave-current interaction
- Effect of time-varying water depth and flooding and drying.

The discretization of the governing equation in geographical and spectral space is performed using cell-centred finite volume method. In the geographical domain, an unstructured mesh technique is used. The time integration is performed using a fractional step approach where a multi-sequence explicit method is applied for the propagation of wave action.

MIKE 21 SW is also used in connection with the calculation of the sediment transport, which for a large part is determined by wave conditions and associated wave-induced currents. The wave-induced current is generated by the gradients in radiation stresses that occur in the surf zone. MIKE 21 SW can be used to calculate the wave conditions and associated radiation stresses. Subsequently the wave-induced flow is calculated using the MIKE 21 Flow Model FM.

2.3 Cross-shore hydrodynamic model

The cross-shore hydrodynamic engine of the LITPACK model (DHI, 2008b) has been applied to model wave setup and the transformation of wave heights across the surf-zone.

The hydrodynamic model includes a description of propagation, shoaling and breaking of waves, calculation of the driving forces due to radiation stress gradients, momentum balance for the cross-shore and longshore direction giving the wave setup and the longshore current velocities. The model can be applied on complex coastal profiles with longshore bars. In the case of a longshore bar the broken waves can reform in the trough onshore of the bar. The waves can be treated as regular or irregular, and the effect of directional spreading can be included in the description.

For irregular waves, the Battjes and Janssen approach is applied in this study. The statistical description of the wave heights is a truncated Rayleigh distribution where the upper bound is the local maximum wave height. The mean wave energy balance equation is applied to calculate the RMS-value of the wave heights across the coastal/beach profile. The wave period is fixed.

2.4 Two-dimensional hydrodynamic model

The two-dimensional hydrodynamic model used is the MIKE 21 Flow Model (DHI, 2008c). The model is used to simulate tsunami propagation and transformation. MIKE 21 is a general purpose numerical modelling system for the simulation of water levels and flows in estuaries, bays and coastal areas. The model solves the two-dimensional shallow water equations (conservation of mass and vertically-integrated momentum) on a series of dynamically-nested rectangular grids using the Alternating Direction Implicit (ADI) technique. The solver is second to third-order accurate in the convective momentum terms.

MIKE 21 Flow includes the following physical phenomena relevant to tsunami simulations:

- Bottom friction
- Flooding and drying, i.e. tsunami run-up on a beach
- Coriolis forcing.

2.5 Three-dimensional hydrodynamic model

The three-dimensional hydrodynamic model used is the MIKE 3 Flow Flexible Mesh Model (DHI, 2008d). The model is used to simulate the three-dimensional tidal, wind and wave-driven currents and the thermal plume dispersion. The model is based on the numerical solution of the three-dimensional incompressible Reynolds averaged Navier-Stokes equations invoking the assumptions of Boussinesq and of hydrostatic pressure. The model consists of the continuity, momentum, temperature, salinity and density equations and is closed by a k - ϵ vertical turbulence closure scheme. Horizontal eddy viscosity is modelled with the Smagorinsky formulation.

The time integration of the shallow water equations and the transport equations is performed using a semi-implicit scheme, where the horizontal terms are treated explicitly and the vertical terms are treated implicitly. In the vertical direction a structured mesh, based on a sigma-coordinate transformation is used, while the geometrical flexibility of the unstructured flexible mesh comprising triangles or rectangles is utilised in the horizontal plane.

MIKE 3 Flow Model includes the following physical phenomena:

- Currents due to tides
- Currents due to wind stress on the water surface
- Currents due to waves: the second order stresses due to breaking of short period waves can be included using the radiation stresses computed in the MIKE 21 SW model
- Coriolis forcing
- Bottom friction
- Flooding and drying

- Advection and dispersion of heat, salt and other constituents
- Effect of water temperature and salinity on density and turbulence (baroclinic mode)
- Heat exchange with the atmosphere: the exchange is calculated for the processes of long wave radiation, sensible heat flux (convection), short wave radiation and latent heat flux (evaporation).

2.6 Two-dimensional sediment transport model

The sediment transport model used is the MIKE 21 Flow Model FM, Sand Transport Model (DHI, 2008e). The model comprises a dynamic coupling between the following modules:

- Spectral wave module
- Hydrodynamic module
- Sand transport module.

The spectral wave module is MIKE 21 SW as described in Section 2.2. The hydrodynamic module is the MIKE 21 Flow Flexible Mesh Model, which is the two-dimensional version of the model described in Section 2.5.

The Sand Transport Module calculates the transport of non-cohesive sediment based on the combination of flow conditions from the hydrodynamic module and wave conditions from the wave module. For the case of combined wave and currents, sediment transport rates are derived by linear interpolation in a sediment transport lookup table. The values in the table are calculated by the quasi three-dimensional sediment transport model (STPQ3D). STPQ3D calculates instantaneous and time-averaged hydrodynamics and sediment transport in two horizontal directions. As the model calculates the bed load and the suspended load separately, the values in the sediment transport table are the total load.

The temporal and vertical variations of shear stress, turbulence, flow velocity and sediment concentrations are resolved. The time evolution of the boundary layer due to combined wave/current motion is solved by means of an integrated momentum approach. The force balance includes contributions from the near bed wave orbital motion, forces associated with wave breaking (gradients of radiation stresses) and the sloping water surface. Note that equilibrium sediment transport conditions are assumed, i.e. the sediment transport reacts instantaneously to the wave and current conditions.

2.7 Suspended sediment model

The LITSTP engine of the LITPACK model (DHI, 2008b) has been applied to model the suspended sediment concentration profiles for estimating the volume of sediment drawn into the cooling water intake. The model solves the vertical diffusion equation on an intrawave period grid to provide a detailed description of the suspended sediment concentration both vertically and over the wave period.

The model accounts for waves and currents at arbitrary angles, breaking/non-breaking waves, plane/ripple-covered bed, uniform/graded bed material, effect of bed slope and the effect of streaming. The sediment is divided into 30 size fractions based on a log-normal grading curve characterized by the median grain diameter D_{50} and the geometrical spreading factor defined by $(D_{84}/D_{16})^{0.5}$. The model output is the time-averaged vertical profile of suspended sediment concentration. The model only simulates non-cohesive sediments with grain sizes greater than 0.063 mm, i.e. sand particles.

2.8 Extreme value analysis

The EVA toolbox (DHI, 2008f) comprises a comprehensive suite of routines for performing extreme value analysis. These include:

- A pre-processing facility for extraction of the extreme value series from the record of observations.
- Support of two different extreme value models, the annual maximum series model and the partial duration series model.
- Support of a large number of probability distributions, including exponential, generalised Pareto, Gumbel, generalised extreme value, Weibull, Frechét, gamma, Pearson Type 3, Log-Pearson Type 3, log-normal, and square-root exponential distributions.
- Three different estimation methods: method of moments, maximum likelihood method, and method of L-moments.
- Three validation tests for independence and homogeneity of the extreme value series.
- Calculation of five different goodness-of-fit statistics.
- Support of two different methods for uncertainty analysis, Monte Carlo simulation and Jackknife resampling.
- Comprehensive graphical tools, including histogram and probability plots.

3. WATER LEVELS

3.1 Tides

The closest port to the Thyspunt site for which long-term tidal data is available is Port Elizabeth. The predicted tidal levels at Port Elizabeth are as follows (South African Tide Tables, 2008):

TABLE 3.1: PREDICTED TIDAL LEVELS FOR PORT ELIZABETH

Parameter	Level [m CD]
Lowest Astronomical Tide (LAT)	0.00
Mean Low Water Springs (MLWS)	0.21
Mean Low Water Neaps (MLWN)	0.79
Mean Level (ML)	1.04
Mean High Water Neaps (MHWN)	1.29
Mean High Water Springs (MHWS)	1.86
Highest Astronomical Tide (HAT)	2.12

These levels are relative to Chart Datum, which is 0.836 m below Mean Sea Level or Land Levelling Datum (South African Tide Tables, 2008).

3.2 Water levels measured at the site

Water levels have been measured at the Thyspunt site starting in February 2008. The location of the tide gauge is shown in Figure 3.1 and the available data is plotted in Figure 3.2. Full details of these measurements are given in Appendix E (Lwandle, 2008a,b,c).

During the storm of 31 August 2008 a maximum water level of +2.9 m CD was recorded, which is 0.9 m above the predicted tide at the corresponding time. Since tide gauge is located in a coastal gully in a water depth of only 2 m below Mean Level, these recorded water levels will include a localised wave setup component in addition to tide, atmospheric pressure and wind setup. This wave setup component will be largely absent in the case of a tide gauge located inside a port, and these levels are thus not directly comparable to the tidal residuals described in the following section.

Since the currently available dataset at Thyspunt has a duration of only approximately 6 months, the 23 year dataset from Port Elizabeth has been used for the extreme value analysis of tidal residuals. The tidal measurements at Thyspunt are ongoing and will provide valuable design data in the future.

3.3 Extraction of tidal residuals

The actual water level differs from the predicted tidal level due to factors such as changes in atmospheric pressure, wind setup, shelf waves and edge waves. The difference between the actual water level and the predicted tide is termed the tidal residual and may be positive (actual water level

higher than predicted tide) or negative (actual water level lower than predicted tide). These residuals form one component of the extreme high and low water levels determined at the site - refer to the Coastal Engineering Investigations Report (PRDW, 2009a) for details of the superposition of all components to obtain the extreme water levels.

The procedure described below has been used to analyse the residuals. The hourly measured tides for Port Elizabeth for the period 1973 to 2007 were kindly provided by the Hydrographer of the South African Navy (who is not responsible for any transcription errors or errors due to calculations using the data). These were corrected to account for the changes in Chart Datum level in use between 1978 and 2003 (South African Tide Tables, 2008). The data was then 'cleaned' by removing obviously incorrect spikes and other errors. The MIKE tidal analysis toolkit was then used to perform a tidal analysis on the data to obtain the tidal constituents and to subsequently perform a tidal prediction for the full period.

The measured tide was then subtracted from predicted tide to obtain the tidal residuals. These residuals were again 'cleaned' to remove additional spikes and other errors in the data. Attention was paid to removing as far as possible errors caused by timing errors in the measurements, since these can significantly corrupt the residual signal. The resulting dataset comprises 22.9 years of residual data. The measured tide, predicted tide and residuals are plotted in Figure 3.3 (the full time-series) and Figure 3.4 (fourteen days including the May 1984 storm when one of the largest residuals was recorded).

3.4 Extreme value analysis of tidal residuals

The residuals have been analysed to estimate the positive and negative residuals with return periods of 1:1, 1:10, 1:100 and 1:1 000 000 years. As discussed in Section 1.3, the results for the 1:1 000 000 year return period need to be interpreted with caution.

The analysis is performed using the EVA (Extreme Value Analysis) toolbox (as described in Section 2.8). The analysis comprises fitting a three parameter Weibull distribution using the Method of Moments to an extreme value series extracted from the input time-series. The extreme value series is selected using the 'peaks over threshold' or 'partial duration series' method, with the threshold defined as the value that is exceeded 8 times per year on average. To ensure independence, two successive events are extracted only if the time between the events exceeds 24 hours. The 95% confidence level to the best estimate is calculated using the Monte Carlo method. The results of the extreme value analysis are presented in Figures 3.5 and 3.6, and Table 3.2.

TABLE 3.2: EXTREME TIDAL RESIDUALS AT PORT ELIZABETH

Return Period [years]	Best estimate positive residual [m]	Upper 95% confidence positive residual [m]	Best estimate negative residual [m]	Upper 95% confidence negative residual [m]
1	0.57	0.60	-0.53	-0.55
10	0.74	0.80	-0.73	-0.80
100	0.90	1.00	-0.93	-1.06
1 000 000	1.43	1.75	-1.73	-2.23

4. TSUNAMI FLOODING

4.1 Background

A tsunami is a train of water waves generated by impulsive disturbances of the water surface due to non-meteorological but geophysical phenomena such as submarine earthquakes, volcanic eruptions, submarine slumps and landslides or ice falls into a body of water. A conservative analysis of the potential effects produced by tsunamis should be performed and the nuclear plant should be designed for a design basis flood with a probable maximum tsunami taken into consideration (IAEA, 2003).

The approach adopted in this study was for the Council for Geoscience to define the distant and local tsunamigenic sources and for PRDW to then model the propagation of the tsunami from the source to the nuclear site.

4.2 Distant tsunamis

4.2.1 Sources

The Council for Geoscience compiled a report (CGS, 2008a) titled 'A Probabilistic Tsunami Hazard Assessment for Coastal South Africa from Distant Tsunamogenic Areas', which is included as Appendix C of this report. The report identifies Sumatra, Karachi and the South Sandwich Islands as tsunamigenic regions which can affect the coastal areas of South Africa. For each region the report provides the maximum credible earthquake magnitude and the corresponding fault parameters.

Given the fault parameters (origin, strike, length, width, dislocation, depth and dip), the vertical displacement of the seabed caused by the earthquake is estimated using the method of Okada (1985). This method assumes that the displacement of the seabed is a result of the fault movement in a semi-infinite elastic homogeneous body. The vertical displacement of the seabed induces a corresponding displacement of the water surface, which is applied as the initial condition for the hydrodynamic model.

For each source region, a number of tests were performed using the hydrodynamic model to investigate which combination of fault parameters resulted in the worst tsunami reaching the nuclear site. Based on these tests, the six tsunami events described in Table 4.1 are presented in this report. The fault parameters and the resulting maximum vertical seabed displacements for each tsunami event are provided in Table 4.2.

TABLE 4.1: DISTANT TSUNAMI SOURCES MODELLED

Earthquake event	Description
Sumatra A	This is the actual tsunami event of 26 December 2004. It is used to calibrate the numerical model. The fault parameters applied are those from Grilli <i>et al</i> (2007).
Sumatra B	This is the maximum credible Sumatra earthquake as determined by CGS (2008a). The fault dip is set to the maximum value and the fault depth to the minimum value recommended in CGS (2008a), since model tests indicated that these values resulted in the largest tsunami. As recommended by CGS (2008a), the fault position and strike were selected to result in the highest tsunami reaching South Africa, as determined from model sensitivity tests. This results in the position being moved south of the 26 December 2004 event to near the Mentawai Islands.
Sumatra C	This is a maximum plausible future rupture of the Mentawai section of the Sunda megathrust, as described by Borrero <i>et al</i> (2006).
Karachi A	This is the maximum credible Karachi earthquake as determined by CGS (2008a). The fault dip is set to the maximum value and the fault depth to the minimum value recommended by CGS (2008a), since model tests indicated that these values resulted in the largest tsunami. As recommended by CGS (2008a), the fault position and strike were selected to result in the highest tsunami reaching South Africa, as determined from model sensitivity tests.
South Sandwich Islands A	This is the maximum credible South Sandwich Islands earthquake determined by CGS (2008a). The fault dip is set to 70° and the fault depth to 1 km, since model sensitivity tests indicated that these values resulted in the largest tsunami. As recommended by CGS (2008a), the fault position and strike were selected to result in the highest tsunami reaching South Africa, as determined from model sensitivity tests.
South Sandwich Islands B	This has the same location as South Sandwich Islands A, but the moment magnitude is increased from 7.6 to 8.0 as a sensitivity test.

TABLE 4.2: FAULT PARAMETERS AND VERTICAL SEABED DISPLACEMENT

Fault parameter	Segment number ⁽¹⁾	Sumatra A (26 Dec 2004 event)	Sumatra B (max credible CGS)	Sumatra C (max plausible Borrero)	Karachi A (max credible CGS)	South Sandwich A (max credible CGS)	South Sandwich B (M _w = 8.0)
Origin longitude ⁽²⁾ [degrees, +ve East, -ve West]	1	94.10	98.55	98.30	63.00	-26.00	-26.00
	2	93.33	-	100.00	-	-	-
	3	92.71	-	101.40	-	-	-
	4	92.17	-	-	-	-	-
	5	92.44	-	-	-	-	-
Origin latitude ⁽²⁾ [degrees, +ve North, -ve South]	1	3.48	-2.08	-2.00	24.5	-56.00	-56.00
	2	5.10	-	-4.20	-	-	-
	3	7.21	-	-6.00	-	-	-
	4	9.68	-	-	-	-	-
	5	11.78	-	-	-	-	-
Strike [degrees] ⁽³⁾	1	323	321	321	270	160	160
	2	348	-	321	-	-	-
	3	338	-	321	-	-	-
	4	356	-	-	-	-	-
	5	10	-	-	-	-	-
Length [km]	1	220	741.3	260	283.1	102.8	162
	2	150	-	360	-	-	-
	3	390	-	140	-	-	-
	4	150	-	-	-	-	-
	5	350	-	-	-	-	-
Width [km]	1	130	166.72	130	96.92	54.75	71
	2	130	-	180	-	-	-
	3	120	-	70	-	-	-
	4	95	-	-	-	-	-
	5	95	-	-	-	-	-
Mean dislocation [m]	1	18	12.82	20	4.18	1.29	2.2
	2	23	-	20	-	-	-
	3	12	-	20	-	-	-
	4	12	-	-	-	-	-
	5	12	-	-	-	-	-
Depth [km] ⁽⁴⁾		25	25	15	25	1	1
Dip [degrees]		12	15	15	27	70	70
Seismic moment M ₀ [N/m] ⁽⁵⁾		8.3 x 10 ²²	6.4 x 10 ²²	8.7 x 10 ²²	4.6 x 10 ²¹	2.9 x 10 ²⁰	1.0 x 10 ²¹
Moment magnitude M _w [-] ⁽⁶⁾		9.2	9.2	9.3	8.4	7.6	8.0
Max displacement up [m] ⁽⁷⁾		9.6	5.4	9.0	1.8	0.8	1.3
Max displacement down [m]		-5.7	-2.3	-3.6	-0.4	-0.4	-0.7

- Notes:
- (1) The fault may comprise between 1 and 5 fault segments
 - (2) The origin is defined as the mid-point of the upper border of the fault
 - (3) An observer facing along strike should see the fault dip to the right (degrees clockwise from north)
 - (4) Depth is defined as depth from the seabed to the upper border of the fault
 - (5) $M_0 = \mu LWD$, with μ = shear modulus $\approx 4 \times 10^{10}$ Pa, L = Fault Length, W = Width, D = Dislocation
 - (6) $M_w = (\log_{10} M_0 - 9) / \log_{10} 32$
 - (7) The seabed displacement modelled has a complex three-dimensional shape - only the maximum upward and downward displacements are given here.

4.2.2 Model setup

The MIKE 21 HD hydrodynamic model (as described in Section 2.4) is used to simulate the propagation of the tsunami wave from the source to the nuclear site. The model solves the two-dimensional shallow water equations (conservation of mass and vertically-integrated momentum) on a series of dynamically-nested rectangular grids using an implicit time scheme. Processes simulated include Coriolis force, bottom shear stress, flooding and drying. The waves are assumed to be non-breaking and the loss of energy and momentum by wave breaking is not simulated.

Nine nested grids were used, with the grid spacing varying from 120 m near the nuclear site to 9720 m at the model boundaries. The model bathymetry is obtained from the following sources:

- ETOPO 2 minute global bathymetry dataset for depths greater than approximately 200 m.
- MIKE C-MAP electronic hydrographic charts (DHI, 2008g) for depths from 200 m to 100 m.
- Multi-beam bathymetric surveys by the Council for GeoScience for depths from 100 m to 30 m.
- Multi-beam bathymetric survey of the inshore zone by Tritan Survey cc for depths from 30 m to 5 m.
- Beach profiles by Tritan Survey cc
- Lidar survey by Southern Mapping Company for land.

The model domain and bathymetry used to simulate tsunamis from the Sumatra and Karachi regions is shown in Figure 4.1, while the bathymetry for the South Sandwich Islands tsunamis is shown in Figure 4.11.

The model time step was 6 s, which ensured a Courant Number of less than 1.0 (although a Courant number up to 20 may be acceptable for model stability, in this case a value of 1 is required for model accuracy). The grid spacings were selected to ensure at least 20 to 30 grid points per tsunami wavelength. The drying depth is set at 0.2 m and the flooding depth is 0.3 m. Bed resistance is specified by a Manning number of 32 m^{1/3}/s. Eddy viscosity is found to have an insignificant influence on these simulations and is set to zero. The water level modelled is Mean Sea Level.

The fault parameters (Table 4.2) are used to calculate the vertical displacement of the seabed caused by the earthquake, which induces a corresponding displacement of the water surface and is applied as the initial condition for the hydrodynamic model.

4.2.3 Model calibration

The model was calibrated by simulating the Sumatra tsunami of 26 December 2004. The fault parameters and associated maximum vertical seabed displacement are shown in Table 4.2.

The 26 December 2004 event was measured at a number of tidal stations along the South African coastline, with the largest water level variation measured in the Port of Port Elizabeth (Rabinovich and Thomson, 2007). The measured tidal data for Port Elizabeth was kindly provided by the Hydrographer of the South African Navy. The measured tide was subtracted from predicted tide and then adjusted for the average storm surge of 0.18 m measured during the tsunami. The resulting tsunami signal is shown in Figure 4.2. It should be noted that the maximum crest of the tsunami was not recorded due to an instrument problem. Hartnady and Okal (2007) estimate the maximum crest level to have been approximately 2.11 m above the predicted tidal level. If the 0.18 m average storm surge is taken into account the maximum crest level reduces to 1.93 m.

The modelled tsunami levels inside the Port of Port Elizabeth compare well to the measurements (Figure 4.2). In this case the model slightly under-predicts the maximum water level (model: 1.7 m, measured: approximately 1.93 m) while over-predicting the minimum water level (model: -2.0 m, measured: -1.5 m). The tsunami has a period of between 30 and 40 minutes. These results provide confidence that the model is capable of simulating the tsunami propagation and transformation processes.

4.2.4 Results

Results are presented for each of the six tsunami events described in Tables 4.1 and 4.2. Each simulation continues for approximately 24 hours after the tsunami wave reaches the site, to ensure that the maximum and minimum water levels are simulated. For each tsunami, the results are presented as two figures showing the maximum and minimum water levels relative to Still Water Level at any time during the simulation. Each figure includes a plot of the larger model domain as well as a zoomed-in view near each of the three proposed nuclear sites (Thyspunt, Bantamsklip and Duynefontein). For reference purposes, Port Elizabeth is also shown. The maximum and minimum water levels in the larger model domain are calculated from model output intervals of 10 minutes, which allows the tsunami wave crests to be visualised in the plots. The maximum and minimum water levels in the zoomed-in views are calculated from model output intervals of 1 minute, which ensures that the maximum levels are accurately detected.

The contour plots are presented in Figures 4.3 to 4.15. It can be seen that for tsunamis in the Indian Ocean, the Thyspunt site is relatively sheltered compared to Port Elizabeth. The Mentawai Islands earthquakes (Sumatra B and C) are seen to direct the tsunami south-westwards towards South Africa, compared to the 26 December 2004 event, which directed more energy westwards towards Sri Lanka.

The maximum and minimum water levels at any position within a 3 km radius of the Thyspunt site have been extracted from the results and are presented below. The 3 km radius accounts for uncertainty regarding the exact location of the nuclear plant, as well as the possibility of flooding from a flank rather than frontally. The maximum and minimum levels generally occur at the shoreline due to shoaling and run-up/run-down effects.

TABLE 4.3: MODELLED WATER LEVELS AT THYSPUNT DUE TO DISTANT TSUNAMIS

Earthquake event	Maximum water level [m above SWL]	Minimum water level [m below SWL]
Sumatra A	0.5	-0.5
Sumatra B	1.5	-1.0
Sumatra C	2.0	-1.5
Karachi A	0.2	-0.1
South Sandwich Islands A	0.5	-0.5
South Sandwich Islands B	0.7	-0.7

The Sumatra C tsunami is seen to result in the most extreme water levels. To account for uncertainties in the source parameters as well as in the modelled tsunami propagation and transformation, it is recommended to increase the modelled results by 0.5 m. This results in a recommended maximum level of 2.5 m and a minimum level of -2.0 m. These are the maximum tsunami-induced water levels relative to Still Water Level. The total water level will additionally include the effect of tide, wave run-up, wave set-up and storm surge, as described in PRDW (2009a).

4.3 Local tsunamis

4.3.1 Sources

The Council for Geoscience compiled a report (CGS, 2008b) titled 'Potential Sources of Tsunami along the South African Coast', which is included as Appendix D of this report. The possible tsunamigenic sources identified include: cosmic impact, remote submarine seismicity, submarine slides and slumps, meteotsunami, volcanic activity, terrestrial landslides and rockfalls. The summary and recommendations section of the report (CGS, 2008b) is reproduced below:

- The report provides a qualitative account of possible tsunamigenic sources that could threaten the South African coastline. To adequately assess the risk, a quantitative assessment of each source category is required.
- Offshore slump generated tsunami are considered the largest unknown risk factor. Holocene and recent historical records provide graphic evidence of their destructive capability on regional scales. Further research including all available stratigraphic/sedimentological/geomorphological data should be undertaken to better define the risk.
- Meteotsunami (edge waves) may well have been responsible for the 1969 and 2008 tsunami events along the southern African west coast. In depth research into the global frequency, locality and magnitude of meteotsunami should be undertaken to further quantify the risk. In particular,

the atmospheric conditions along the west coast prior to the 1969 event should be compared with those of its 2008 counterpart.

- Worst case scenarios need to be defined. For instance, the potential impacts of the coincidence of maximum storm waves, storm surge, astronomical tides and meteotsunami should be modelled.
- Because of the relatively short history of tsunami records along the South African coast, the database should be extended by conducting an investigation of palaeotsunami in the stratigraphic record. No systematic work has yet been conducted along this coast. Areas of focus should be in the vicinity of planned nuclear facilities.

4.3.2 Modelling approach

The Council for Geoscience report (CGS, 2008b) considers offshore slump generated tsunamis as the largest unknown risk factor for the South African coast. A number of slump regions have been documented where historical slumping has occurred on massive scales in various phases including late Mesozoic (148 million years ago-65 million years ago), early to late Tertiary (65 Ma-1.8 Ma) and possibly Quaternary (1.8 Ma-present). However, a quantitative assessment of the risk of occurrence and geometry of future slump events along the South African shelf margin is not available at present. This is in contrast to the distant tsunamigenic sources which are comparatively well defined (Section 4.2).

After discussion with the external reviewer for this study (Prof. C A Fleming), the modelling approach adopted in this study is to simulate the tsunamis generated by a number of theoretical offshore slumps in order to estimate the slump volume required to generate a tsunami at the nuclear sites of comparable size to that from the maximum credible distant earthquake described in Section 4.2.

4.3.3 Model setup

The MIKE 21 HD hydrodynamic model (as described in Section 2.4) is used to simulate the propagation of the tsunami wave from the source to the nuclear site. The model grid and parameters are the same as used for the distant earthquake sources (Section 4.2.2), except that the time-step is reduced from 6 to 3 s, and for numerical stability the eddy viscosity is increased from 0 to 20 m²/s.

Submarine mass failures can be categorised as either slip events, which are typically large translations in landslide masses, or rotational failure leading to a slump event. Since most of the South African events are categorised as slumps (CGS, 2008b), only slumps will be considered in this study. Unlike tsunami generation by earthquakes, which can be accurately modelled using the instantaneous co-seismic displacement of the water surface as an initial condition, submarine slumps or slides typically take place over an extended period of time. To simulate slumps or slides the MIKE 21 HD hydrodynamic model has the facility to dynamically change the seabed level as a function of time.

A numerical routine is developed to define the dynamic changes in seabed level arising from a slump. The submarine slump is simulated as a rigid body moving down a slope (Figure 4.16). The body has a Gaussian shape as specified in Grilli and Watts (2005). The equation describing the slump motion follows Watts *et al* (2003), where the slump motion is modelled as a rigid body undergoing a rotation around a point described as the centre of rotation of a circle prescribed by the arc of the circular failure plane. The rigid body is subject to external moments due to gravity, added mass and shear stress summed over the failure plane. The slump motion is described with a cosine function and as such experiences an initial angular acceleration, relatively constant maximum angular velocity and a subsequent deceleration before coming to rest in a position such that the centre of mass of the slump is vertically under the axis of rotation. The input parameters required for the slump model are described in the following section.

4.3.4 Slumps modelled

CGS (2008b) describes two historical slump regions relevant to the proposed nuclear sites: the Cape Town and Agulhas Slumps, shown in Figure 4.17. Three theoretical slumps have been modelled, with each slump located within one of the historical slumping regions and directly opposite one of the three proposed nuclear sites, as shown in Figure 4.18.

The magnitude of tsunami generated by a slump depends on a number of parameters, including slump volume, water depth, slump thickness, initial acceleration and maximum velocity of the slump. The geometry of the slumps which have been modelled is based on the measured geometry of the upper or proximal part of the Agulhas Slump, as indicated in Figure 4.19. Setting the slump width equal to the slump length gives a slump volume of 80 km³. The slump parameters modelled are given in Table 4.4.

TABLE 4.4: SLUMP PARAMETERS MODELLED

Parameter	Agulhas Slump	Cape Town Slump (South)	Cape Town Slump (North)
Volume [km ³] ⁽¹⁾	80	80	80
Length [km] ⁽²⁾	18	18	18
Width [km] ⁽³⁾	18	18	18
Thickness [km] ⁽⁴⁾	0.3	0.3	0.3
Rotation [deg] ⁽⁵⁾	0.4	0.4	0.4
Radius [km] ⁽⁶⁾	135	135	135
Displacement [km] ⁽⁷⁾	1.0	1.0	1.0
Centroid longitude [deg]	24.89	18.38	17.18
Centroid latitude [deg]	-35.22	-35.44	-34.37
Strike [deg] ⁽⁸⁾	75	140	160
Water depth [m]	2000	2000	2000
Initial acceleration [m/s ²]	0.011	0.011	0.011
Maximum velocity [m/s]	2.3	2.3	2.3
Duration [minutes] ⁽⁹⁾	11.3	11.3	11.3

- Notes: (1) Since the slump is elliptic, the volume = $\pi/4$ x length x width x thickness
(2) Length of the slump is measured down the slope, see 'b' in Figure 4.16
(3) Width of the slump is measured across the slope.
(4) See 'T' in Figure 4.16
(5) See ' ϕ ' in Figure 4.16
(6) See 'R' in Figure 4.16
(7) See 'S' in Figure 4.16
(8) An observer facing along the strike will see the slump moving down to the right (degrees clockwise from north)
(9) This is the total duration of the slump movement

4.3.5 Results

Results are presented for each of the three slump-generated tsunamis described in Table 4.4. Each simulation continues for approximately 10 hours after the tsunami wave reaches the site, to ensure that the maximum and minimum water levels are simulated. For each tsunami, the results are presented as two figures showing the maximum and minimum water levels relative to Still Water Level at any time during the simulation. Each figure includes a plot of the larger model domain as well as a zoomed-in view near each of the three proposed nuclear sites (Thyspunt, Bantamsklip and Duynefontein). The maximum and minimum water levels in the larger model domain are calculated from model output intervals of 10 minutes, which allows the tsunami wave crests to be visualised in the plots. The maximum and minimum water levels in the zoomed-in views are calculated from model output intervals of 1 minute, which ensures that the maximum levels are accurately detected. The contour plots are presented in Figures 4.20 to 4.25.

The maximum and minimum water levels at any position within a 3 km radius of the Thyspunt site have been extracted from the results and are presented below. The 3 km radius accounts for uncertainty regarding the exact location of the nuclear plant, as well as the possibility of flooding from a flank rather than frontally. The maximum and minimum levels generally occur at the shoreline due to shoaling and run-up/run-down effects.

**TABLE 4.5: MODELLED WATER LEVELS AT THYSPUNT
DUE TO A THEORETICAL 80 km³ SLUMP**

Slump event	Maximum water level [m above SWL]	Minimum water level [m below SWL]
Agulhas Slump	2.5	-2.8
Cape Town Slump (South)	0.2	-0.5
Cape Town Slump (North)	0.2	-0.1

4.3.6 Discussion

The hydrodynamic modelling indicates that an 80 km³ slump in the historical Agulhas Slump region is likely to result in a tsunami amplitude of approximately 2.5 m at the Thyspunt site.

The historical Agulhas Slump is one of the largest identified world-wide with an estimated length of 750 km, width of 106 km and volume of 20 000 km³ (Dingle, 1977). According to Dingle (1977), the slump involved Pliocene sediments and may therefore be Quaternary (1.8 million years to present) in age. The volume of this slump implies a devastating tsunami, evidence of which should presumably be contained in the stratigraphic record.

An important factor, however, is whether the slump occurred as a single unit or as a number of smaller events over time. Preliminary numerical modelling indicates that for the Agulhas and Cape Town slump regions, the duration of the tsunami-induced water level disturbance at the shore is 1 to 2 hours, implying that slumps separated by longer than this time are effectively separate smaller events rather than one large event.

4.4 Conclusions

The maximum tsunami risk from distant earthquake sources is found to be from the Sumatra region, which results in a maximum tsunami level of 2.5 m and a minimum level of -2.0 m (including a 0.5 m safety factor) at the Thyspunt site.

The maximum risk to the Thyspunt site from local sources is likely to be a submarine slump in the historical Agulhas Slump region. The hydrodynamic modelling indicates that a slump volume of approximately 80 km³ is required to generate a tsunami at the Thyspunt site that exceeds the tsunami

from the distant Sumatra earthquake. However, a quantitative assessment of the risk of occurrence and geometry of future slump events along the South African shelf margin is not available at present.

Until further geological research is undertaken, it is proposed to base the tsunami risk on the relatively well defined distant earthquake sources. This results in a recommended maximum level of 2.5 m and a minimum level of -2.0 m. These are the maximum tsunami-induced water levels relative to Still Water Level. The total water level will additionally include the effect of tide, wave run-up, wave set-up and storm surge, as described in PRDW (2009a).

4.5 Recommendations

Additional research is required to better define the risk from local tsunamigenic sources. The CGS (2008b) report recommends the following approach:

- Further research including all available stratigraphic/sedimentological/geomorphological data should be undertaken to better define the risk from offshore slump generated tsunami.
- In depth research into the global frequency, locality and magnitude of meteotsunami should be undertaken to further quantify the risk. In particular, the atmospheric conditions along the west coast prior to the 1969 event should be compared with those of its 2008 counterpart.
- Because of the relatively short history of tsunami records along the South African coast, the database should be extended by conducting an investigation of palaeotsunami in the stratigraphic record. No systematic work has yet been conducted along this coast. Areas of focus should be in the vicinity of planned nuclear facilities.

5. WAVES

5.1 Waves measured at the site

Waves have been measured at the Thyspunt site starting in February 2008. The location of the two wave meters is shown in Figure 3.1 and the available data is plotted in Figures 5.1 to 5.3. A number of problems including fouling by fishing nets and instrument firmware issues have reduced the data return, particularly at Site B. The position of Site B has thus been moved (as shown in Figure 3.1) and these issues have now been addressed. Full details of the measurements are given in Appendix E (Lwandle, 2008a,b,c).

The largest storm recorded to date occurred on 1 September 2008 during which the maximum waves measured at Site A were $H_{m0} = 5.6$ m, $T_p = 19.4$ s and mean direction = 210° . The instrument at Site B was not operational during the storm.

These data have been used to calibrate the wave models, as described in Section 5.4. Since the currently available dataset has a duration of only 7 months, the 15 year wave hindcast dataset has been refracted inshore and then used for the extreme value analysis of wave height. The wave measurements are ongoing and will provide valuable design data in the future.

5.2 Offshore hindcast data

Fifteen years of offshore wave hindcast data was purchased from Fugro Oceanor in Norway. The data covers the period from November 1990 to October 2007, but excluding the period June 1991 to May 1993 (during which the data quality is lower). The data position is approximately 90 km south of the Thyspunt site in 900 m water depth at E 24.50° , S 35.0° (Figure 5.6). The data comprises two-dimensional wave spectra and wave parameters (H_{m0} , T_p , mean direction) at 6 hourly intervals.

The basic source of the data is the directional wave spectra from the WAM (WAVE Model) model run at the European Centre for Medium Range Weather Forecasting (ECMWF). The model data has been calibrated by Fugro Oceanor against available satellite altimeter data. A full description of the data sources and the calibration and verification procedure is provided in Appendix B.

The full dataset is plotted in the form of a time-series (Figure 5.4) as well as a wave rose and wave height histogram (Figure 5.5). The dominant wave direction is 225° , the median H_{m0} is 2.86 m and the maximum H_{m0} is 13.03 m.

5.3 Model setup

The wave modelling has been conducted using the MIKE Spectral Waves model (as described in Section 2.2). The objective is to transform the hindcast data from offshore to nearshore where it will be

used for a number of applications including wave runup, wave-driven currents for plume dispersion and sediment transport.

The model mesh extends from the offshore wave hindcast position in 900 m depth to the shoreline. The mesh size varies from 50 m in the area of interest to 2000 m at the offshore boundary (Figure 5.6).

The model bathymetry is obtained from the following sources:

- MIKE C-MAP electronic hydrographic charts (DHI, 2008g) for depths from 200 m to 100 m.
- Multi-beam bathymetric surveys by the Council for GeoScience for depths from 100 m to 30 m.
- Multi-beam bathymetric survey of the inshore zone by Tritan Survey cc for depths from 30 m to 5 m.
- Beach profiles by Tritan Survey cc
- Lidar survey by Southern Mapping Company for land.

5.4 Model calibration

The model is calibrated by refracting the offshore hindcast data to the inshore measurement positions (Sites A and B, Figure 3.1) for the period February to July 2008. The model parameter settings based on this calibration are described below.

The directionally decoupled parametric formulation was found to give comparable results to the fully spectral formulation and is adopted due to its lower computational cost. For the directional spreading a $\cos^n(\theta-\theta_m)$ distribution is used, where n is the directional spreading index and θ_m is the mean wave direction. A constant spreading index of $n = 1.6$ (directional standard deviation = 35°) gives superior results to more complex formulations where the spreading is made a function of wave period or direction. The directional discretization in the model is 10° . The wave breaking index is 0.8.

Bottom friction is identified as an important calibration parameter. Referring to Figures 1.3 and 3.1, it is seen that one measurement station (Site A) lies inshore of the reef and one offshore of the reef (Site B). The measurements indicate significant wave energy losses across the very jagged reef structure. The best calibration was obtained using the friction factor formulation for bottom friction and setting f_w to the default value of 0.02 over the whole model domain, except over the reef where it is increased to 0.2.

The resulting model calibration is considered to be good (Figures 5.7 and 5.8). Since the boundary condition used for the calibration is the offshore wave hindcast data and not measured data, the calibration confirms the accuracy of these hindcast data.

Figure 5.9 shows an example of the wave refraction from offshore towards the site, while Figure 5.10 shows a more detailed view near the Thyspunt site, including the model output position located at -30 m CD.

5.5 Extreme value analysis of wave height

The calibrated wave model has been used to transform the offshore hindcast data inshore to the -30 m CD depth contour. Since the objective is to determine the extreme inshore wave climate, the refraction has been performed only at the times in the 15 year record when the offshore H_{m0} exceeded 5.0 m.

Results are extracted at the five points along the -30 m CD depth contour shown in Figure 5.10. The wave rose for the storm waves refracted to Point 1 is shown in Figure 5.11, as well as the H_{m0} - T_p relationship.

The wave data refracted to the -30 m CD position have been analysed to estimate the H_{m0} with return periods of 1:1, 1:10, 1:100 and 1:1 000 000 years. As discussed in Section 1.3, the results for the 1:1 000 000 year return period need to be interpreted with extreme caution.

The analysis is performed using the EVA (Extreme Value Analysis) toolbox (as described in Section 2.8). The analysis comprises fitting a three parameter Weibull distribution using the Method of Moments to an extreme value series extracted from the input time-series. The extreme value series is selected using the 'peaks over threshold' or 'partial duration series' method, with the threshold defined as the value that is exceeded 8 times per year on average. To ensure independence, two successive events are extracted only if the time between the events exceeds 48 hours. The 95% confidence level to the best estimate is calculated using the Monte Carlo method. The results of the extreme value analysis are presented in Figure 5.12 and Table 5.1.

Included in Table 5.1 are the increased wave heights taking climate change into account, which is assumed to increase the heights by 17% - refer to PRDW (2009a) for details on climate change. Also included in Table 5.1 is the estimated T_p for each wave height, based on the relationship between T_p^2 and H_{m0} at -30 m CD (refer to Figure 5.11).

TABLE 5.1: EXTREME WAVE CLIMATE AT -30 m CD

	Return Period [years]	No climate change				Climate change (17% increase in H_{m0})			
		H_{m0} best estimate [m]	T_p [s]	H_{m0} upper 95% confidence [m]	T_p [s]	H_{m0} best estimate [m]	T_p [s]	H_{m0} upper 95% confidence [m]	T_p [s]
Point 1	1	6.7	15.8	6.9	16.1	7.8	17.1	8.1	17.5
	10	8.2	17.5	8.7	18.1	9.6	19.0	10.2	19.6
	100	9.5	18.9	10.5	19.9	11.2	20.5	12.3	21.5
	1 000 000	14.4	23.3	17.5	25.6	16.8	25.2	20.4	27.7
Point 2	1	6.8	16.0	7.1	16.4	8.0	17.3	8.3	17.7
	10	8.4	17.8	9.0	18.4	9.8	19.2	10.5	19.9
	100	9.8	19.2	10.9	20.2	11.5	20.8	12.7	21.9
	1 000 000	15.0	23.7	18.2	26.2	17.5	25.6	21.3	28.3
Point 3	1	6.7	15.8	6.9	16.2	7.8	17.1	8.1	17.5
	10	8.2	17.5	8.7	18.1	9.6	19.0	10.2	19.6
	100	9.6	19.0	10.5	19.9	11.2	20.5	12.3	21.5
	1 000 000	14.4	23.3	17.5	25.6	16.9	25.2	20.5	27.7
Point 4	1	6.7	15.9	7.0	16.2	7.9	17.2	8.2	17.5
	10	8.2	17.5	8.7	18.1	9.6	19.0	10.2	19.6
	100	9.5	18.9	10.5	19.8	11.1	20.5	12.2	21.5
	1 000 000	14.2	23.1	17.1	25.4	16.6	25.0	20.0	27.4
Point 5	1	6.9	16.1	7.1	16.4	8.0	17.4	8.3	17.7
	10	8.4	17.7	8.9	18.3	9.8	19.2	10.4	19.8
	100	9.7	19.1	10.7	20.0	11.4	20.7	12.5	21.7
	1 000 000	14.4	23.3	17.4	25.6	16.9	25.2	20.4	27.7

5.6 Wave transformation across surf-zone

The cross-shore hydrodynamic engine of the LITPACK model (as described in Section 2.3) was used to transfer each of the extreme wave conditions at the -30 m CD position (Table 5.1) inshore to the -5 m CD position, where the resulting wave conditions are required as input to the wave setup and run-up computations as described in the Coastal Engineering Investigations Report (PRDW, 2009a). An example of the model output is shown in Figure 5.13.

6. SEA TEMPERATURE

6.1 Temperature measured at site

Water temperature has been measured at the Thyspunt site starting in February 2008. Temperature is measured by the Acoustic Doppler Current Profiler (ADCP) instruments deployed at Sites A and B, and by temperature sensors at two depths on a mooring at Site B. More recently, temperature data has been obtained from the tide gauge (refer to Figure 3.1 for the positions of these instruments). Full details of the these measurements are given in Appendix E (Lwandle, 2008a,b,c). The available data to date is plotted in Figure 6.1 and summarised in Table 6.1.

TABLE 6.1: SUMMARY STATISTICS OF WATER TEMPERATURES MEASURED AT THE THYSPUNT SITE

Instrument type	Total water depth [m]	Instrument depth [m]	Length of dataset [months]	Minimum temperature [°C]	Mean temperature [°C]	Maximum temperature [°C]
Tide gauge	2	1.8	3.5	12.0	15.7	18.7
Mooring at Site B	28	10	2.0	12.4	15.3	17.5
ADCP at Site A	16	15	7.0	9.1	15.2	20.1
ADCP at Site B	28	27	2.0	10.1	14.8	19.1
Mooring at Site B	28	27	6.0	9.8	14.4	18.1

The data shows water column stratification of up to 7°C on occasion, while the water column is well-mixed on other occasions. The available data indicates an average decrease in temperature of approximately 1.3°C between a depth of 2 m and a depth of 27 m. These temperature measurements are ongoing and will provide valuable design data in the future, specifically once more than one year of data is available.

Since the temperature data at the site have a duration of only 7 months, the 24 year temperature dataset measured at Tsitsikamma has been used for the extreme value analysis of temperature, as described in the next section.

6.2 Long-term data

The South African Weather Service maintains a database of sea temperatures measured daily in the surf-zone at a number of locations along the South African coastline. The closest measurement locations to the Thyspunt site are Tsitsikamma and Storms River Mouth (refer to Figure 1.1 for locations) and these datasets were purchased from the South African Weather Service. At the Tsitsikamma location both morning and afternoon measurements are available, while only morning measurements are available at Storms River Mouth.

The datasets comprise 15.3, 13.1 and 24.1 years of valid data for the Tsitsikamma (morning), Tsitsikamma (afternoon) and Storms River Mouth locations, respectively. The data is presented as a

time-series plot in Figure 6.2 and as histogram plots in Figure 6.3. The temperature statistics are summarised below:

TABLE 6.2: SUMMARY STATISTICS OF MEASURED SURF-ZONE TEMPERATURES AT THREE LOCATIONS

	Tsitsikamma (morning)	Tsitsikamma (afternoon)	Storms River Mouth
Minimum [°C]	10.0	10.0	9.4
Median [°C]	16.9	17.5	16.7
Maximum [°C]	26.0	27.0	24.4
Standard deviation [°C]	2.6	2.6	2.5

6.3 Extreme value analysis of temperature

The data has been analysed to estimate the temperatures with return periods of 1:1, 1:10, 1:100 and 1:1 000 000 years. As discussed in Section 1.3, the results for the 1:1 000 000 year return period need to be interpreted with caution.

The analysis is performed using the EVA (Extreme Value Analysis) toolbox (as described in Section 2.8). The analysis comprises fitting a three parameter Weibull distribution using the Method of Moments to an extreme value series extracted from the input time-series. The extreme value series is selected using the ‘peaks over threshold’ or ‘partial duration series’ method, with the threshold defined as the value that is exceeded 8 times per year on average. To ensure independence, two successive events are extracted only if the time between the events exceeds 48 hours. The 95% confidence level to the best estimate is calculated using the Monte Carlo method. The results of the extreme value analysis are presented in Figures 6.4 to 6.6 and Table 6.3.

TABLE 6.3: EXTREME SEA TEMPERATURES AT THREE LOCATIONS

Return Period [years]	Tsitsikamma (morning)		Tsitsikamma (afternoon)		Storms River Mouth	
	Best estimate [°C]	Upper 95% confidence [°C]	Best estimate [°C]	Upper 95% confidence [°C]	Best estimate [°C]	Upper 95% confidence [°C]
1	23.7	24.0	24.6	24.9	22.6	22.8
10	25.4	26.0	26.0	26.5	23.5	23.9
100	26.8	27.9	27.2	28.0	24.3	24.9
1 000 000	31.7	34.8	31.1	33.6	26.8	28.3

The highest extreme temperatures generally occur in the afternoon at the Tsitsikamma location and these results are thus used in the Site Safety Report. Should the new seawater intake be located offshore in deep water it is likely that the temperatures will be lower than these surf-zone temperatures (refer to Section 6.1).

7. CURRENTS AND THERMAL PLUME DISPERSION

7.1 Background

The advantage of locating the power station at the coast is that it allows a once-through seawater cooling system to be used. However, the intake and outfall structures need to be designed to minimize recirculation between the outfall and the intake, and to ensure that the potential ecological impacts due to the discharge of heated water and other co-discharges such as chlorine and nuclides are acceptable.

The MIKE 3 Flow Flexible Mesh three-dimensional hydrodynamic model (as described in Section 2.5) has been set up to simulate the currents and the dispersion of the thermal plume due to winds, waves, tides and buoyancy effects. Two conceptual intake and outfall layouts have been tested for a representative 42 day simulation period.

7.2 Currents measured at site

Currents have been measured at the Thyspunt site starting in February 2008. The location of the two Acoustic Doppler Current Profiler (ADCP) instruments is shown in Figure 3.1 and the available data is plotted in Figures 7.1 to 7.3. The instruments measure the current speed and direction in 0.5 m intervals from the surface to the seabed. A number of problems including fouling by fishing nets and instrument firmware issues have reduced the data return, particularly at Site B. The position of Site B has thus been moved (as shown in Figure 3.1) and these issues have now been addressed. Full details of the measurements are given in Appendix E (Lwandle, 2008a,b,c).

The dominant current direction is towards the east and the current speeds are moderate near the surface and low near the seabed, as shown in Table 7.1.

TABLE 7.1: SUMMARY STATISTICS OF CURRENT SPEEDS MEASURED AT THE THYSPUNT SITE

	Site A		Site B	
	Near surface (-2.3 m)	Near seabed (-12.4 m)	Near surface (-2.2 m)	Near seabed (-23.2 m)
Mean current speed [m/s]	0.11	0.05	0.20	0.10
Maximum current speed [m/s]	0.70	0.45	0.72	0.57

These data have been used to calibrate the hydrodynamic model, as described in Section 7.3.2. The current measurements are ongoing and will provide valuable design data in the future.

7.3 Hydrodynamic modelling

7.3.1 Model setup

The model bathymetry is obtained from the following sources:

- MIKE C-MAP electronic hydrographic charts (DHI, 2008g) for depths from 200 m to 100 m.
- Multi-beam bathymetric surveys by the Council for GeoScience for depths from 100 m to 30 m.
- Multi-beam bathymetric survey of the inshore zone by Tritan Survey cc for depths from 30 m to 5 m.
- Beach profiles by Tritan Survey cc
- Lidar survey by Southern Mapping Company for land.

The horizontal model grid comprises both triangular and quadrilateral elements with sizes ranging from 30 m at the outfall to 1000 m at the offshore boundaries (Figures 7.4 and 7.5). The vertical grid has five layers having thicknesses from seabed to surface of 20%, 30%, 20%, 20% and 10% of the local water depth.

7.3.2 Model calibration

The model was calibrated by comparing the measured and modelled currents at Sites A and B (Figure 3.1). The model parameter settings based on this calibration are described below.

The predicted tide is applied along the three open boundaries of the model. Since a weak tidal signal is evident in the measured currents, the tidal levels applied in the model are varied along the boundaries. The tidal levels are obtained from a global tide model including the major diurnal (K_1 , O_1 , P_1 and Q_1) and semidiurnal tidal constituents (M_2 , S_2 , N_2 and K_2) with a spatial resolution of $0.25^\circ \times 0.25^\circ$ based on TOPEX/POSEIDON altimetry data (DHI, 2008c).

A wind that varies in time but is constant over the model domain is applied. The wind data used for the calibration is the data measured at the Thyspunt site by Airshed Planning Professionals (Pty) Ltd. The model calibration indicates a constant wind drag coefficient $C_d = 0.0012$.

Wave-driven currents are included by first running the calibrated MIKE Spectral Waves model (refer to Section 5) and saving the radiation stresses at three hour intervals. The numerical grid for the refraction model corresponds to the hydrodynamic grid in the hydrodynamic domain, but extends further offshore to the 900 m contour (Figure 5.7).

Bottom friction is identified as an important calibration parameter. Referring to Figures 1.3 and 3.1, it is seen that one measurement station (Site A) lies inshore of the reef and one offshore of the reef (Site B). The wave model calibration (Section 5.4) found significant wave energy losses across the very jagged reef structure and the wave friction factor was thus increased over the reef. This effect is also evident in the currents and hydrodynamic model calibration indicates the use of the default bottom roughness height of 0.05 m over the whole model domain, except over the reef where it is increased to 1.0 m.

Horizontal eddy viscosity and dispersion are computed using the Smagorinsky formulation with a default constant of 0.28. Vertical eddy viscosity is computed using the k- ϵ vertical turbulence closure scheme, while the vertical eddy dispersion is set to 0.1 times the vertical eddy viscosity. This scaling factor is applied to compensate for additional vertical mixing caused by the use of only 5 vertical layers and the potential smoothing of the vertical density gradient between the buoyant thermal plume and the ambient water. Model sensitivity tests for the Duynefontein site (PRDW, 2009a) indicate that using a scaling factor of 0.1 does result in a small increase in the vertical stratification compared to a default factor of 1.0.

Model sensitivity tests were performed for the Duynefontein site in which ambient thermal stratification as well as heat exchange between the atmosphere and the sea surface are included in the simulation (PRDW, 2009a). These two processes were found to have a relatively small influence on the model results (in terms of the temperature increase in the plume over background) and the remaining simulations have been performed using a constant background temperature of 17°C, corresponding to the median temperature measured at Tsitsikamma (Section 6.2). It should be borne in mind that the background sea temperature varies on a seasonal, synoptic and diurnal time-scale (refer to Figures 6.1 and 6.2) and the temperature increase due to the thermal plume will be superimposed on this background variability. A constant salinity of 35.0 psu is specified.

The resulting model calibration is shown in Figures 7.6 to 7.9. The model is seen to reproduce the main features of the measured currents including wind, wave and tidal forcing. Based on these calibration results, the model is expected to reliably simulate the thermal plume advection and dispersion.

In addition, the thermal plume dispersion capabilities of the model have been calibrated against measured thermal plume temperatures. In the absence of an existing thermal plume at Thyspunt, the plume at the existing Koeberg Nuclear Power Station is employed. Full details are provided in the Duynefontein Modelling Report (PRDW, 2009b).

7.3.3 Selection of wind and wave forcing

The Oceanor hindcast dataset (Section 5.2) includes 10 years of simultaneous wave and wind data which are required as input forcing to the hydrodynamic model, along with tidal forcing. However, the computer run-times for the three-dimensional hydrodynamic model limit the period that can be simulated to a number of months. A rigorous procedure was thus developed to select the following periods from the 10 year dataset:

- A 14 day period with typical summer conditions
- A 14 day period with typical winter conditions
- A 14 day period with calm conditions (low waves and wind).

The procedure first calculates the following parameters for each consecutive 14 day period in the 10 year dataset (values in brackets are the weighting factor applied in the cost function):

- The mean wave height (1.0)
- The standard deviation of the wave height (0.2)
- The mean wave direction, weighted by the wave height (1.0)
- The mean peak period (0.4)
- The mean wind speed (1.0)
- The standard deviation of the wind speed (0.2)
- The mean wind direction, weighted by the wind speed (1.0).

The procedure then uses a cost function (i.e. a function that minimises the difference between two values) to locate the 14 day period having parameters closest to the average conditions for each season. The calmest 14 day period was located using a weighting factor of 2.0 for mean wave height and 1.0 for mean wind speed, with all other weights set to zero. The periods located by this process are given below, and the wind and wave conditions for each period are plotted in Figures 7.10 to 7.12.

- 14 day summer period: 2006-01-21 to 2006-02-03
- 14 day winter period: 2000-08-01 to 2000-08-15
- 14 day calm period: 2004-02-14 to 2004-02-27

For the plume dispersion modelling, these three periods have been run sequentially giving a total simulation time of 42 days.

7.3.4 Discharge characteristics

The current Environmental Impact Assessment for Nuclear-1 being conducted by Arcus Gibb is based on a maximum power output of 4 000 MWe, with provision made for future expansion as, when and if appropriate.

The Site Safety Report is based on the Plant Parameter Envelope (PPE) of 10 000 MWe (Eskom, 2008a). The seawater cooling water requirement is based on information provided by Eskom (2008b), which indicates that a Pressurised Water Reactor (PWR) with a power of 1 650 MWe requires 76 m³/s of cooling water and increases the water temperature by 12°C. By assuming the flow rate to increase linearly with power output and the temperature increase to remain constant, the seawater flow rates are as follows:

TABLE 7.2: SEAWATER COOLING REQUIREMENTS

Power output [MWe]	Seawater flow rate [m ³ /s]	ΔT [°C]	Comment
4 000	184	12	Nuclear-1 EIA Study
10 000	460	12	Site Safety Report

In addition to the increased temperature, the cooling water discharge may also contain co-discharges such as chlorine, nuclides, etc. Since these co-discharges have not yet been quantified, for this modelling study these are treated as conservative tracers, i.e. they undergo dilution by physical mixing only and any additional biochemical or physical processes are not modelled. The model results provide the achievable dilutions for any discharged constituent. Once the concentration of these constituents has been quantified, the potential impact of these constituents can be assessed by comparing the achievable dilutions from the model results to the dilution required to reduce the concentration at discharge to a level at which no impacts occur.

Reverse Osmosis desalination is being considered to provide fresh water during the earthworks, construction and operation stages of the power station (Eskom, 2008b). During operation of the power plant, the brine discharge from the desalination plant will be mixed with the once-through cooling water discharge from the power station and discharged at the cooling water outfall. The operational stage desalination plant fresh water output is 4000 m³/day (Eskom, 2008b). The brine output flow associated with this is 6000 m³/day (or 0.069 m³/s), while the cooling water discharge rate for Nuclear-1 with a power output of 3300 MWe will be approximately 152 m³/s (Eskom 2008b). This means that the brine will be diluted 2200 times in the pipe prior to discharge into the sea, making the brine effectively undetectable.

During the earthworks and construction stages, however, the cooling water outfall structure will not be completed and the brine will have to be discharged independently of the cooling water. The dilution of the construction stage brine has been modelled in PRDW (2008a). Since the brine is not considered to be a site safety issue, it is not considered further in this report.

7.4 Intake and outfall layouts tested

Since no engineering feasibility studies on the intake and outfall structures have been completed, conceptual layouts were developed which serve to illustrate the thermal plumes that can be anticipated for typical combinations of intake and outfall types. On 29 September 2008, Eskom advised PRDW that the basin intake options should not be considered any further for purposes of the Thyspunt SSR. Only two conceptual intake and outfall layouts have thus been tested.

Layout 1 has been tested for a power output of 4 000 MWe (as required for the Nuclear-1 EIA study) as well as a power output of 10 000 MWe (as required for the Site Safety Report). Layout 2 has been tested for a power output of 10 000 MWe only.

7.4.1 Layout 1: Offshore tunnel intake and nearshore pipeline outfall

This is based on the conceptual intake and outfall layout for Nuclear-1 as provided by Eskom (2008c). Only the details that are of relevance for the thermal plume dispersion modelling are described here.

The intake is a submarine tunnel extending to a depth of -29 m CD approximately 1000 m offshore. An intake structure will be positioned at the end of the intake tunnel with the intake openings positioned 3 to 5 m above the sea bed to prevent the drawing in of large quantities of sediment. For Nuclear-1 (maximum power of 4 000 MWe and maximum seawater flow of 184 m³/s), either a single tunnel with an internal diameter of approximately 9 m, or two tunnels with diameters of approximately 6.4 m will be used. The velocity of the water in the intake tunnel will be in the range 2.5 to 3.0 m/s to avoid sedimentation.

The outfall for Nuclear-1 as described in Eskom (2008c) comprises six 3 m diameter pipes buried below the seabed in a 27.5 m wide trench and discharging approximately 250 m offshore in a water depth of approximately -5 m CD. The velocity of the water in the pipes will be approximately 4.5 m/s and the ends of the pipes will be raised above the seabed to prevent erosion of the seabed.

In the case of the full PPE, the power output will increase to 10 000 MWe and for this modelling study it is assumed that three 9 m diameter intake tunnels will be required. The positions of the three intakes tested in this study are shown in Figure 7.13. These positions will need to be refined based on geotechnical and engineering considerations.

In the case of the full PPE, it is also assumed that the number outfall pipes will triple to eighteen. The position of the outfall tested in this study is shown in Figure 7.13. The position will need to be refined based on geotechnical and engineering considerations.

7.4.2 Layout 2: Offshore tunnel intake and nearshore channel outfall

This layout comprises the same tunnel intake modelled for Layout 1. The outfall is now a 90 m wide channel discharging at the same position as before, i.e. approximately 250 m offshore in a water depth of approximately -5 m CD. The bottom of the channel is at -1 m CD. Note that this channel width is for the full PPE of 10 000 MWe and for Nuclear-1 a narrower channel would be recommended to maintain the same velocity in the channel. This layout is shown in Figure 7.14.

Both Layouts 1 and 2 have the intake openings located approximately 25 m below the water surface. The available measurements (Section 6.1) indicate that the temperature at this depth is on average 1.3°C colder than near the surface. This difference has not been included in the modelling which makes the model results conservative.

7.5 Results

7.5.1 Currents

The currents are predominantly wave-driven in the surf-zone and wind- and tidally-driven beyond the surf-zone. Figure 7.15 illustrates an example of a wave-driven current caused by obliquely-breaking waves. Figure 7.16 shows an example of a westward current generated by a wind from the east.

7.5.2 Temperature and dilution

The thermal plume from the outfall is advected and dispersed by the ambient currents. Since these currents are continually changing as the wave, wind and tidal conditions change, the plume behaviour is dynamic. This is illustrated in Figures 7.15 and 7.16 which show the thermal plume at two moments in time.

The model results for each layout have been post-processed to determine the maximum and mean (i.e. time-averaged) increase in temperature over the full 42 day simulation period. This has been done for both the surface and seabed layers of the model. The results are presented in Figures 7.17 to 7.29. These results can also be interpreted as dilution factors for any co-discharges such as chlorine, nuclides, etc. as follows: divide 12 (the initial temperature increase) by the temperature increase shown in the plots, e.g. the 2°C contour in the plots represents a dilution factor of $12/2 = 6$. If the co-discharge is mixed with the cooling water prior to discharge into the sea, the co-discharge will undergo a pre-dilution in the pipe in addition to the subsequent dilution in the sea.

These results show that the maximum increase in temperature is significantly larger and more extensive than the mean increase in temperature. This is due to the dynamic plume behaviour which results in the plume remaining at one position for short periods of time only. The results also illustrate the effect of the buoyancy of the plume due to the increased temperature, which tends to keep the plume near the water surface rather than the seabed, particularly as the plume is advected into deeper water. In the shallow water (less than 5 m) the plume tends to be mixed throughout the water column.

The plume for Nuclear-1 (power output: 4 000 MWe) is significantly smaller than for the PPE (power output: 10 000 MWe). Compare for example Figures 7.17 and 7.21, or Figures 7.19 and 7.23.

The plumes predicted for Layouts 1 and 2 are similar. The main difference is that the channel outfall structure (Layout 2) tends to jet the plume slightly further offshore than the pipeline outfall (Layout 1). Compare for example Figures 7.21 and 7.25, or Figures 7.23 and 7.27.

The sensitivity of the plume dispersion to climate change is also investigated by increasing the wind speed by 10% and the wave height by 17%, which are the increases anticipated by the year 2100 (PRDW, 2009a). Refer to PRDW (2009a) for further details on climate change. The predicted

influence of these changes is to slightly improve the dispersion of the plume due to the increased current speeds (compare Figures 7.21 and 7.29). As discussed in PRDW (2009a), climate change may also increase the background water temperature by 3°C, which will result in a corresponding increase in the intake and discharge temperatures.

These model results can be used to assess the potential ecological impacts due to the discharge of heated water and other co-discharges such as chlorine and nuclides.

7.5.3 Recirculation

The model results have been analysed to determine the recirculation of the thermal plume from the outfall back to the intake. Note that the hydrodynamic model automatically accounts for recirculation by constantly adjusting the outfall temperature to be 12°C above the intake temperature at each time-step.

The results are plotted in Figures 7.30 to 7.32. These plots show how the plume tends to be located in the upper half of the water column, with temperature increases up to 7°C near the surface and less than 0.9°C near the seabed, which is where the intake is located. The plots also show that the recirculation events occur in cycles of approximately 5 days. The plots show no trend for the temperature to build up over the simulation period.

The recirculation results for a power output of 10 000 MWe are summarised in Table 7.3. The recirculation temperatures for Layouts 1 and 2 are very similar and only a small influence of climate change is evident. These results indicate that recirculation is unlikely to be a problem for either Layouts 1 or 2, due to the outfall being located near the surface and intake near the seabed.

**TABLE 7.3: RECIRCULATION RESULTS:
INCREASE IN TEMPERATURE AT INTAKE**

	Layout 1	Layout 2	Layout 1 including climate change
Mean increase [°C]	0.2	0.2	0.2
Maximum increase [°C]	0.9	0.9	1.0
Standard deviation [°C]	0.2	0.1	0.2

8. SEDIMENT TRANSPORT

8.1 Background

The aim of this section is to estimate the net and gross sediment transport rates in the vicinity of the Thyspunt site. In addition, the concentration of suspended sediment in the water column is modelled for various intake depths and wave conditions.

Additional sediment related studies are described in the Coastal Engineering Report (PRDW, 2009a). These include the analysis of historical beach plan shapes, beach erosion by storms, setback due to sea level rise and sediment movement by tsunamis.

8.2 Sediment grain size

Sediment samples were taken from the nearshore (using a Van Veen grab) and from the beach (near the high and low water marks) on 5 and 6 April 2008, respectively. The grain size analysis is given in Table 8.1 and the spatial variation of the D_{50} grain size is plotted in Figure 8.1 (D_N is the diameter for which N% of the sediment, by weight, has a smaller diameter.) The sand on the beaches has a D_{50} of 0.2 to 0.4 mm, while further offshore D_{50} is generally 0.1 to 0.2 mm, except on the reef where larger sized gravel and shell fragments are found. The sediment grading, defined as $(D_{84}/D_{16})^{0.5}$, averages 1.5.

TABLE 8.1: SEDIMENT GRAIN SIZE ANALYSIS FOR THYSPUNT

Longitude [deg]	Latitude [deg]	D ₉₅ [mm]	D ₉₀ [mm]	D ₈₄ [mm]	D ₇₅ [mm]	D ₅₀ [mm]	D ₂₅ [mm]	D ₁₆ [mm]	D ₁₀ [mm]	D ₅ [mm]	Grading [-]
24.6470	-34.1796	0.457	0.362	0.298	0.259	0.195	0.158	0.145	0.135	0.125	1.4
24.6833	-34.1873	0.458	0.383	0.330	0.287	0.233	0.195	0.181	0.169	0.155	1.4
24.6824	-34.1873	0.386	0.286	0.253	0.227	0.188	0.161	0.150	0.142	0.133	1.3
24.6806	-34.1914	0.490	0.404	0.344	0.291	0.234	0.195	0.181	0.169	0.156	1.4
24.6938	-34.1973	0.438	0.304	0.257	0.224	0.188	0.164	0.154	0.145	0.136	1.3
24.6995	-34.1938	0.000	0.000	1.732	1.277	0.581	0.313	0.267	0.237	0.205	2.5
24.7028	-34.1972	0.354	0.263	0.235	0.211	0.184	0.162	0.153	0.145	0.136	1.2
24.7021	-34.1987	0.350	0.268	0.238	0.214	0.185	0.163	0.153	0.145	0.136	1.2
24.7092	-34.2000	0.342	0.250	0.225	0.206	0.181	0.159	0.150	0.142	0.132	1.2
24.7154	-34.1979	0.000	1.961	1.407	0.933	0.518	0.370	0.319	0.255	0.199	2.1
24.7333	-34.1911	0.486	0.389	0.322	0.276	0.215	0.183	0.171	0.160	0.149	1.4
24.7439	-34.1947	0.446	0.259	0.220	0.197	0.167	0.147	0.139	0.132	0.125	1.3
24.6087	-34.1807	0.381	0.326	0.293	0.272	0.231	0.198	0.185	0.175	0.163	1.3
24.6137	-34.1765	0.287	0.258	0.241	0.225	0.199	0.179	0.169	0.160	0.151	1.2
24.6194	-34.1741	0.305	0.280	0.264	0.246	0.211	0.189	0.179	0.170	0.159	1.2
24.6289	-34.1723	0.504	0.438	0.391	0.342	0.271	0.226	0.209	0.196	0.182	1.4
24.6290	-34.1724	0.475	0.412	0.365	0.318	0.260	0.219	0.204	0.192	0.178	1.3
24.6474	-34.1727	0.523	0.454	0.411	0.367	0.290	0.243	0.222	0.206	0.190	1.4
24.6558	-34.1742	0.450	0.411	0.380	0.347	0.289	0.249	0.229	0.213	0.195	1.3
24.6608	-34.1753	0.429	0.372	0.330	0.294	0.255	0.221	0.207	0.195	0.182	1.3
24.6850	-34.1834	0.661	0.564	0.496	0.457	0.381	0.319	0.294	0.275	0.255	1.3
24.6859	-34.1839	0.920	0.687	0.572	0.483	0.392	0.318	0.290	0.271	0.249	1.4
24.6994	-34.1896	0.000	1.896	1.489	1.122	0.409	0.211	0.190	0.175	0.159	2.8
24.6996	-34.1885	0.000	1.134	0.724	0.475	0.284	0.223	0.204	0.190	0.174	1.9
24.7164	-34.1910	0.551	0.471	0.429	0.386	0.306	0.250	0.228	0.211	0.193	1.4
24.7190	-34.1894	0.776	0.646	0.562	0.484	0.376	0.294	0.267	0.245	0.221	1.5
24.7244	-34.1870	0.507	0.462	0.428	0.392	0.324	0.271	0.251	0.231	0.210	1.3
24.7269	-34.1864	0.488	0.438	0.399	0.358	0.288	0.244	0.225	0.209	0.193	1.3
24.7299	-34.1863	0.491	0.439	0.399	0.357	0.287	0.245	0.227	0.212	0.195	1.3
24.7328	-34.1862	0.528	0.482	0.450	0.416	0.350	0.295	0.271	0.252	0.227	1.3
24.7359	-34.1867	0.459	0.413	0.378	0.341	0.281	0.241	0.224	0.210	0.194	1.3
24.6089	-34.1807	0.518	0.409	0.339	0.289	0.241	0.205	0.193	0.183	0.170	1.3
24.6138	-34.1766	0.463	0.359	0.296	0.271	0.227	0.198	0.188	0.179	0.166	1.3
24.6195	-34.1742	0.463	0.359	0.296	0.271	0.227	0.198	0.188	0.179	0.166	1.3
24.6290	-34.1724	0.653	0.508	0.450	0.394	0.297	0.245	0.224	0.208	0.190	1.4
24.6381	-34.1723	0.488	0.435	0.395	0.353	0.284	0.242	0.224	0.210	0.193	1.3
24.6473	-34.1728	0.487	0.431	0.389	0.345	0.280	0.240	0.224	0.210	0.194	1.3
24.6557	-34.1742	0.488	0.421	0.371	0.321	0.266	0.228	0.212	0.200	0.186	1.3
24.6607	-34.1756	0.492	0.433	0.389	0.343	0.280	0.242	0.225	0.212	0.197	1.3
24.6850	-34.1834	0.712	0.605	0.526	0.467	0.378	0.305	0.284	0.268	0.250	1.4
24.6858	-34.1840	0.617	0.494	0.454	0.412	0.334	0.280	0.262	0.247	0.227	1.3
24.6994	-34.1896	1.839	1.458	1.185	0.900	0.298	0.202	0.182	0.168	0.153	2.6
24.6996	-34.1885	0.000	0.000	1.838	1.206	0.448	0.239	0.207	0.189	0.171	3.0
24.7167	-34.1912	0.572	0.442	0.382	0.323	0.255	0.213	0.199	0.188	0.176	1.4
24.7191	-34.1895	0.558	0.461	0.413	0.364	0.285	0.240	0.222	0.207	0.192	1.4
24.7219	-34.1881	0.500	0.438	0.391	0.344	0.275	0.234	0.218	0.205	0.192	1.3
24.7244	-34.1872	0.451	0.414	0.386	0.355	0.298	0.259	0.241	0.225	0.207	1.3
24.7270	-34.1866	0.495	0.431	0.383	0.334	0.272	0.233	0.216	0.203	0.189	1.3
24.7299	-34.1864	0.518	0.426	0.367	0.308	0.270	0.237	0.220	0.207	0.191	1.3
24.7328	-34.1864	0.570	0.478	0.441	0.402	0.329	0.275	0.256	0.239	0.219	1.3
24.7360	-34.1869	0.716	0.588	0.497	0.444	0.347	0.279	0.257	0.237	0.215	1.4

8.3 Sediment transport rates

8.3.1 Model setup

The MIKE 21 Coupled Flexible Mesh model (as described in Section 2.6) is used. The model simulates wave refraction, wave-driven currents, wind-driven currents and non-cohesive sediment transport over a two-dimensional domain. A simpler approach would be to use a one-dimensional model such as LITPACK (DHI, 2008b) to estimate the sediment transport at specific profile positions. However, the complex bathymetry in this area requires a two-dimensional approach.

The model grid and bathymetry are similar to that used in the wave modelling (Figure 5.7) and the plume dispersion modelling (Figure 7.4). The grid is refined to less than 50 m in the nearshore areas.

8.3.2 Schematisation of wave and wind climate

The deepwater wave and wind hindcast data described in Section 5.2 is used to drive the model. The dataset used is the 10 year period from 1997 to 2006 at 6 hourly intervals. These data are binned into 163 conditions which are then simulated in the model.

The bin sizes used for the deepwater wave conditions are as follows: 2 m bins for H_{m0} , 25° bins for wave direction and 4 s bins for T_p . Only the longshore component of the wind is considered, since this component drives the longshore currents. The bin size for the longshore wind speed is 10 m/s.

To obtain one representative condition to model from all the conditions falling into a particular bin, H_{m0} and the wave direction are weighted by the wave energy flux $H_{m0}^2 T_p$ and the wind speed is weighted by the wind speed squared.

Each of the 163 conditions is modelled for 12 hours to achieve steady state current speeds under the imposed wave and wind forcing. The sediment transport rate and the rate of bed level change at the end of each 12 hour simulation are saved. The sediment transport rates are then weighted by the occurrence of each condition to obtain the annual sediment transport rates. Note that a fixed bed level is applied, i.e. no morphodynamic updating.

8.3.3 Model calibration

The model parameters used in the wave refraction model follow from the model calibration described in Section 5.4. The model parameters used in the hydrodynamic model follow from the model calibration described in Section 7.3.2.

The inputs to the sediment transport model include the grain size. Since this varies over the domain (Figure 8.1), separate simulations are performed using D_{50} grain sizes of 0.15, 0.2 and 0.3 mm. Based on a number of preliminary tests the additional parameter settings for the sediment transport model are

selected as follows: critical Shields parameter = 0.05, ripples are included, bed slope effects are excluded, the deterministic formulation is used for the bed concentration, streaming is excluded, density currents are excluded, helical flow is excluded, undertow is excluded, the wave theory is Stokes 1st order and the wave breaker index = 0.8.

The coupled wave, current and sediment transport model was first tested for a simplified case with a uniform 1:67 beach slope and a wave approaching 30° from normal. The results are seen to be qualitatively correct (Figures 8.2 and 8.3).

The model calibration was to set up the model for the existing Koeberg layout and to compare the modelled net sediment transport entering the intake basin to the measured maintenance dredging volumes. The model includes the Koeberg cooling water intake pumps with an average flow rate of 86 m³/s. The grain size is set to $D_{50} = 0.2$ mm, which is the typical grain size measured inside the basin (PRDW, 2002). The model gives a net sediment transport into the basin of 140 000 m³/year (Figure 8.4), which compares well to the average maintenance dredging volume of approximately 132 000 m³/year (PRDW, 2002).

8.3.4 Results

The modelled net sediment transport in the vicinity of the Thyspunt site for a D_{50} of 0.2 mm is shown in Figures 8.5 to 8.7. It is important to note that these are the potential sediment transport rates, assuming that the seabed is covered with sand. In rocky areas the actual sediment transport rates will be lower, and will tend to occur as a 'slug' of sand moving over the rock under particular conditions.

The sediment transport has been integrated across the 46 beach profiles shown in blue in Figures 8.5 to 8.7. For each profile, the accumulated westward transport, the accumulated eastward transport, the net transport and the gross transport have been calculated and are presented in Figure 8.8.

West of Klippen Point at Profile 1 the potential net transport is westwards, which suggests little sediment is being supplied to the system from the west. The beach at Oyster Bay (Profiles 7 to 18) is characterised by rip cells and variable net transport directions. The rocky coastline between Profiles 19 and 24 generally has a westward potential net transport, which implies little sediment supply to Thysbaai from the west. Near Thyspunt (Profiles 25 to 29) the potential transport is strongly eastwards, but the sediment supply is low and any sand arriving from the west will be rapidly transported eastwards. The beach at Thysbaai (Profiles 30 to 36) has a small net westwards transport due to the eddy formed in the lee of Thyspunt. The rocky area to the east of Thysbaai (Profiles 37 to 46) has a strong eastward potential net transport, but will be limited by the sediment supply.

The sensitivity of the model results to grain size is shown in Figure 8.9. The D_{50} of 0.15 mm has approximately twice the transport rate of the larger 0.2 and 0.3 mm sizes.

The model results are also processed to obtain the maximum daily accretion and erosion rates for any of the 163 wave/wind conditions simulated (Figures 8.10 and 8.11). These are again the potential rates, assuming a sufficient supply of sand. These results give an indication of the short term erosion and accretion that an intake or outfall structure would be subjected to at various locations. The reduction in seabed level changes with increasing water depth is clearly shown. The predicted bed level change over the reef area would be limited by the presence of the reef and availability of sand.

8.3.5 Conclusions

The model results indicate that although there are areas of high potential sediment transport towards the east, there is a limited supply of sediment available from the west and the actual net transport near Thyspunt is thus likely to be low. Further more detailed morphodynamic modelling will however need to be undertaken as part of the detailed design phase. An assessment of the coastline stability based on aerial photographs, beach profile measurements and cross-shore sediment transport modelling is presented in PRDW (2009a).

8.4 Suspended sediment concentrations

8.4.1 Background

The proposed seawater intake is a tunnel extending to approximately 30 m water depth with the intake opening positioned 3 to 5 m above the seabed (Eskom, 2008c). One of the design parameters will be the volume of sand drawn into the intake which will have to be removed from the proposed settling basin located on land in front of the cooling water pump house (Eskom, 2008c). Preliminary modelling is performed to estimate the volume of sand drawn into the intakes. Note that this work applies only to the proposed tunnel intake system. In the case of a basin intake, more detailed three-dimensional sediment transport modelling will be required.

8.4.2 Measured suspended sediment concentrations

One set of 11 water samples has been taken at the Thyspunt site on 20 July 2008. The samples were taken between 2 and 8 m below the water surface in water depths between 4 and 30 m. The measured suspended solids concentrations are between 2 and 10 mg/L, with an average of 3 mg/L. Additional samples have been taken and will be included in the final SSR report.

The ADCP instruments are also able to estimate suspended sediment concentrations, using specialised software (the ViSea Plume Detection Toolbox). Based on a preliminary calibration using the limited sampling data presently available, the suspended sediment concentrations are estimated from the ADCP located in 16 m water depth (Site B in Figure 3.1). The predicted suspended sediment concentrations are generally below 5 mg/L in the lower half of the water column. Refer to Lwandle (2008d) for further information.

Both the measured and predicted suspended sediment concentration profiles are approximately uniform throughout the water column, implying that these are smaller cohesive sediment particles ($D_{50} < 0.063$ mm) rather than larger sand particles (which would show a higher concentration near the seabed). These measurements are ongoing and will provide valuable design data in the future, specifically once more than one year of data is available.

8.4.3 Model setup

The modelling is performed using the LITPACK model, as described in Section 2.7. The model inputs are the water depth, D_{50} grain size, the sediment grading defined by $(D_{84}/D_{16})^{0.5}$, the root-mean-square wave height $H_{rms} \approx H_{m0}/1.41$, the zero-crossing wave period $T_z \approx T_p/1.3$, wave direction, current speed and current direction. The model output is the vertical profile of suspended sand concentration. The model only simulates non-cohesive sediments with grain sizes greater than 0.063 mm, i.e. sand particles.

Based on the settings established in the two-dimensional sediment transport modelling (Section 8.3.3) the parameter settings for the model are selected as follows: critical Shields parameter = 0.05, wave breaking dissipation factor beta = 0.15, ripples are included, bed slope effects are excluded, the deterministic formulation is used for the bed concentration, convective terms are included, density currents are excluded, the wave theory is Stokes 5th order and the wave breaker index = 0.8. A graded sand with 30 size fractions is modelled.

8.4.4 Conditions modelled

The conditions modelled are the same 163 binned wave/wind conditions used for the two-dimensional sediment transport simulations (Section 8.3.2). For each condition the two-dimensional model provides the waves and currents throughout the model domain. The wave and current parameters for each condition are extracted at the proposed intake position in 30 m water depth (as shown in Figure 7.13) for use in the suspended sediment model.

The measured sediment grain sizes are presented in Table 8.1 and Figure 8.1. The four sampling positions in the vicinity of the proposed intake have D_{50} in the range 0.181 to 0.188 mm. A D_{50} of 0.18 mm with the average measured sediment grading of 1.5 has thus been modelled.

8.4.5 Results

An example of the vertical profile of suspended sand concentration modelled for one input wave/current condition is shown in Figure 8.12. It is seen that the sand concentration increases logarithmically near the seabed.

The proposed intake opening is positioned 3 to 5 m above the seabed (Eskom, 2008c), while the intake flow rate for the Plant Parameter Envelope of 10 000 MWe is 460 m³/s (Section 7.3.4). For a particular

wave/current condition, a preliminary estimate of the volume of sand drawn into the intake can be calculated as the suspended sand concentration at the vertical position of the intake opening multiplied by the intake flow rate. It is assumed that the intake structure itself does not influence the suspended sand profile and that the seabed is covered in sand, i.e. no rocks. The extent to which this assumption is true will depend on the detailed design of the intake structure: the intake geometry, the number of intake openings, the intake velocities, the extent of scour protection around the structure, etc. Since these details are not yet available, the results below should be viewed as preliminary.

The sand volume drawn into the intake is calculated for each of the 163 wave/current conditions. The annual sand volume is then calculated by adding the volumes for each condition, taking into account the percentage occurrence of each condition. The final volume is then adjusted from solid volume to bulk volume assuming a sediment porosity of 0.4. In addition to the annual average sand volume, the maximum sand concentration and the maximum short-term sand volume are obtained from the 163 conditions. Results are presented for the proposed intake levels of 3 and 5 m above the seabed, as well as 1 m above seabed to account for the drawing in of sand from below the level of the intake, or for sand build-up around the intake.

TABLE 8.2: PRELIMINARY ESTIMATE OF SAND VOLUME DRAWN INTO COOLING WATER INTAKE IN 30 M DEPTH

	Annual sand volume [m³/year]	Short-term maximum sand volume [m³/day]	Maximum sand concentration [mg/L = ppm by mass]
Intake 1 m above seabed	8 000	950	40
Intake 3 m above seabed	2 900	250	10
Intake 5 m above seabed	2 000	190	8

Note that the model only simulates non-cohesive sediments with grain sizes greater than 0.063 mm, i.e. sand particles. Finer mud and clay particles that may be present in the water column as a background concentration are not modelled. Assuming an average background concentration of 3 mg/L (Section 8.4.2) and a porosity of 0.4, the annual cohesive sediment volume drawn into the cooling water intake would be 27 400 m³/year. This is significantly higher than the sand volumes given in Table 8.2. Whether these cohesive particles will have time to settle in the settling basin, or pass through the heat exchangers and be discharged back to sea, will depend on the design of the settling basin.

The volumes predicted above are significantly lower than the average maintenance dredging at the present Koeberg intake basin of approximately 132 000 m³/year (PRDW, 2002).

8.4.6 Conclusions

The preliminary modelling presented above indicates that only limited volumes of sand are likely to be drawn into the proposed cooling water intake, which is a tunnel intake located in 30 m water depth with the intake openings located 3 to 5 m above the seabed.

9. CONCLUSIONS AND RECOMMENDATIONS

Numerical models and data analysis frameworks have been set up to characterise the following parameters at the Thyspunt site:

- Water levels
- Tsunami flooding
- Wave height, period and direction
- Sea temperatures
- Currents
- Thermal plume dispersion for typical intake and outfall configurations
- Sediment transport
- Suspended sediment concentrations.

The numerical models have been calibrated using measurements undertaken at the site as part of the ongoing measurement programme.

The results will be used in the Nuclear-1 EIA, the Coastal Engineering Investigations Report (PRDW, 2009a), the SSR Chapter on Oceanography and Coastal Engineering, as well as other chapters in the SSR dealing with marine ecology and risk assessment.

The oceanographic measurement programme is scheduled to run until August 2010 and it is strongly recommended that the programme continue as scheduled.

It is also recommended that engineering feasibility studies be undertaken to identify the optimum intake and outfall structures.

Additional research is required to better define the risk from local tsunamigenic sources. The Council for Geoscience report (CGS, 2008b) recommends the following approach:

- Further research including all available stratigraphic/sedimentological/geomorphological data should be undertaken to better define the risk from offshore slump generated tsunami.
- In depth research into the global frequency, locality and magnitude of meteotsunami should be undertaken to further quantify the risk. In particular, the atmospheric conditions along the west coast prior to the 1969 event should be compared with those of its 2008 counterpart.
- Because of the relatively short history of tsunami records along the South African coast, the database should be extended by conducting an investigation of palaeotsunami in the stratigraphic record. No systematic work has yet been conducted along this coast. Areas of focus should be in the vicinity of planned nuclear facilities.

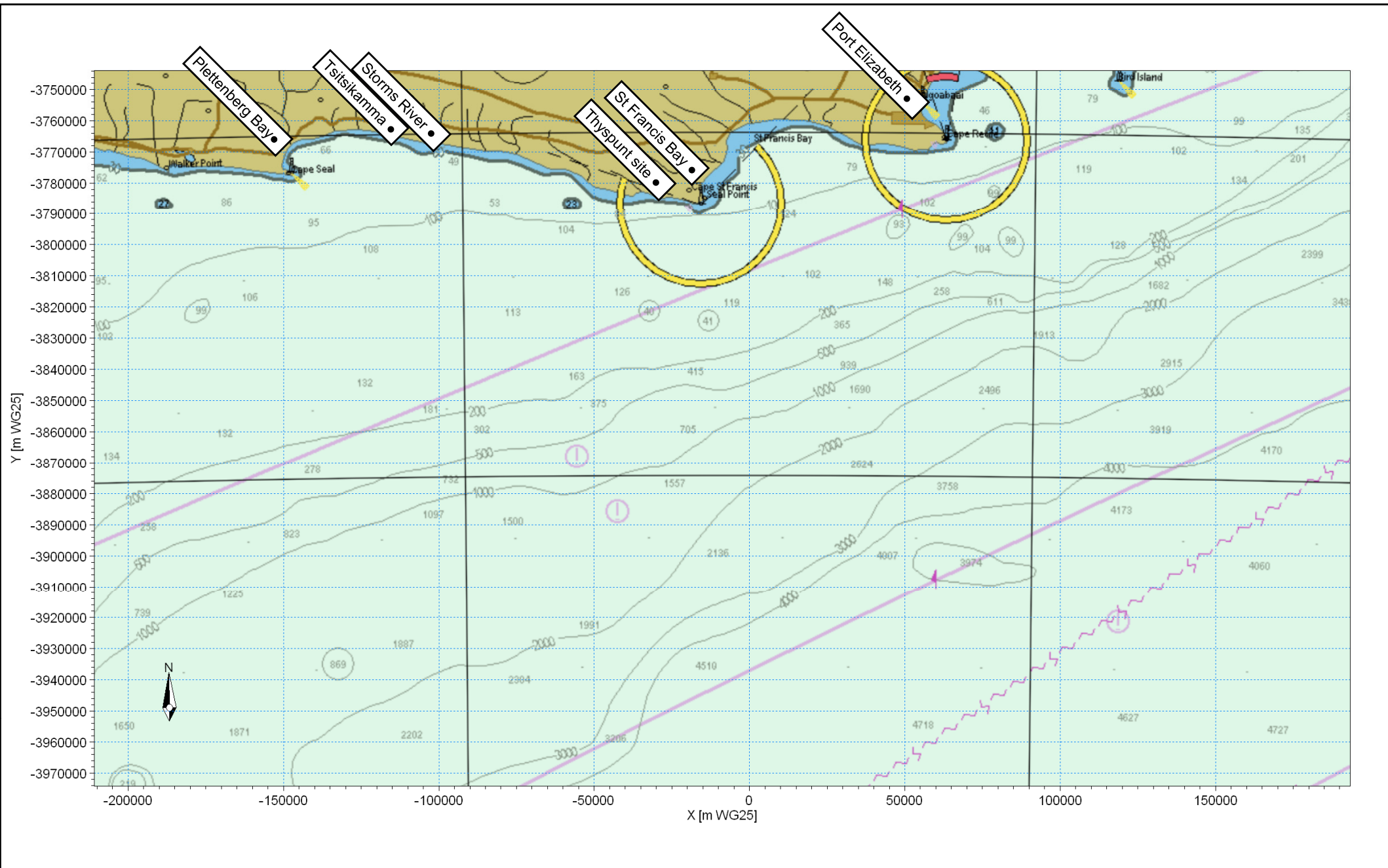
REFERENCES

1. Borrero J, Sieh K, Chlieh M and Synolakis C (2006). Tsunami Inundation Modeling for Western Sumatra, PNAS, 26 December 2006, vol. 103, no. 52.
2. CGS (2008a) A Probabilistic Tsunami Hazard Assessment for Coastal South Africa from Distant Tsunamogenic areas. By A. Kijko, V. Midzi, J. Ramperthap and M. Singh. Council for Geoscience Report No. 2008 – 0156, Revision 2.
3. CGS (2008b) Potential Sources of Tsunami Along the South African Coast. By D.L. Roberts. Council for Geoscience Report Number: 2008 - 0220 .
4. DHI (2008a) MIKE 21 SW, Spectral Waves FM Module, User Guide, Danish Hydraulics Software.
5. DHI (2008b) LITPACK, An Integrated Modelling System for Littoral Processes and Coastline Kinetics, User Guide, Danish Hydraulics Software.
6. DHI (2008c) MIKE 21 Flow Model, User Guide, Danish Hydraulics Software
7. DHI (2008d) MIKE 21/3 Coupled Model FM, User Guide, Danish Hydraulics Software.
8. DHI (2008e) MIKE 21 Flow Model FM, Sand Transport Model, User Guide, Danish Hydraulics Software.
9. DHI (2008f) EVA, Extreme Value Analysis, User Guide, Danish Hydraulics Software
10. DHI (2008g) MIKE C-MAP, Extraction of World Wide Bathymetry Data and Tidal Information, User Guide, 2008.
11. Dingle R (1977) The anatomy of a large submarine slump on a sheared continental margin (SE Africa. Journal of the Geological Society of London 134; 293-310.
12. Dingle R, Birch G, Bremner J, de Decker R, du Plessis A, Engelbrecht J, Fincham M, Fitton T, Flemming B, Gentle R, Goodlad S, Martin A, Mills E, Moir G, Parker R, Robson S, Rogers J, Salmon D, Siesser W, Simpson E, Summerhayes C, Westall C and Winter A (1987). Deep-sea sedimentary environments around southern Africa, South-East Atlantic and South-West Indian Oceans. Annals of the South African Museum 98, 1–27.
13. Eskom (2006) Koeberg Site Safety Report, Chapter 8, Oceanography and Cooling Supply, Rev 3.
14. Eskom (2008a) Plant Parameter Envelope for 10 000 MWe for NSIP Site Safety Reports, Document provided by Israel Sekoko, Eskom, on 1 September 2008.
15. Eskom (2008b) Nuclear-1 consistent EIA data set (Rev. 2). Document (Excel spreadsheet) provided by Andre Nel, Eskom, on 2 October 2008.
16. Eskom (2008c) Cooling Water Intake and Outfall Works for the Eskom Nuclear-1 Sites, Conceptual Arrangements, Nuclear Programmes Department Nuclear-1, Document No. 300-9, September 2008.
17. Grilli S and Watts P (2005) Tsunami Generation by Submarine Mass Failure, 1: Modelling, Experimental Validation and Sensitivity Analysis, Journal of Waterway, Port, Coastal and Ocean Engineering, November/December 2005.

18. Grilli S, Ioualalen M, Asavanant J, Shi F, Kirby J and Watts P (2007). Source constraints and model simulation of the December 26, 2005, Indian Ocean tsunami, *Journal of Waterway, Port, Coastal, and Ocean Engineering*, Vol. 133, No. 6, November, 2007.
19. Hartnady C and Okal E (2007). Mentawai tsunami effect at Port Elizabeth, South Africa on 12-14 September 2007, *South Afr. J. Sci.*, submitted, 2007.
20. IAEA (2003) Flood Hazard for Nuclear Power Plants on Coastal and River Sites, Safety Guide No. NS-G-3.5, International Atomic Energy Agency.
21. Lwandle (2008a) Data Report, Thyspunt Site – Deployment 1, Prepared for Retief Dresner Wijnberg (Pty) Ltd, Prepared by Lwandle Technologies (Pty) Ltd, Job No. LT-JOB-50, 24 June 2008.
22. Lwandle (2008b) Data Report, Thyspunt Site – Deployment 2, Prepared for Retief Dresner Wijnberg (Pty) Ltd, Prepared by Lwandle Technologies (Pty) Ltd, Job No. LT-JOB-50, 16 July 2008.
23. Lwandle (2008c) Data Report, Thyspunt Site – Deployment 3, Prepared for Retief Dresner Wijnberg (Pty) Ltd, Prepared by Lwandle Technologies (Pty) Ltd, Job No. LT-JOB-50, 19 September 2008.
24. Lwandle (2008d) Data Report, Thyspunt Site – Turbidity Data, Prepared for Retief Dresner Wijnberg (Pty) Ltd, Prepared by Lwandle Technologies (Pty) Ltd, Job No. LT-JOB-50, 3 October 2008.
25. Okada Y (1985) Surface deformation to shear and tensile faults in a half-space, *Bull. Seism. Soc. Am.*, 75, [4], 1135-1154.
26. PRDW (2002) Eskom, Koeberg Nuclear Power Station, Cooling Water Intake Basin, Dredging Strategy, Updated Strategy – May 2002, PRDW Report 201/2/01, May 2002.
27. PRDW (2008a) Eskom, Nuclear1 EIA: Modelling of Construction Stage Brine Discharge, Report No. 1010/5/001, October 2008.
28. PRDW (2009a) Eskom Site Safety Reports, Coastal Engineering Investigations Report, Thyspunt, Prestedge Retief Dresner Wijnberg (Pty) Ltd, Report 1010/2/102 Rev 04.
29. PRDW (2009b) Eskom Site Safety Reports, Numerical Modelling of Coastal Processes, Duynefontein, Prestedge Retief Dresner Wijnberg (Pty) Ltd, Report 1010/4/101 Rev 04.
30. Rabinovich A and Thomson R (2007). The 26 December 2004 Sumatra Tsunami: Analysis of Tide Gauge Data from the World Ocean Part 1. Indian Ocean and South Africa, *Pure and Applied Geophysics*, 164 (2007), 261–308.
31. South African Tide Tables (2008) SAN HO-2, Published by the Hydrographer, South African Navy, ISBN 0-9584817-3-3.

32. Watts P, Grilli S, Kirby J, Fryer G and Tappin D (2003). Landslide Tsunami Case Studies Using a Boussinesq Model and a Fully Nonlinear Tsunami Generation Model, Natural Hazards and Earth System Sciences, Vol. 3, 2003, pp. 391-402.

FIGURES

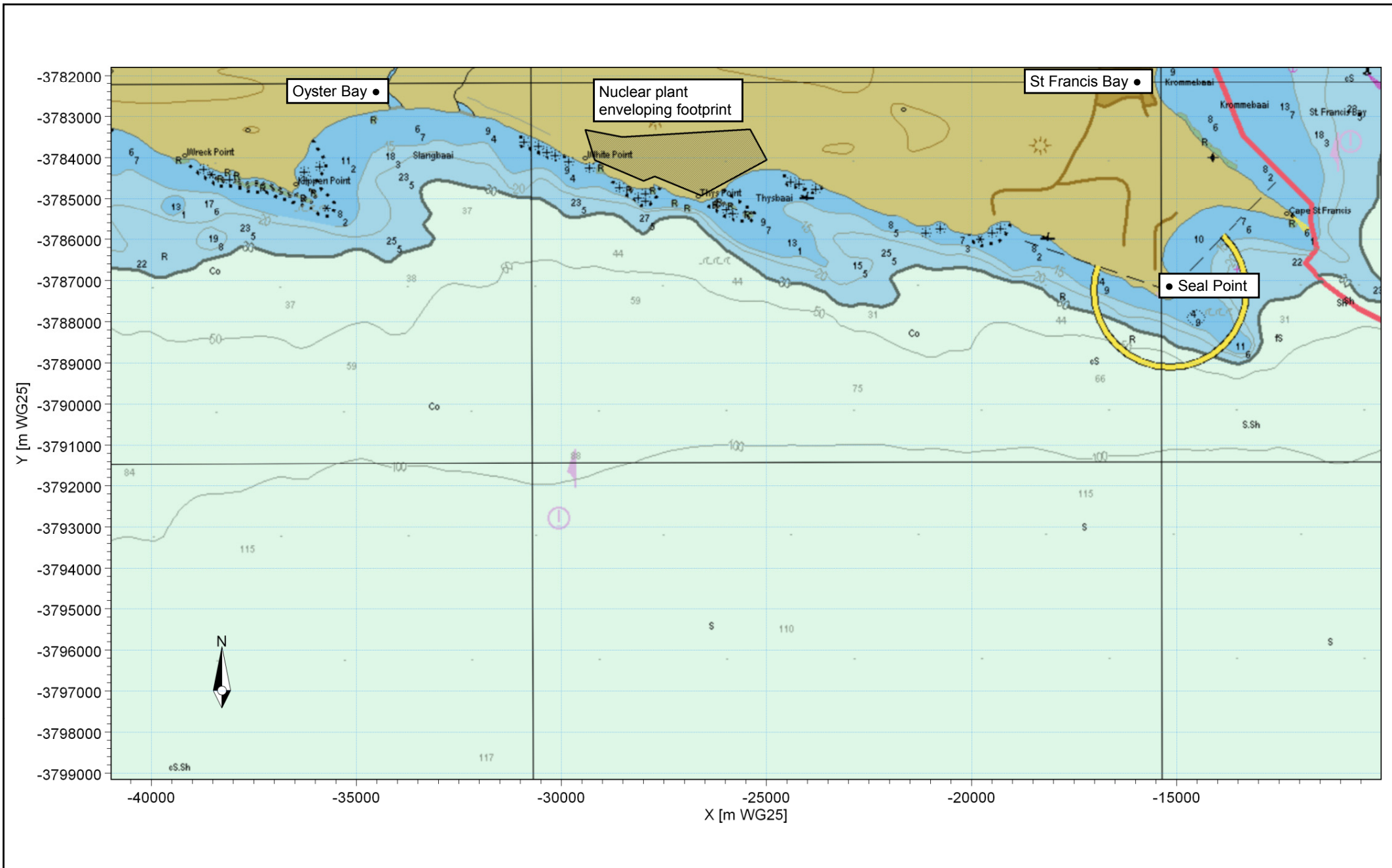


Title:

Locality map for Thyspunt site.

Figure No.

1.1

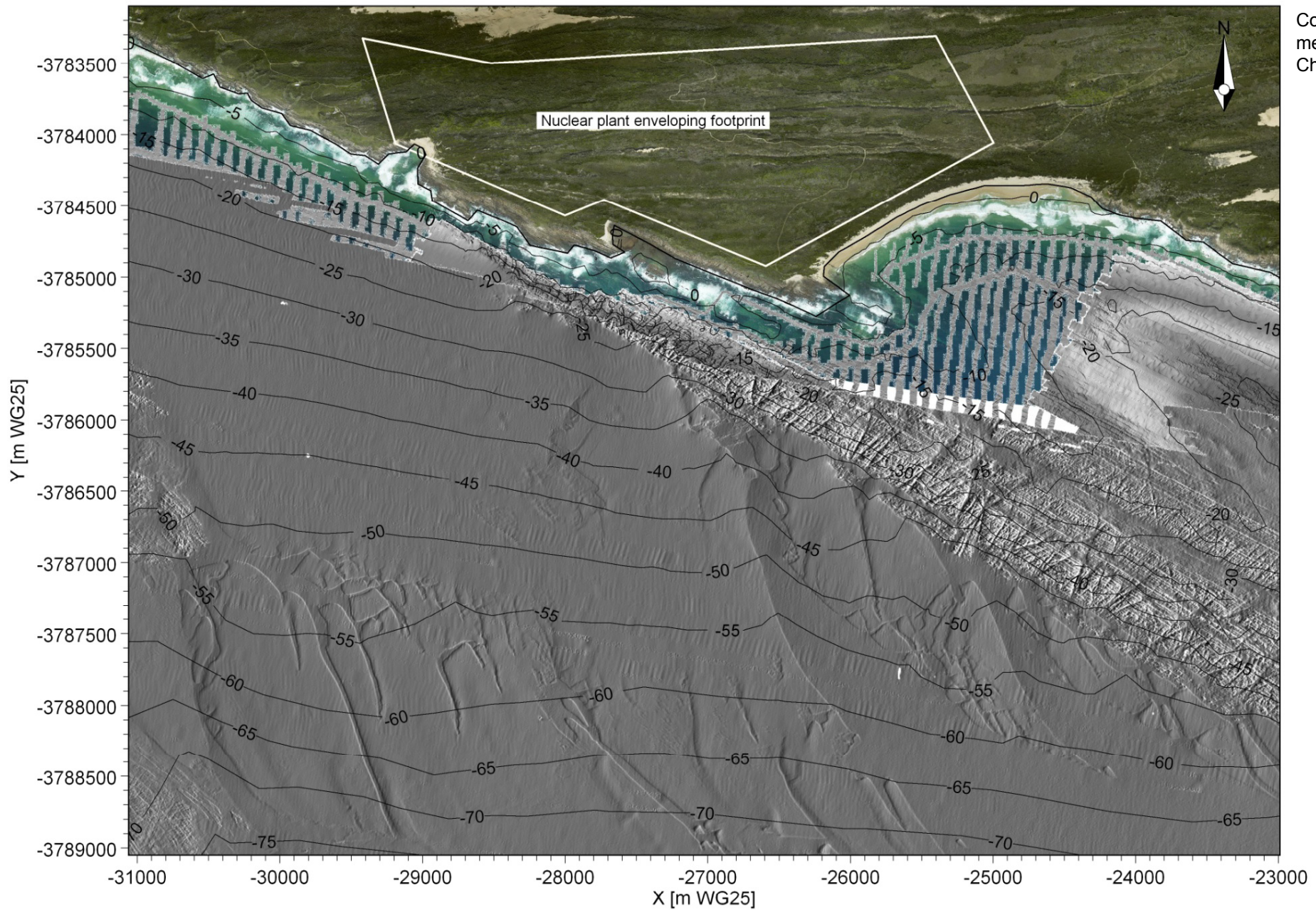


Title:

Detailed locality map for Thyspunt site.

Figure No.

1.2



Contours are in meters below Chart Datum

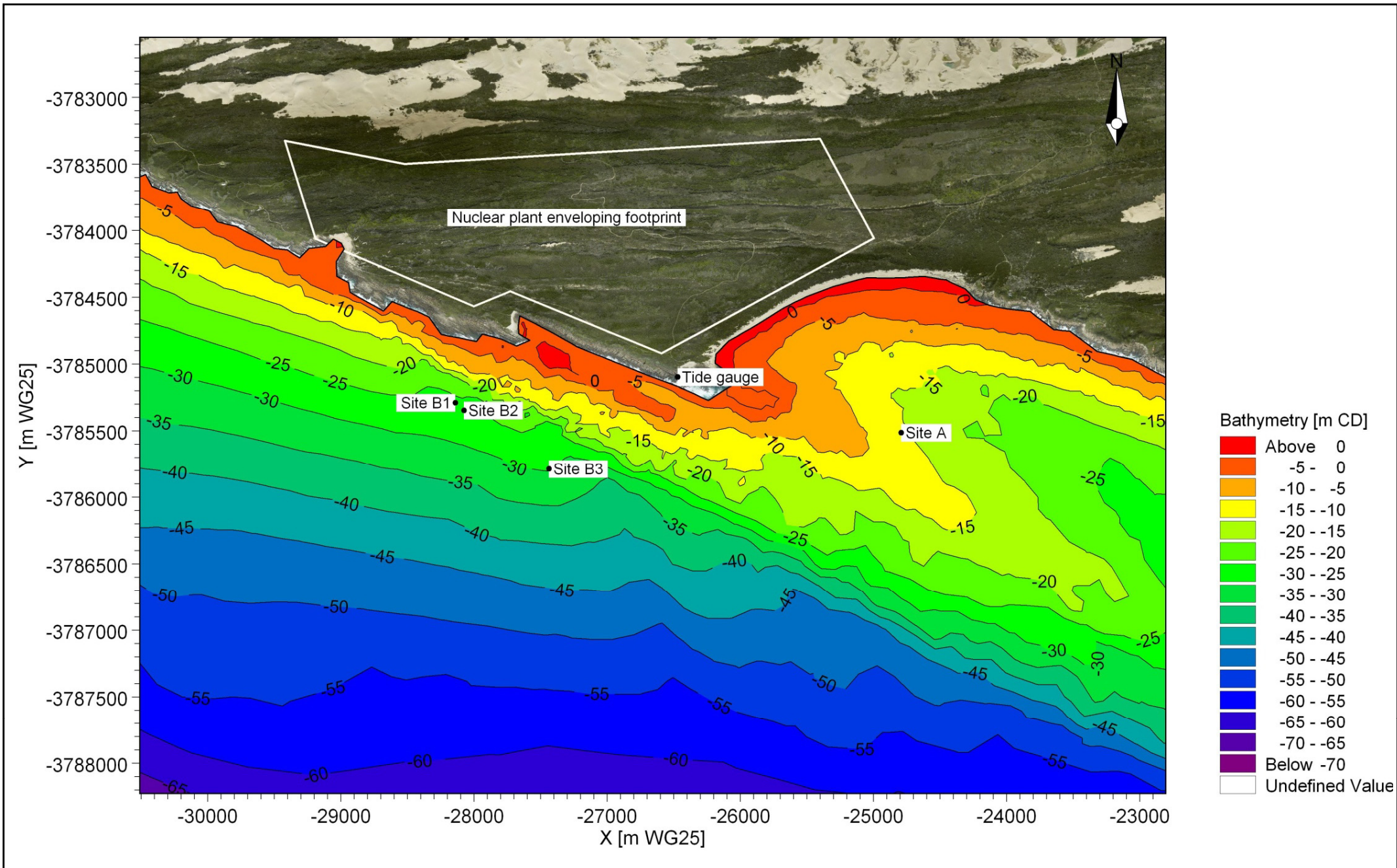


Title:

Multi-beam bathymetry showing location of the reef at Thyspunt.

Figure No.

1.3

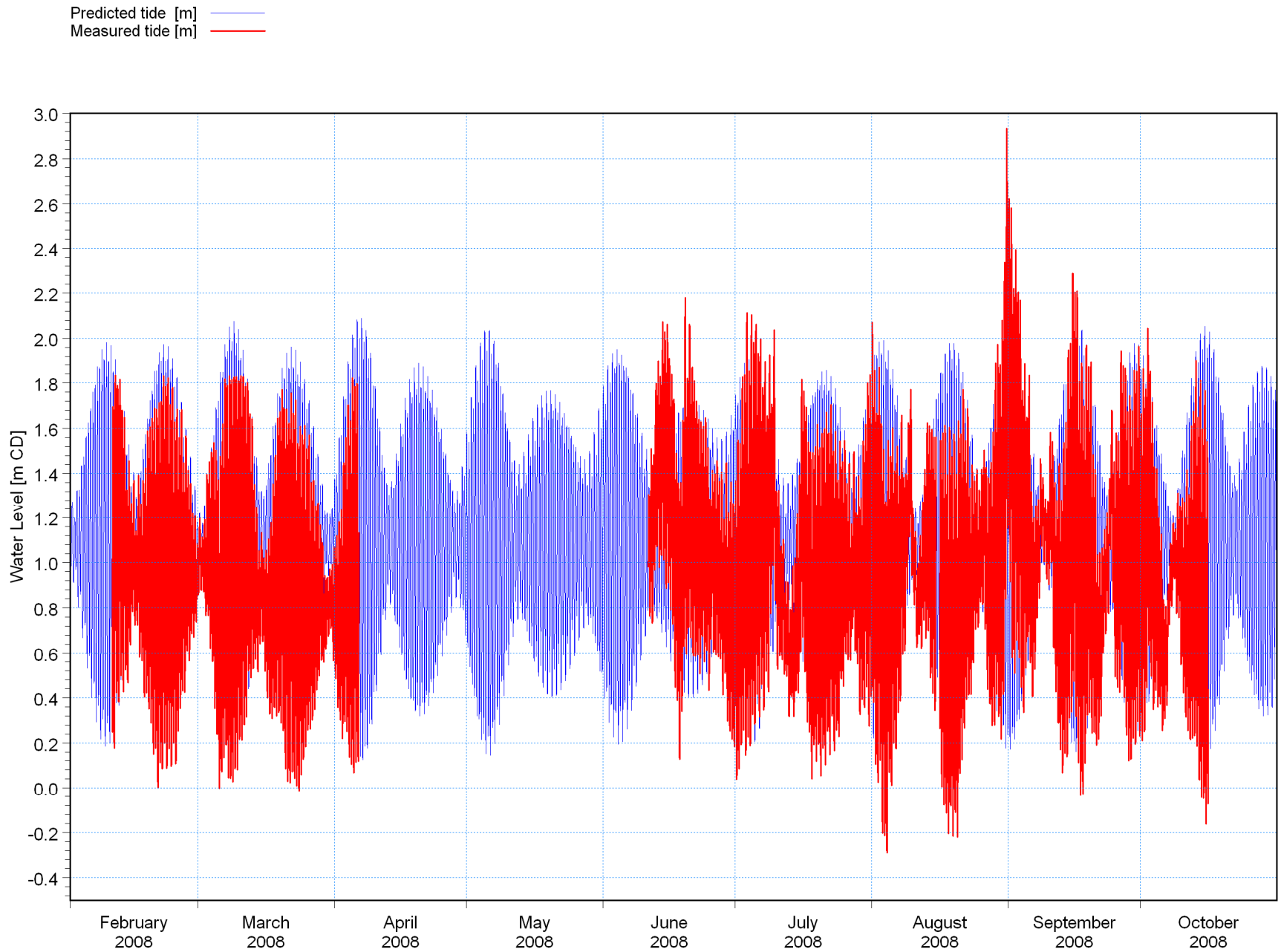


Title:

Location of instruments deployed at Thyspunt.

Figure No.

3.1



G:\Projects\1010_Nuclear\Sites\Thyspunt\Data\Tide_CMap_PortElizabeth_2008.dfs0
 G:\Projects\1010_Nuclear\Sites\Thyspunt\Data\Lwandle\PO1\Processed\Thyspunt_C_T_PO1.dfs0
 G:\Projects\1010_Nuclear\Sites\Thyspunt\Data\Lwandle\PO3\Processed\Thyspunt_C_T_1050_PO3_Cleaned.dfs0
 G:\Projects\1010_Nuclear\Sites\Thyspunt\Data\Lwandle\PO4\Processed\Thyspunt_C_T_2050_PO3.dfs0
 G:\Projects\1010_Nuclear\Sites\Thyspunt\Data\Lwandle\PO4\Processed\Thyspunt_C_T_PO4.dfs0

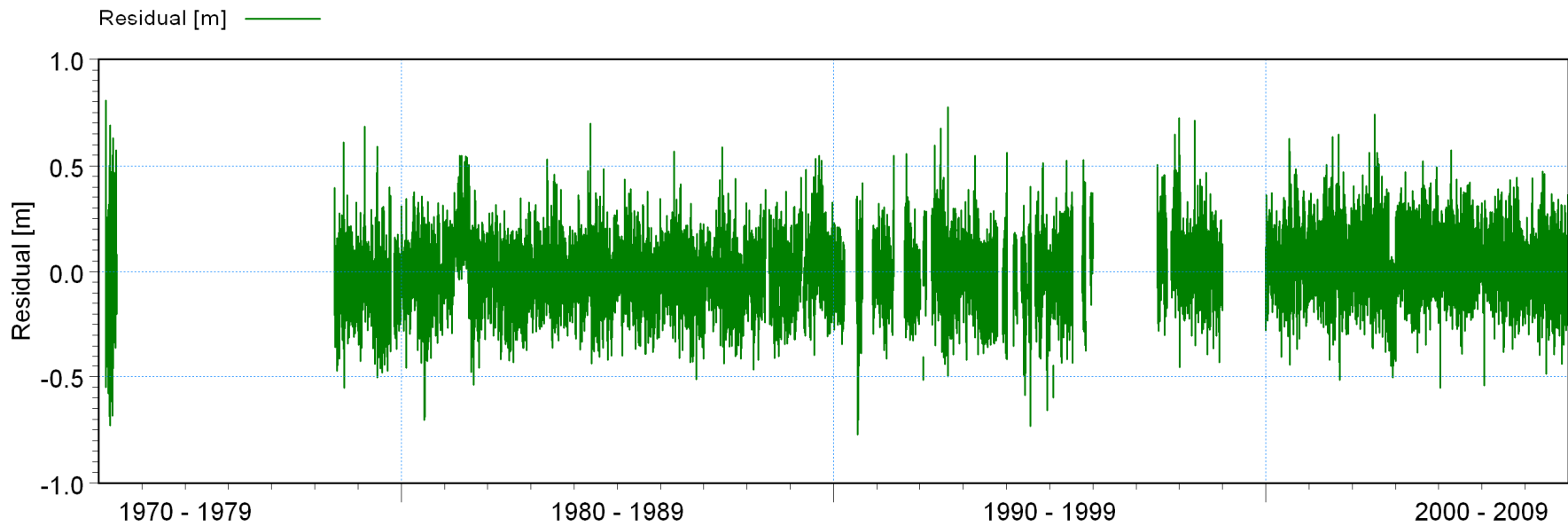
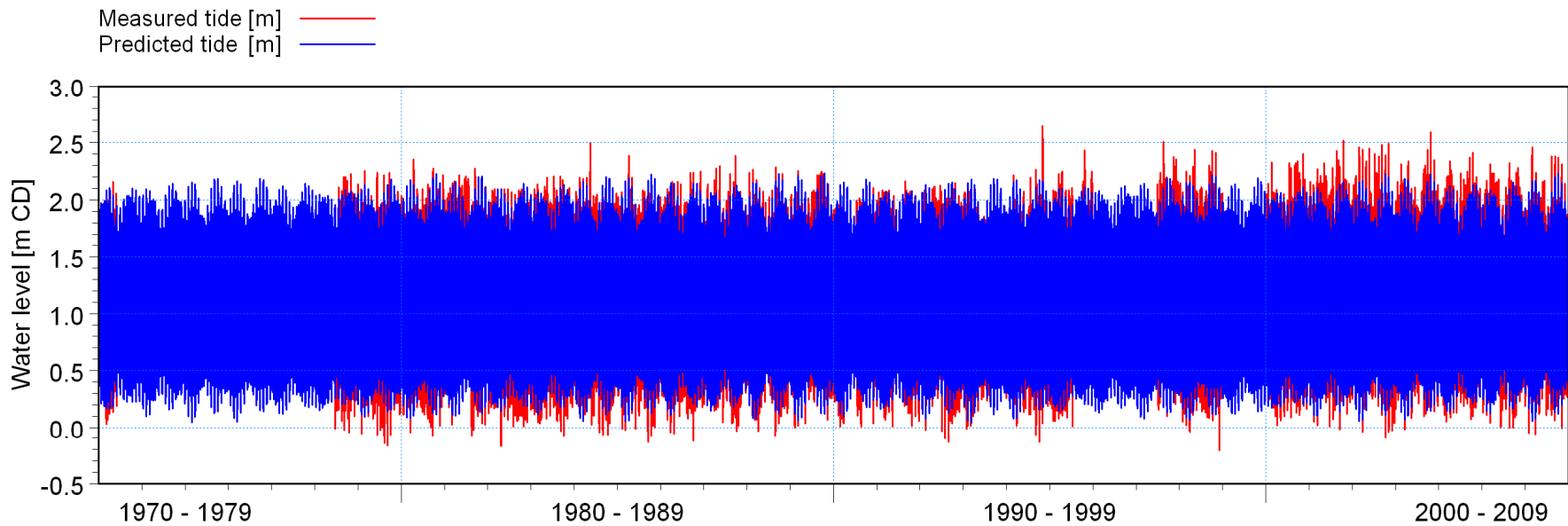


Title:

Water levels measured at Thyspunt (refer to Figure 3.1 for instrument position).

Figure No.

3.2



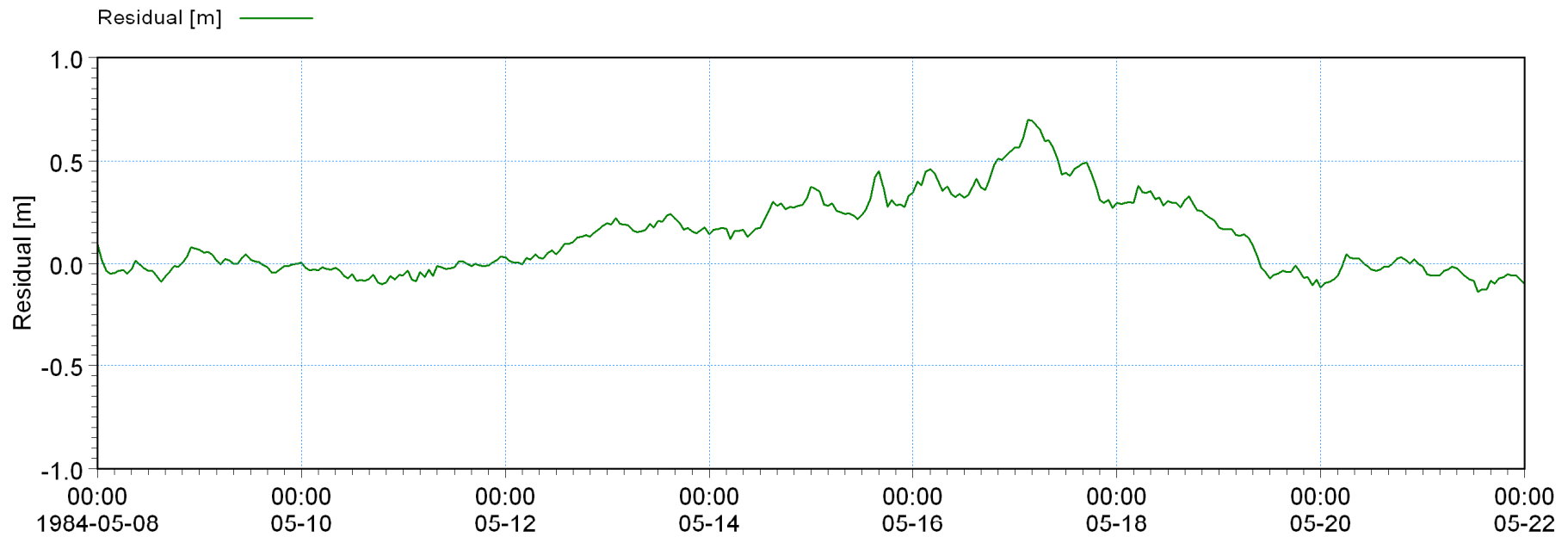
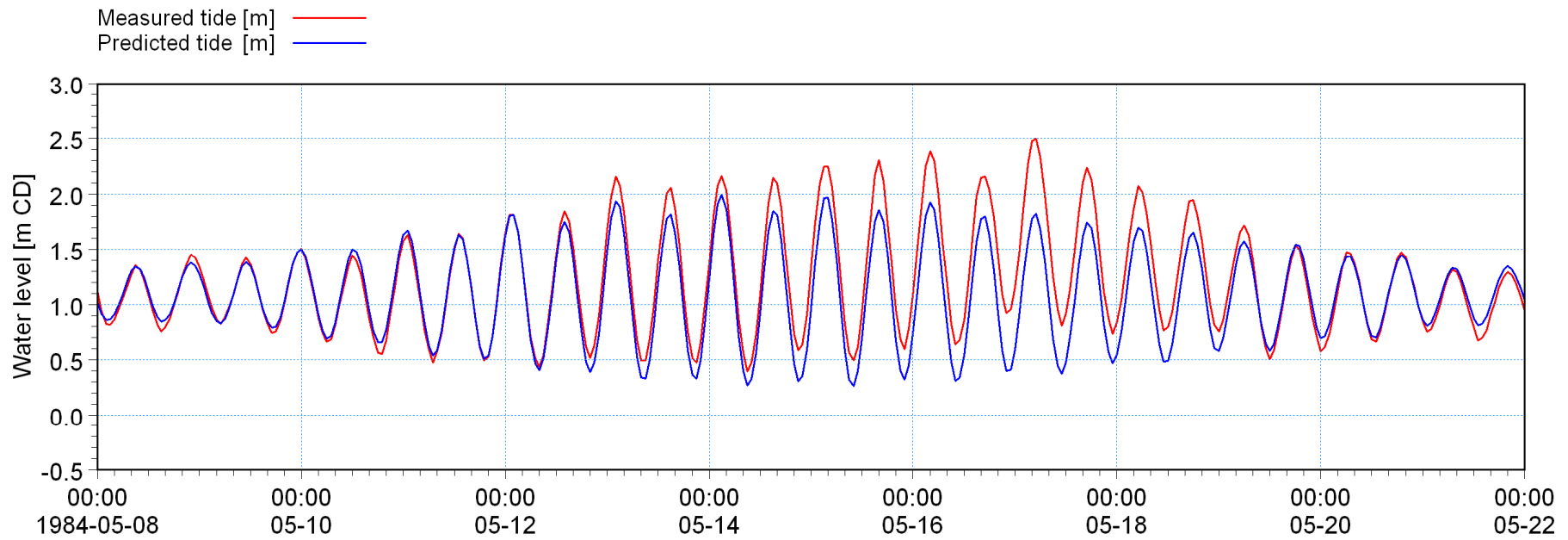
\\Data\Water\Levels\Processed\Tide_Residual_PortElizabeth_Cleaned.dfs0

\\Data\Water\Levels\Processed\Tide_Residual_PortElizabeth_Cleaned.dfs0



Title: Analysis of water level residuals: Measured tide, predicted tide and residual at Port Elizabeth. Full 34 year dataset.

Figure No.
3.3



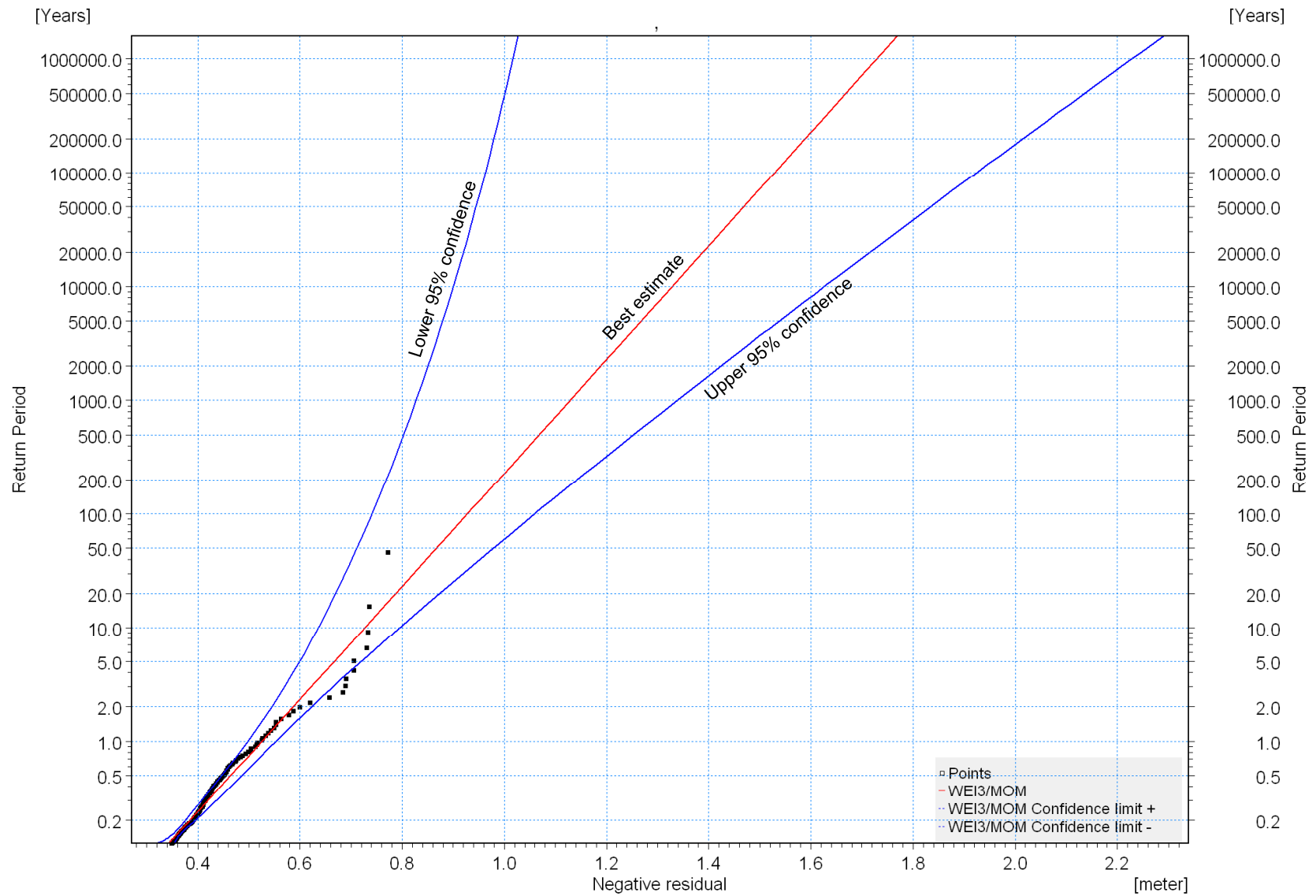
\\Data\WaterLevels\Processed\Tide_Residual_PortElizabeth_Cleaned.dfs0

\\Data\WaterLevels\Processed\Tide_Residual_PortElizabeth_Cleaned.dfs0



Title: Analysis of water level residuals: Measured tide, predicted tide and residual at Port Elizabeth. Fourteen days including the May 1984 storm event.

Figure No.
3.4

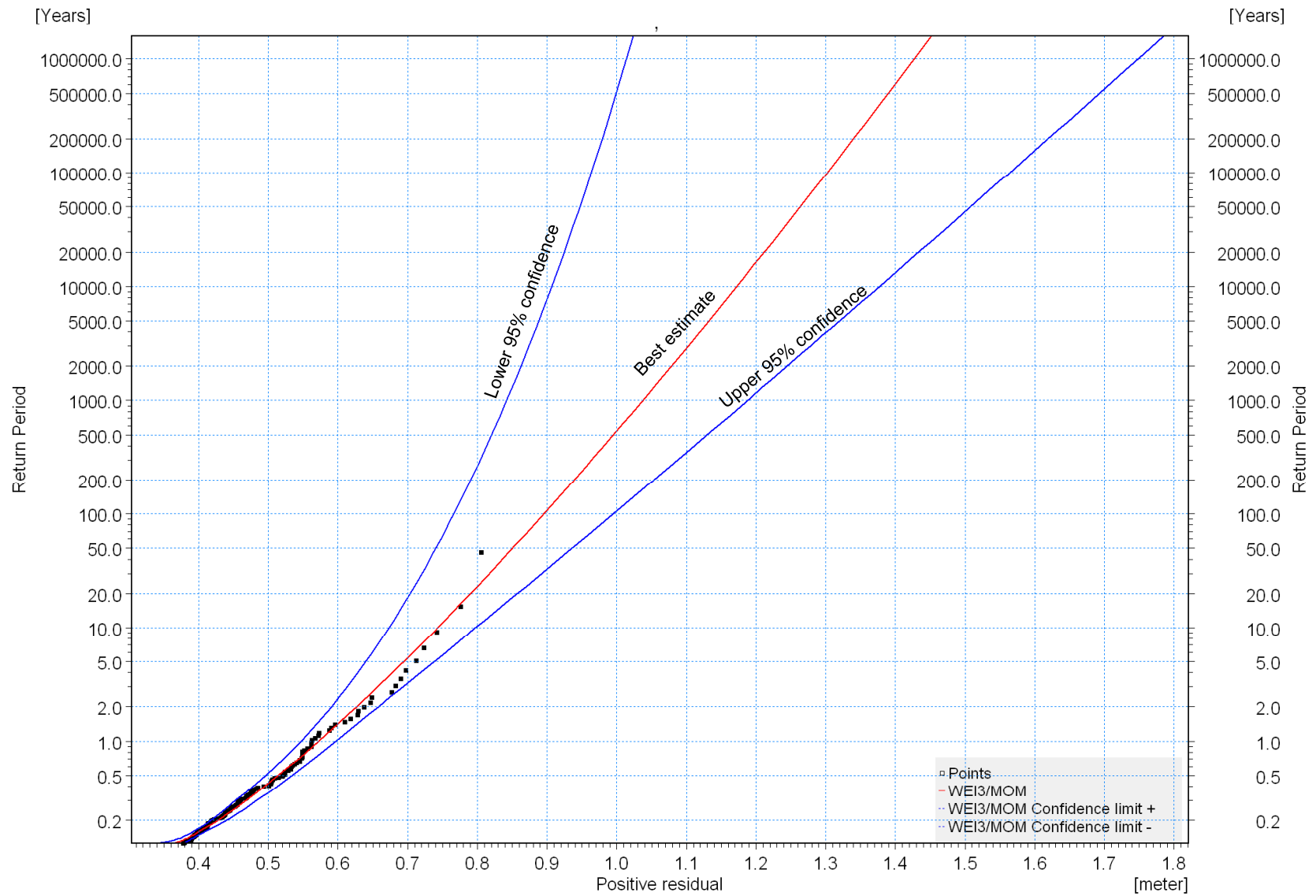


Title:

Extreme value analysis of negative tidal residuals at Port Elizabeth.

Figure No.

3.5

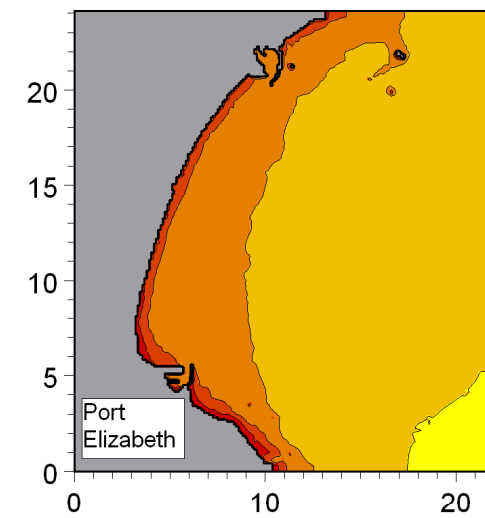
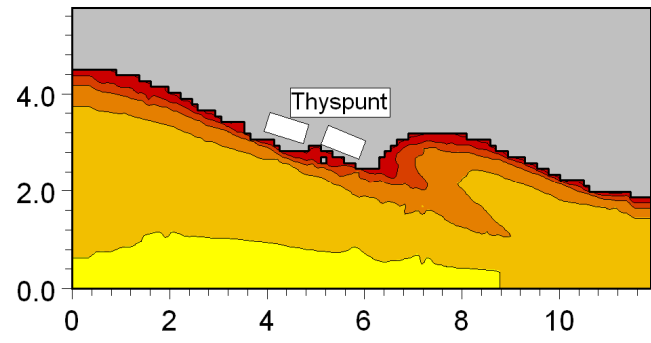
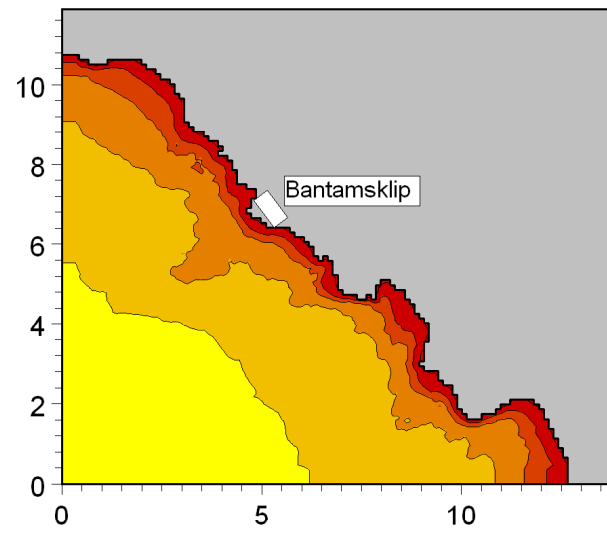
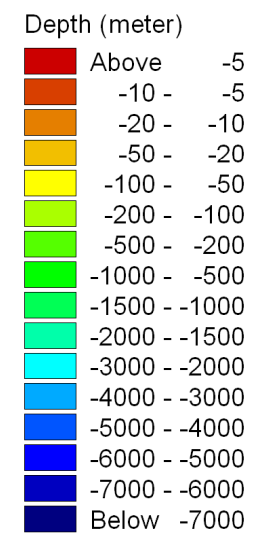
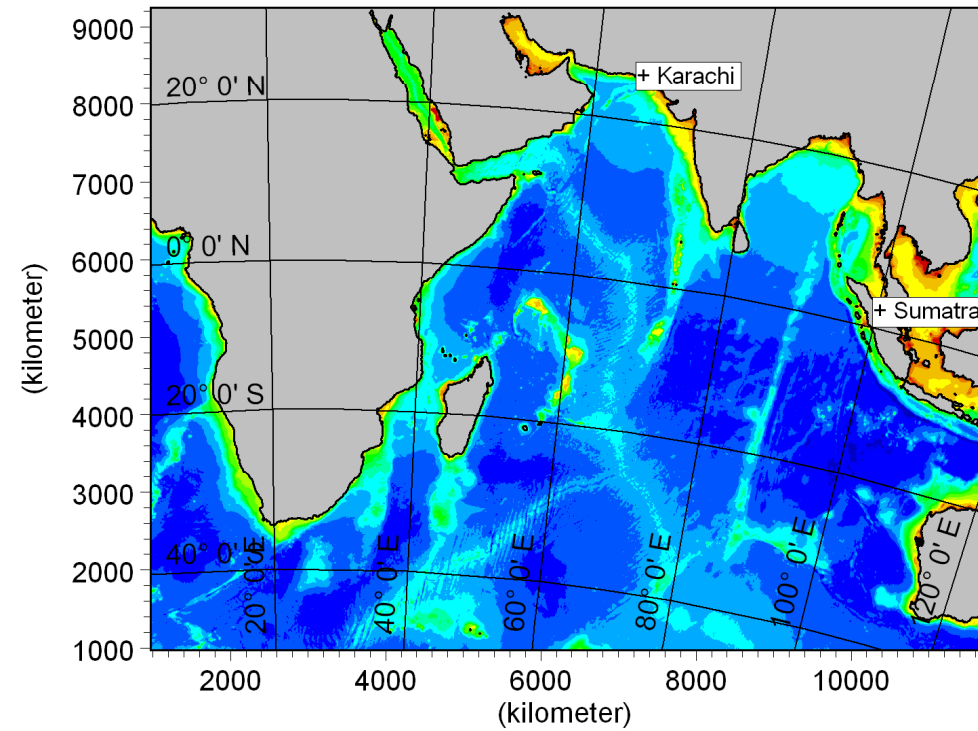
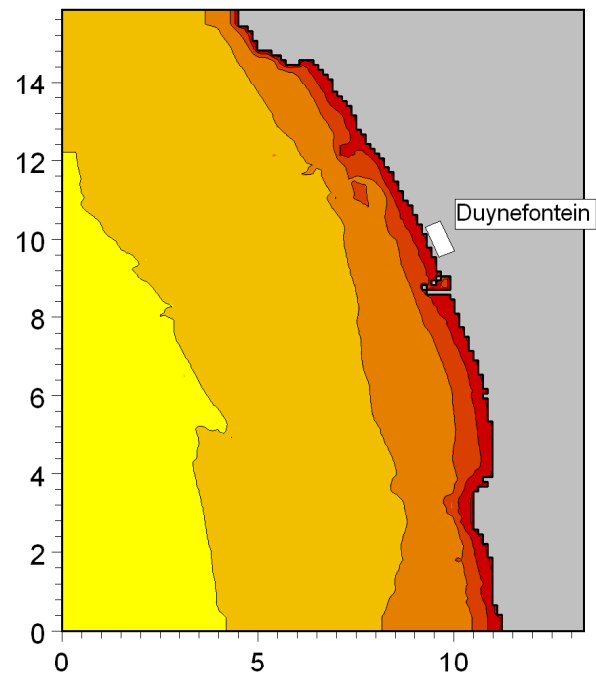


Title:

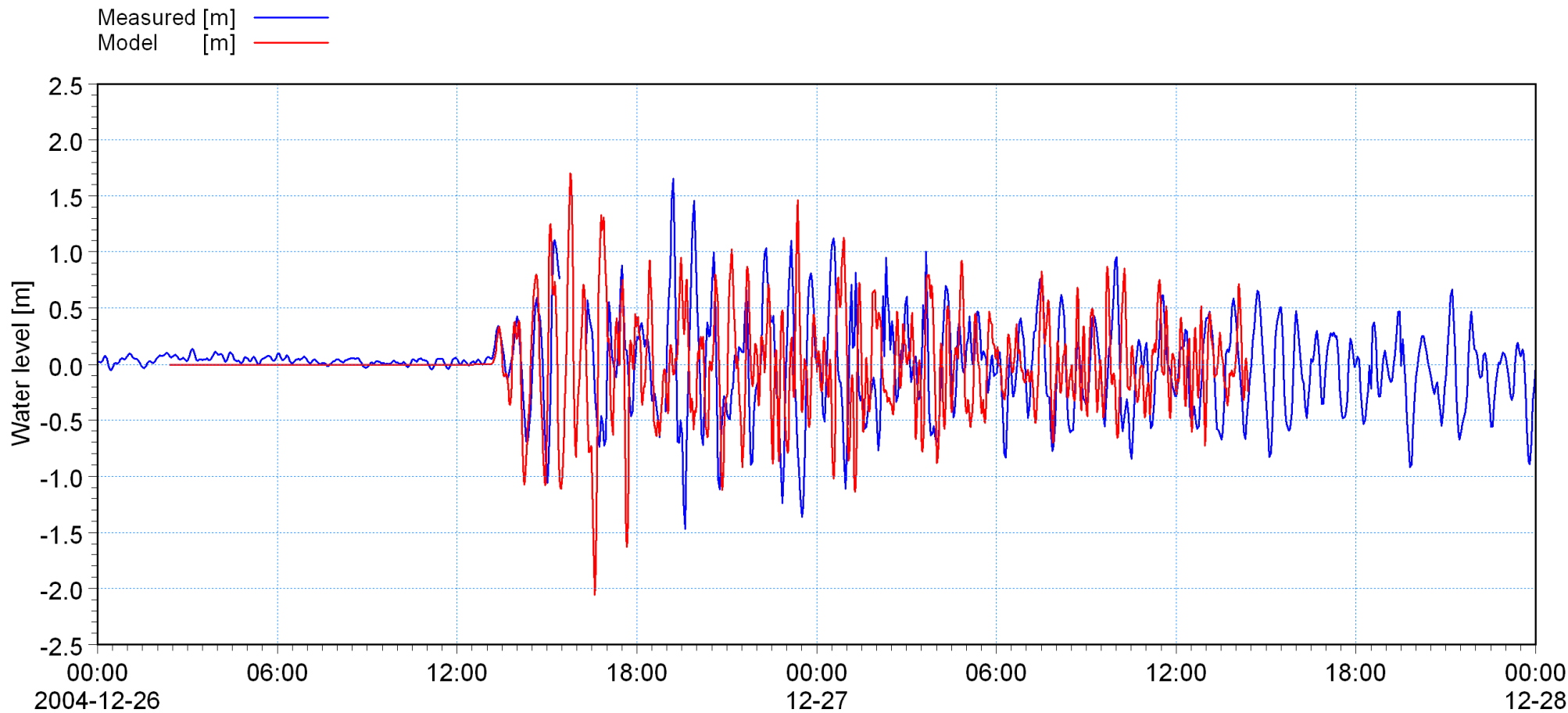
Extreme value analysis of positive tidal residuals at Port Elizabeth.

Figure No.

3.6



Title: **Model bathymetry used for tsunami modelling of Sumatra and Karachi earthquake events.**

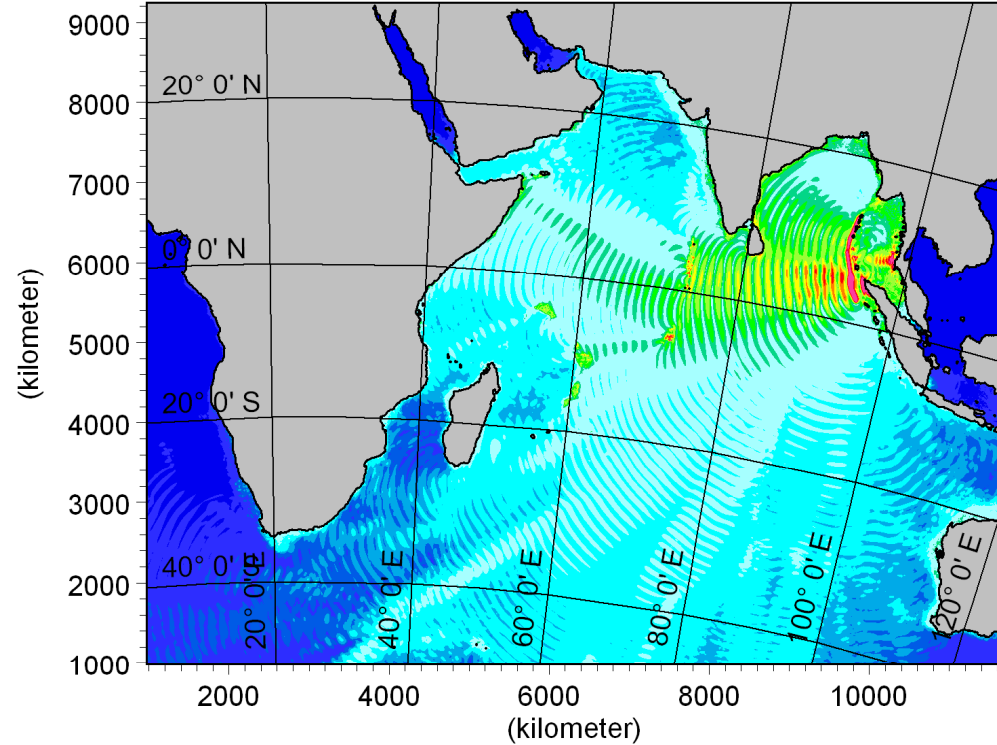
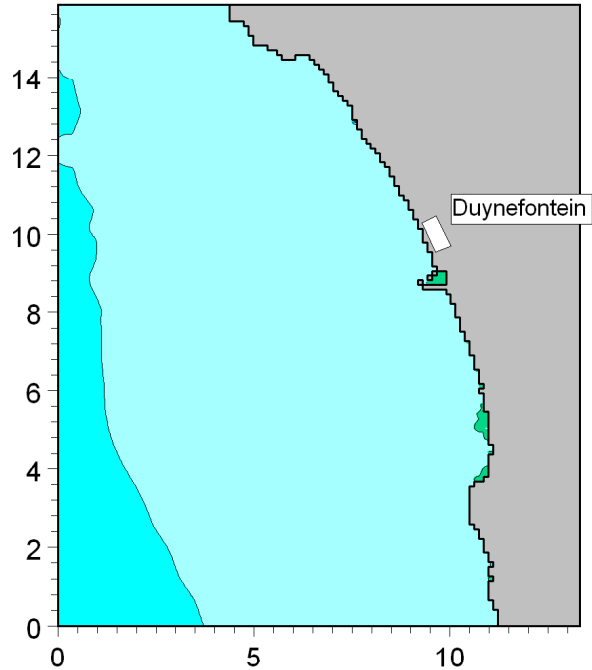


acts\1010_Nuclear\Sites\General\Tsunami\Data\WaterLevels\Measured_Tsunami_PE_2004.dfs0
 \sumami\Models\Runs\Sumatra04_MSL_a_PE.m21 - Result Files\PE_Mid_Forward85mins.dfs0

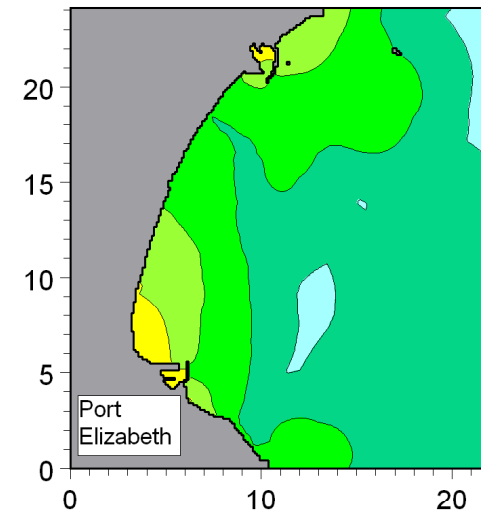
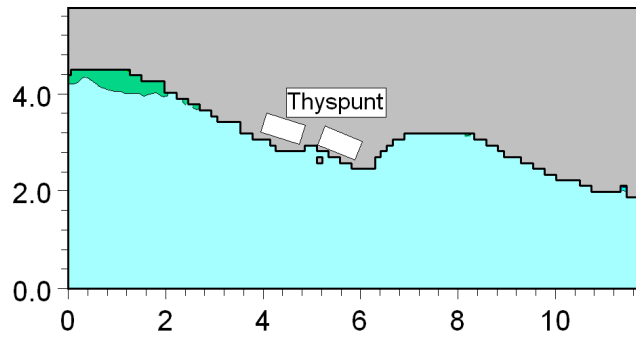
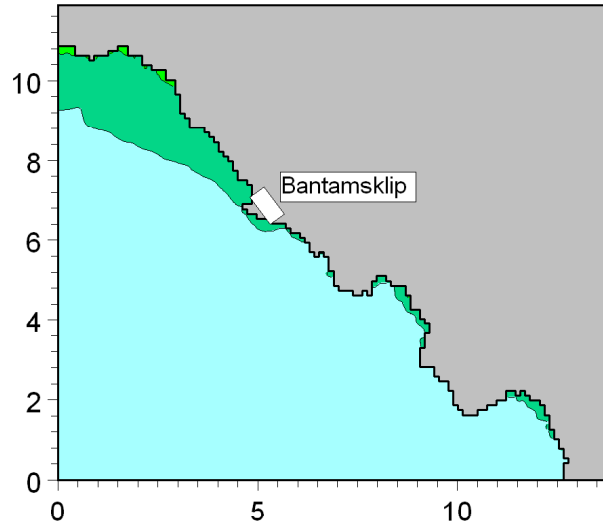
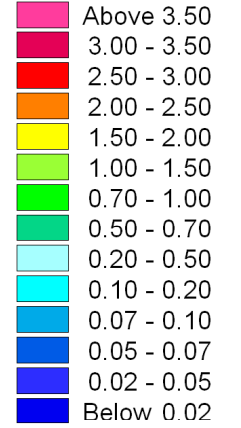


Title: Calibration of tsunami model: Measured and modelled water levels in the port of Port Elizabeth for the 26 December 2004 Sumatra tsunami event.

Figure No.
4.2



Maximum surface elevation (meter)



These are the maximum tsunami-induced water levels above Still Water Level. The total water level will additionally include the effect of tide, wave run-up, wave set-up and storm surge.

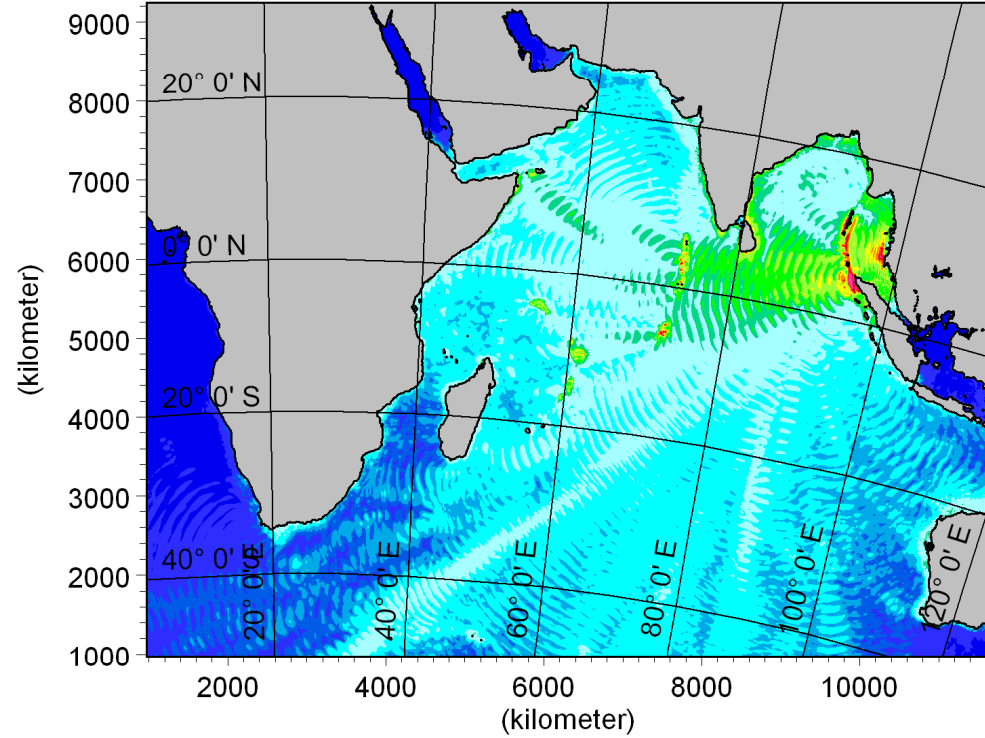
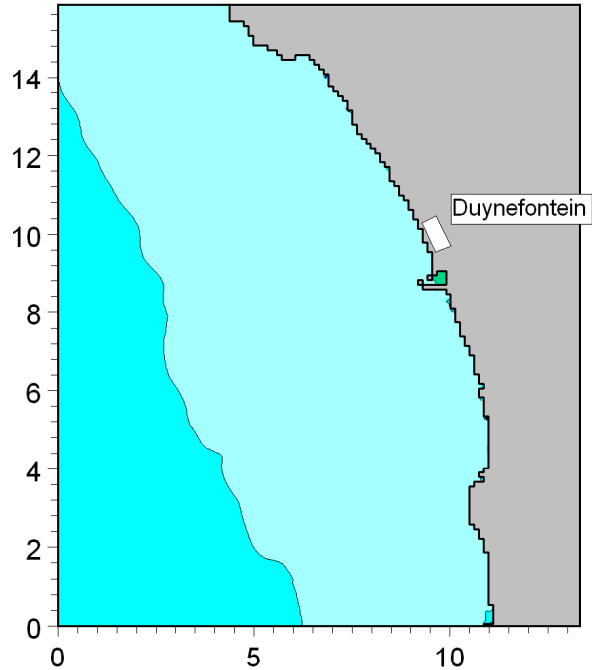


Title:

Maximum water levels predicted during tsunami event.
Source is Sumatra A: 26 December 2004 earthquake, Mw = 9.2.

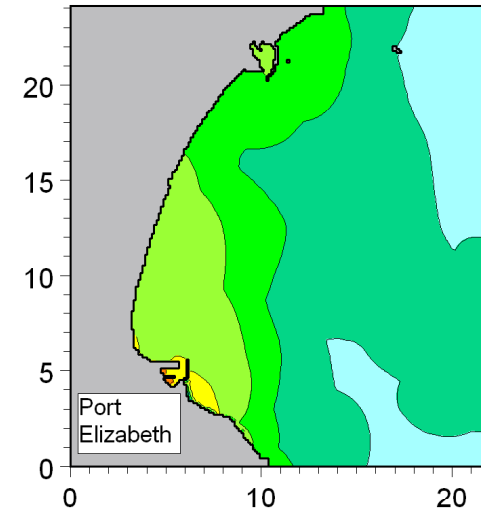
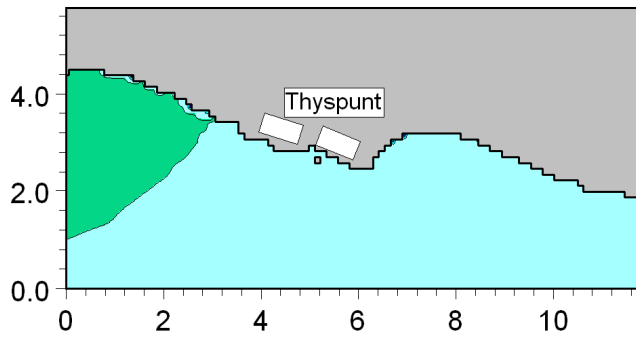
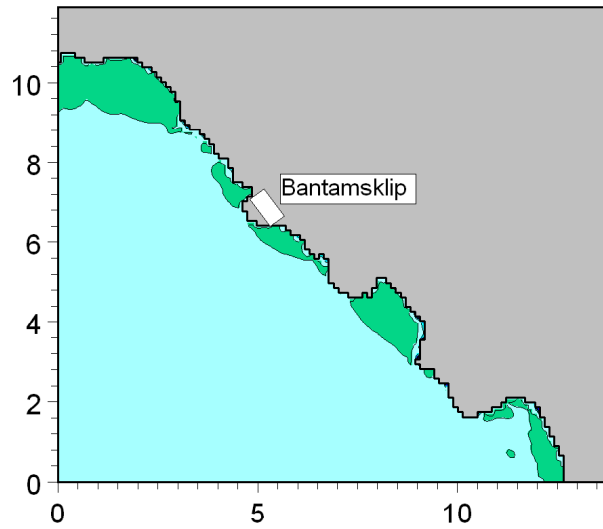
Figure No.

4.3



Minimum surface elevation (meter)

- Above -0.02
- 0.05 - -0.02
- 0.07 - -0.05
- 0.10 - -0.07
- 0.20 - -0.10
- 0.50 - -0.20
- 0.70 - -0.50
- 1.00 - -0.70
- 1.50 - -1.00
- 2.00 - -1.50
- 2.50 - -2.00
- 3.00 - -2.50
- 3.50 - -3.00
- Below -3.50



These are the minimum tsunami-induced water levels below Still Water Level. The total water level will additionally include the effect of tide and storm surge.

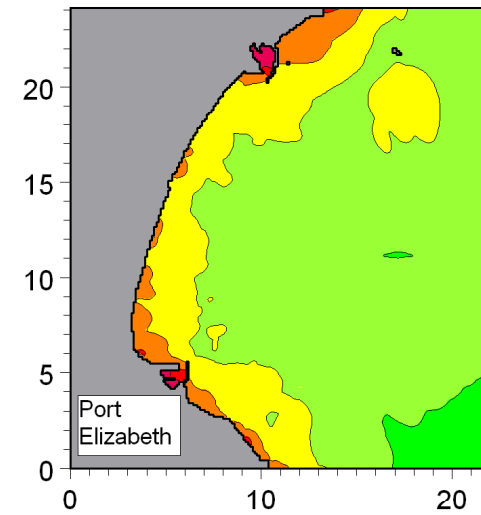
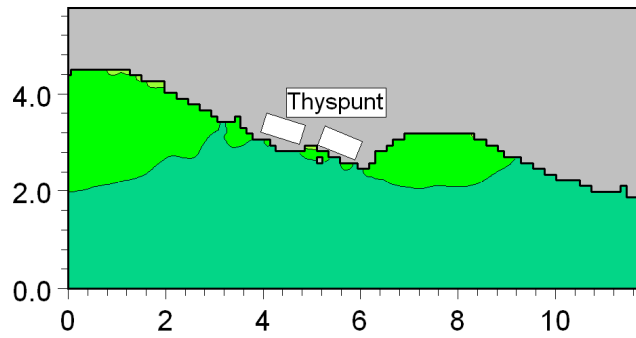
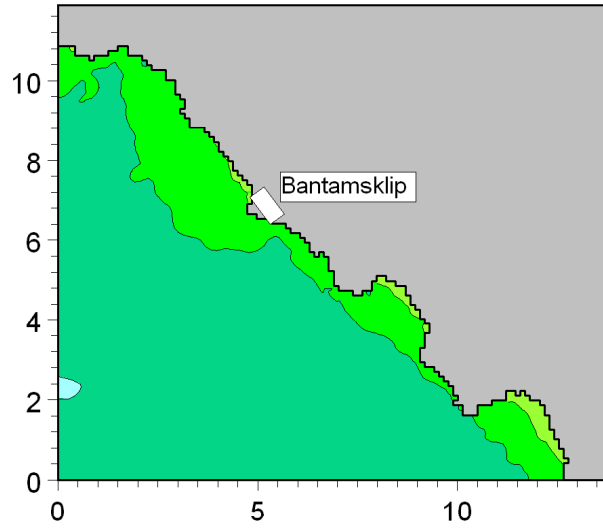
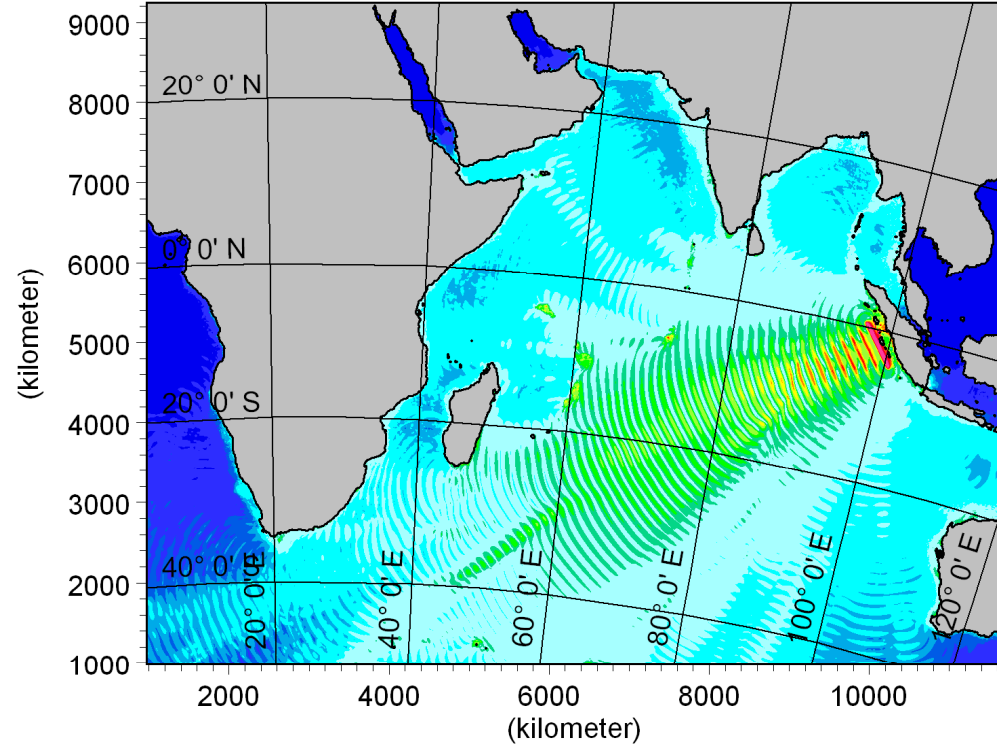
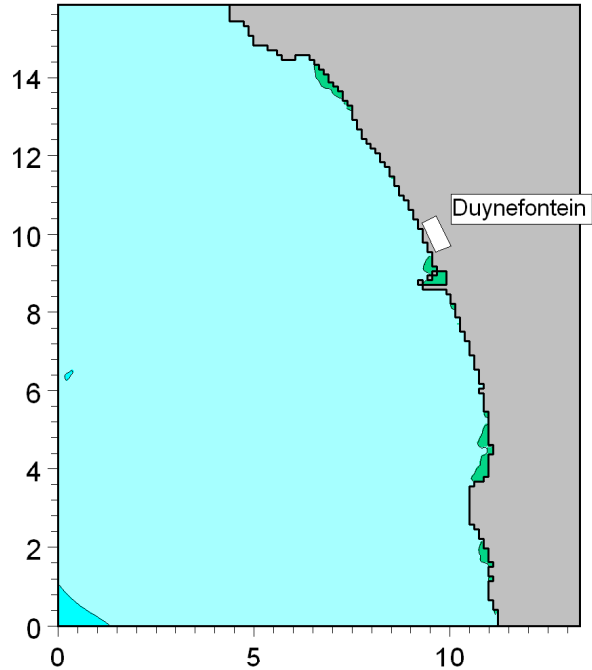


Title:

**Minimum water levels predicted during tsunami event.
Source is Sumatra A: 26 December 2004 earthquake, Mw = 9.2.**

Figure No.

4.4

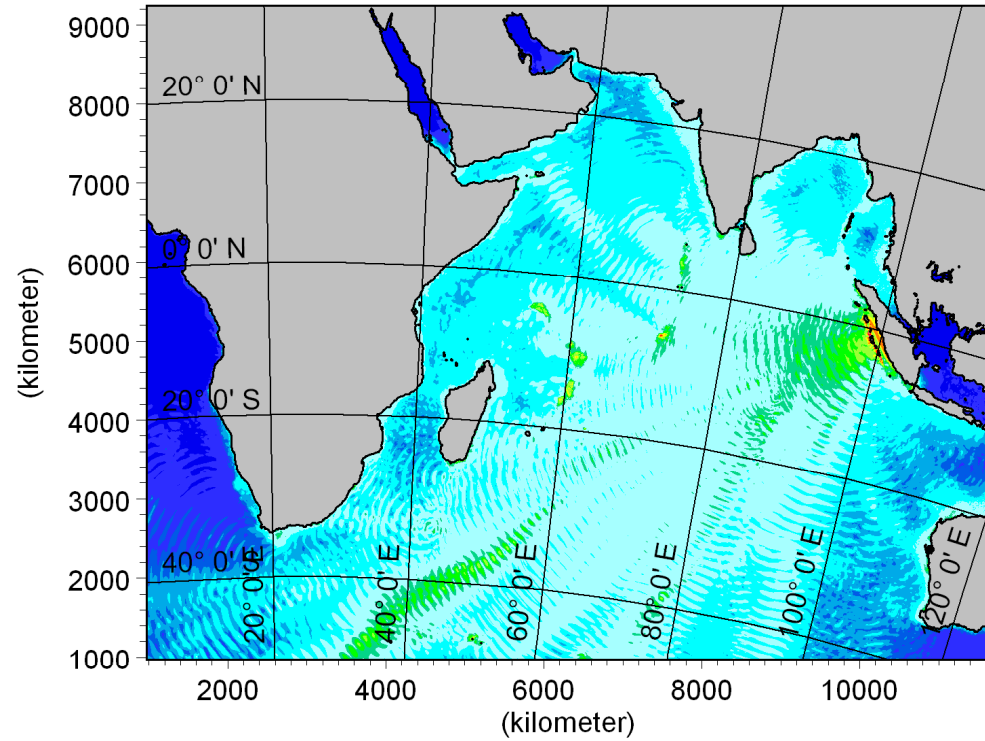
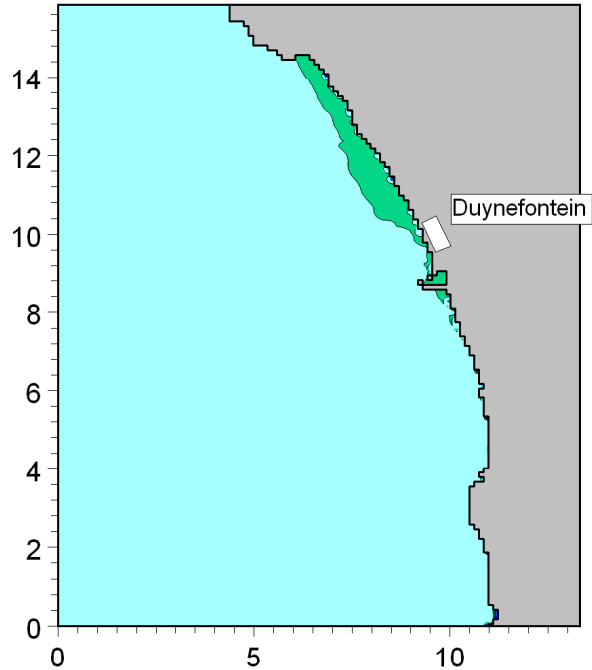


These are the maximum tsunami-induced water levels above Still Water Level. The total water level will additionally include the effect of tide, wave run-up, wave set-up and storm surge.

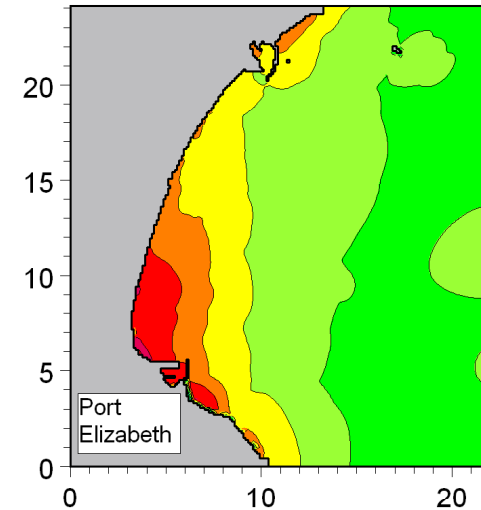
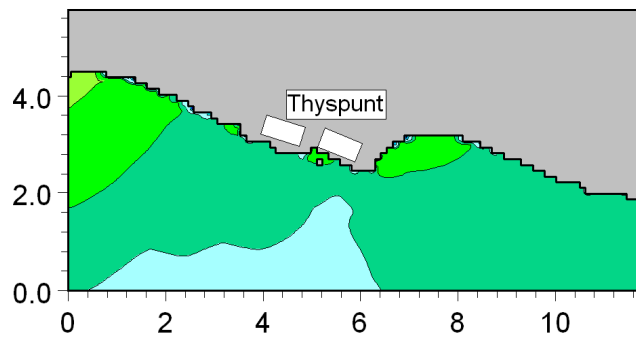
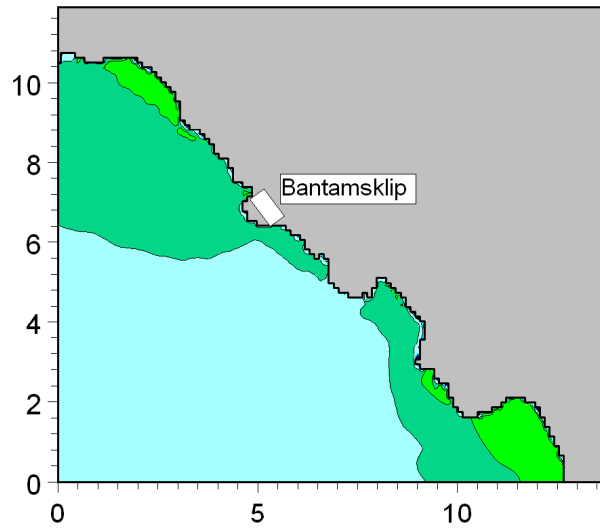
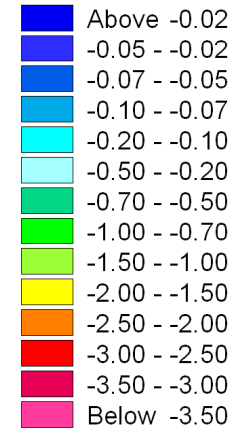


Title: Maximum water levels predicted during tsunami event.
Source is Sumatra B: maximum credible earthquake determined by the Council for Geoscience, Mw = 9.2.

Figure No. 4.5



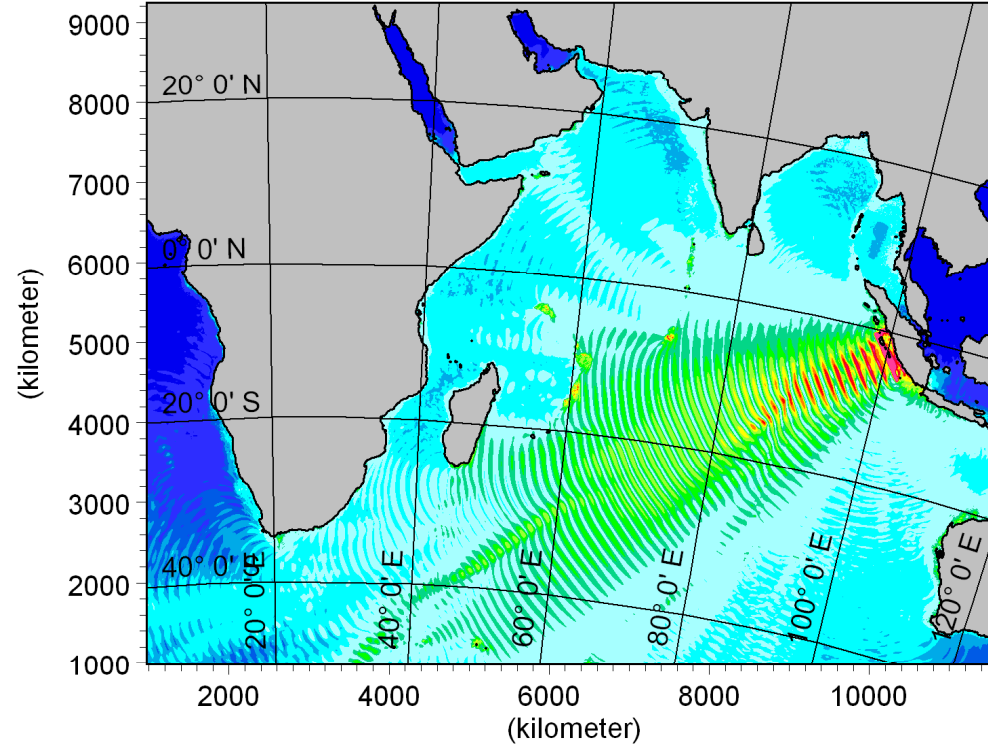
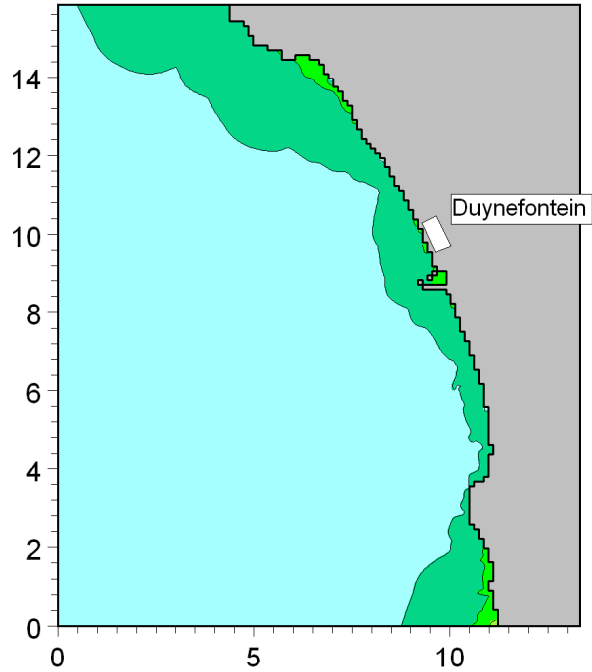
Minimum surface elevation (meter)



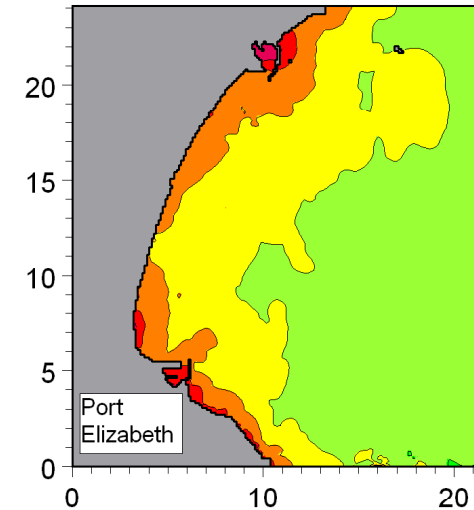
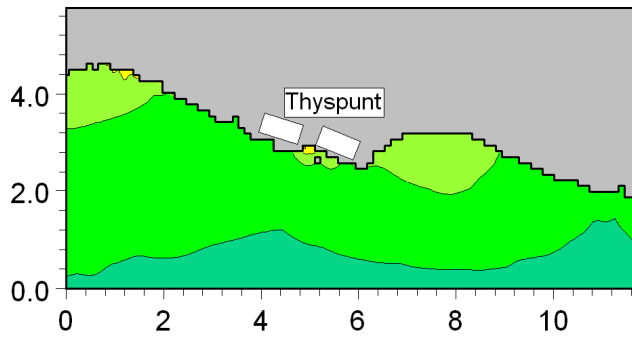
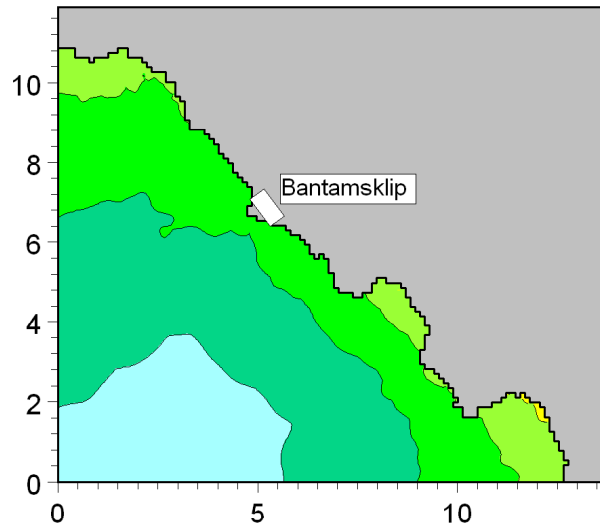
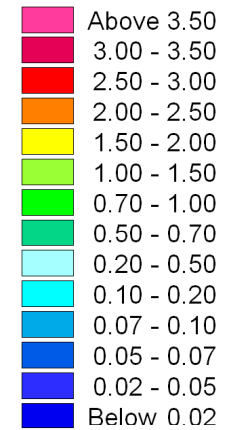
These are the minimum tsunami-induced water levels below Still Water Level. The total water level will additionally include the effect of tide and storm surge.



Title: Minimum water levels predicted during tsunami event.
Source is Sumatra B: maximum credible earthquake determined by the Council for Geoscience, Mw = 9.2.



Maximum surface elevation (meter)



These are the maximum tsunami-induced water levels above Still Water Level. The total water level will additionally include the effect of tide, wave run-up, wave set-up and storm surge.

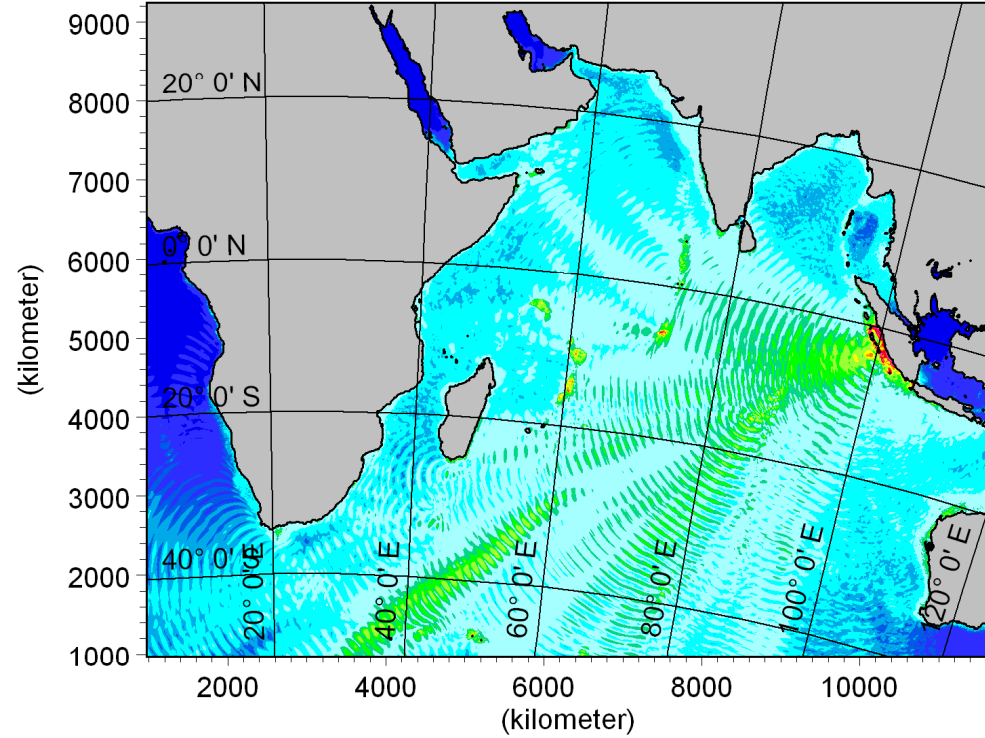
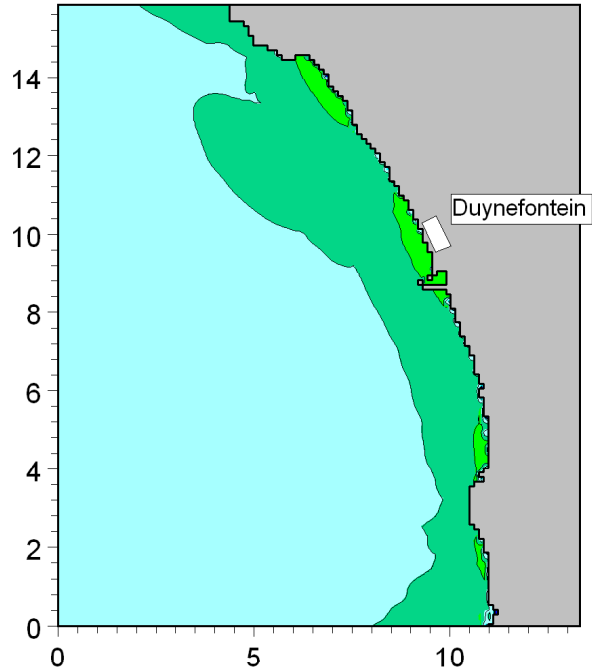


Title:

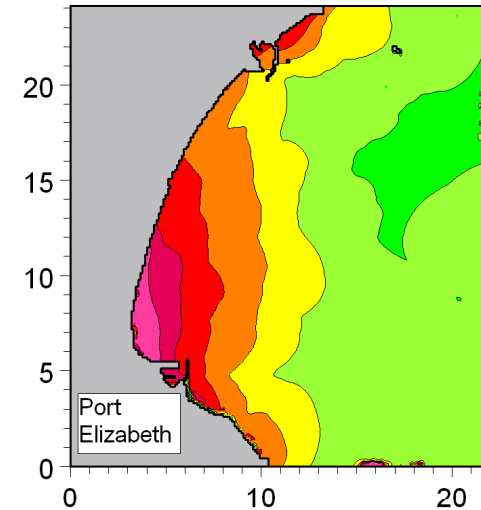
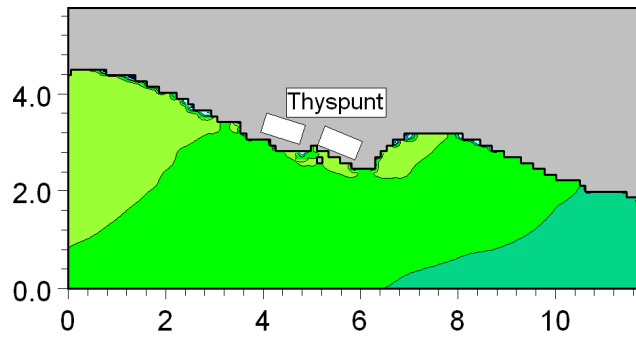
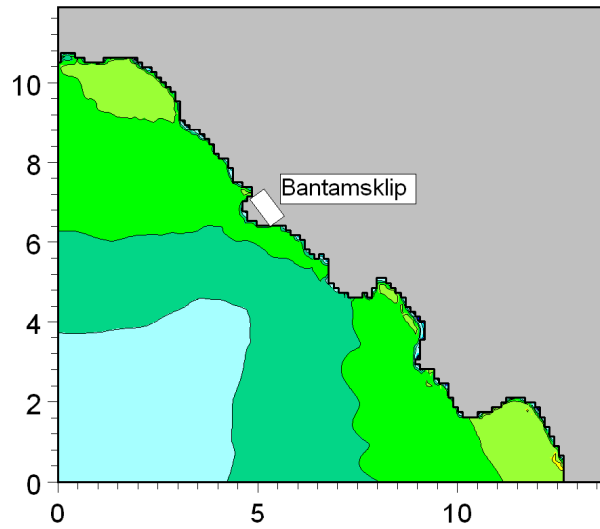
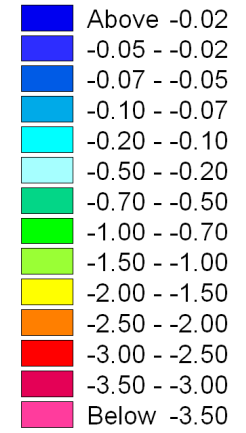
**Maximum water levels predicted during tsunami event.
Source is a Sumatra C: maximum plausible event from Borrero *et al* (2006), Mw = 9.3.**

Figure No.

4.7



Minimum surface elevation (meter)



These are the minimum tsunami-induced water levels below Still Water Level. The total water level will additionally include the effect of tide and storm surge.

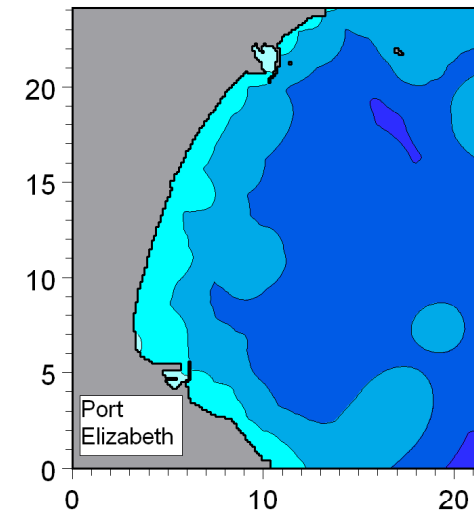
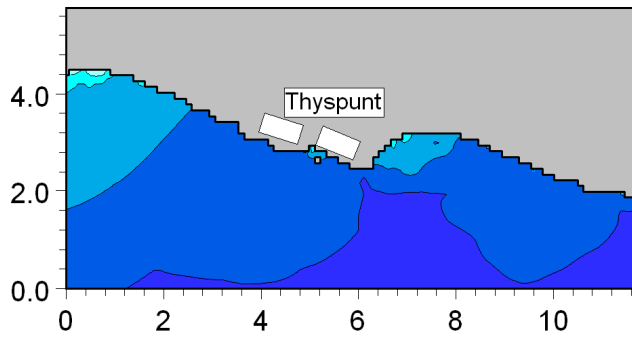
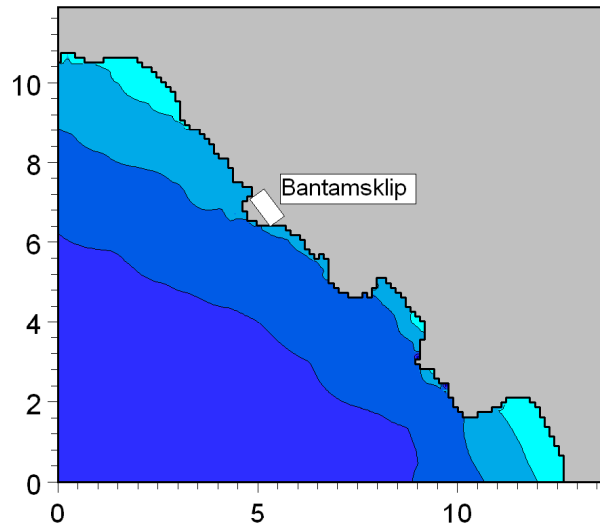
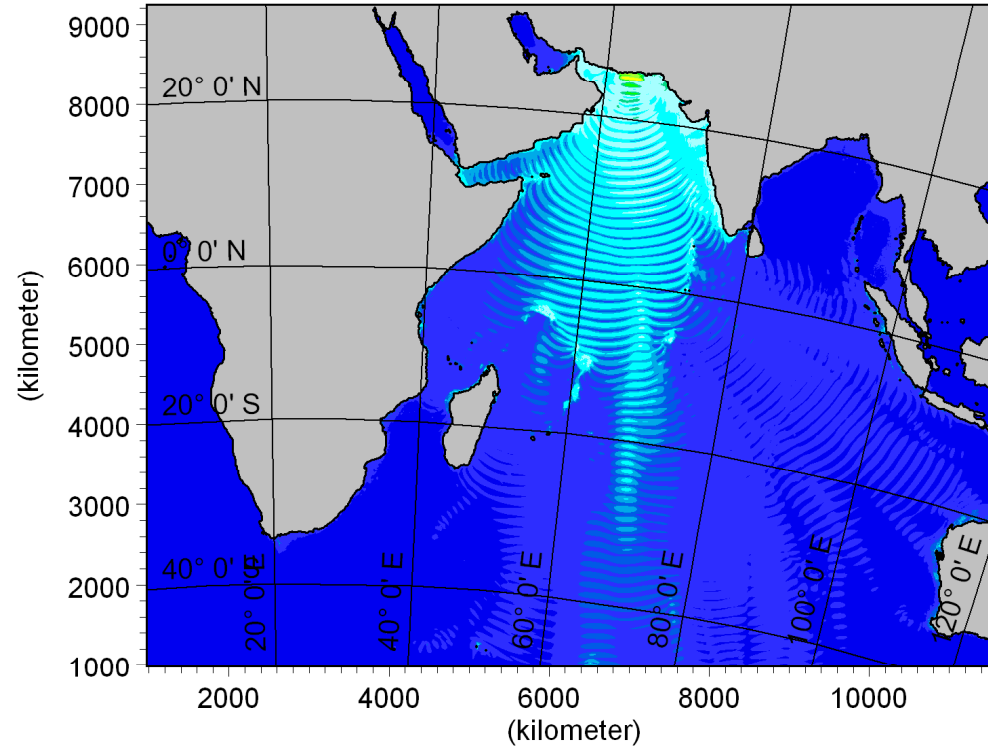
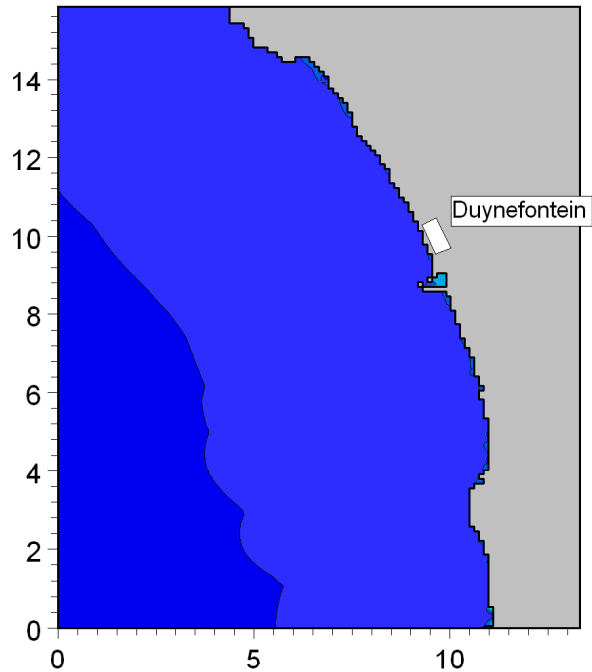


Title:

Minimum water levels predicted during tsunami event.
Source is a Sumatra C: maximum plausible event from Borrero *et al* (2006), Mw = 9.3.

Figure No.

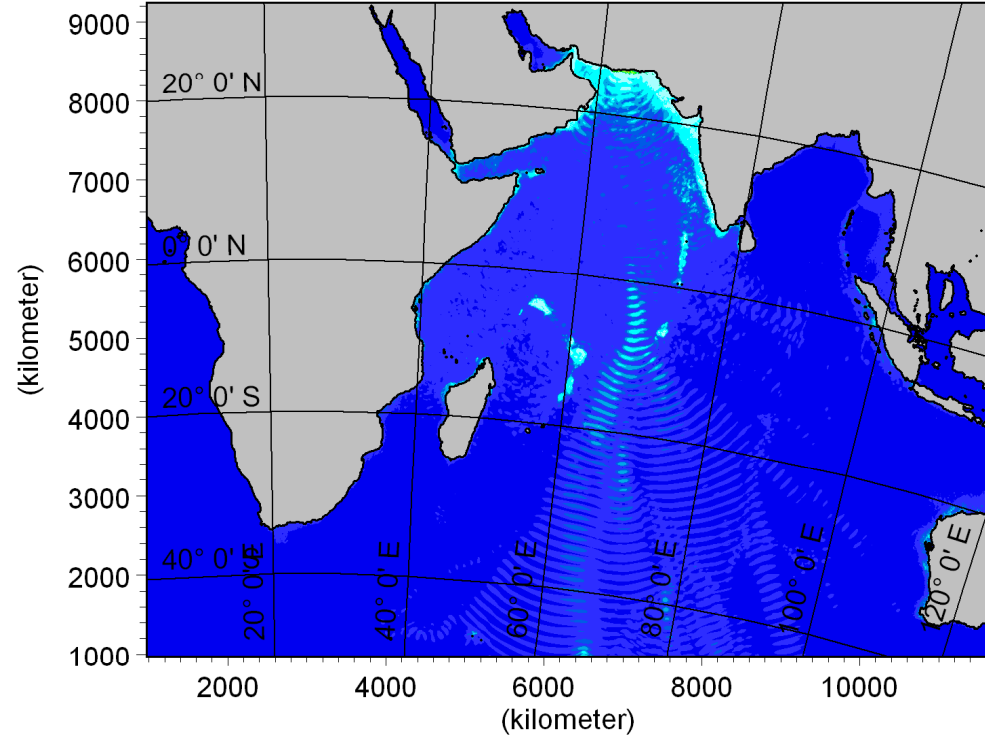
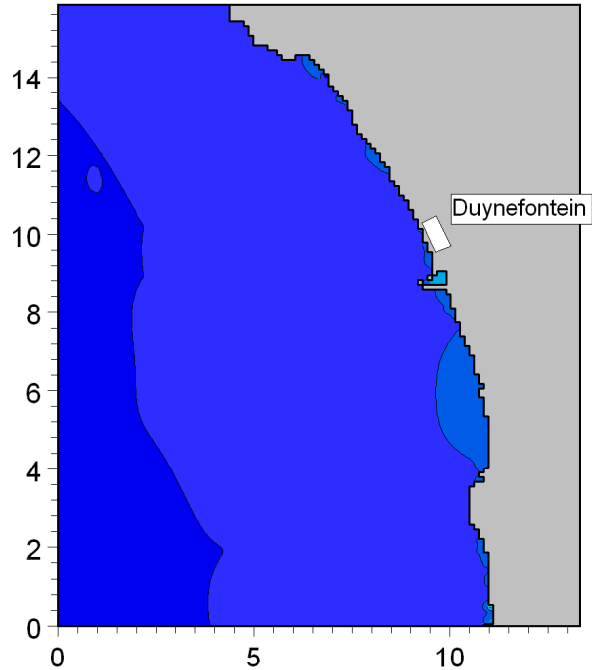
4.8



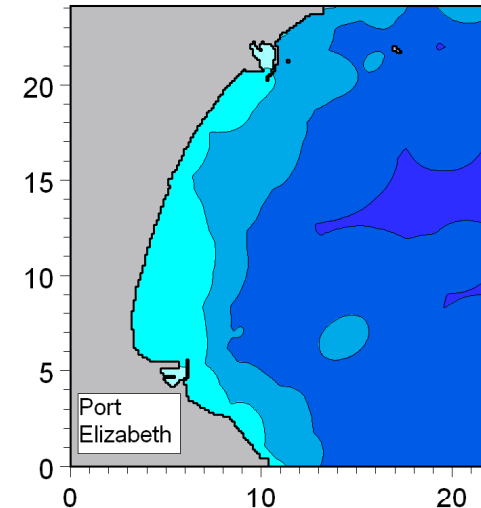
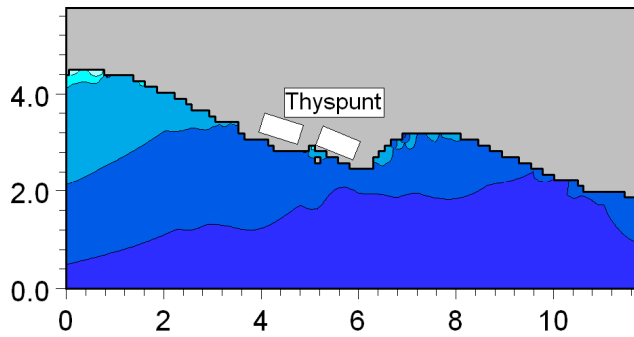
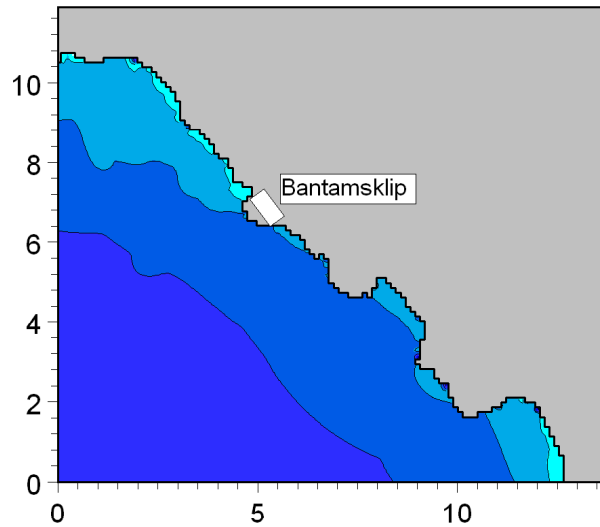
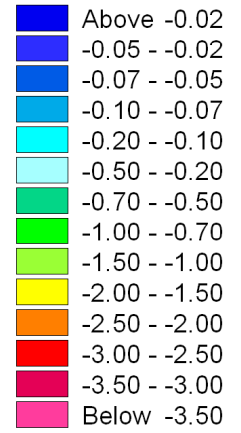
These are the maximum tsunami-induced water levels above Still Water Level. The total water level will additionally include the effect of tide, wave run-up, wave set-up and storm surge.



Title: Maximum water levels predicted during tsunami event.
Source is Karachi A: maximum credible earthquake determined by the Council for Geoscience, Mw =8.4.



Minimum surface elevation (meter)

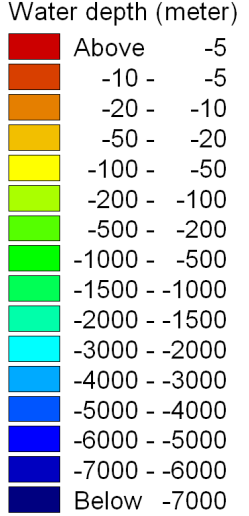
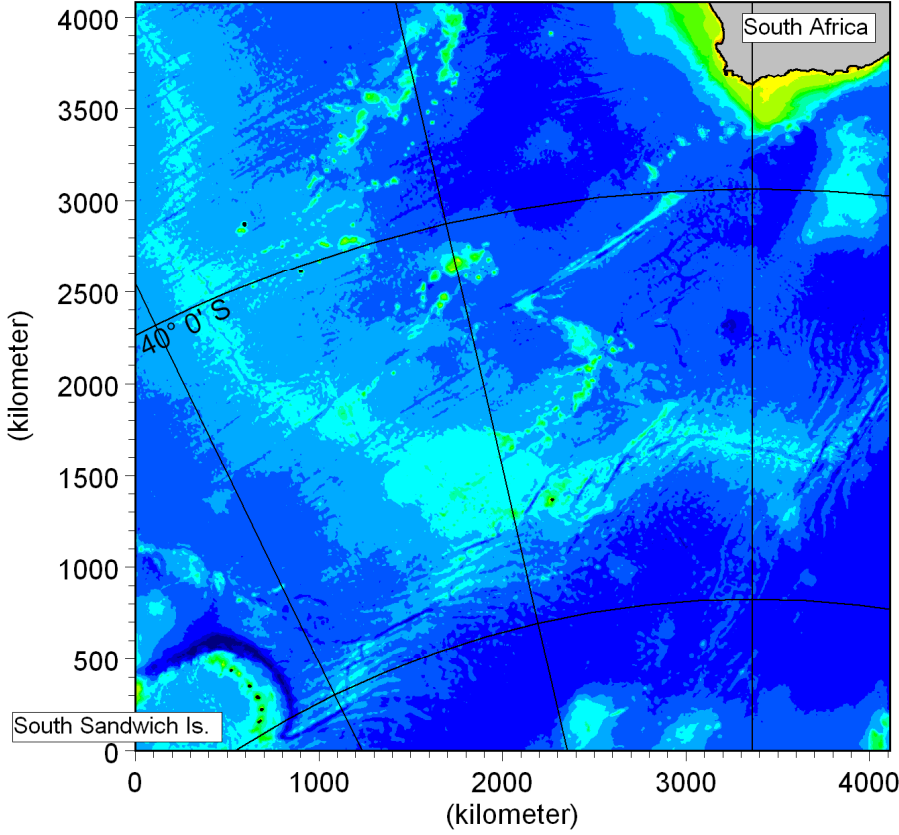
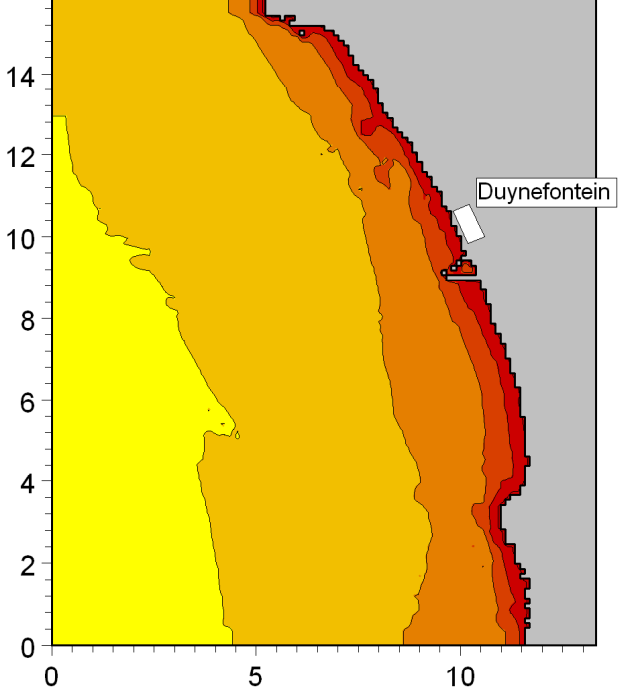
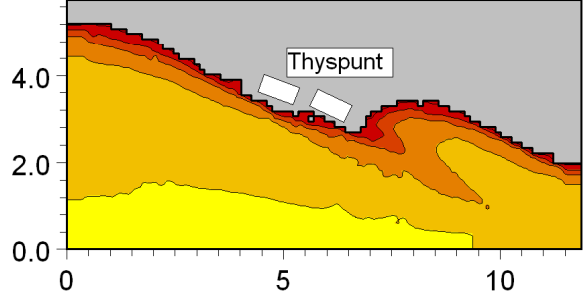
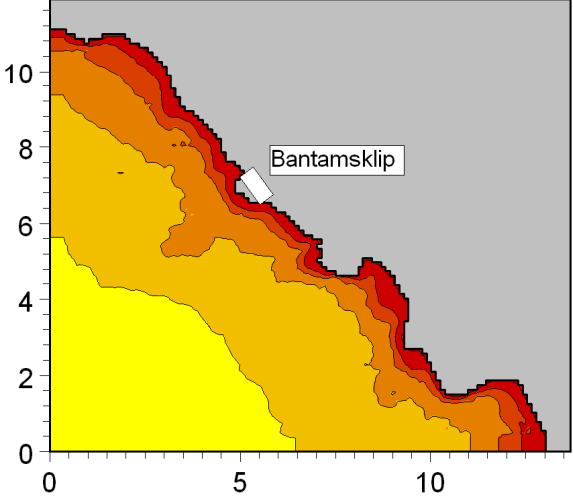


These are the minimum tsunami-induced water levels below Still Water Level. The total water level will additionally include the effect of tide and storm surge.

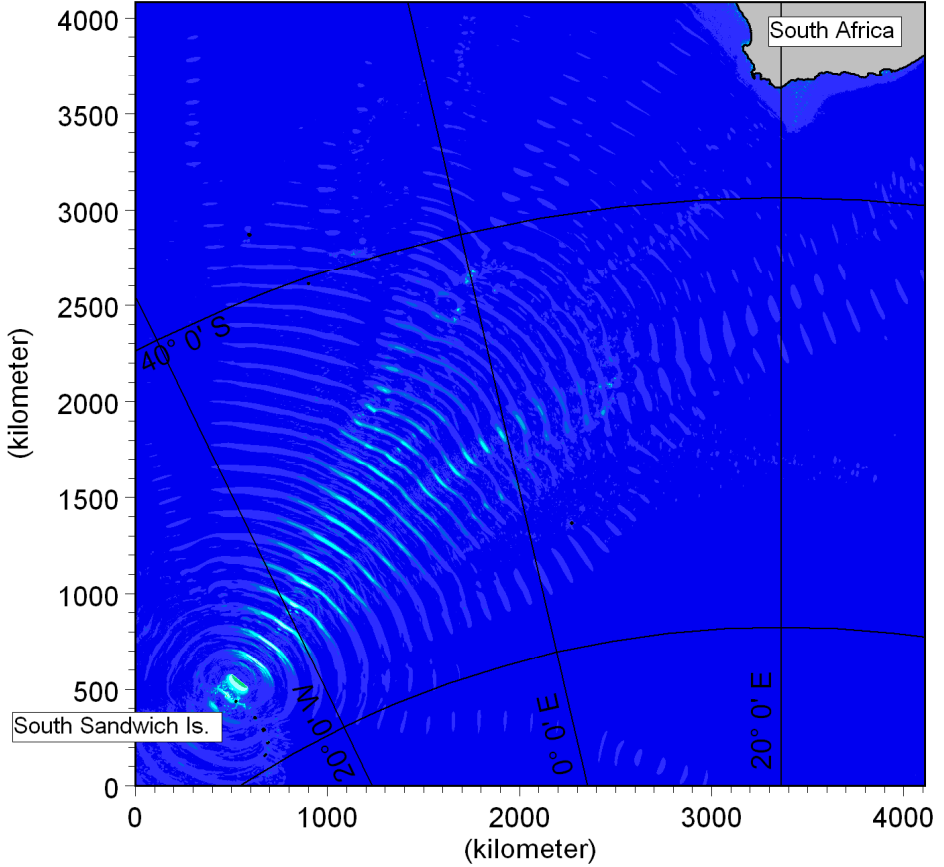
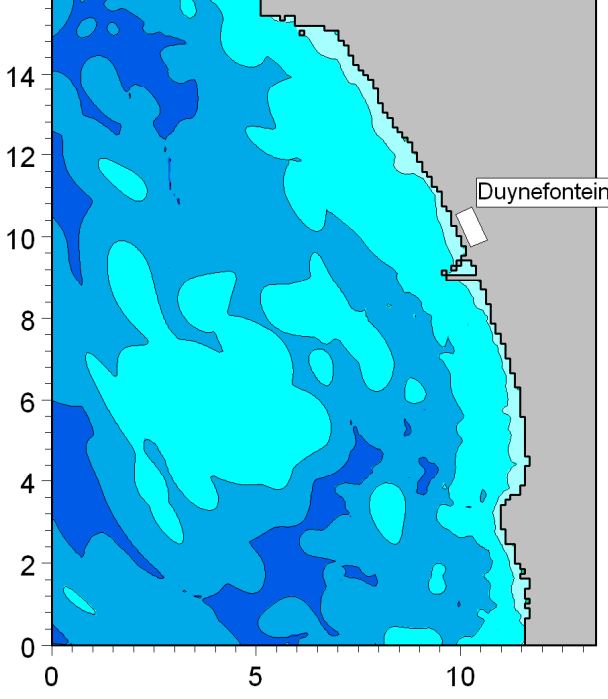
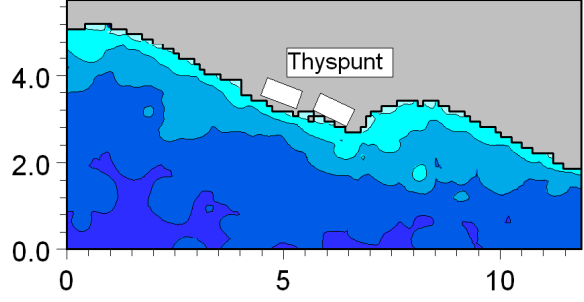
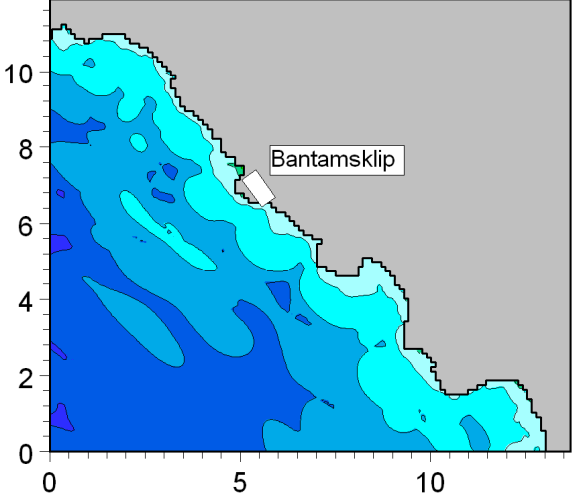


Title: Minimum water levels predicted during tsunami event.
Source is Karachi A: maximum credible earthquake determined by the Council for Geoscience, Mw =8.4.

Run: SouthSandwich01_MSL_a



Title: **Model bathymetry used for tsunami modelling of the South Sandwich Islands earthquake events.**

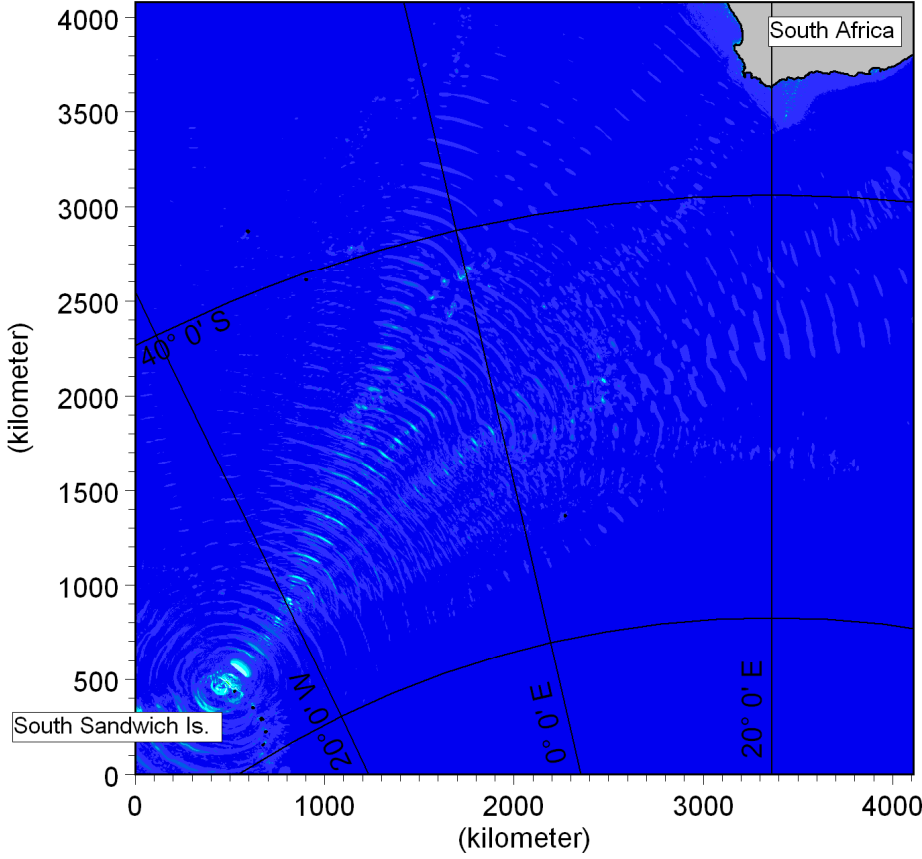
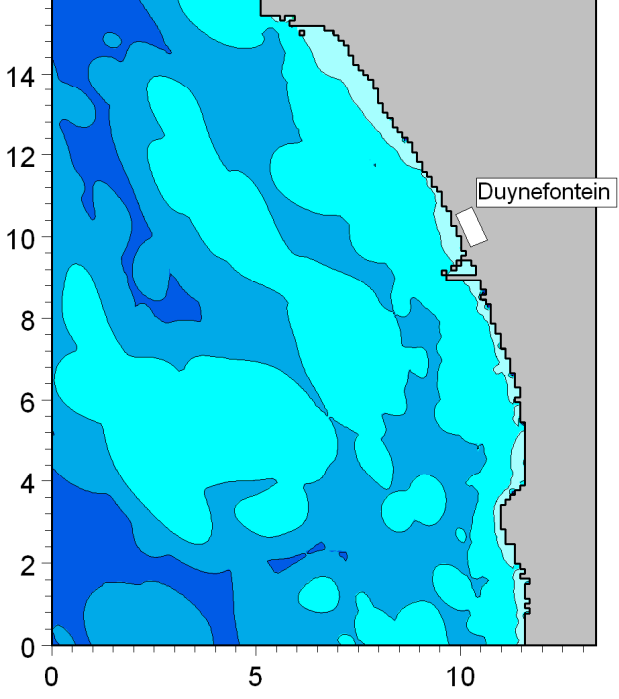
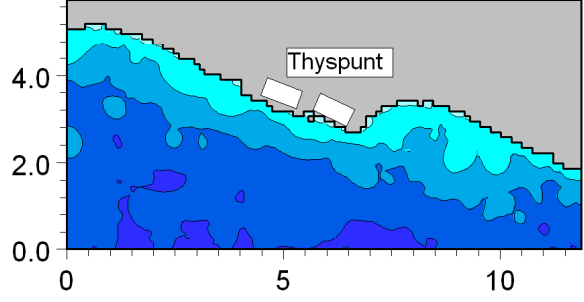
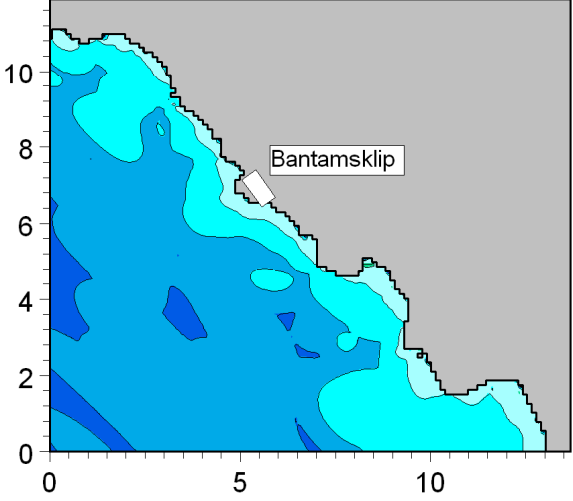


These are the maximum tsunami-induced water levels above Still Water Level. The total water level will additionally include the effect of tide, wave run-up, wave set-up and storm surge.

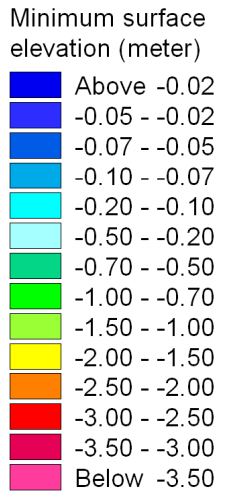
- Maximum surface elevation (meter)
- █ Above 3.50
 - █ 3.00 - 3.50
 - █ 2.50 - 3.00
 - █ 2.00 - 2.50
 - █ 1.50 - 2.00
 - █ 1.00 - 1.50
 - █ 0.70 - 1.00
 - █ 0.50 - 0.70
 - █ 0.20 - 0.50
 - █ 0.10 - 0.20
 - █ 0.07 - 0.10
 - █ 0.05 - 0.07
 - █ 0.02 - 0.05
 - █ Below 0.02



Title: Maximum water levels predicted during tsunami event.
 Source is South Sandwich Islands A: maximum credible earthquake determined by the Council for Geoscience, Mw = 7.6.

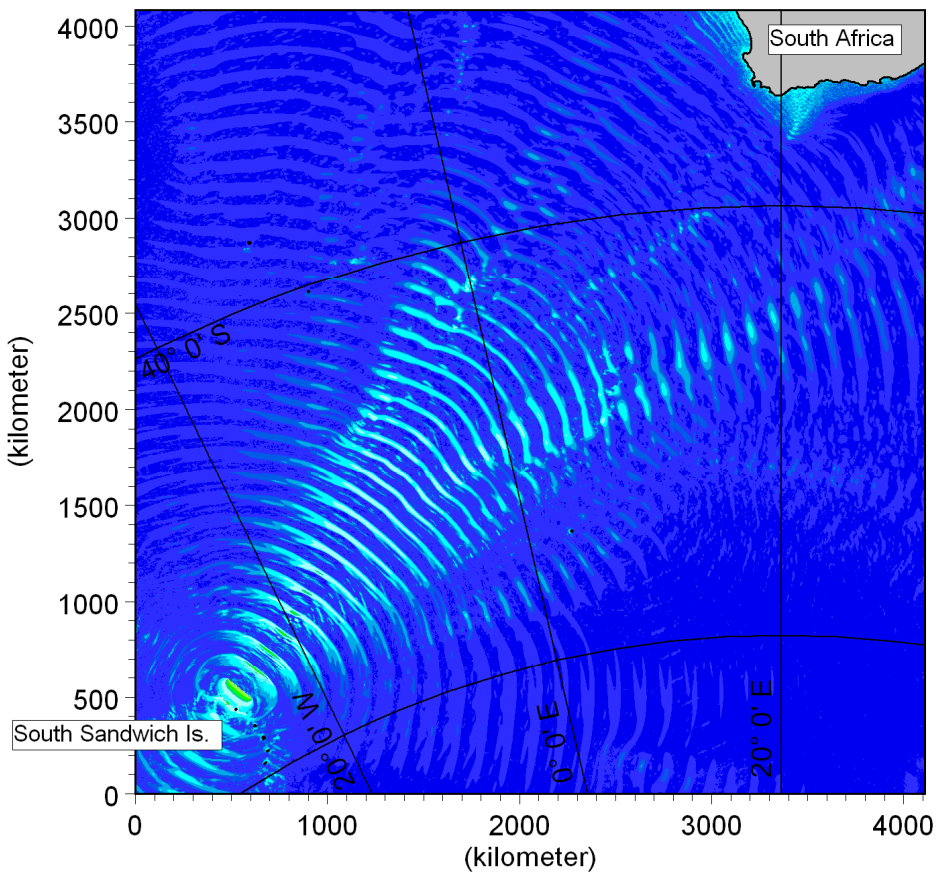
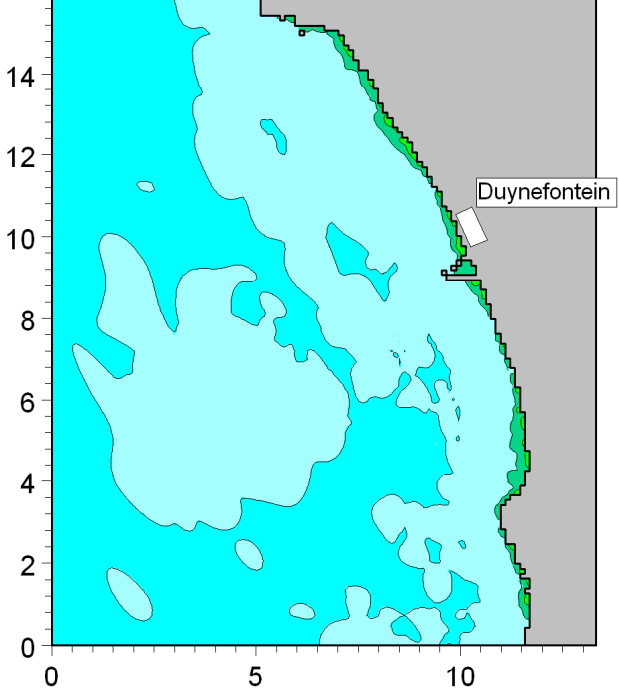
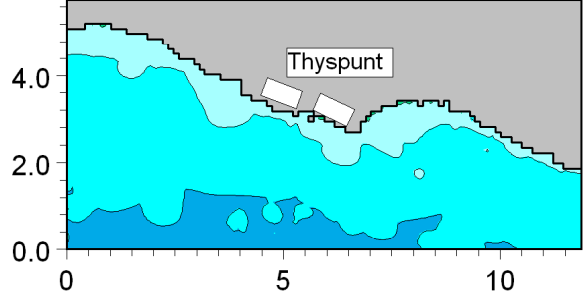
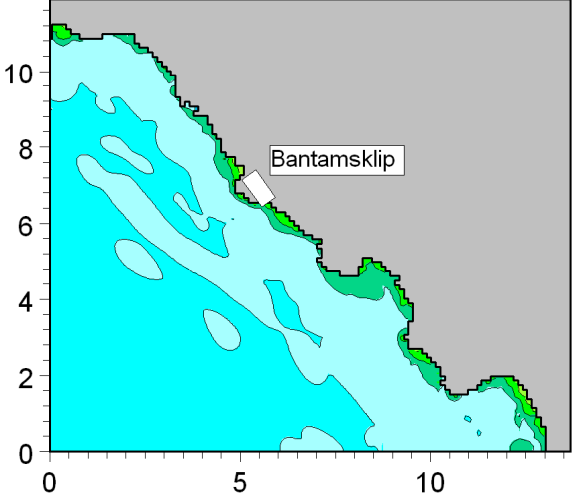


These are the minimum tsunami-induced water levels below Still Water Level. The total water level will additionally include the effect of tide and storm surge.

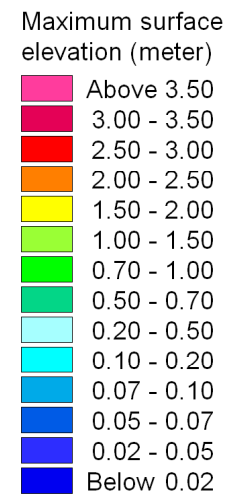


Title: Minimum water levels predicted during tsunami event. Source is South Sandwich Islands A: maximum credible earthquake determined by the Council for Geoscience, Mw = 7.6.

Run: SouthSandwich04_MSL_a



These are the maximum tsunami-induced water levels above Still Water Level. The total water level will additionally include the effect of tide, wave run-up, wave set-up and storm surge.



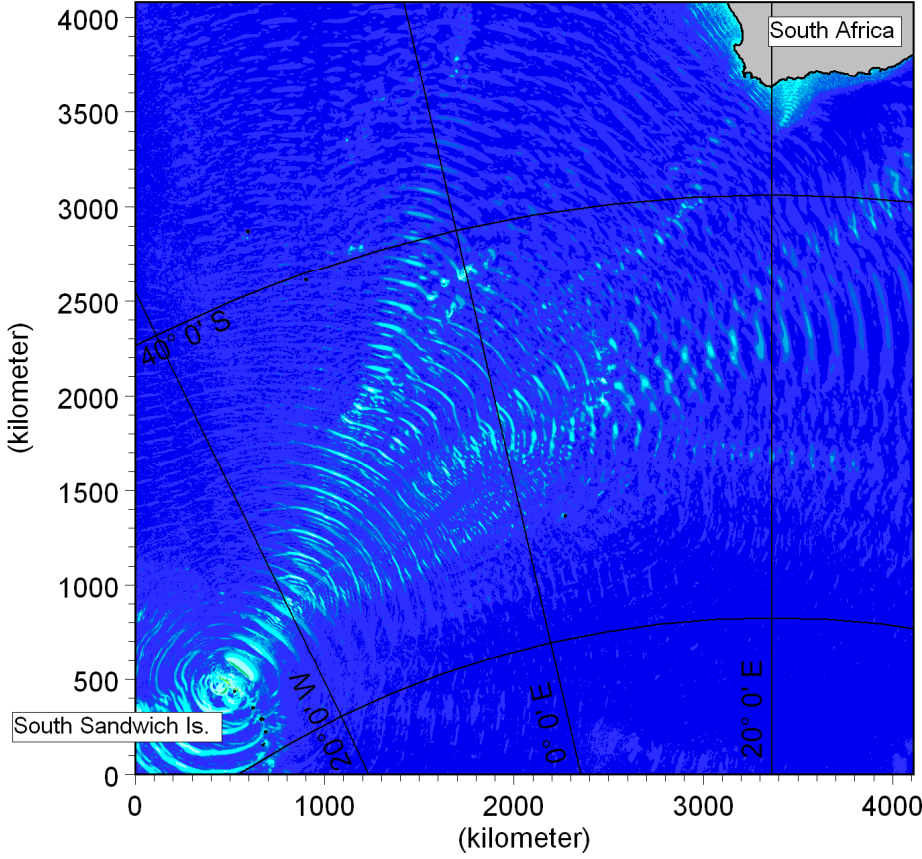
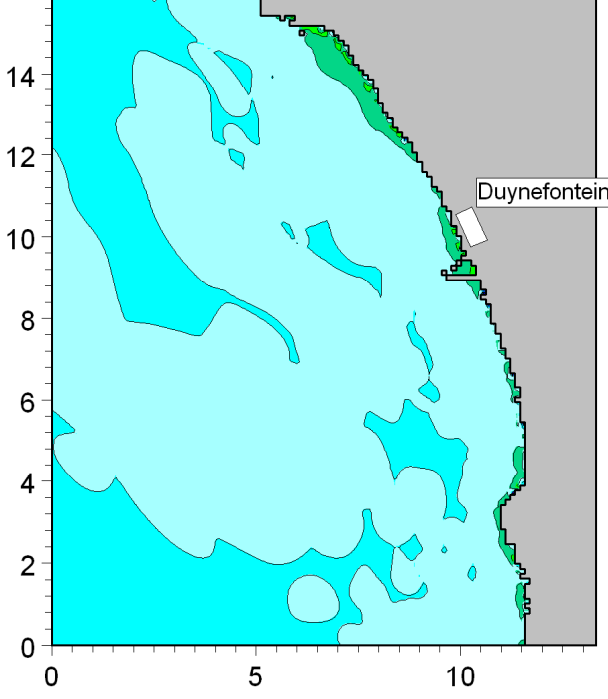
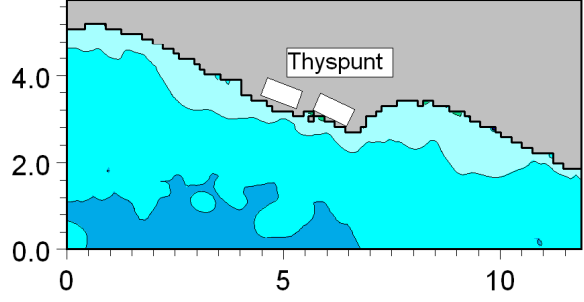
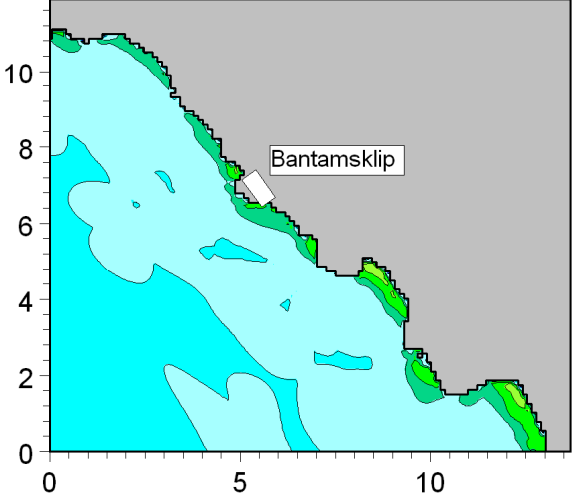
Title:

**Maximum water levels predicted during tsunami event.
Source is South Sandwich Islands B: magnitude increased to Mw = 8.0.**

Figure No.

4.14

Run: SouthSandwich04_MSL_a



These are the minimum tsunami-induced water levels below Still Water Level. The total water level will additionally include the effect of tide and storm surge.

- Minimum surface elevation (meter)
- Above -0.02
 - 0.05 - -0.02
 - 0.07 - -0.05
 - 0.10 - -0.07
 - 0.20 - -0.10
 - 0.50 - -0.20
 - 0.70 - -0.50
 - 1.00 - -0.70
 - 1.50 - -1.00
 - 2.00 - -1.50
 - 2.50 - -2.00
 - 3.00 - -2.50
 - 3.50 - -3.00
 - Below -3.50

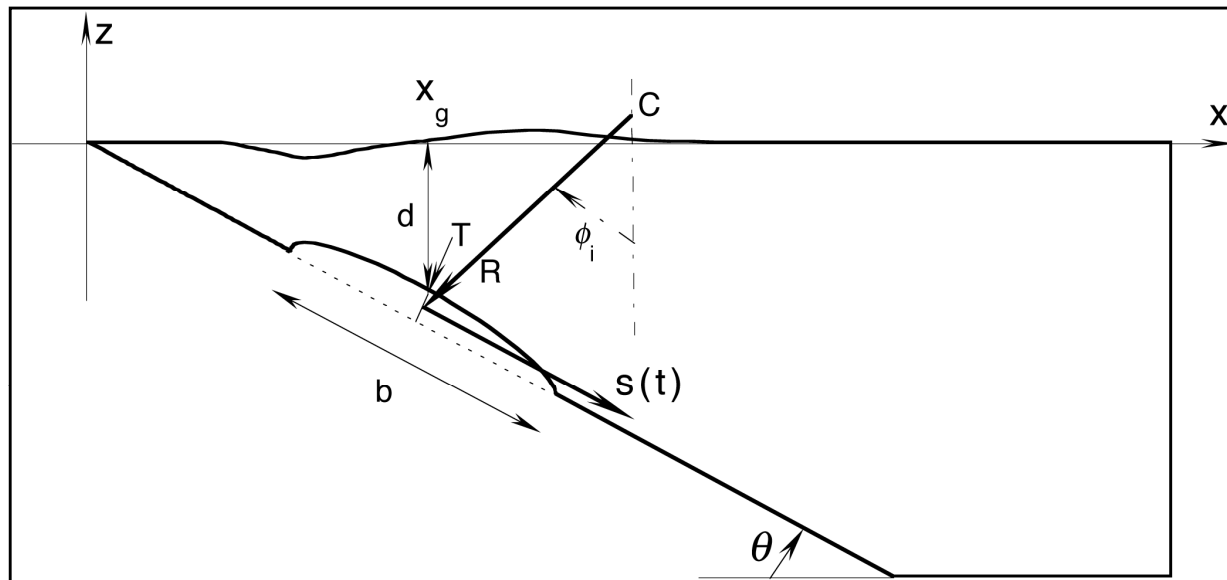
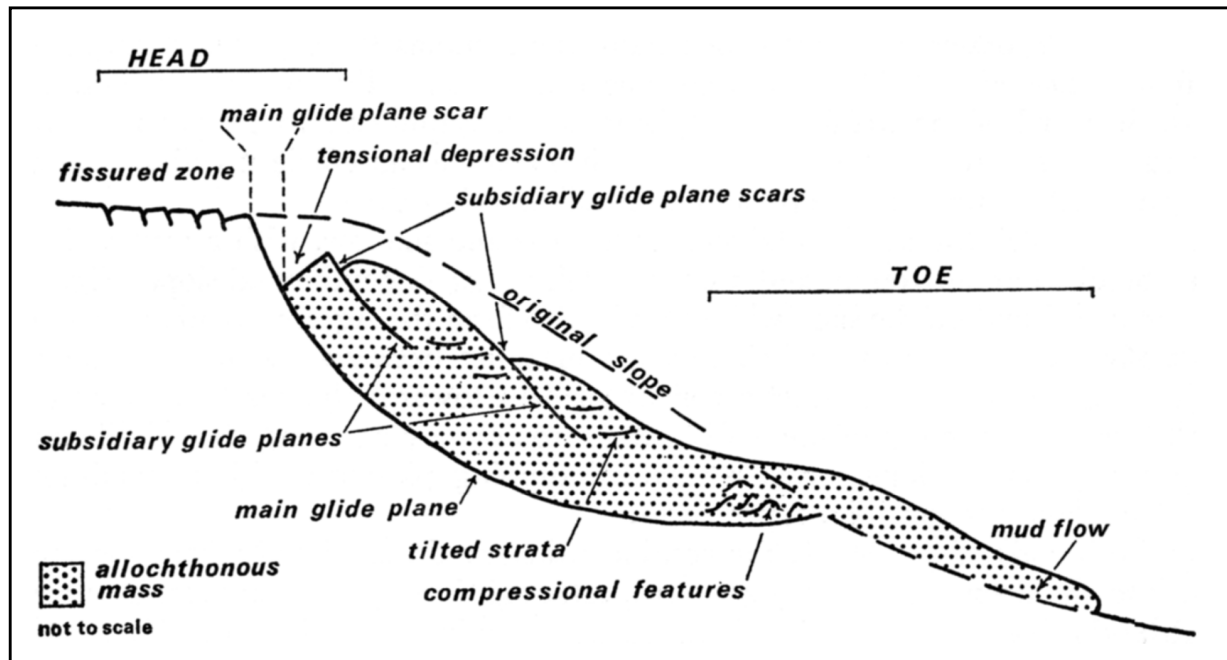


Title:

**Minimum water levels predicted during tsunami event.
Source is South Sandwich Islands B: magnitude increased to Mw = 8.0.**

Figure No.

4.15

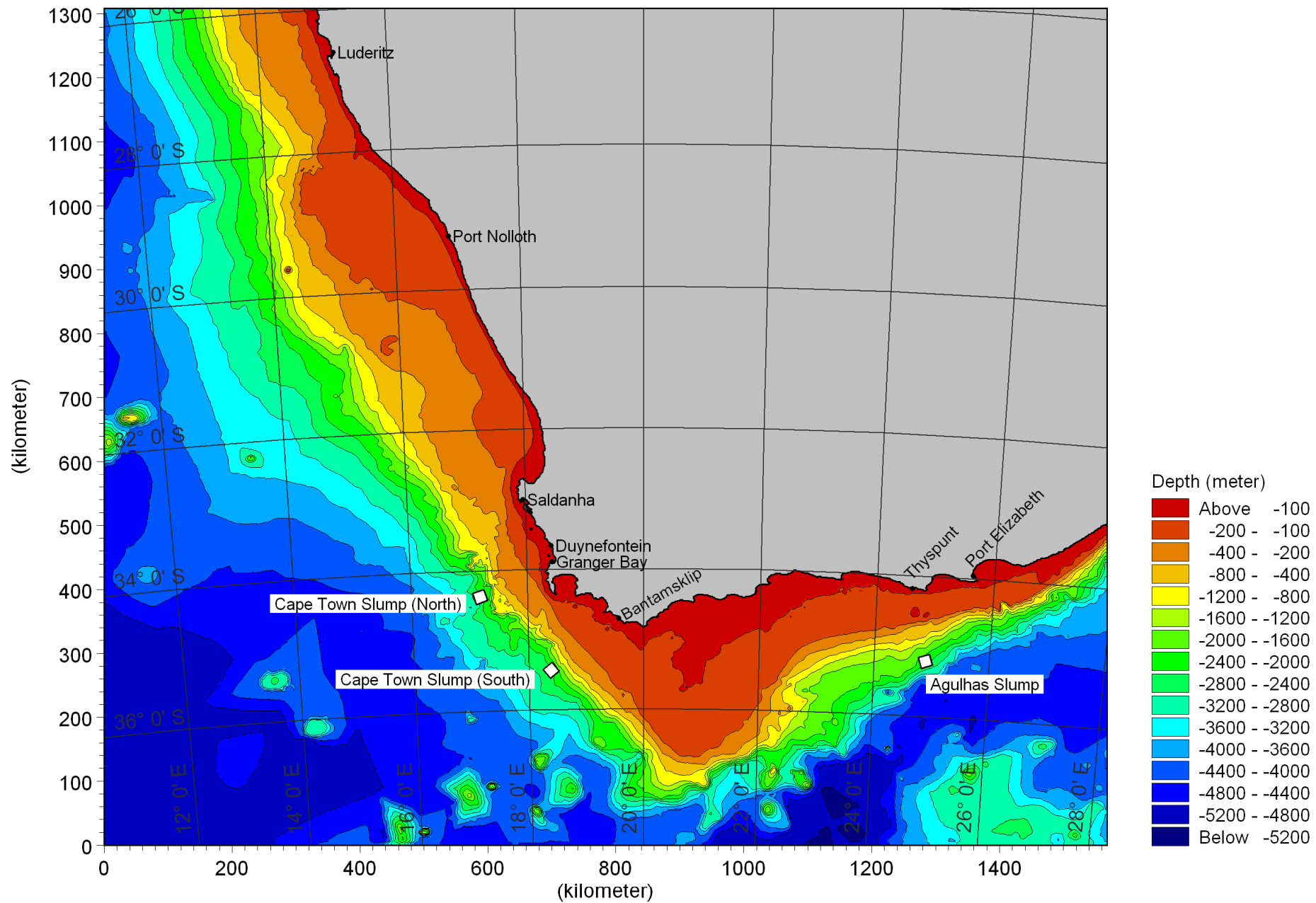


Title:

Top: Main morphological and structural features of submarine slumps (Dingle, 1977).
 Bottom: Parameters defining slump model (Watts et al, 2003).

Figure No.

4.16



Title: Model bathymetry used for tsunami modelling due to slumps on the South African shelf margin. Locations of the three slumps modelled are indicated.

Figure No.
4.18

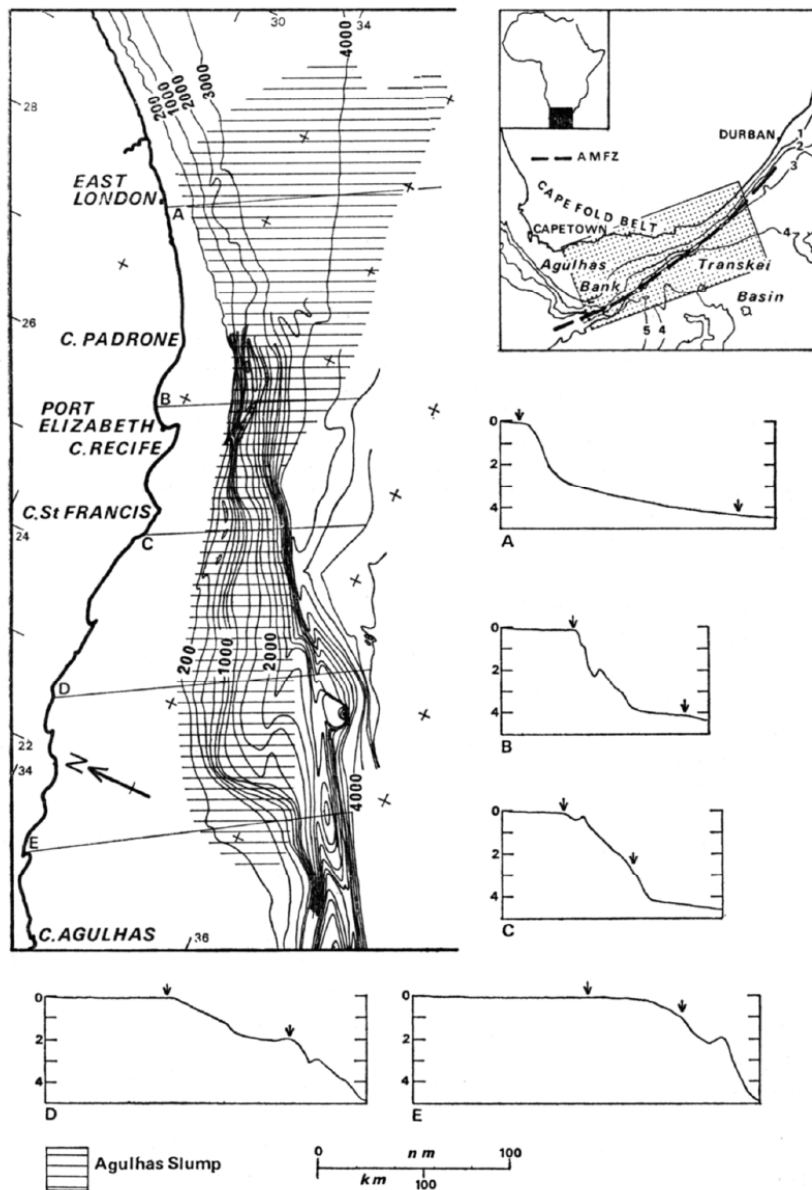


FIG. 1. Bathymetry (in metres) and bathymetric profiles (in kilometres) on the SE Agulhas Bank. Insert shows location of area; AMFZ, Agulhas marginal fracture zone. Arrows on profiles show limits of slump.

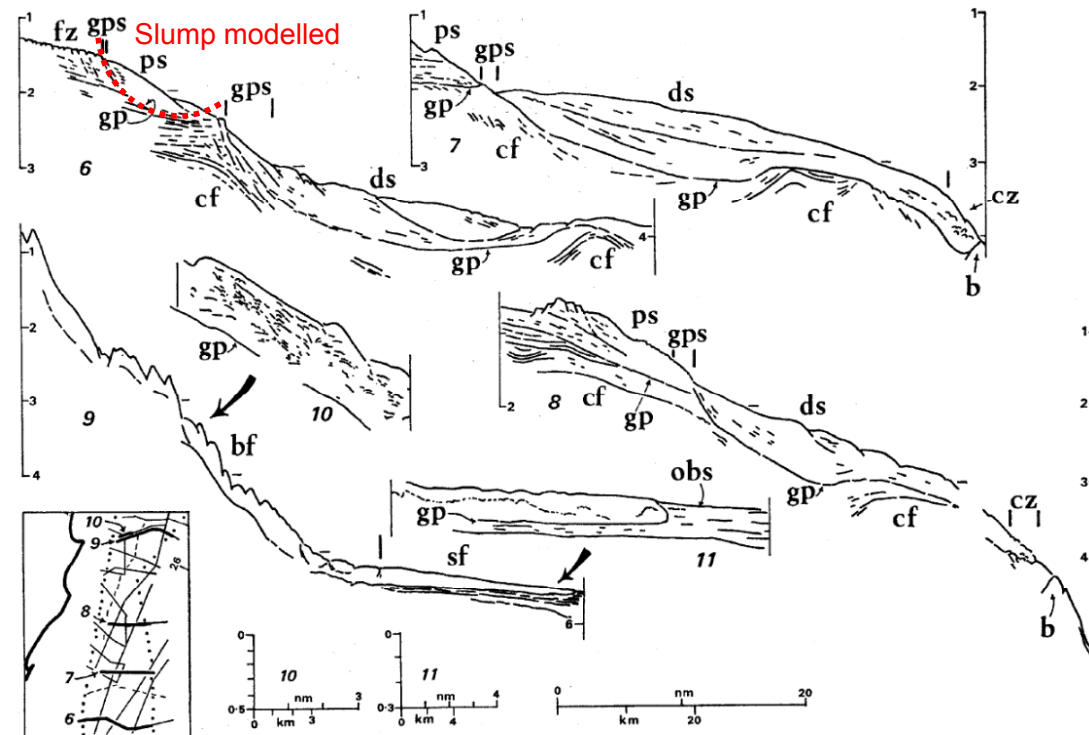


FIG. 6. Replotted (6-9) and traced (10 & 11) seismic profiles across the distal part of the Agulhas Slump. Vertical scales in seconds DT. For abbreviations see explanation to Fig. 4. For location of profile 11 see Fig. 3.

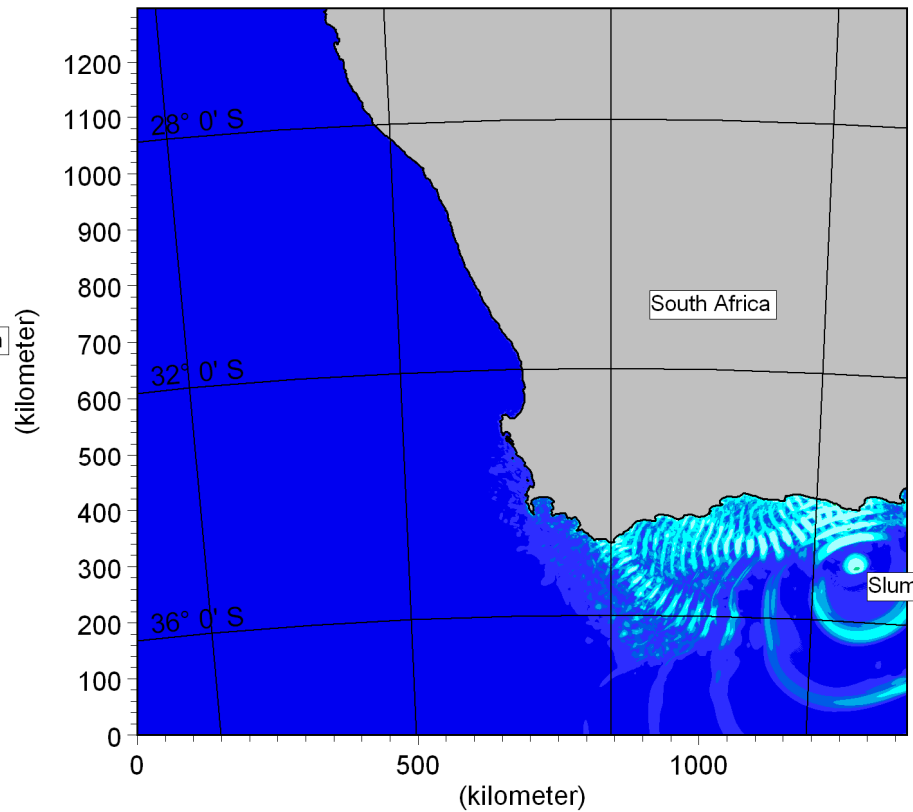
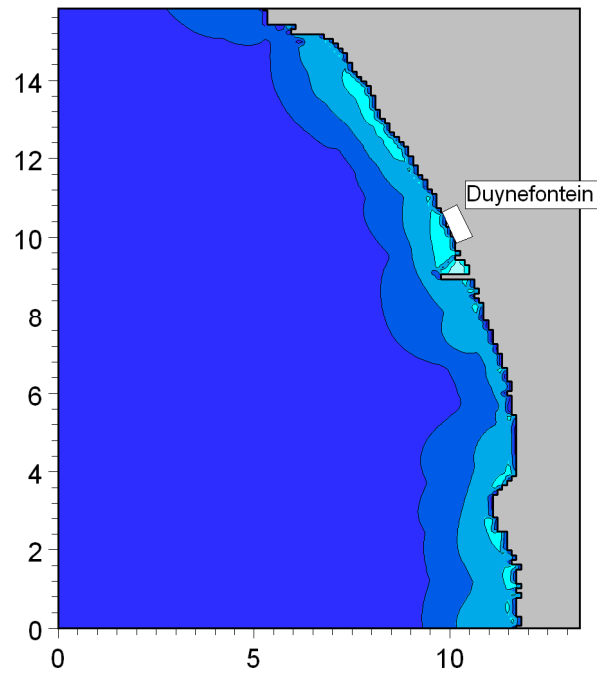
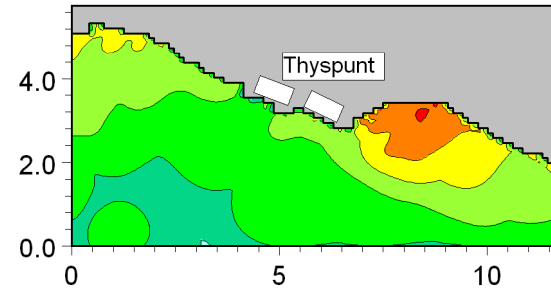
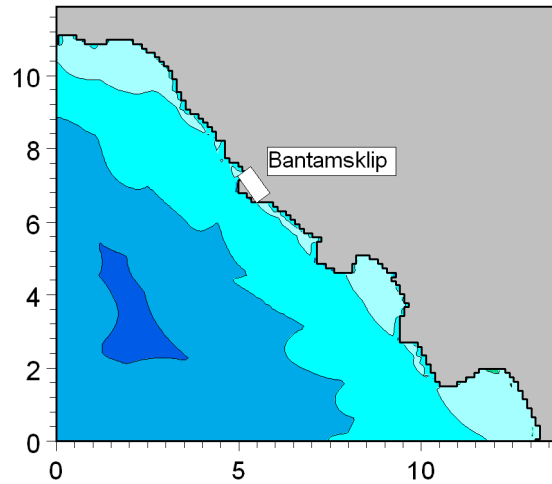


Title:

Details of the Agulhas Slump (Dingle, 1977).

Figure No.

4.19



Maximum surface elevation (meter)

- Above 3.50
- 3.00 - 3.50
- 2.50 - 3.00
- 2.00 - 2.50
- 1.50 - 2.00
- 1.00 - 1.50
- 0.70 - 1.00
- 0.50 - 0.70
- 0.20 - 0.50
- 0.10 - 0.20
- 0.07 - 0.10
- 0.05 - 0.07
- 0.02 - 0.05
- Below 0.02

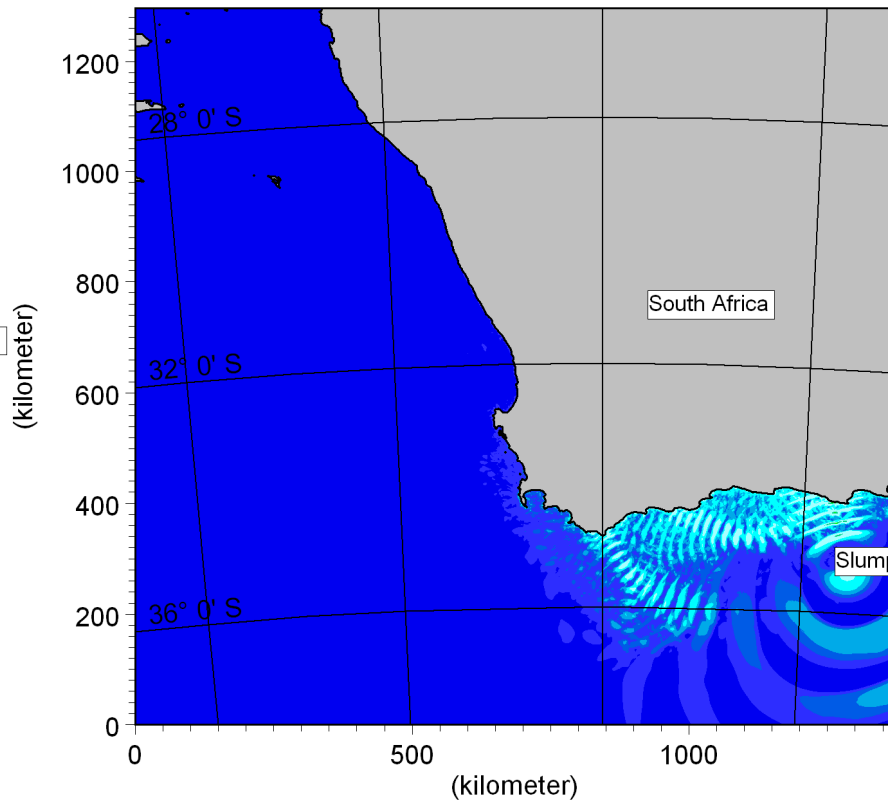
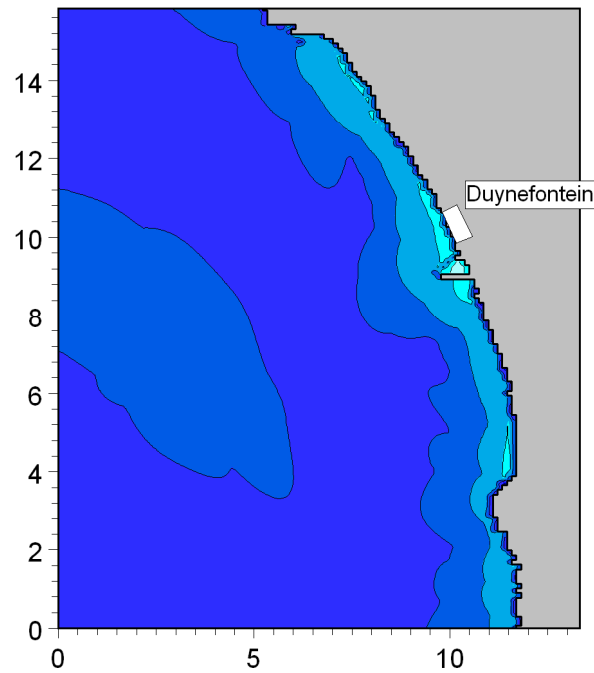
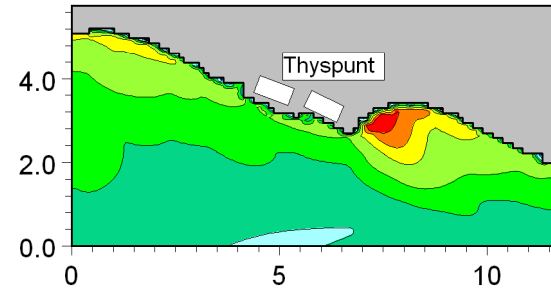
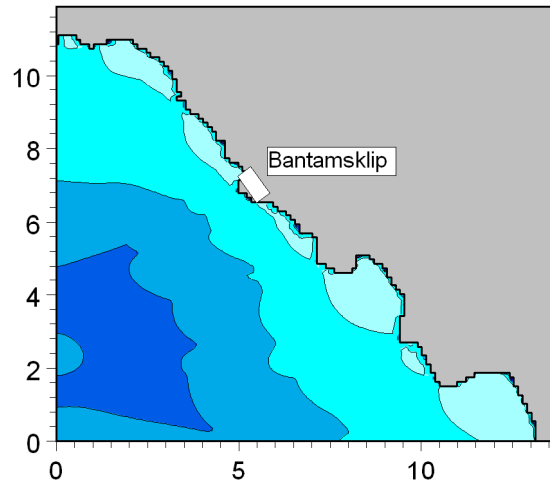


Title:

**Maximum water levels predicted during tsunami event.
Source is theoretical Agulhas Slump with volume of slumped sediment = 80 km³.**

Figure No.

4.20



Minimum surface elevation (meter)

- Above -0.02
- 0.05 - -0.02
- 0.07 - -0.05
- 0.10 - -0.07
- 0.20 - -0.10
- 0.50 - -0.20
- 0.70 - -0.50
- 1.00 - -0.70
- 1.50 - -1.00
- 2.00 - -1.50
- 2.50 - -2.00
- 3.00 - -2.50
- 3.50 - -3.00
- Below -3.50



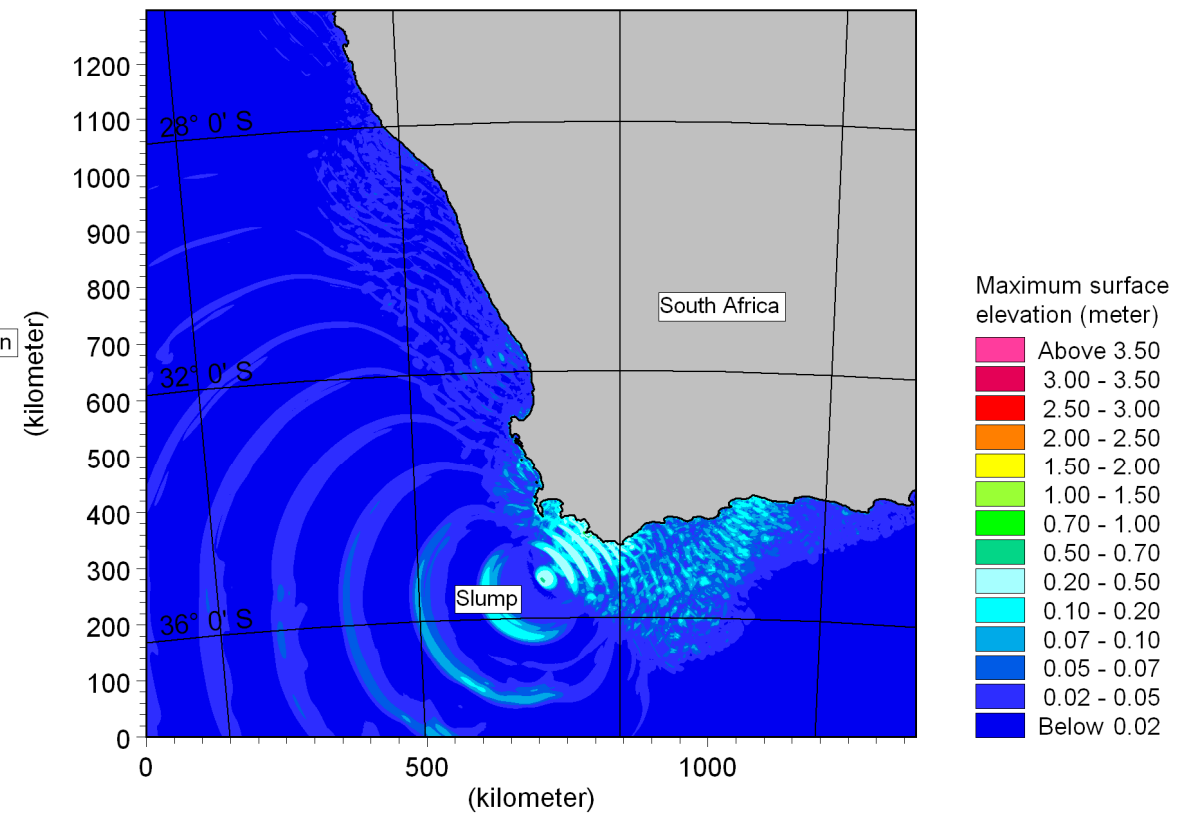
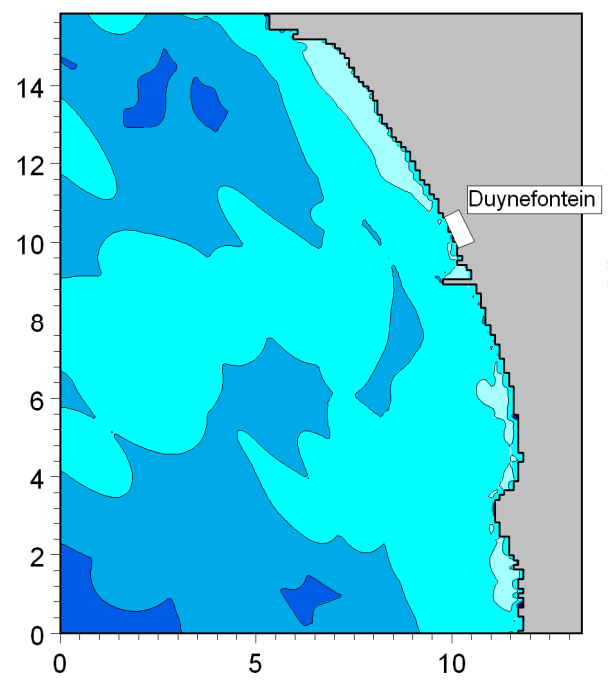
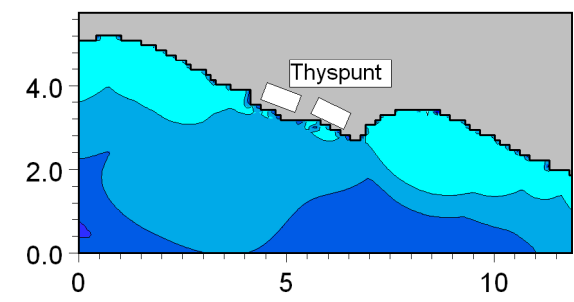
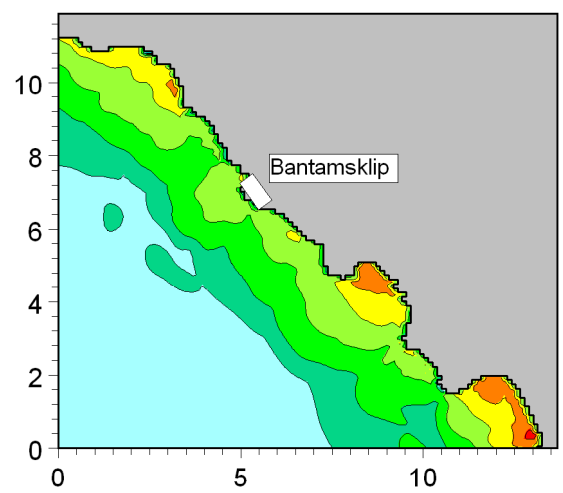
Title:

**Minimum water levels predicted during tsunami event.
Source is theoretical Agulhas Slump with volume of slumped sediment = 80 km³.**

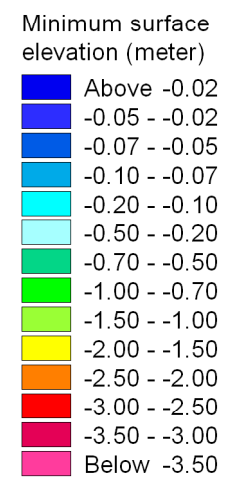
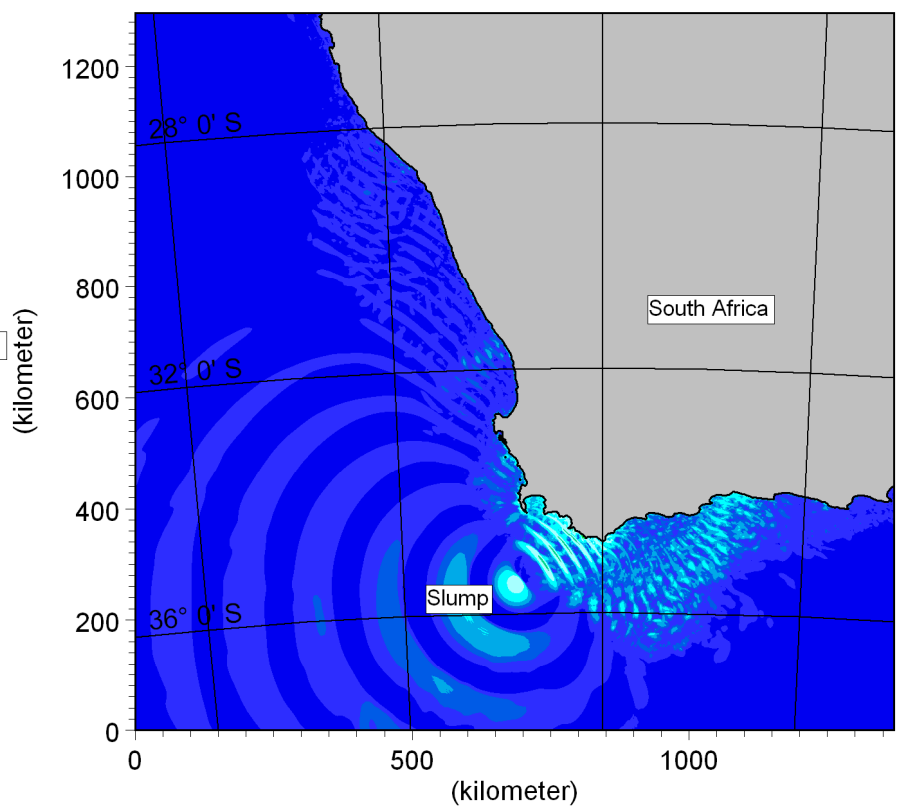
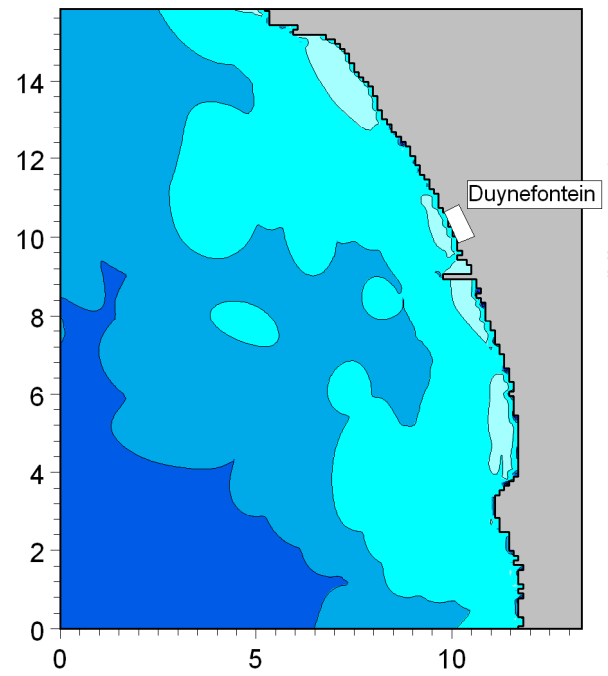
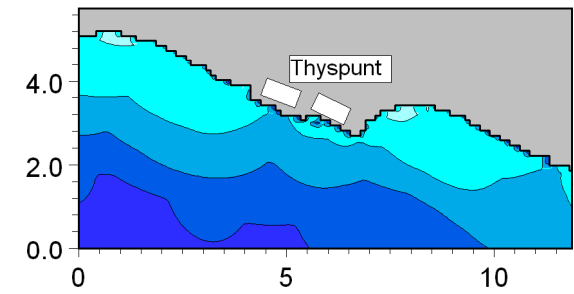
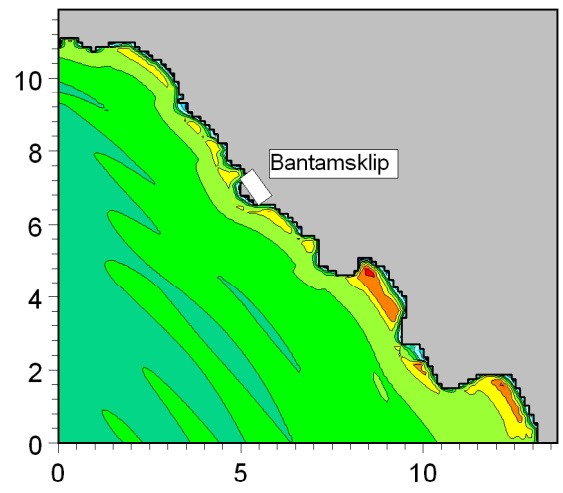
Figure No.

4.21

Run: CapeTownSouth01b



Title: Maximum water levels predicted during tsunami event.
Source is theoretical Cape Town Slump (South) with volume of slumped sediment = 80 km³.



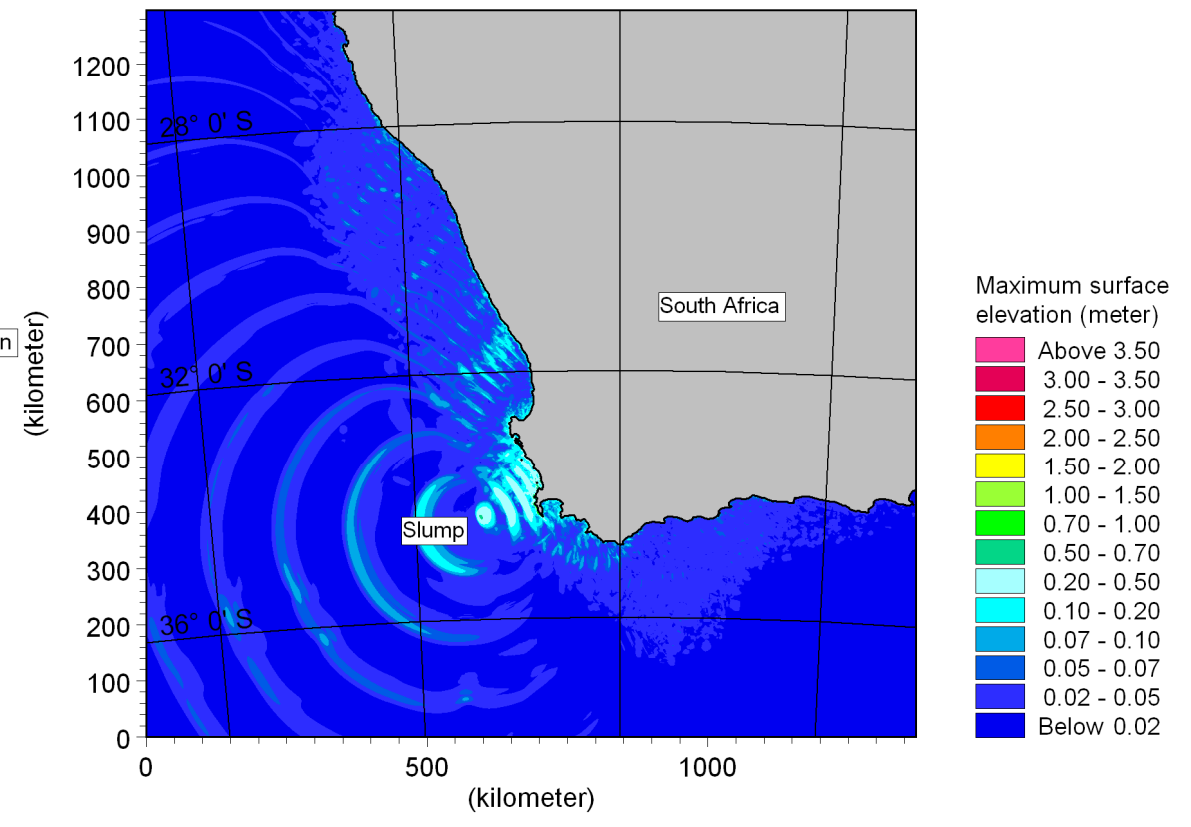
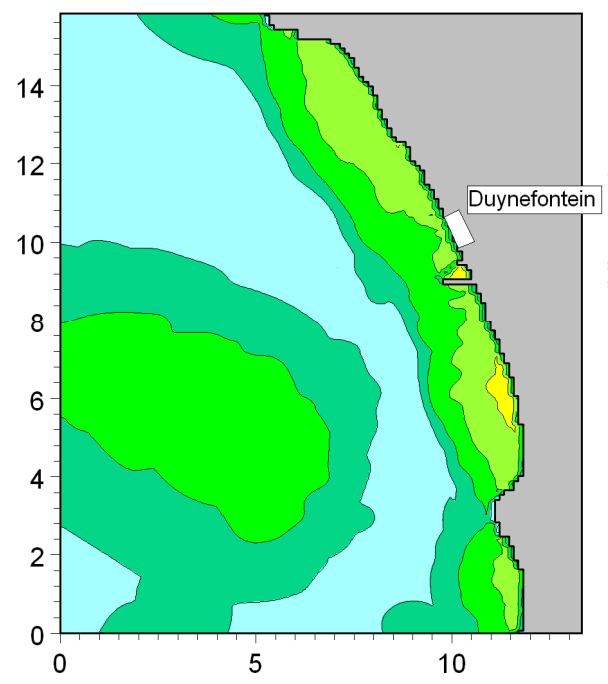
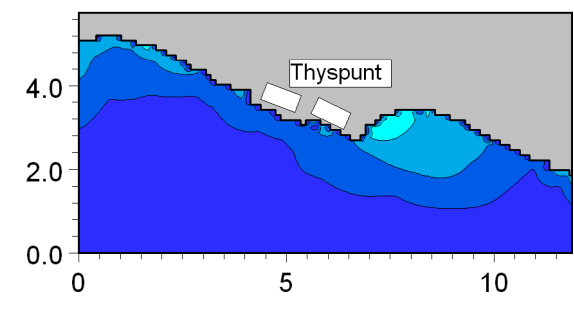
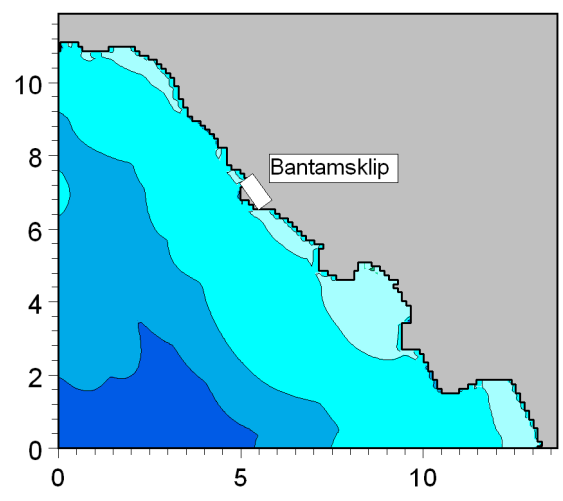
Title:

**Minimum water levels predicted during tsunami event.
Source is theoretical Cape Town Slump (South) with volume of slumped sediment = 80 km³.**

Figure No.

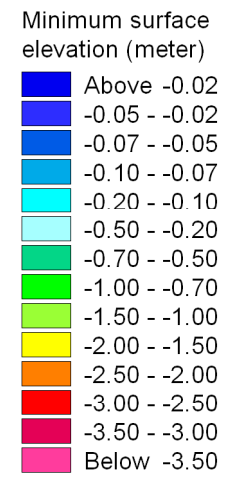
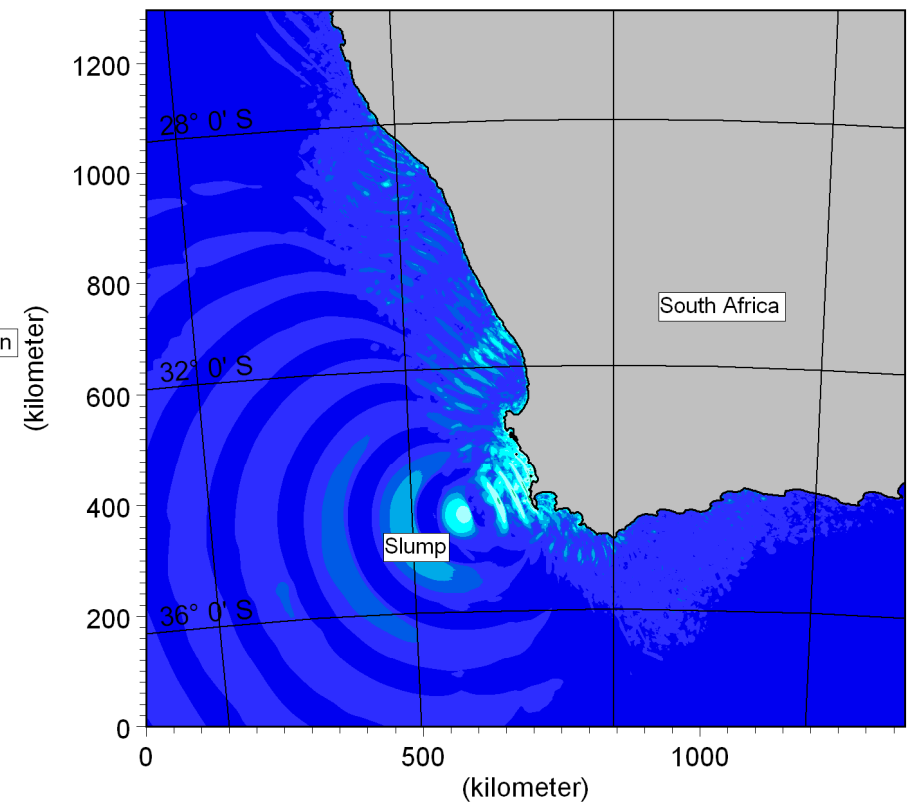
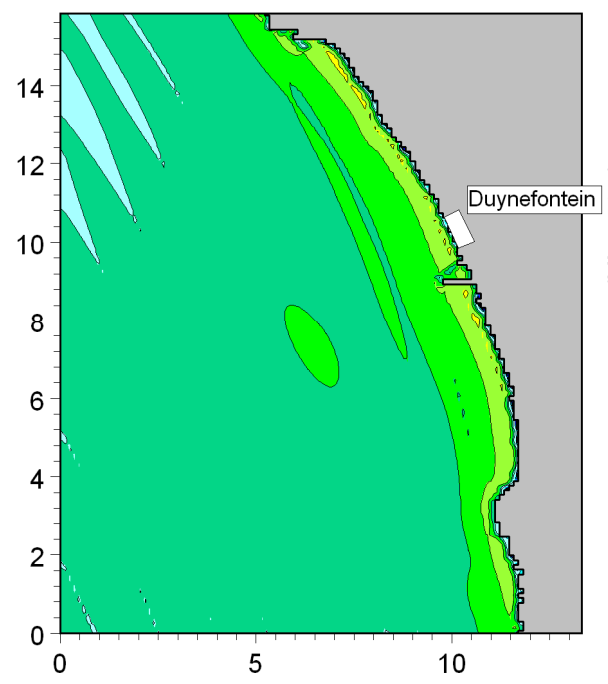
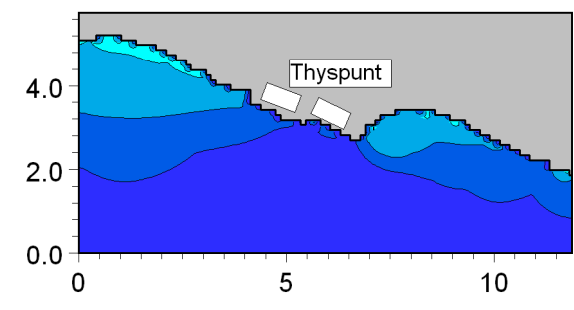
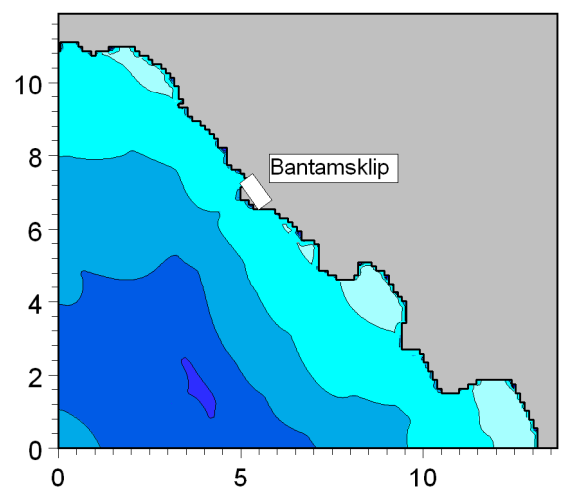
4.23

Run: CapeTownNorth01b

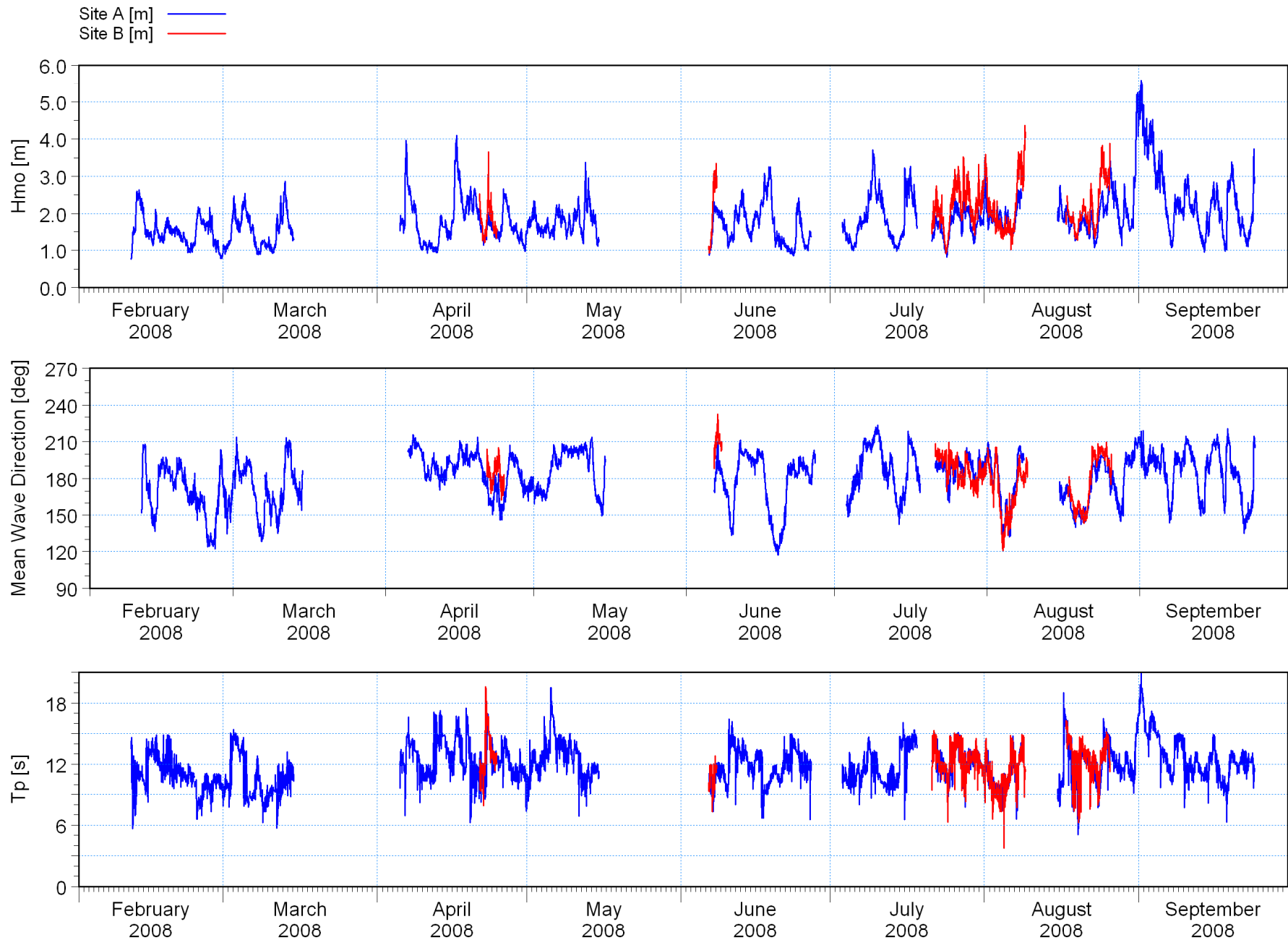


Title: Maximum water levels predicted during tsunami event.
Source is theoretical Cape Town Slump (North) with volume of slumped sediment = 80 km³.

Run: CapeTownNorth01b



Title: Minimum water levels predicted during tsunami event.
Source is theoretical Cape Town Slump (North) with volume of slumped sediment = 80 km³.



le:\Concatenated\Thyspunt_A_W0_P01_02_03_04.dfs0
andle\Concatenated\Thyspunt_B_W0_P02_03_04.dfs0

le:\Concatenated\Thyspunt_A_W0_P01_02_03_04.dfs0
andle\Concatenated\Thyspunt_B_W0_P02_03_04.dfs0

le:\Concatenated\Thyspunt_A_W0_P01_02_03_04.dfs0
andle\Concatenated\Thyspunt_B_W0_P02_03_04.dfs0



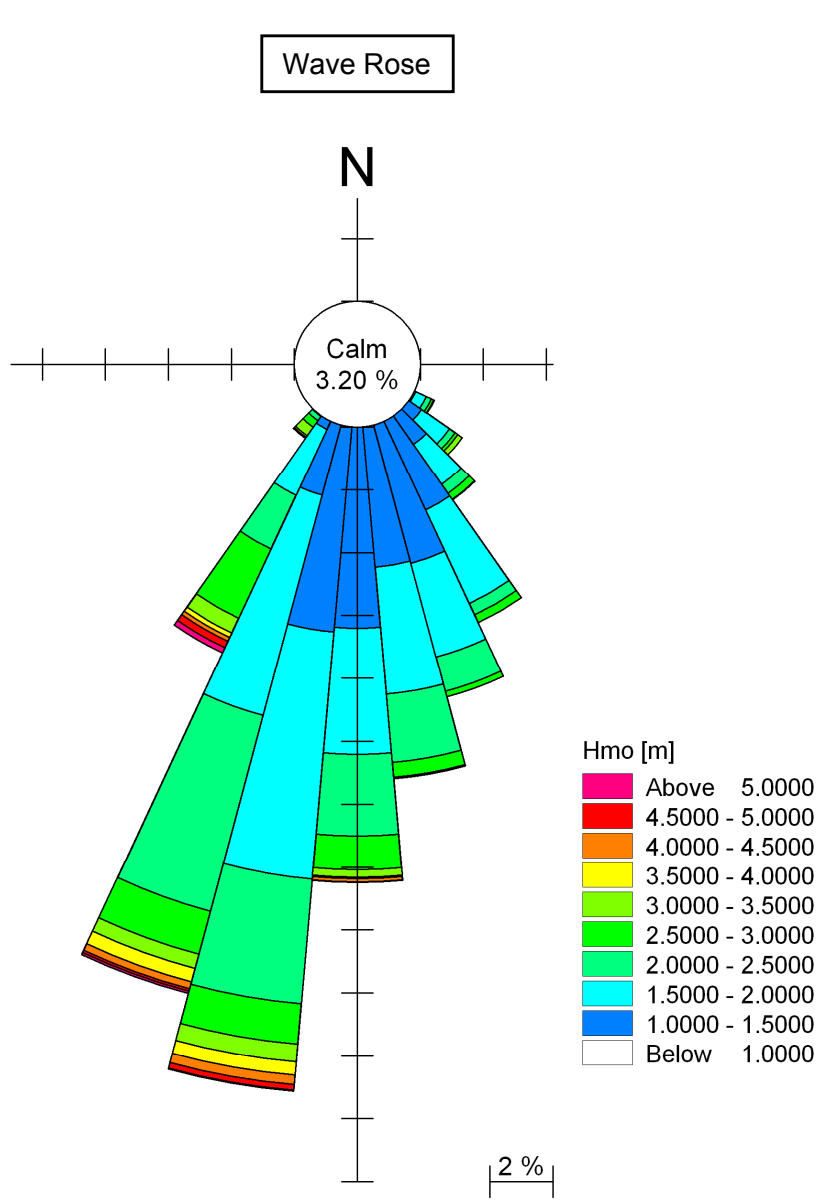
Title:

**Wave measurements at Thyspunt Sites A and B.
Time-series of wave parameters (refer to Figure 3.1 for instrument positions).**

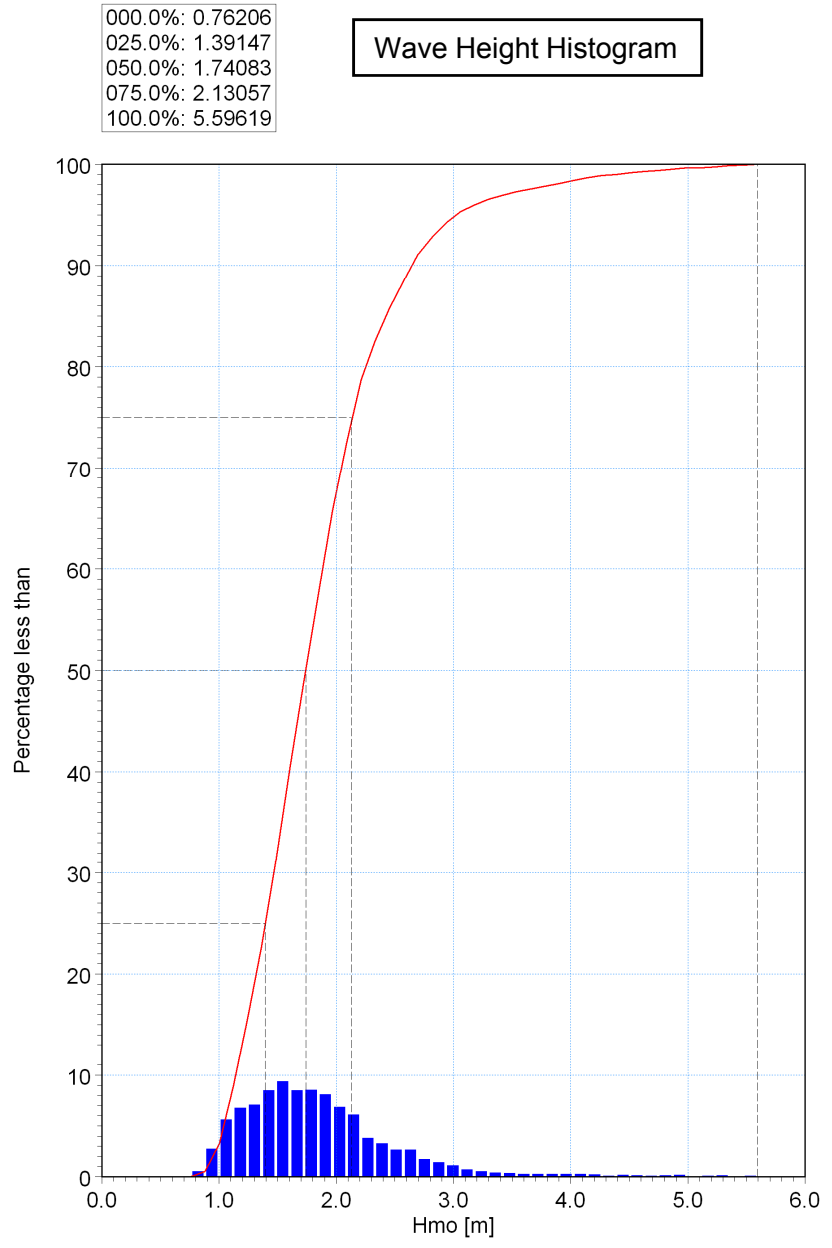
Figure No.

5.1

G:\Projects\1010_NuclearSites\ThyspuntData\Lvandle\Concatenated\Thyspunt_A_WO_P01_02_03_04.dfs0



000.0%: 0.76206
025.0%: 1.39147
050.0%: 1.74083
075.0%: 2.13057
100.0%: 5.59619



G:\Projects\1010_NuclearSites\ThyspuntData\Lvandle\Concatenated\Thyspunt_A_WO_P01_02_03_04.dfs0



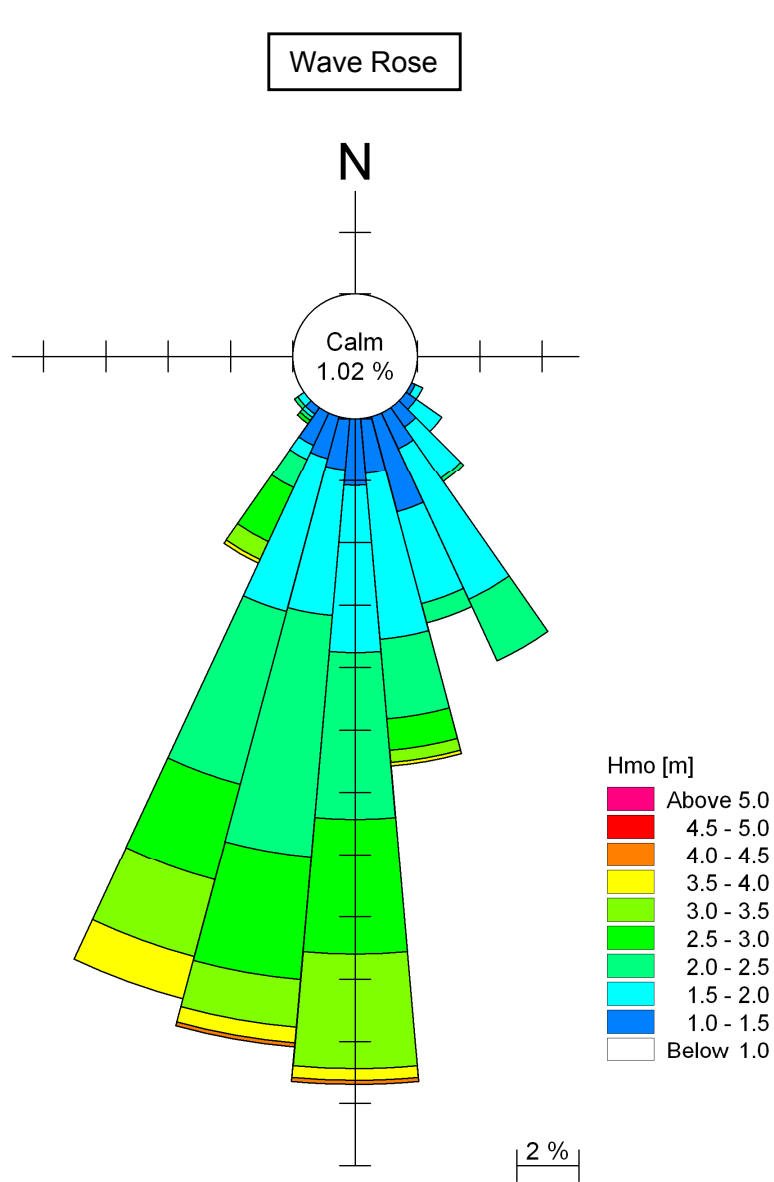
Title:

**Wave measurements at Thyspunt Site A (refer to Figure 3.1 for instrument position).
Wave rose and histogram of wave heights.**

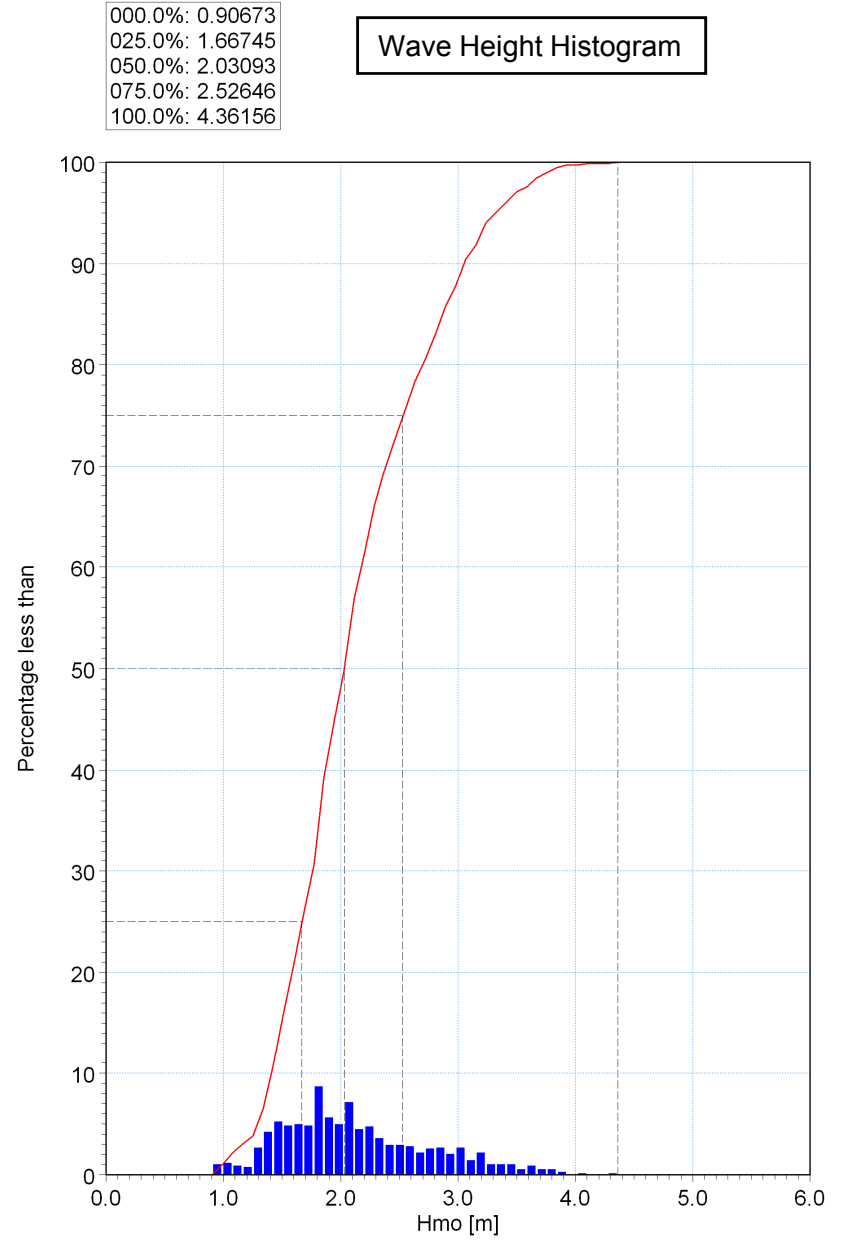
Figure No.

5.2

G:\Projects\1010_Nuclear\Sites\Thyspunt\Data\Lwandle\Concatenated\Thyspunt_B_W0_P02_03_04.dfs0



000.0%: 0.90673
025.0%: 1.66745
050.0%: 2.03093
075.0%: 2.52646
100.0%: 4.36156



G:\Projects\1010_Nuclear\Sites\Thyspunt\Data\Lwandle\Concatenated\Thyspunt_B_W0_P02_03_04.dfs0

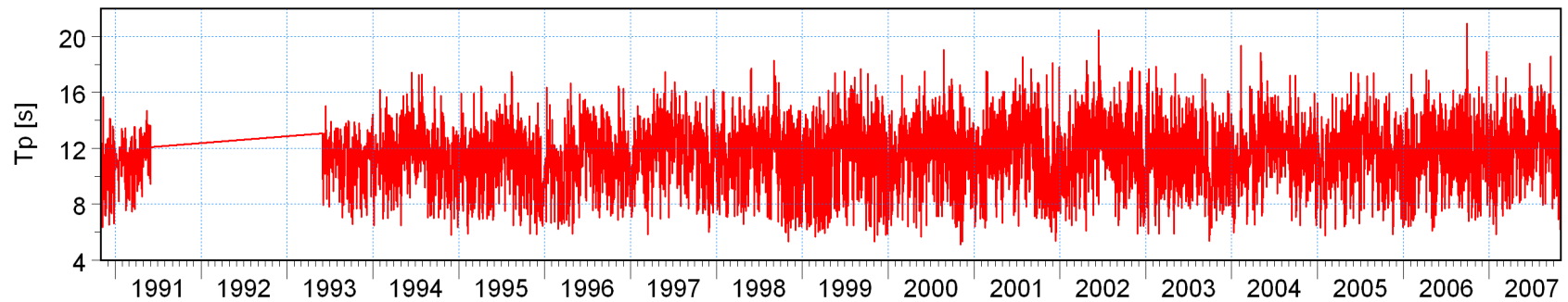
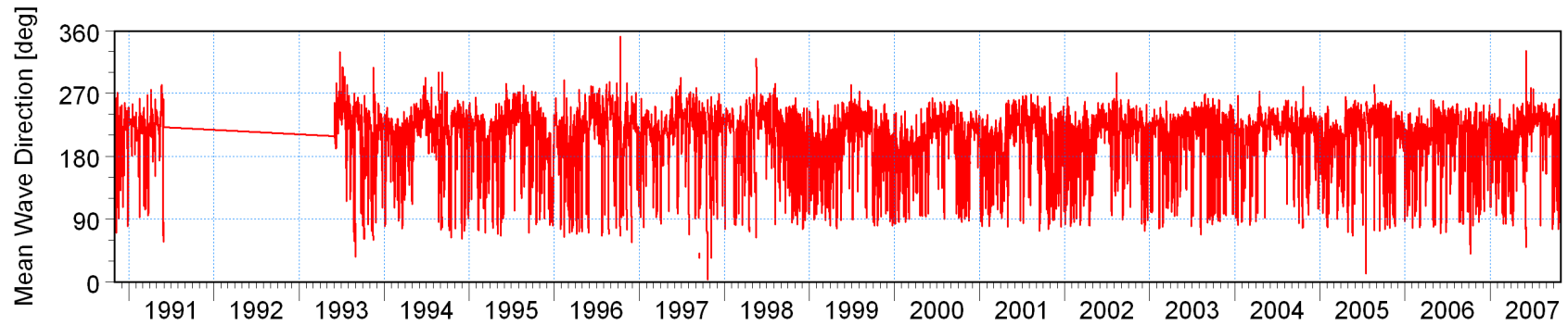
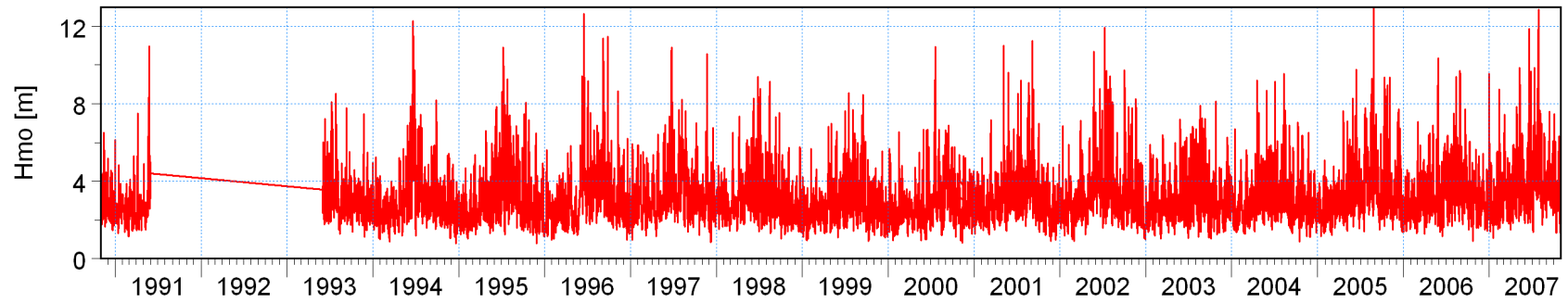


Title:

**Wave measurements at Thyspunt Site B (refer to Figure 3.1 for instrument position).
Wave rose and histogram of wave heights.**

Figure No.

5.3



ised\\Wave_Parameters_Oceanor_e245_s350.dfs0
 cessed\\Wave_Parameters_Oceanor_e245_s350.dfs0
 ised\\Wave_Parameters_Oceanor_e245_s350.dfs0

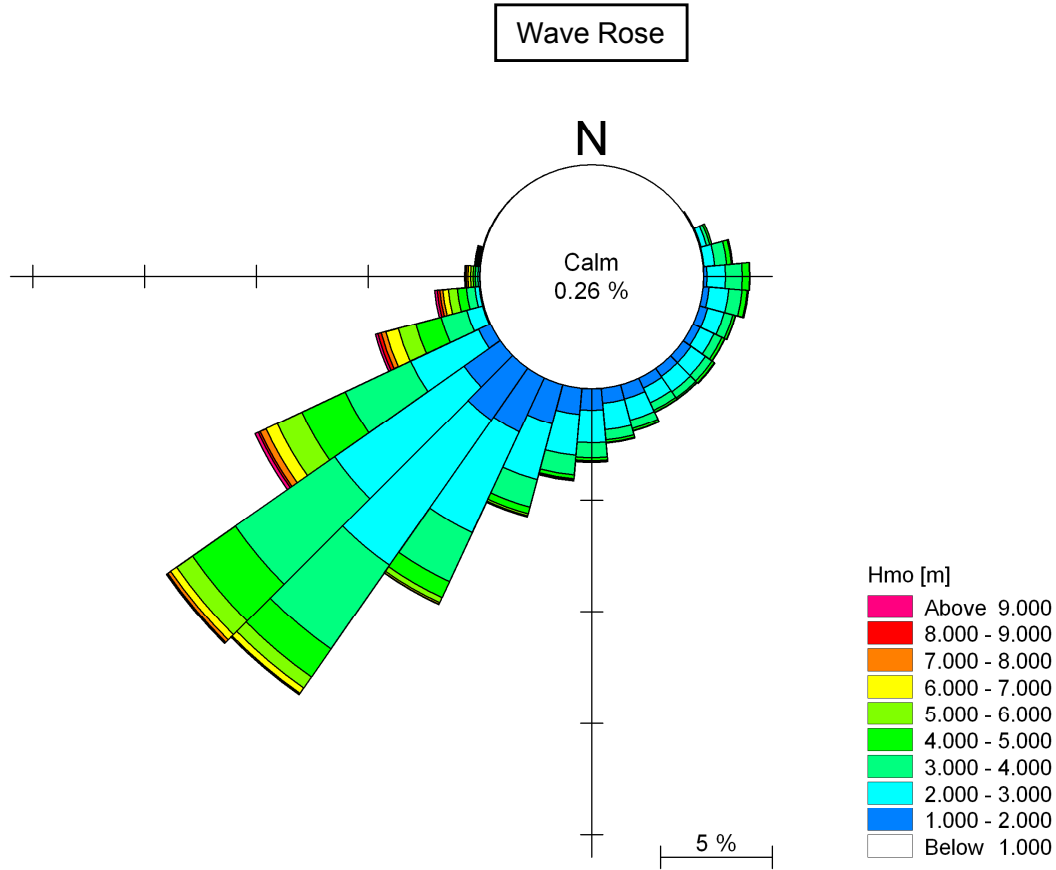


Title:

**Time-series of offshore wave hindcast parameters.
 Position is E 24.5°E, S 35.0° in 900 m depth (refer to Figure 5.6 for position).**

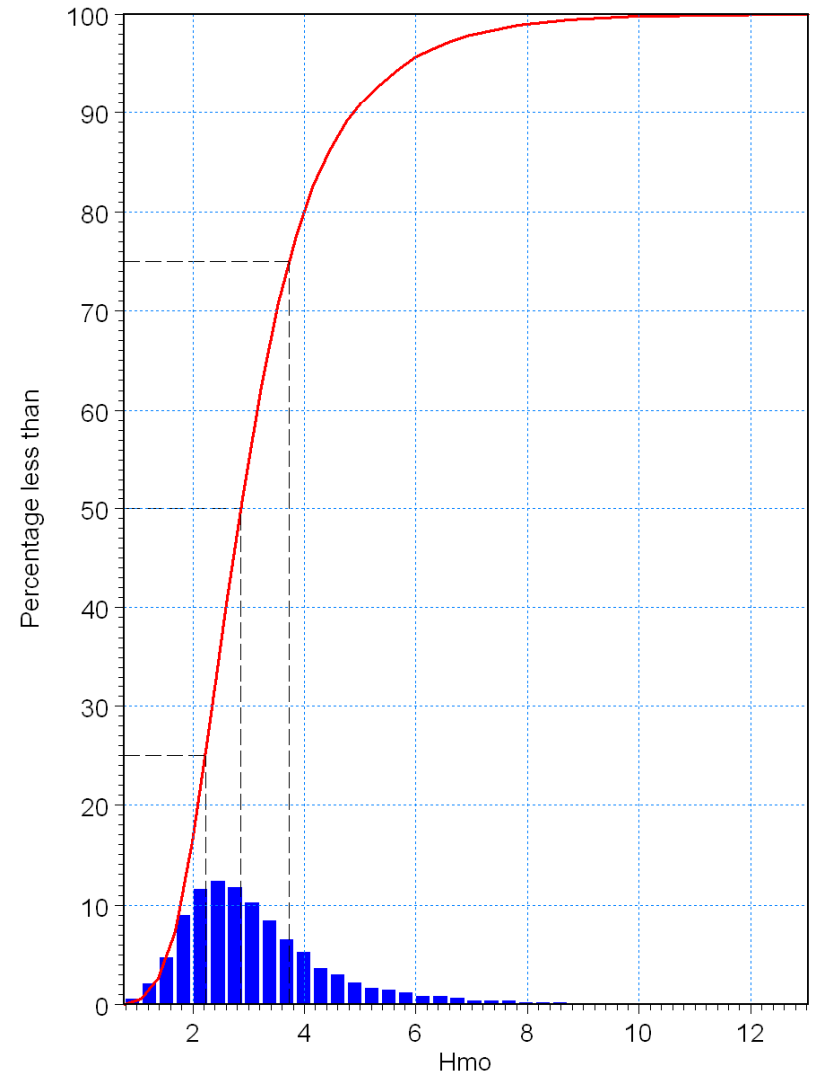
Figure No.

5.4



000.0%: 0.77000
 025.0%: 2.23000
 050.0%: 2.86000
 075.0%: 3.72000
 100.0%: 13.03000

Wave Height Histogram

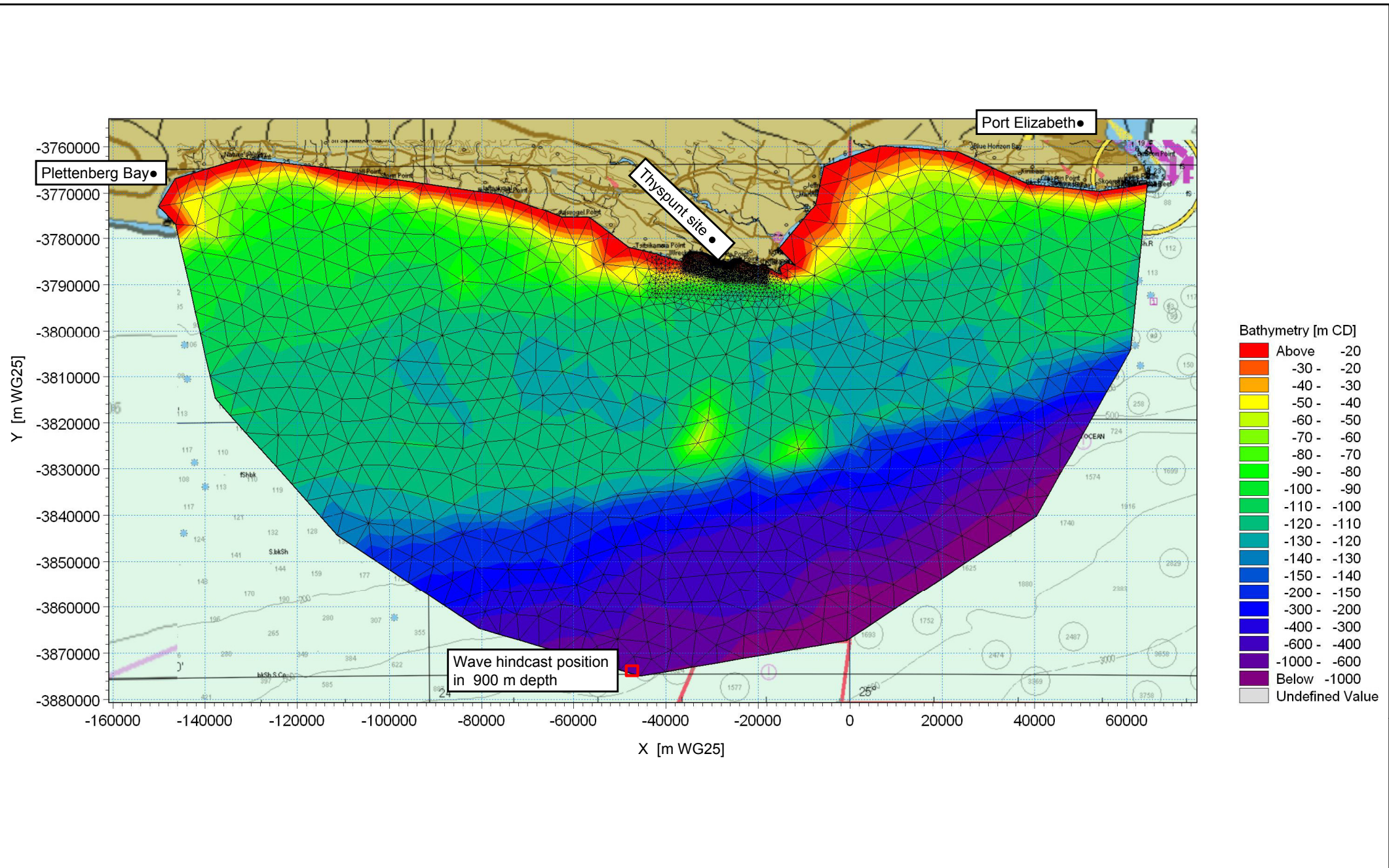


Title:

**Rose and histogram of offshore wave hindcast data.
 Position is E 24.5°, S 35.0° in 900 m depth (refer to Figure 5.6 for position).**

Figure No.

5.5

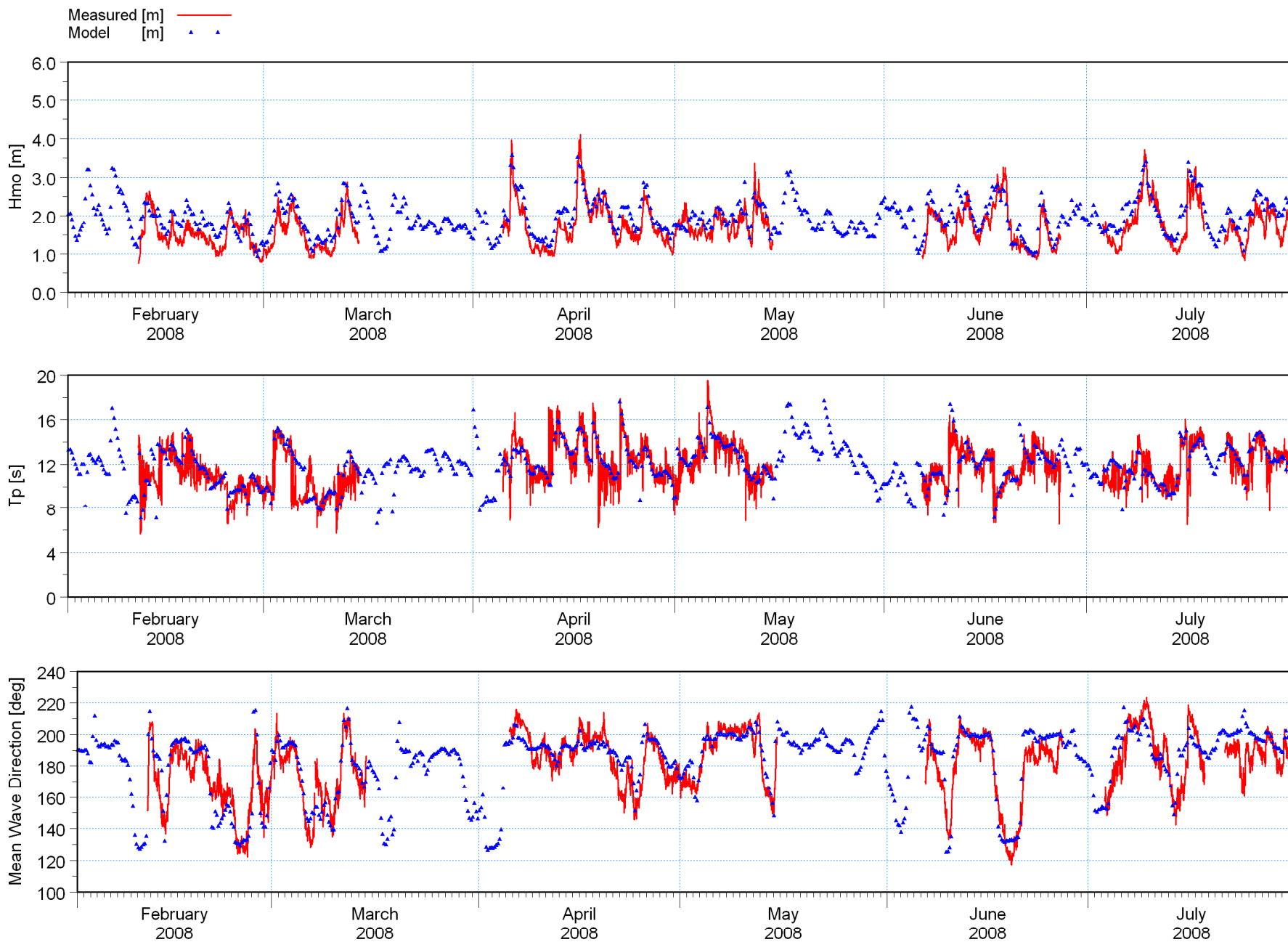


Title:

Numerical mesh used for wave refraction modelling.

Figure No.

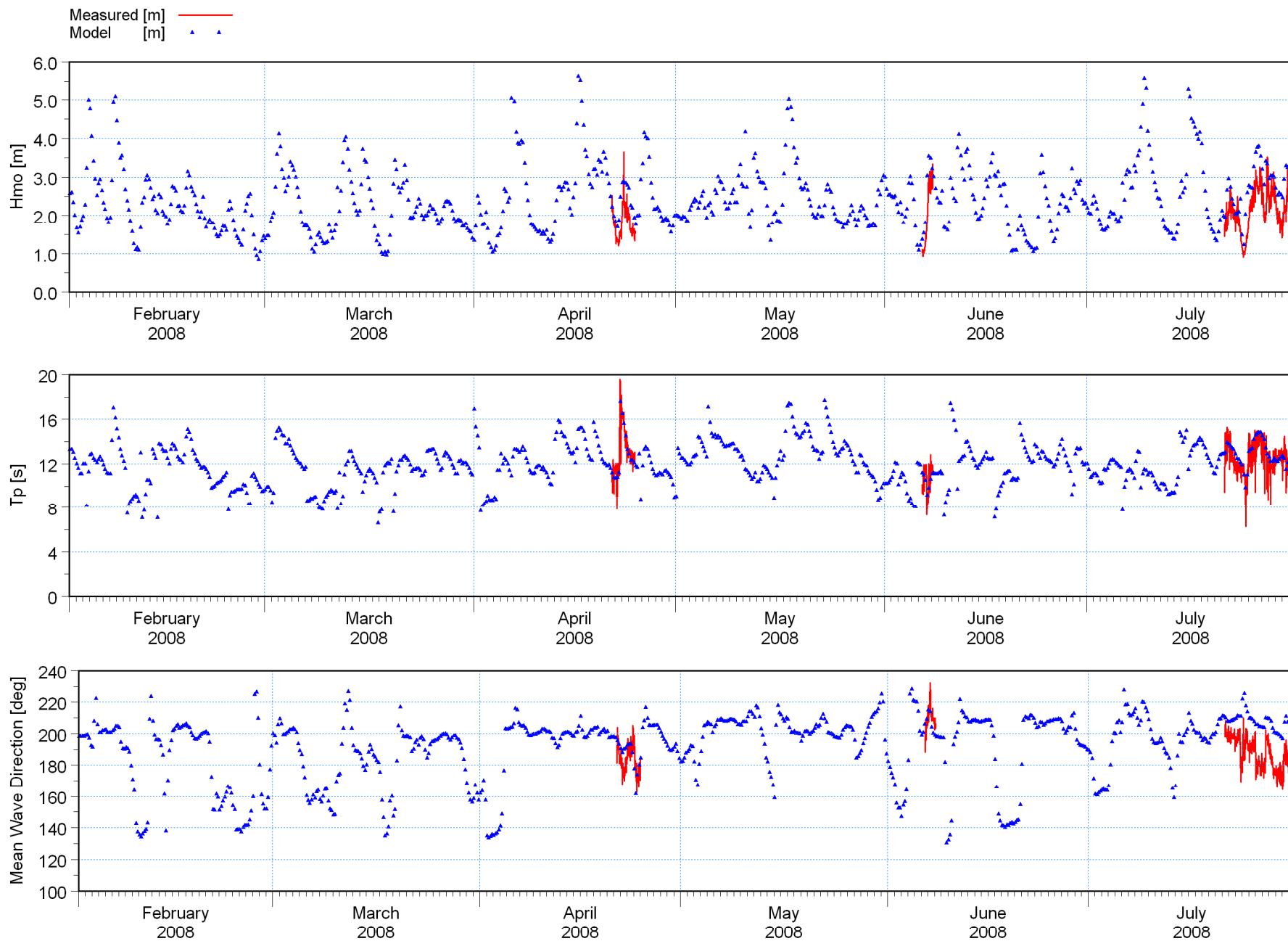
5.6



\\lrvandile\Concatenated\Thyspunt_A_WD_P01_P02_P03.dfs0
 \Models\Plume\00q.sw - Result Files\Parameters_Point.dfs0
 \andile\Concatenated\Thyspunt_A_WD_P01_P02_P03.dfs0
 \deis\Plume\00q.sw - Result Files\Parameters_Point.dfs0
 \andile\Concatenated\Thyspunt_A_WD_P01_P02_P03.dfs0
 \deis\Plume\00q.sw - Result Files\Parameters_Point.dfs0



Title: Calibration of wave model.
Measured and modelled time-series of wave parameters at Site A (refer to Figure 3.1 for location).

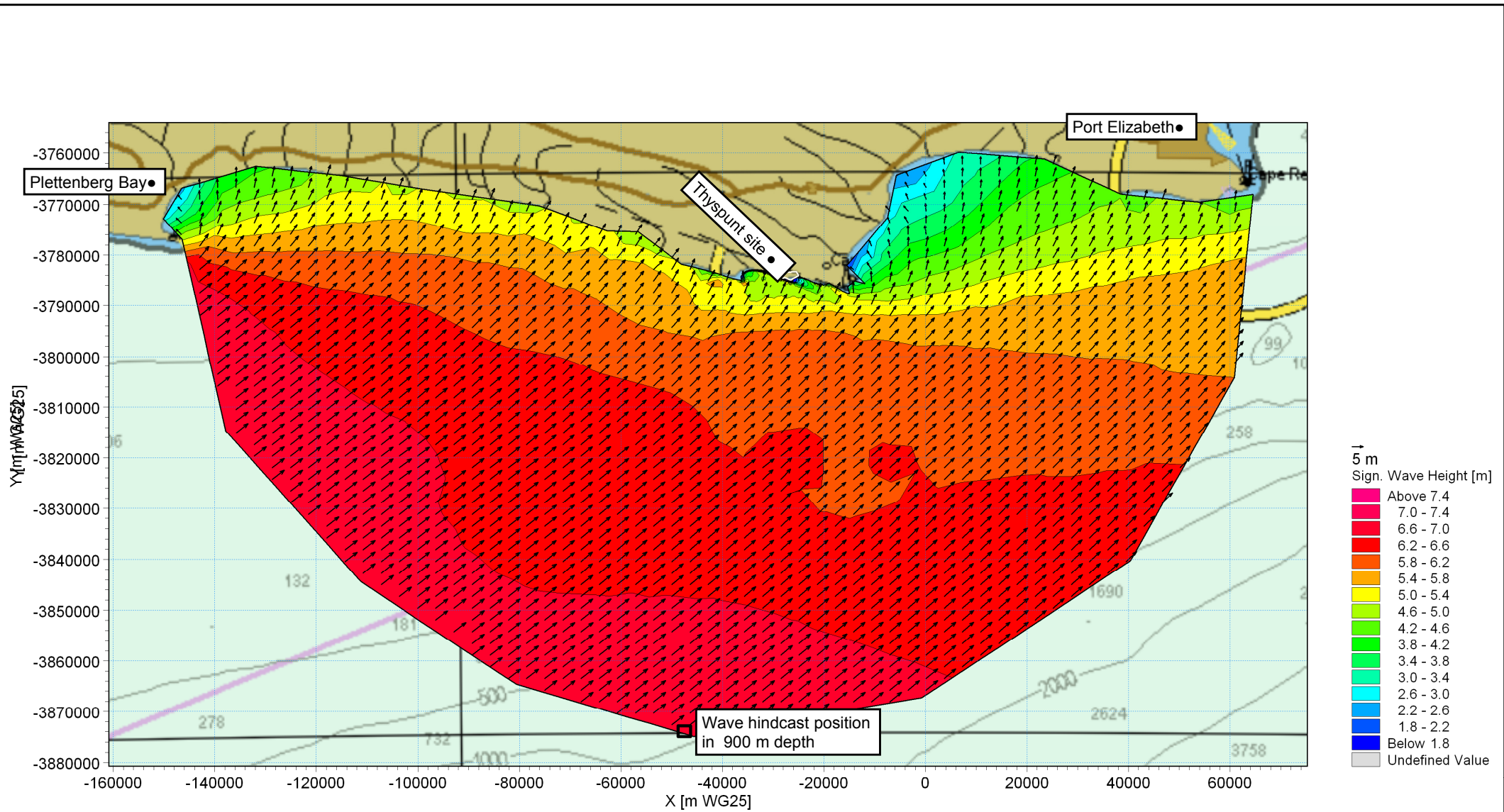


:\Data\Lwandle\Concatenated\Thyspunt_B_WD_P02_P03.dfs0
 \Models\Plume\d00q.sw - Result Files\Parameters_Point.dfs0
 ta\Lwandle\Concatenated\Thyspunt_B_WD_P02_P03.dfs0
 deis\Plume\d00q.sw - Result Files\Parameters_Point.dfs0
 ita\Lwandle\Concatenated\Thyspunt_B_WD_P02_P03.dfs0
 deis\Plume\d00q.sw - Result Files\Parameters_Point.dfs0



Title:
Calibration of wave model.
Measured and modelled time-series of wave parameters at Site B (refer to Figure 3.1 for location).

Figure No.
5.8



17:00:00 2008-05-17 Time Step 853 of 1454.

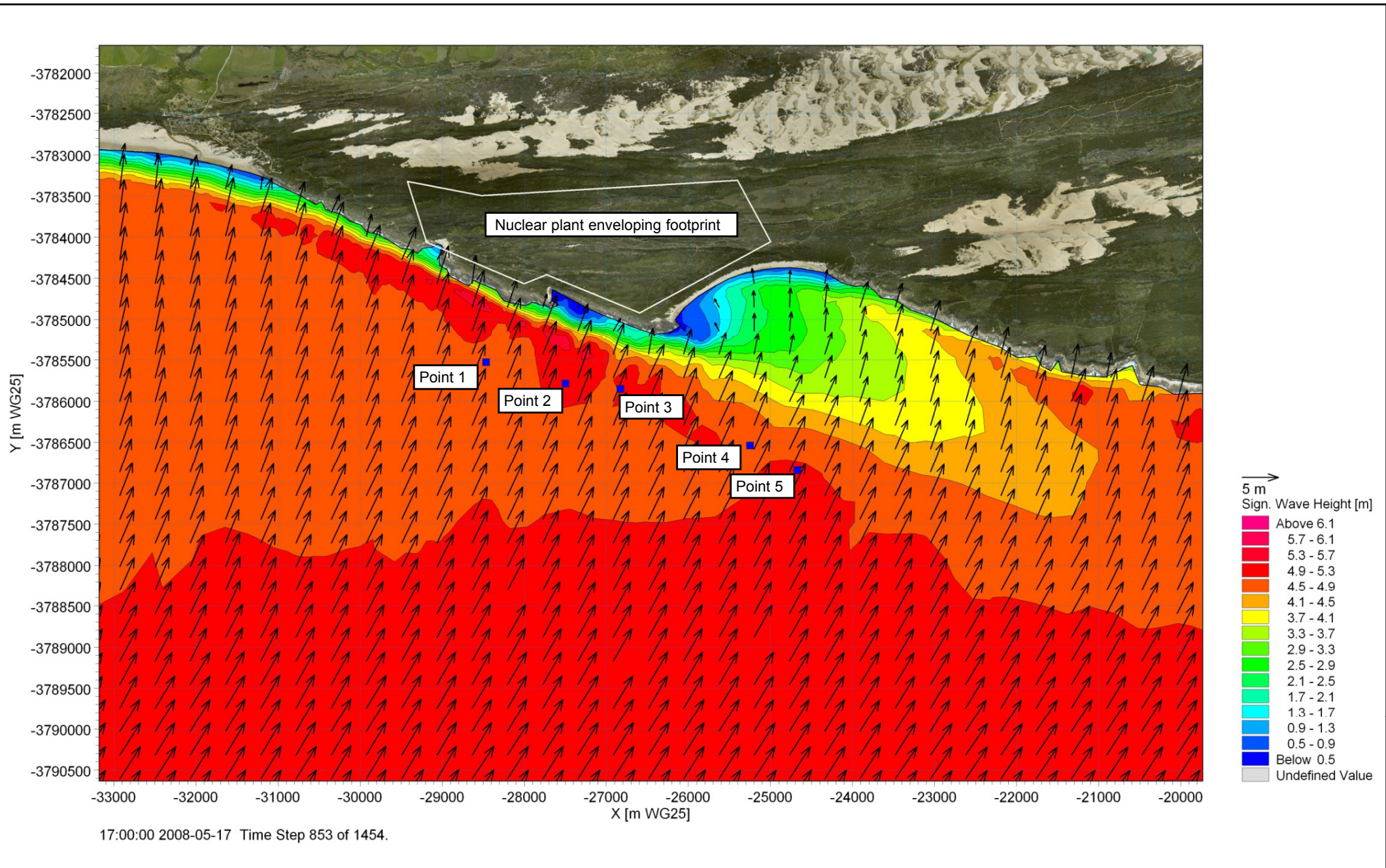


Title:

Example of wave refraction from offshore to Thyspunt site.
 Deepwater wave condition: $H_{m0} = 6.6$ m, $T_p = 17.2$ s, $Dir = 233^\circ$.

Figure No.

5.9



Title:

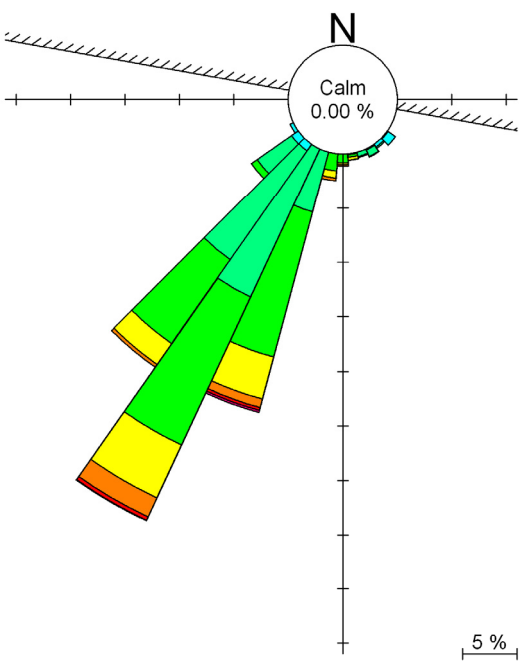
**Example of wave refraction from offshore to Thyspunt site.
 Deepwater wave condition: $H_{m0} = 6.6$ m, $T_p = 17.2$ s, $Dir = 233^\circ$.
 Model output points along -30 m CD contour indicated.**

Figure No.

5.10

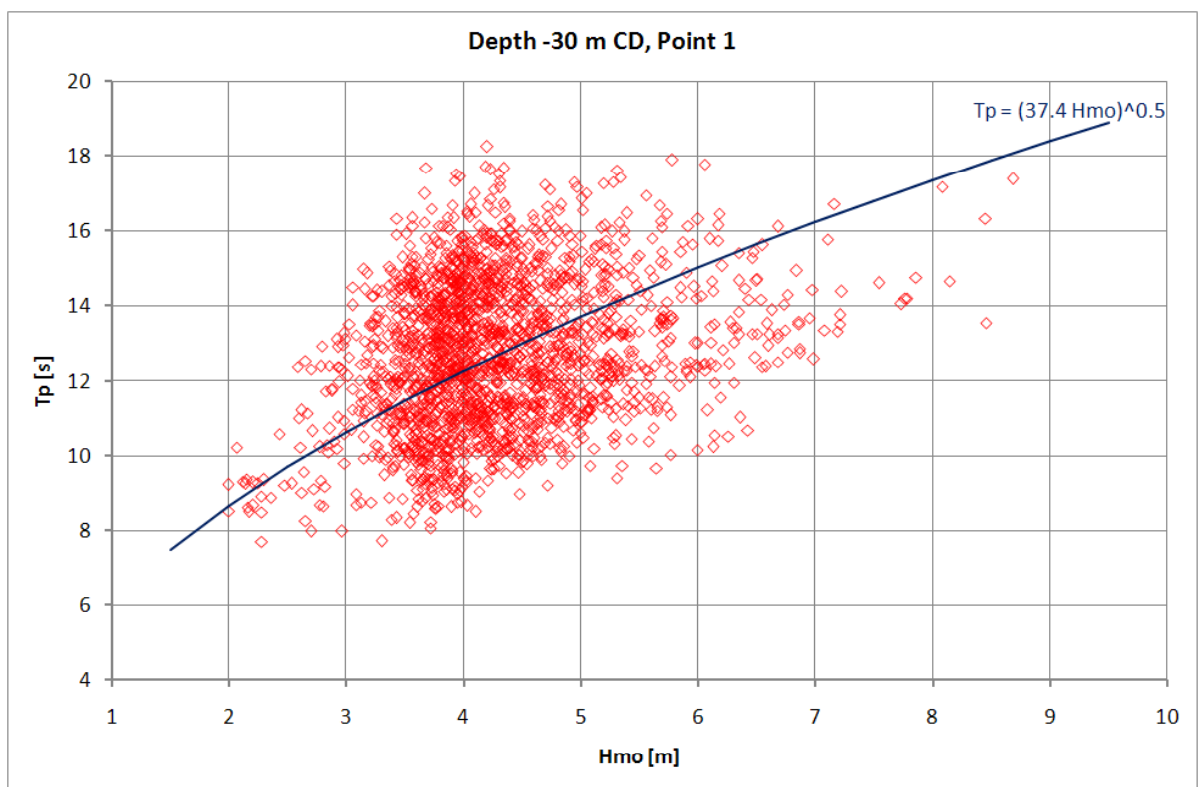
G:\Projects\1010_Nuclear\Sites\Thyspunt\Models\Waves\1a.sv - Result Files\Parameters_Point_Feat.dfs0

Wave Rose



- Hmo [m]
- Above 8.0000
 - 7.0000 - 8.0000
 - 6.0000 - 7.0000
 - 5.0000 - 6.0000
 - 4.0000 - 5.0000
 - 3.0000 - 4.0000
 - 2.0000 - 3.0000
 - 1.0000 - 2.0000
 - Below 1.0000

Wave Height – Period Relationship

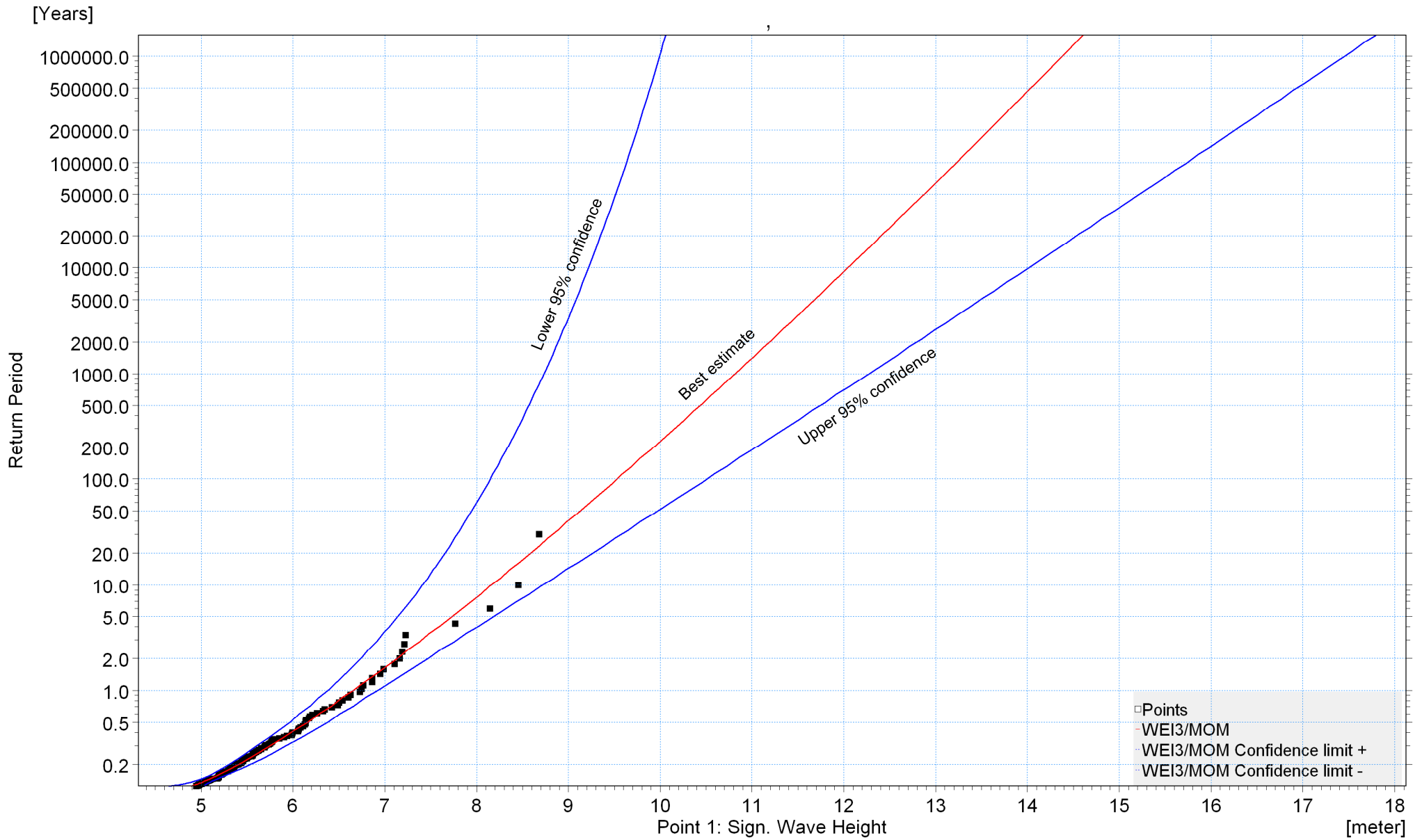


Title:

**Characterisation of storm waves refracted to -30 m CD depth at Thyspunt site.
Includes only storms where the offshore $H_{m0} > 5.0$ m.**

Figure No.

5.11

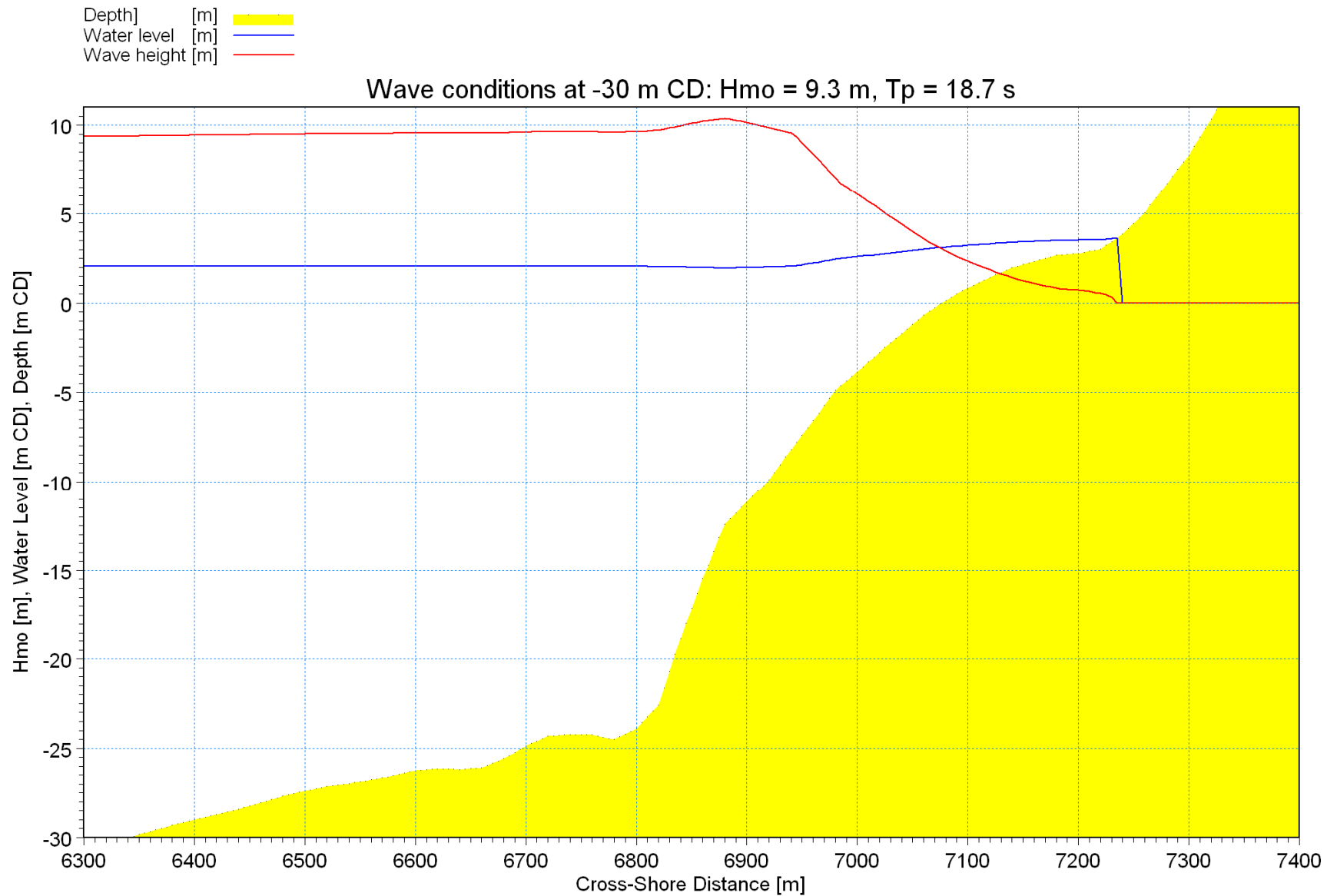


Title:

Extreme value analysis of waves at -30 m CD depth at Point 1.

Figure No.

5.12



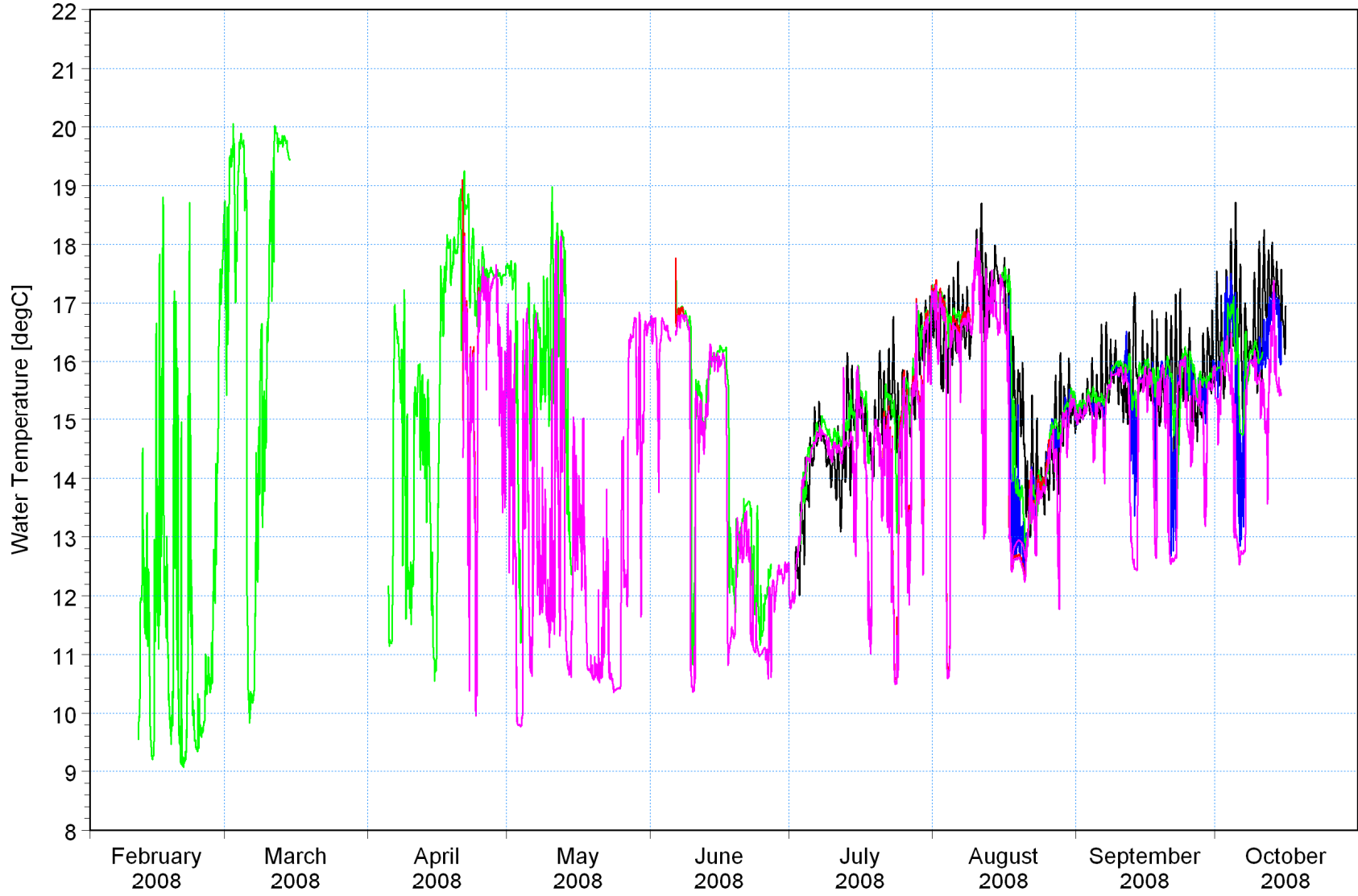
Title:

Example of cross-shore wave transformation modelling from -30 m CD depth to shoreline.

Figure No.

5.13

Instrument depth 1.8 m (Tide Gauge) [deg C] ———
 Instrument depth 10 m (Mooring at Site B) [deg C] ———
 Instrument depth 15 m (ADCP at Site A) [deg C] ———
 Instrument depth 27 m (ADCP at Site B) [deg C] ———
 Instrument depth 27 m (Mooring at Site B) [deg C] ———



G:\Projects\1010_NuclearSites\ThyspuntData\L\wandle\Concatenated\Thyspunt_C_R0_P03_04.dfs0
 G:\Projects\1010_NuclearSites\ThyspuntData\L\wandle\PO4\Processed\Thyspunt_D_R1_P04.dfs0
 G:\Projects\1010_NuclearSites\ThyspuntData\L\wandle\Concatenated\Thyspunt_A_C2_P01_02_03_04.dfs0
 G:\Projects\1010_NuclearSites\ThyspuntData\L\wandle\Concatenated\Thyspunt_B_C2_P02_03_04.dfs0
 G:\Projects\1010_NuclearSites\ThyspuntData\L\wandle\Concatenated\Thyspunt_D_R2_P02_03_04.dfs0

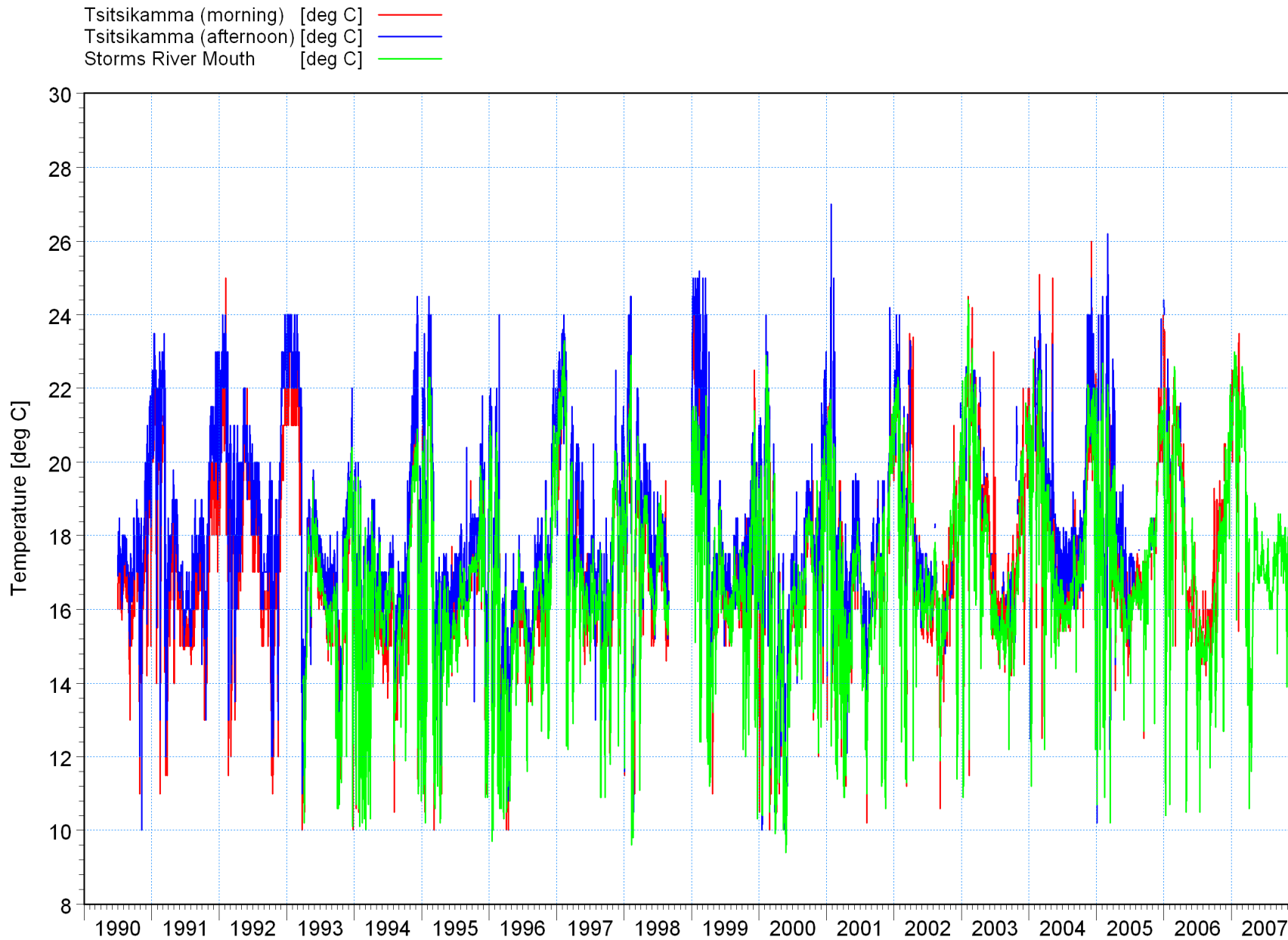


Title:

**Measured water temperatures at Thyspunt
 (Refer to Figure 3.1 for instrument positions).**

Figure No.

6.1



D:\Projects\1010_NuclearSites\Thyspunt\Data\Sea_Temperature\Temperature_SAWS_Tsitsikamma_AM_Station136.dfs0
 D:\Projects\1010_NuclearSites\Thyspunt\Data\Sea_Temperature\Temperature_SAWS_Tsitsikamma_PM_Station137.dfs0
 D:\Projects\1010_NuclearSites\Thyspunt\Data\Sea_Temperature\Temperature_SAWS_Storms_River_Mouth_Station138.dfs0

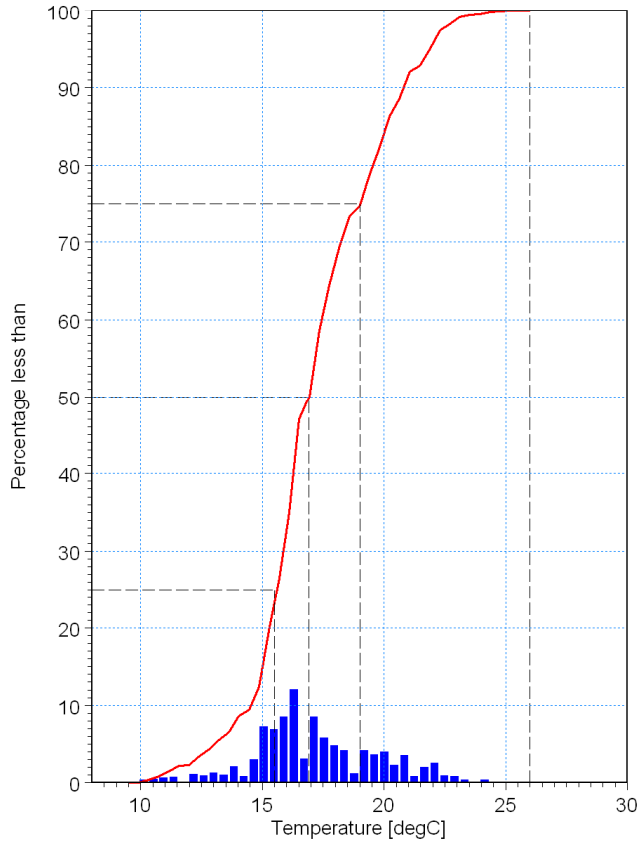


Title:
Time-series of measured sea temperatures (in surf-zone) at Tsitsikamma and Storms River Mouth
(refer to Figure 1.1 for instrument positions).

Figure No.
6.2

Tsitsikamma (morning)

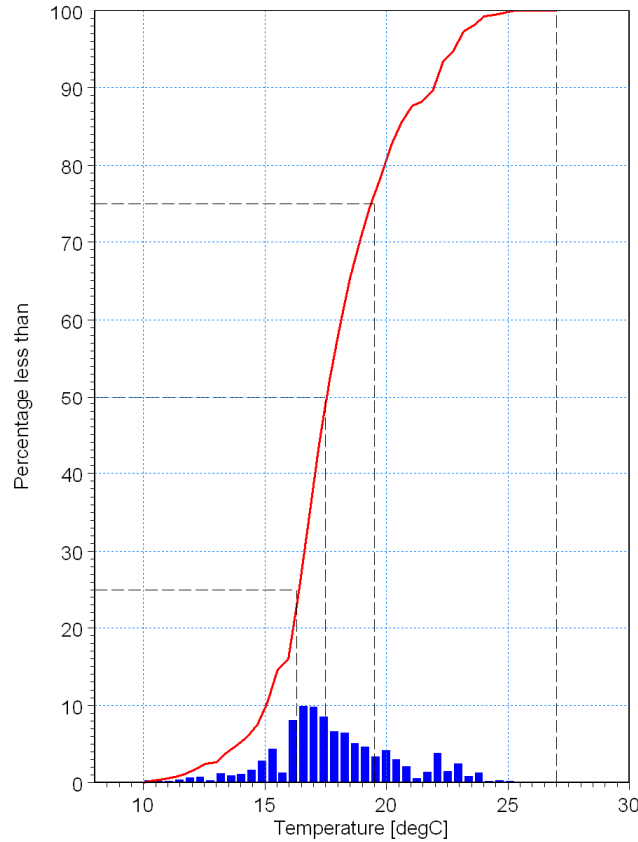
000.0%:	10.00000
025.0%:	15.50000
050.0%:	16.90000
075.0%:	19.00000
100.0%:	26.00000



D:\Projects\1010_NuclearSites\Thyspunt\DataSea_Temperature\Temperature_SAVS_Tsitsikamma_AM_Station136.dfs0

Tsitsikamma (afternoon)

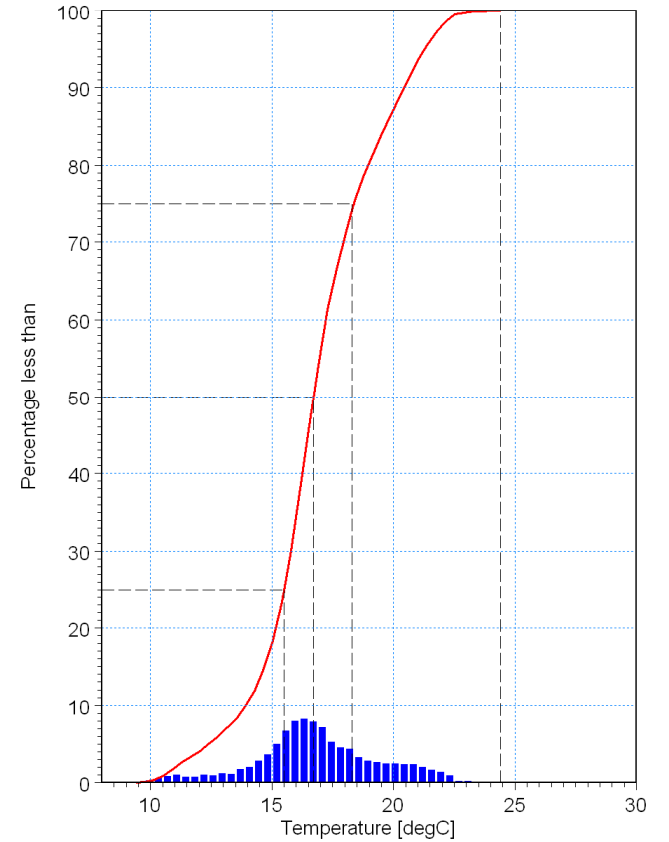
000.0%:	10.00000
025.0%:	16.30000
050.0%:	17.50000
075.0%:	19.50000
100.0%:	27.00000



D:\Projects\1010_NuclearSites\Thyspunt\DataSea_Temperature\Temperature_SAVS_Tsitsikamma_PM_Station137.dfs0

Storms River Mouth

000.0%:	9.40000
025.0%:	15.50000
050.0%:	16.70000
075.0%:	18.30000
100.0%:	24.40000

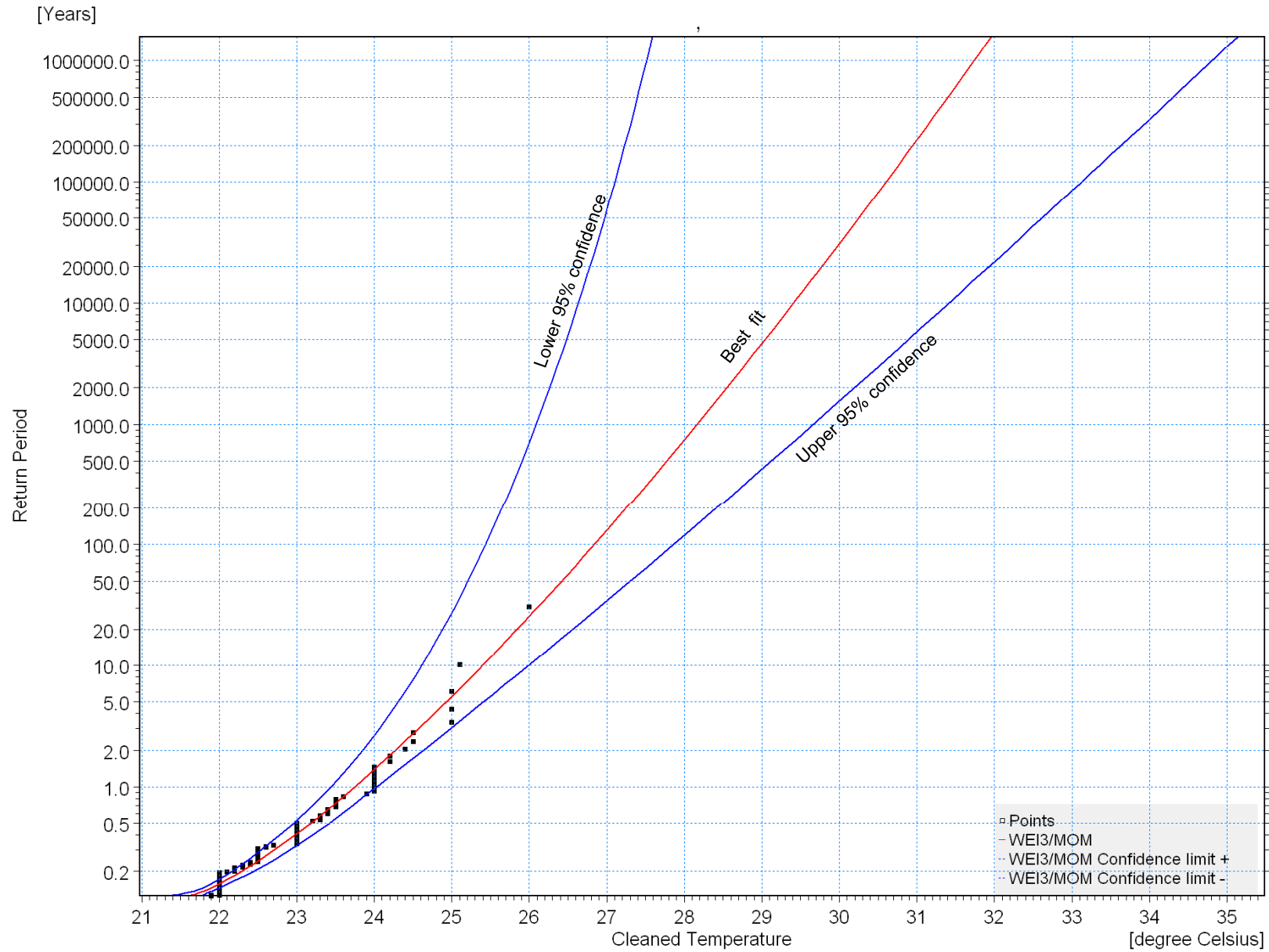


D:\Projects\1010_NuclearSites\Thyspunt\DataSea_Temperature\Temperature_SAVS_Storms_River_Mouth_Station138.dfs0



Title:
Histograms of measured sea temperatures (in surf-zone) at Tsitsikamma and Storms River Mouth (refer to Figure 1.1 for instrument positions).

Figure No.
6.3

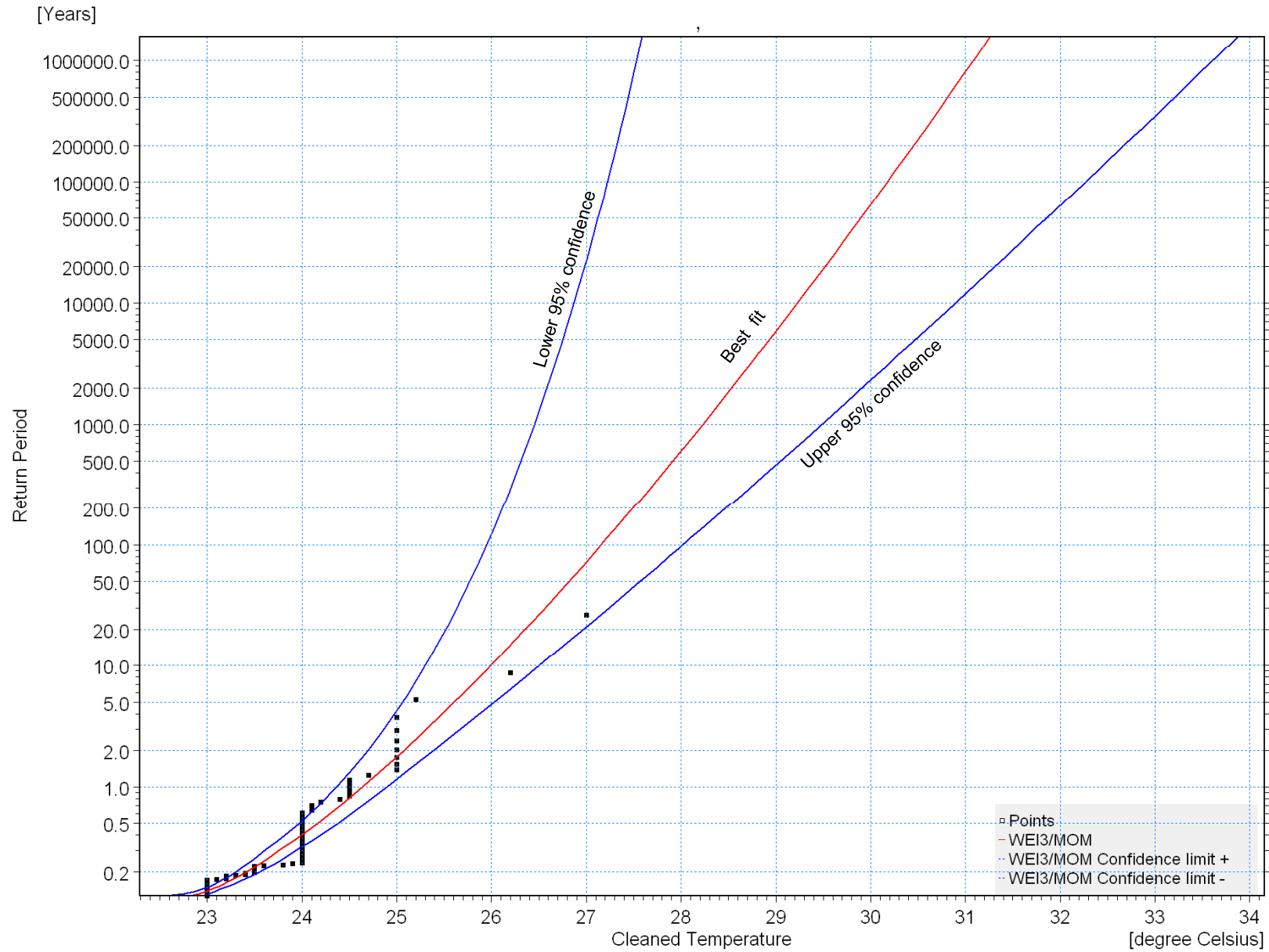


Title:

Extreme Value Analysis of measured sea temperatures (in surf-zone) at Tsitsikamma (morning).

Figure No.

6.4

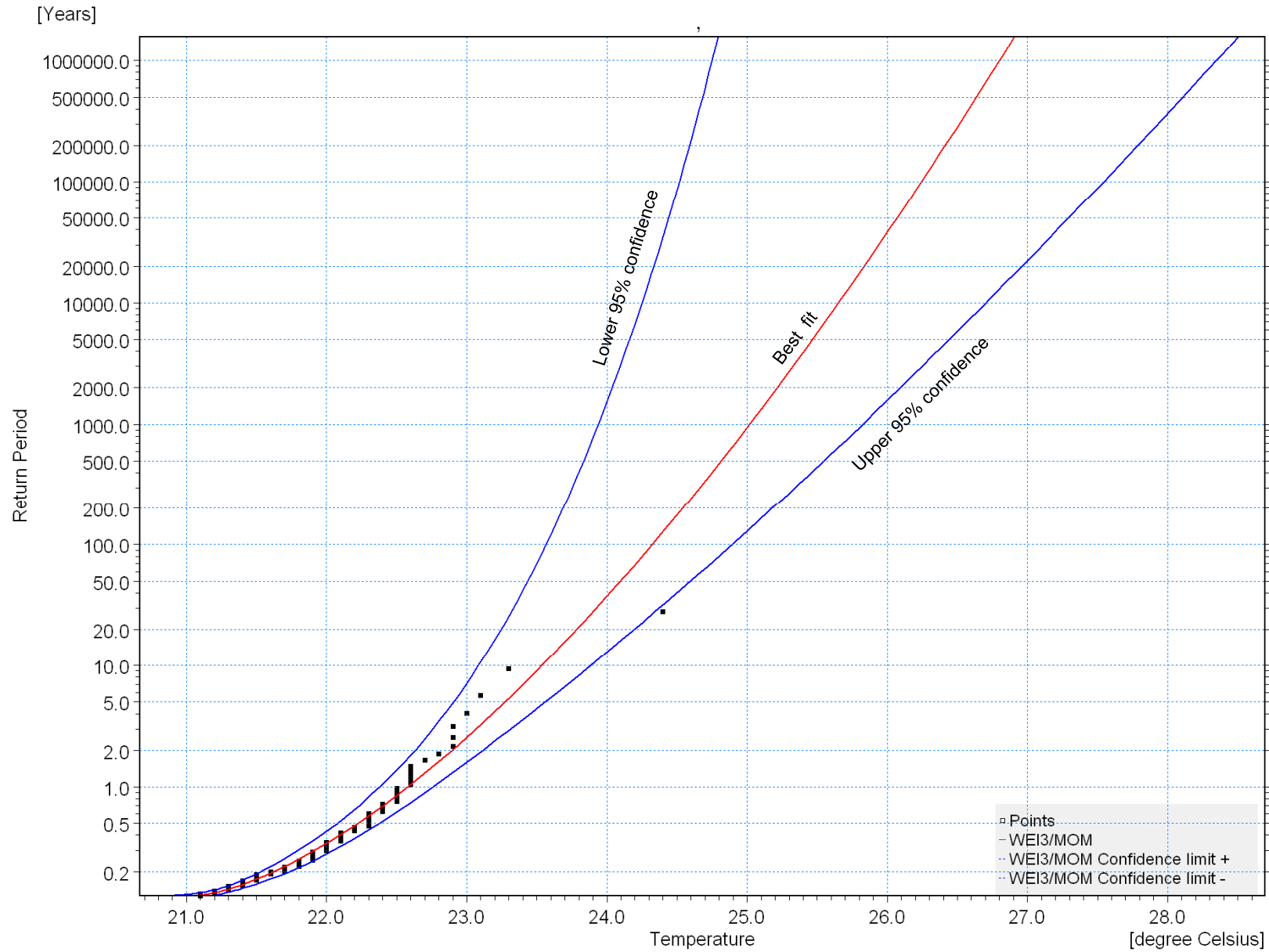


Title:

Extreme Value Analysis of measured sea temperatures (in surf-zone) at Tsitsikamma (evening).

Figure No.

6.5

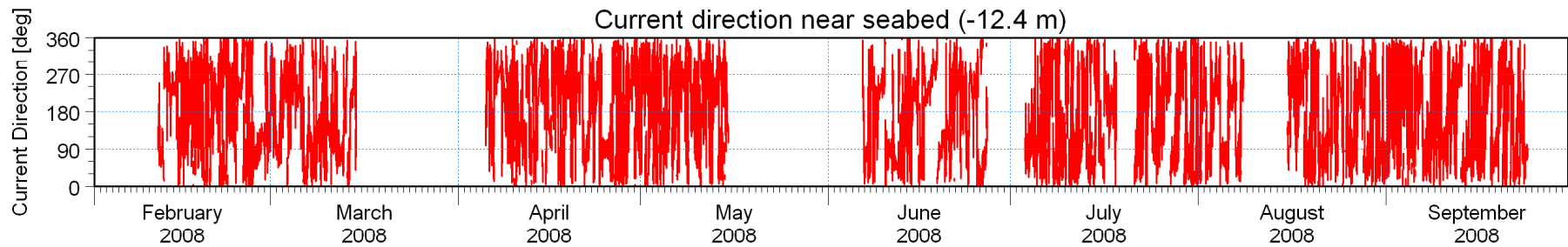
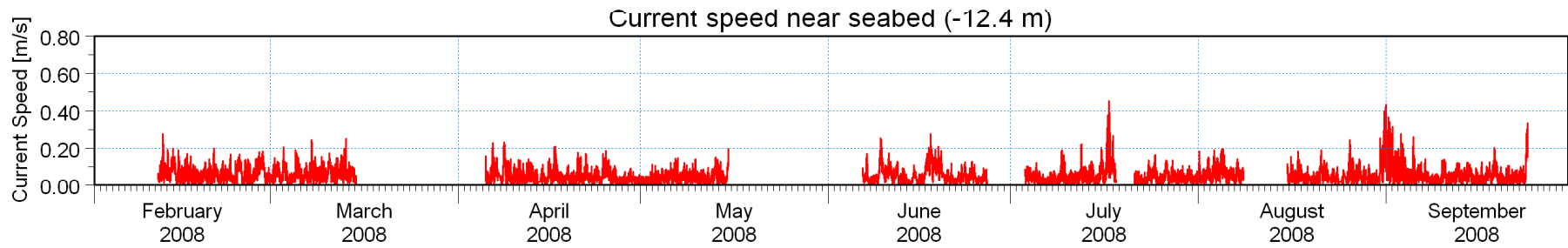
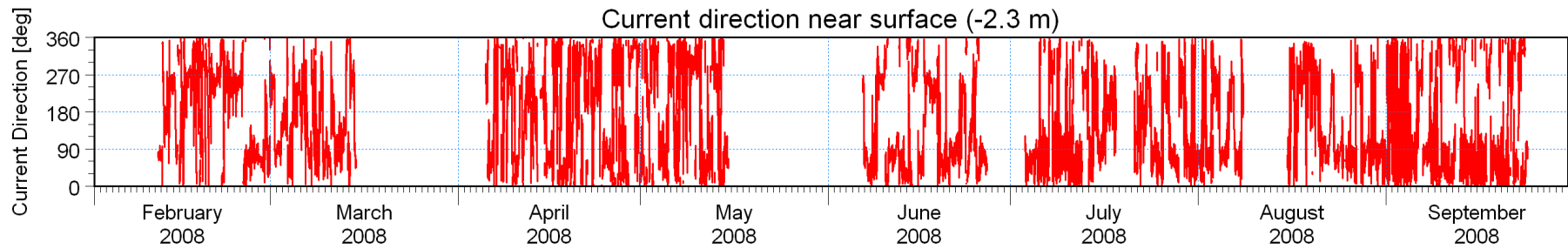
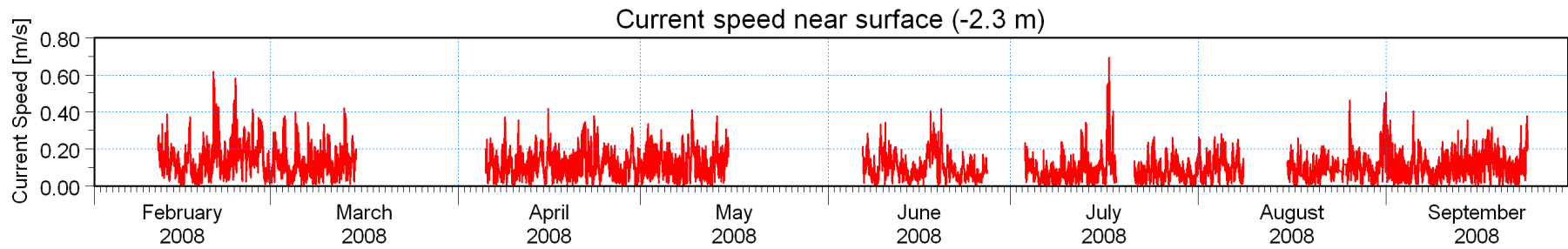


Title:

Extreme Value Analysis of measured sea temperatures (in surf-zone) at Storms River Mouth.

Figure No.

6.6



I:\Thyspunt_A_C1_P01_02_03_04.dfs0

I:\Thyspunt_A_C1_P01_02_03_04.dfs0

I:\Thyspunt_A_C1_P01_02_03_04.dfs0

I:\Thyspunt_A_C1_P01_02_03_04.dfs0

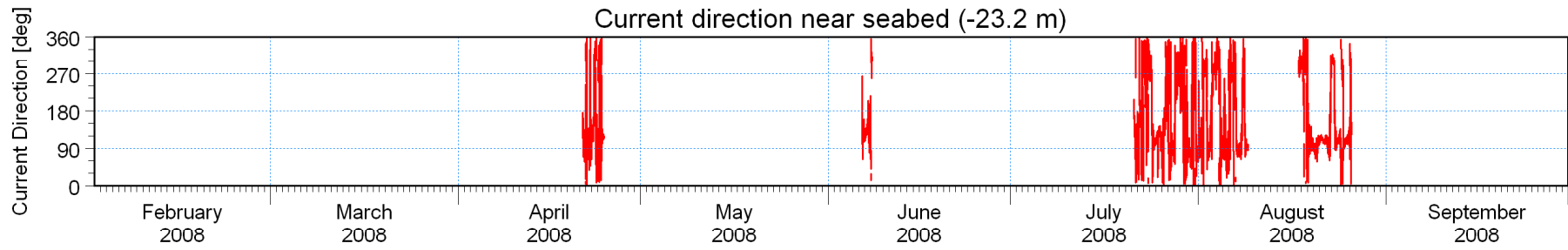
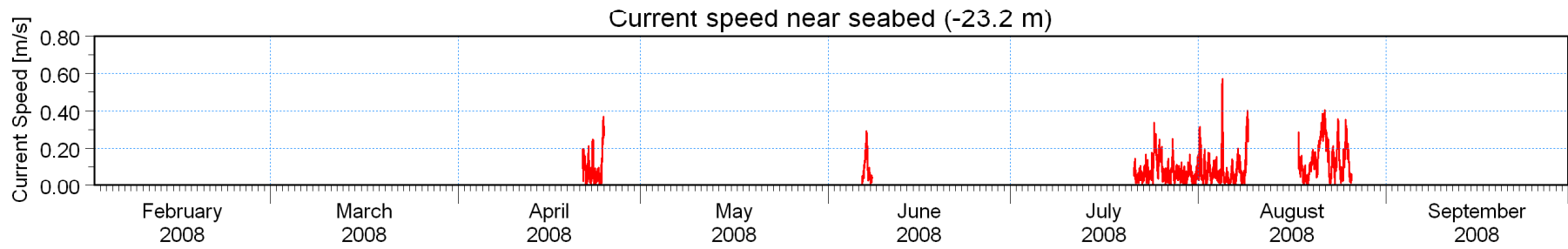
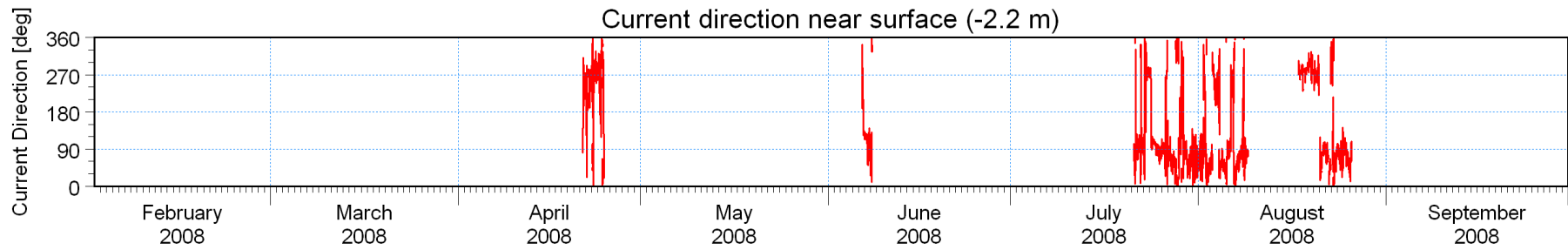
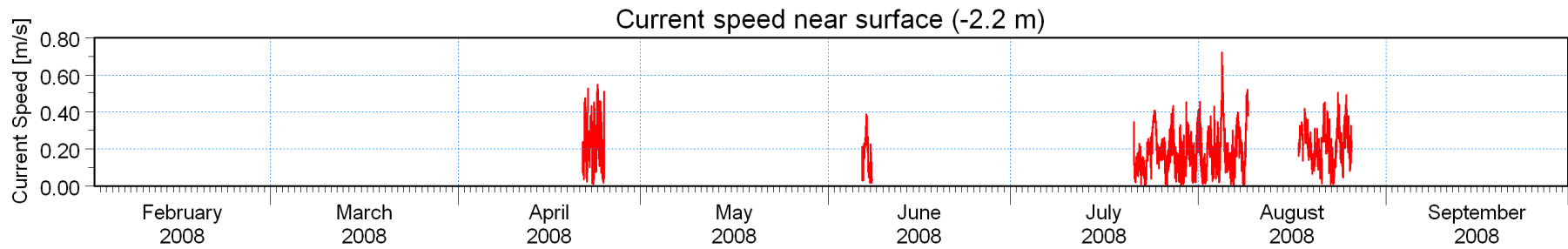


Title:

**Current measurements at Site A (refer to Figure 3.1 for position).
Time-series of surface and bottom currents.**

Figure No.

7.1



atened\Thyspunt_B_C1_P02_03_04.dfs0

atened\Thyspunt_B_C1_P02_03_04.dfs0

atened\Thyspunt_B_C1_P02_03_04.dfs0

ated\Thyspunt_B_C1_P02_03_04.dfs0

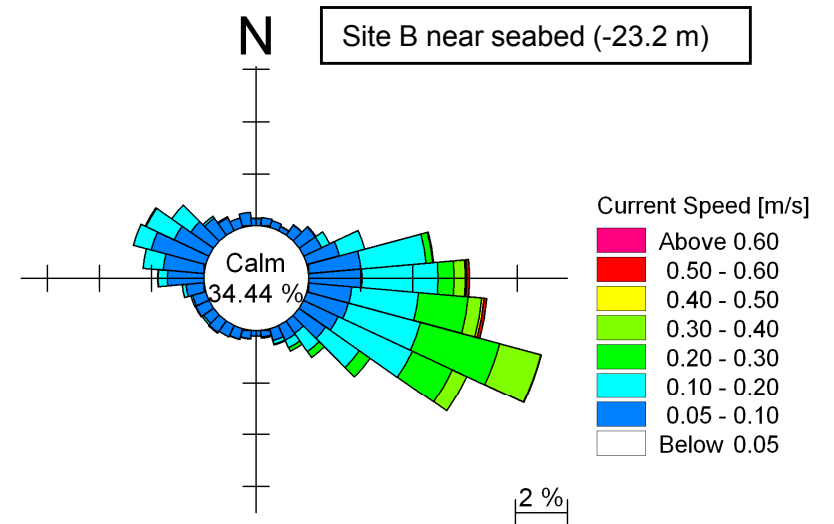
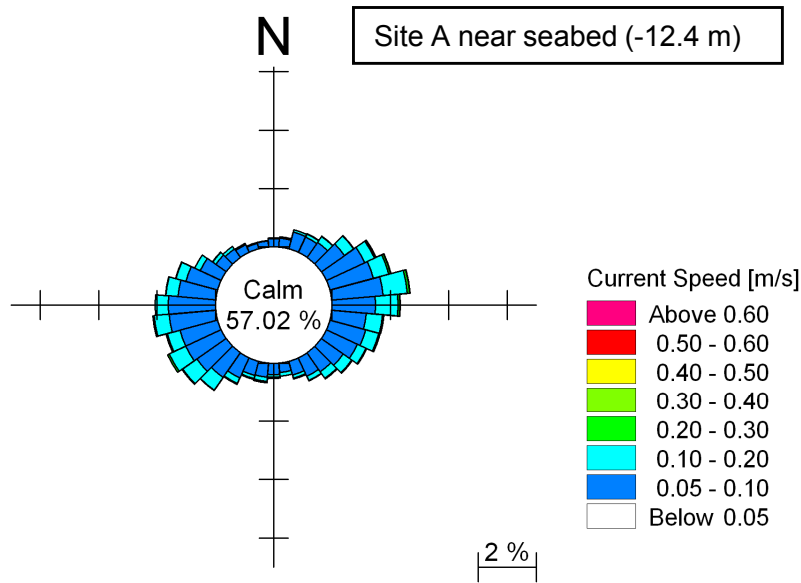
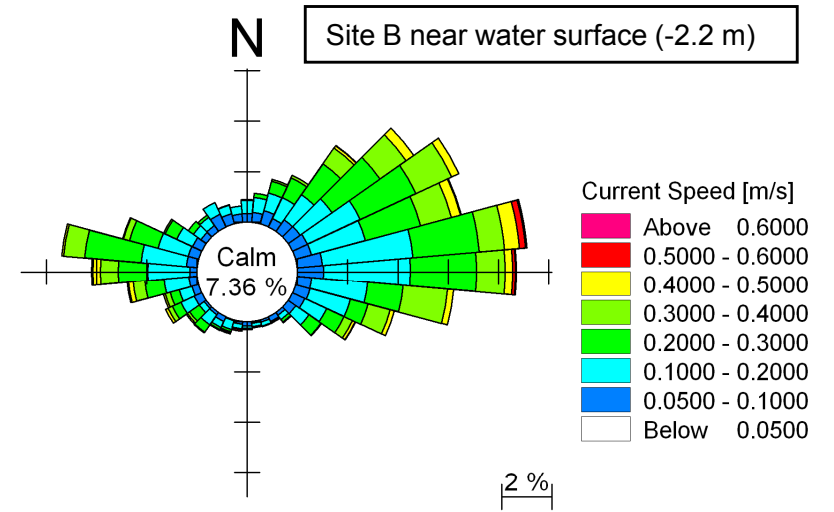
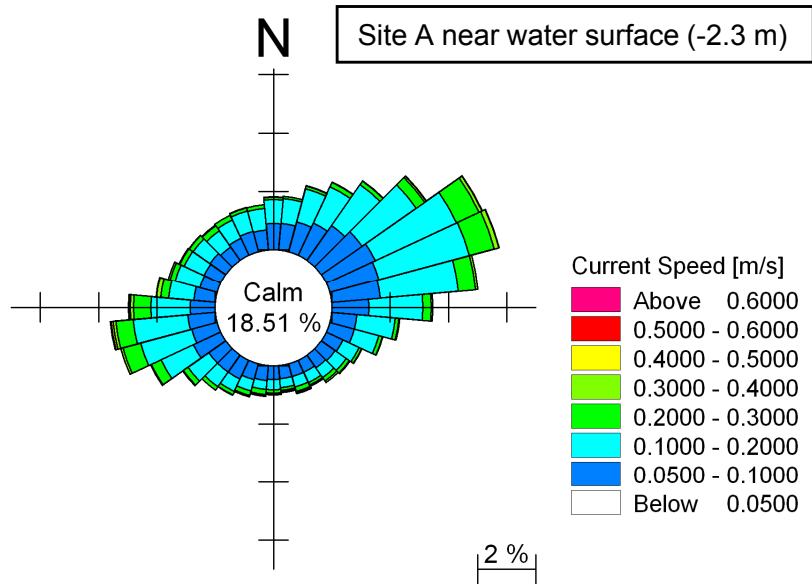


Title:

**Current measurements at Site B (refer to Figure 3.1 for position).
Time-series of surface and bottom currents.**

Figure No.

7.2

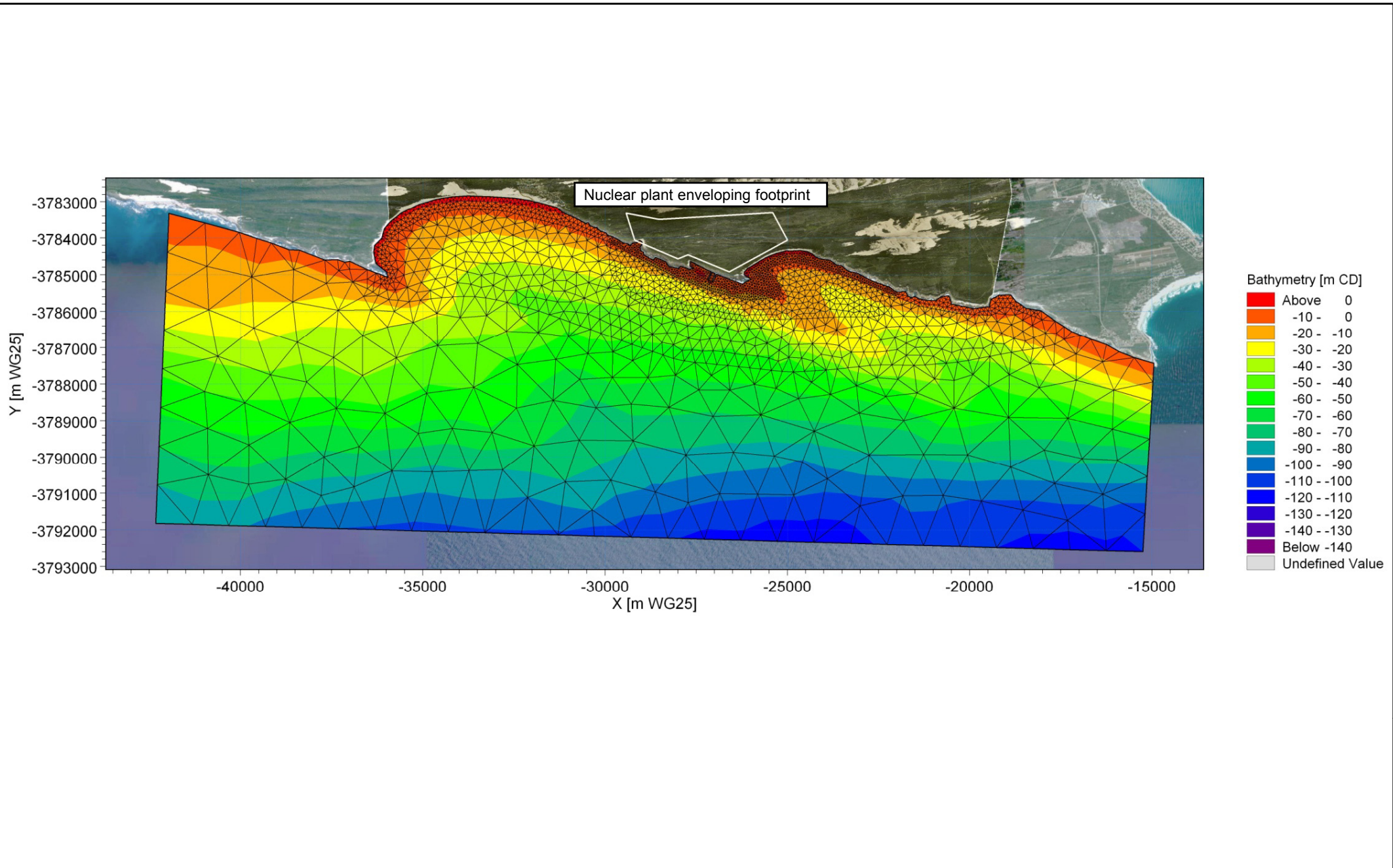


Title:

**Current measurements at Sites A and B (refer to Figure 3.1 for locations).
Surface and seabed rose plots.**

Figure No.

7.3

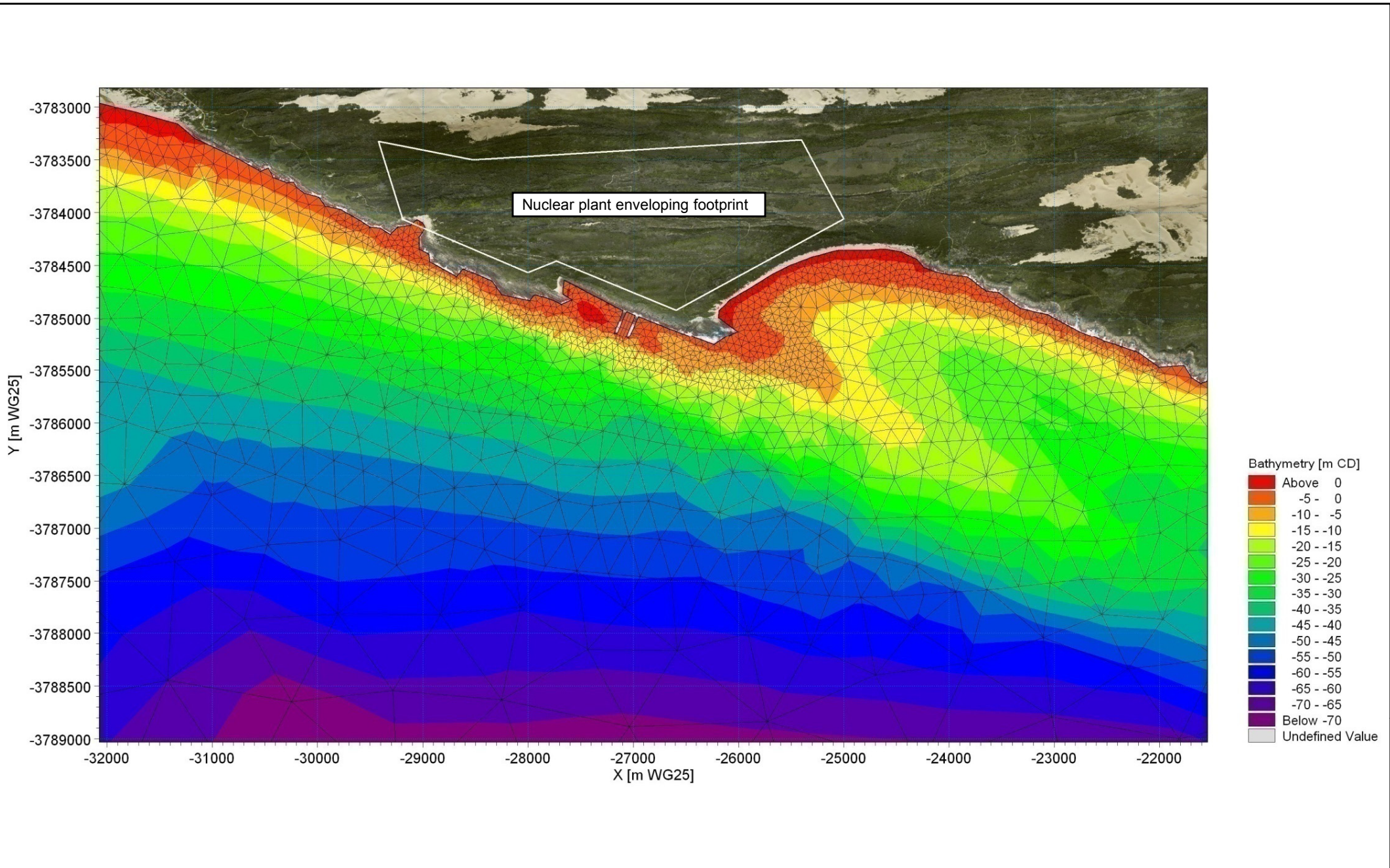


Title:

Numerical mesh and bathymetry used for hydrodynamic modelling.

Figure No.

7.4

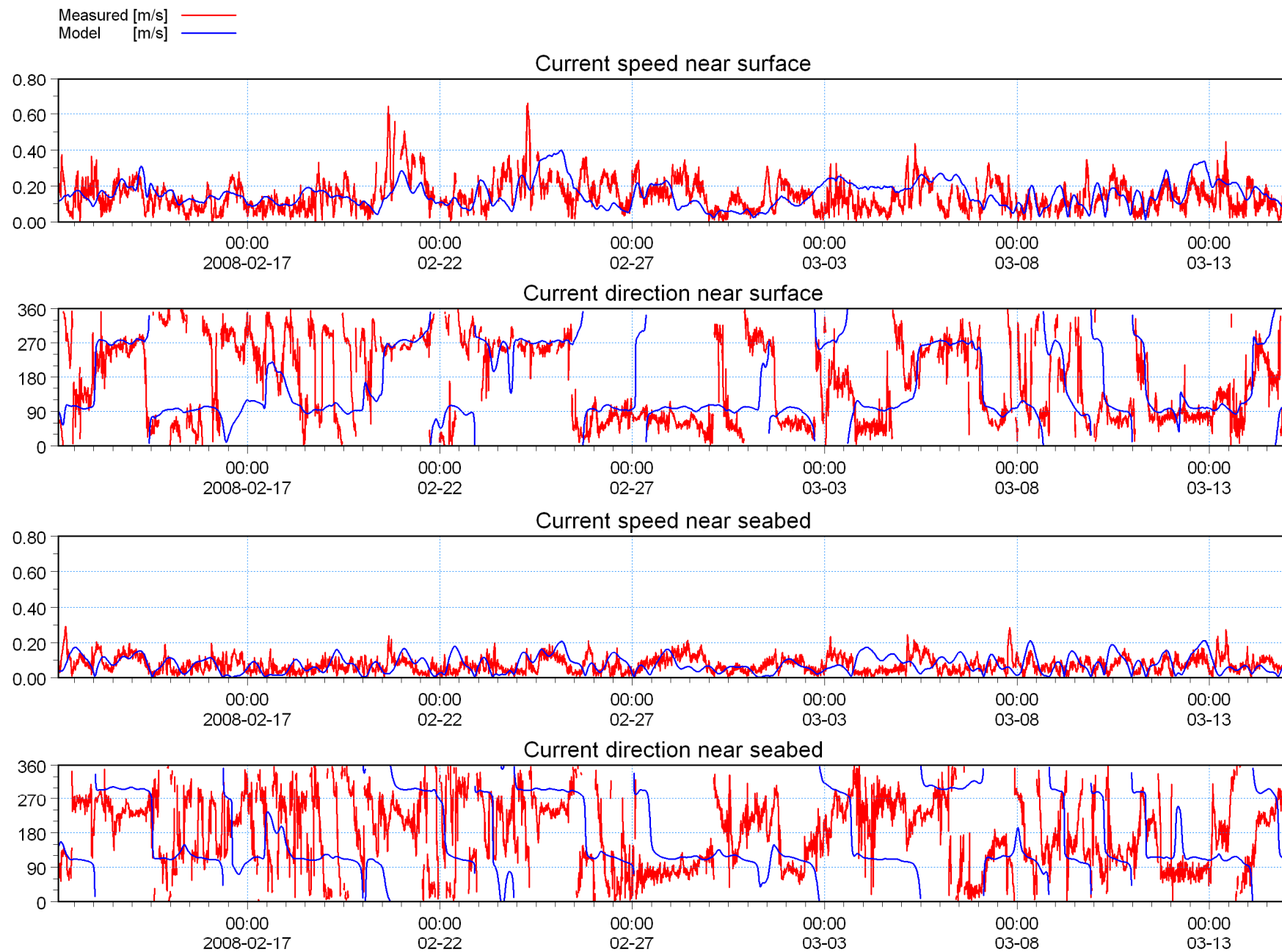


Title:

Detail of numerical mesh and bathymetry used for hydrodynamic modelling.

Figure No.

7.5



ted\Thyspunt_A_C1_P01_P02_P03.dfs0
q00q.m3m - Result Files\3D_Point.dfs0

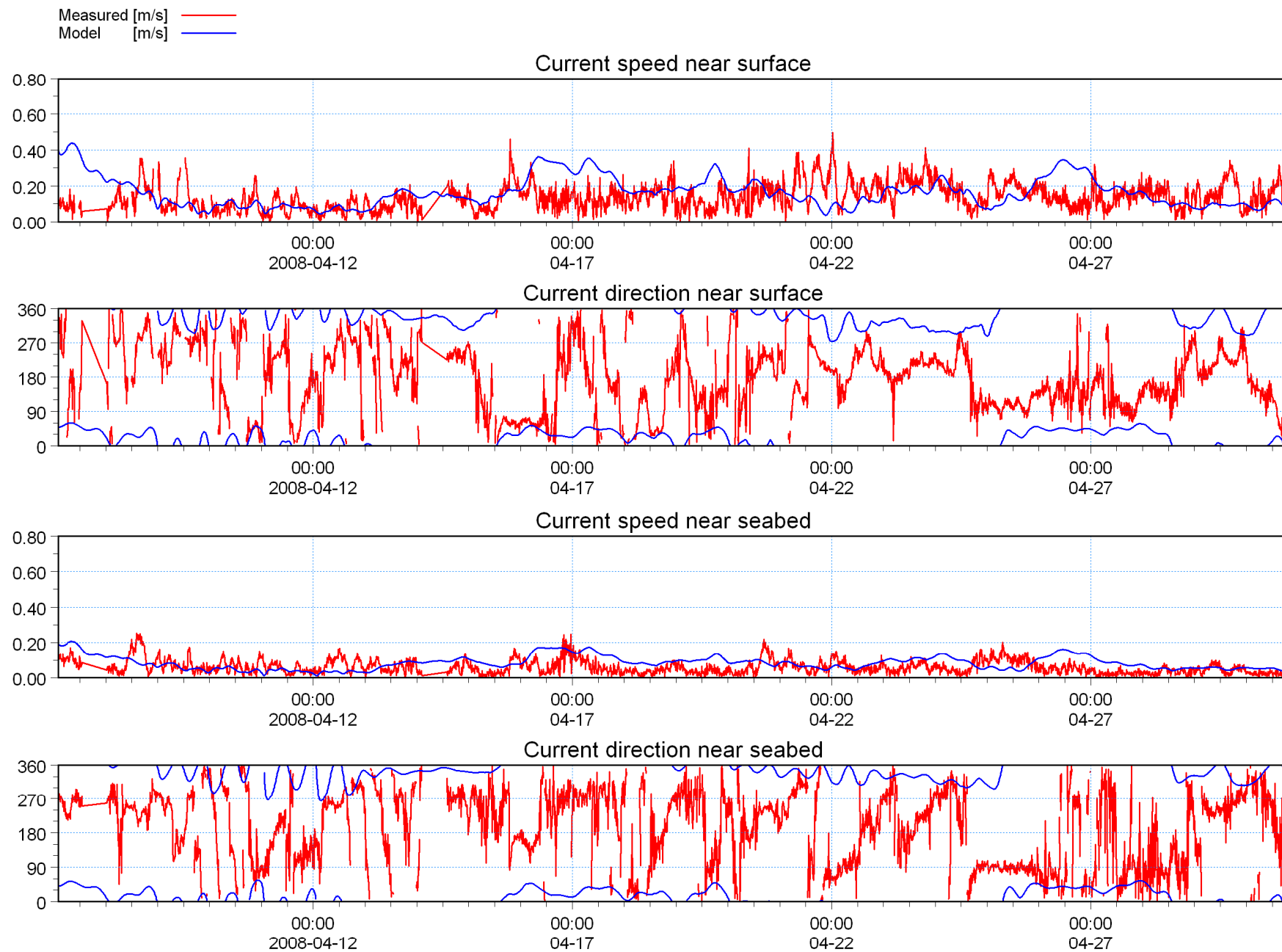


Title:

**Calibration of hydrodynamic model.
Measured and modelled time-series of currents at Site A for period February to March 2008.
(refer to Figure 3.1 for location).**

Figure No.

7.6

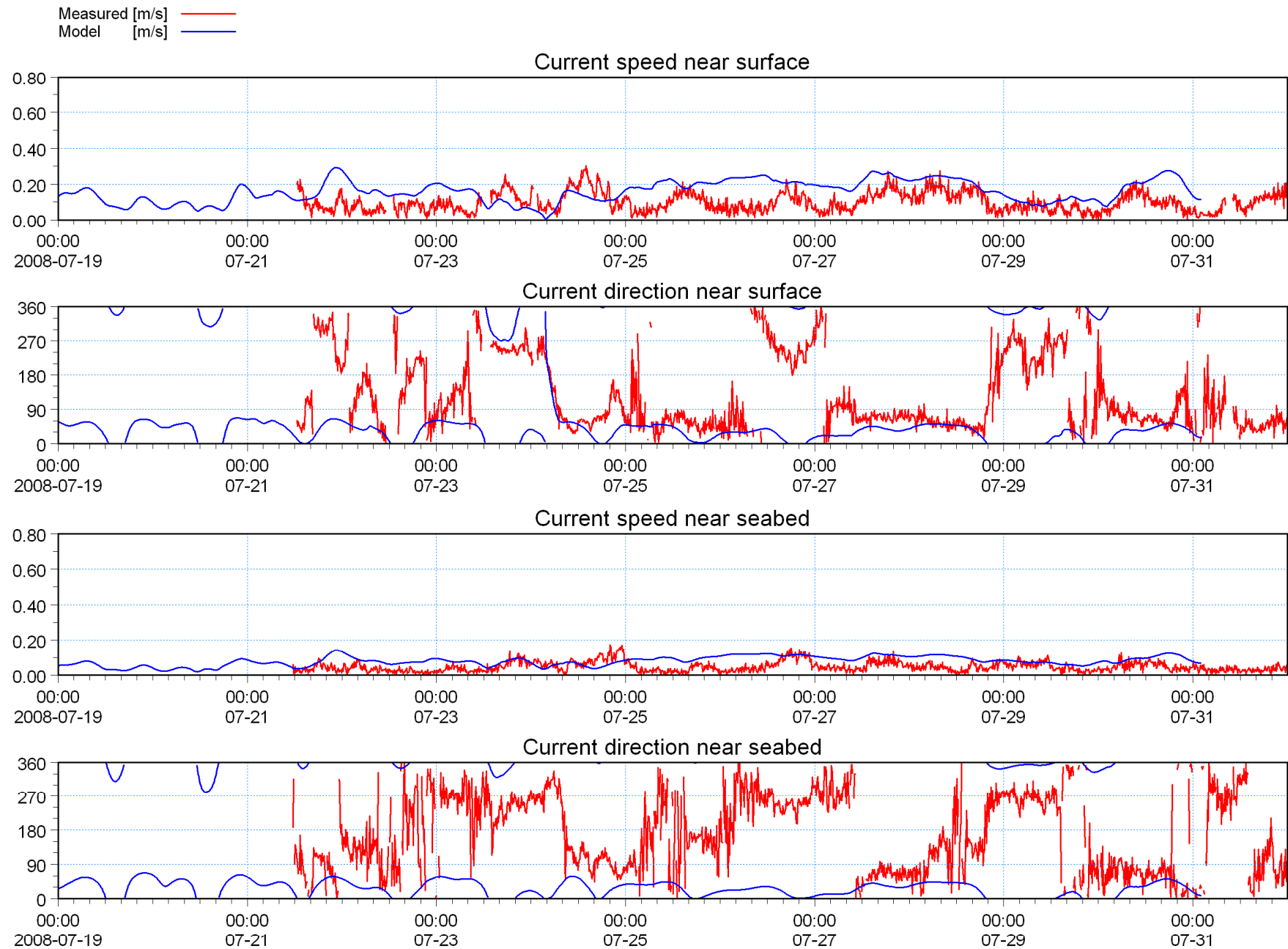


ted\Thyspunt_A_C1_P01_P02_P03.dfs0
 \q00q.m3m - Result Files\3D_Point.dfs0
 ted\Thyspunt_A_C1_P01_P02_P03.dfs0
 \q00q.m3m - Result Files\3D_Point.dfs0
 ted\Thyspunt_A_C1_P01_P02_P03.dfs0
 \q00q.m3m - Result Files\3D_Point.dfs0
 ted\Thyspunt_A_C1_P01_P02_P03.dfs0
 \q00q.m3m - Result Files\3D_Point.dfs0



Title:
Calibration of hydrodynamic model.
Measured and modelled time-series of currents at Site A for period April 2008.
(refer to Figure 3.1 for location).

Figure No.
7.7



ted\Thyspunt_A_C1_P01_P02_P03.dfs0
jq00q.m3m - Result Files\3D_Point.dfs0

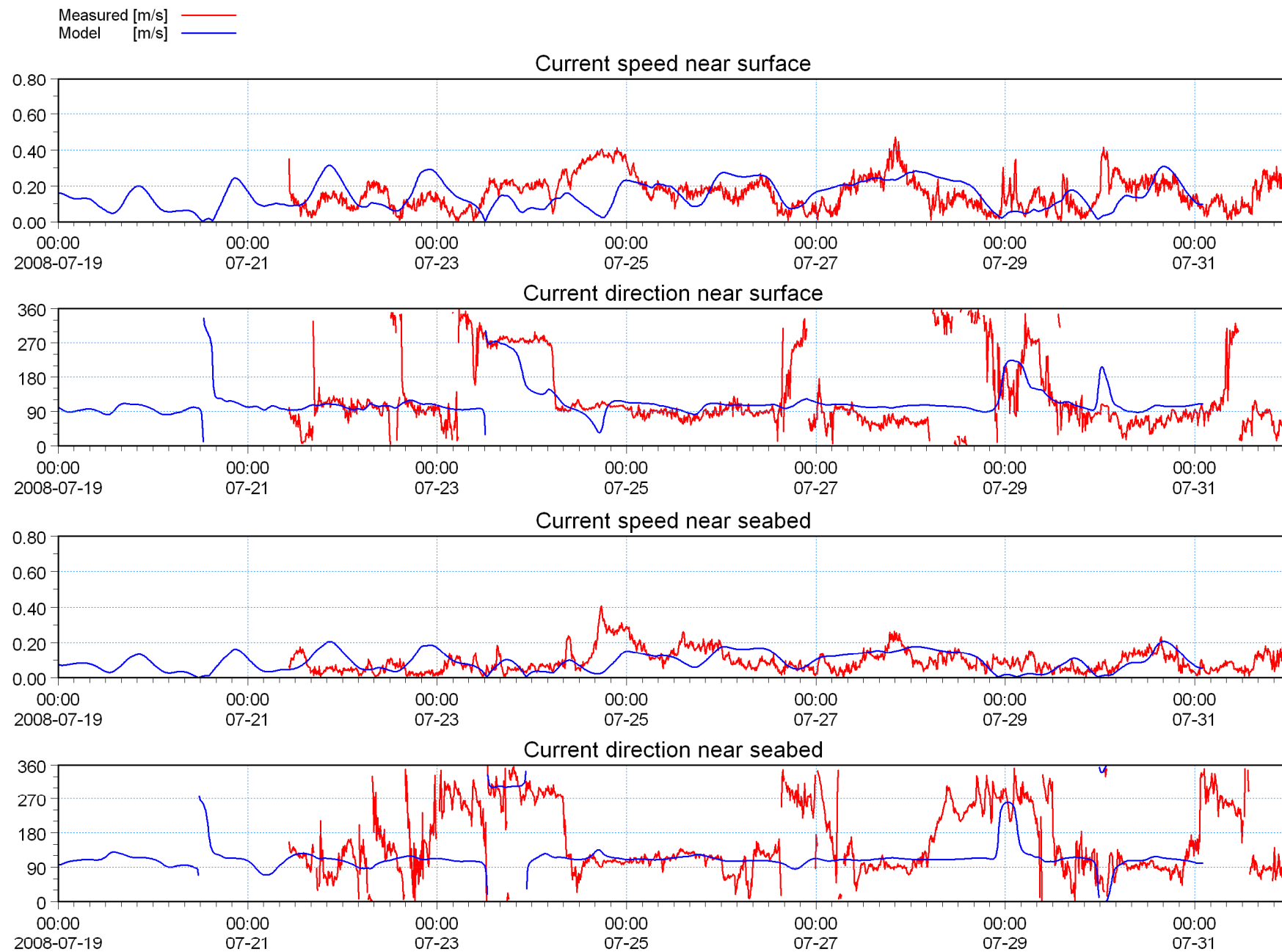


Title:

**Calibration of hydrodynamic model.
Measured and modelled time-series of currents at Site A for period July 2008.
(refer to Figure 3.1 for location).**

Figure No.

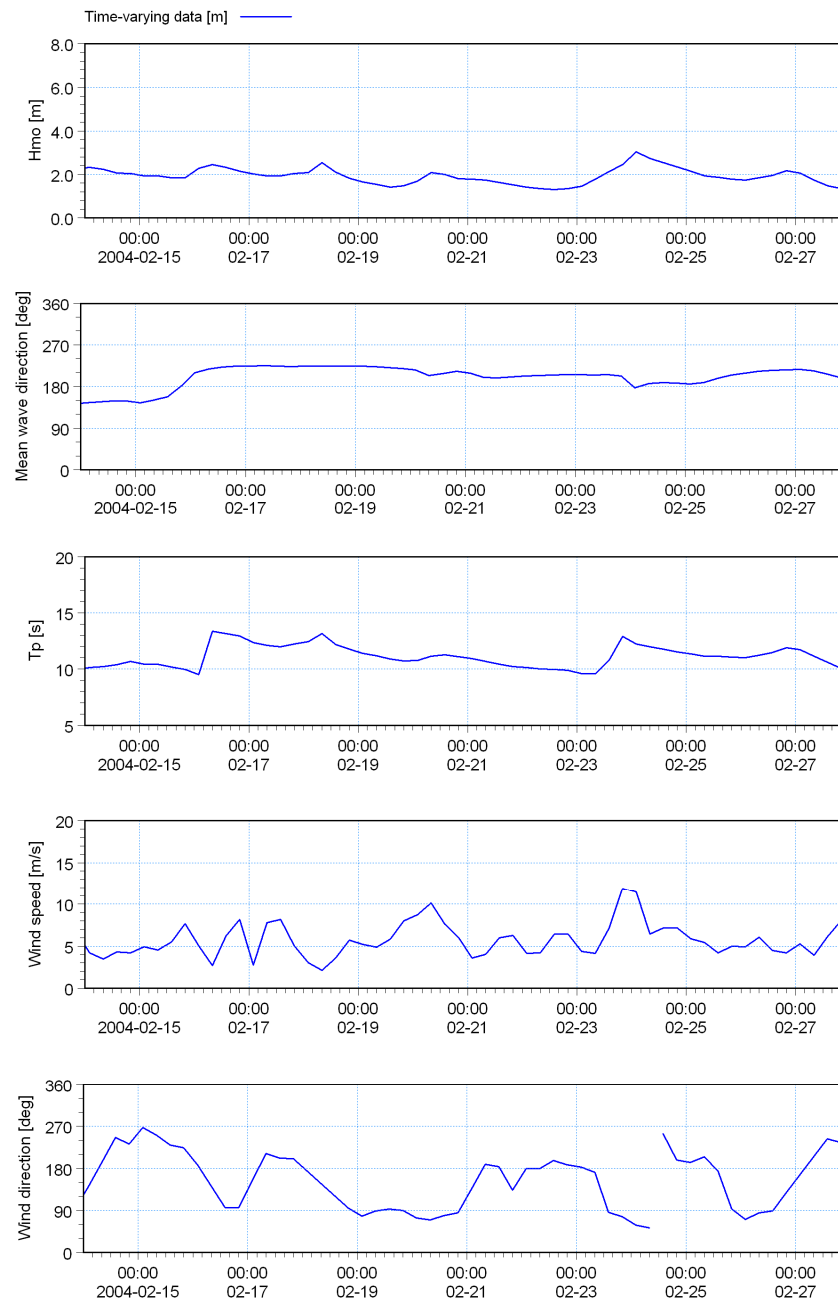
7.8



3:\Processed\ThySpunt_B2_C1_P03.dfs0
 3:\Processed\ThySpunt_B2_C1_P03.dfs0
 3:\Processed\ThySpunt_B2_C1_P03.dfs0
 3:\Processed\ThySpunt_B2_C1_P03.dfs0



Title: Calibration of hydrodynamic model.
 Measured and modelled time-series of currents at Site B for period July 2008.
 (refer to Figure 3.1 for location).



L:\Oceanor_e245_s350_interpolated2_1997_2006.dfo
 L:\Oceanor_e245_s350_interpolated2_1997_2006.dfo
 e_Parameters_Oceanor_e245_s350_1997_2006.dfo
 _Parameters_Oceanor_e245_s350_1997_2006.dfo
 s_Parameters_Oceanor_e245_s350_1997_2006.dfo

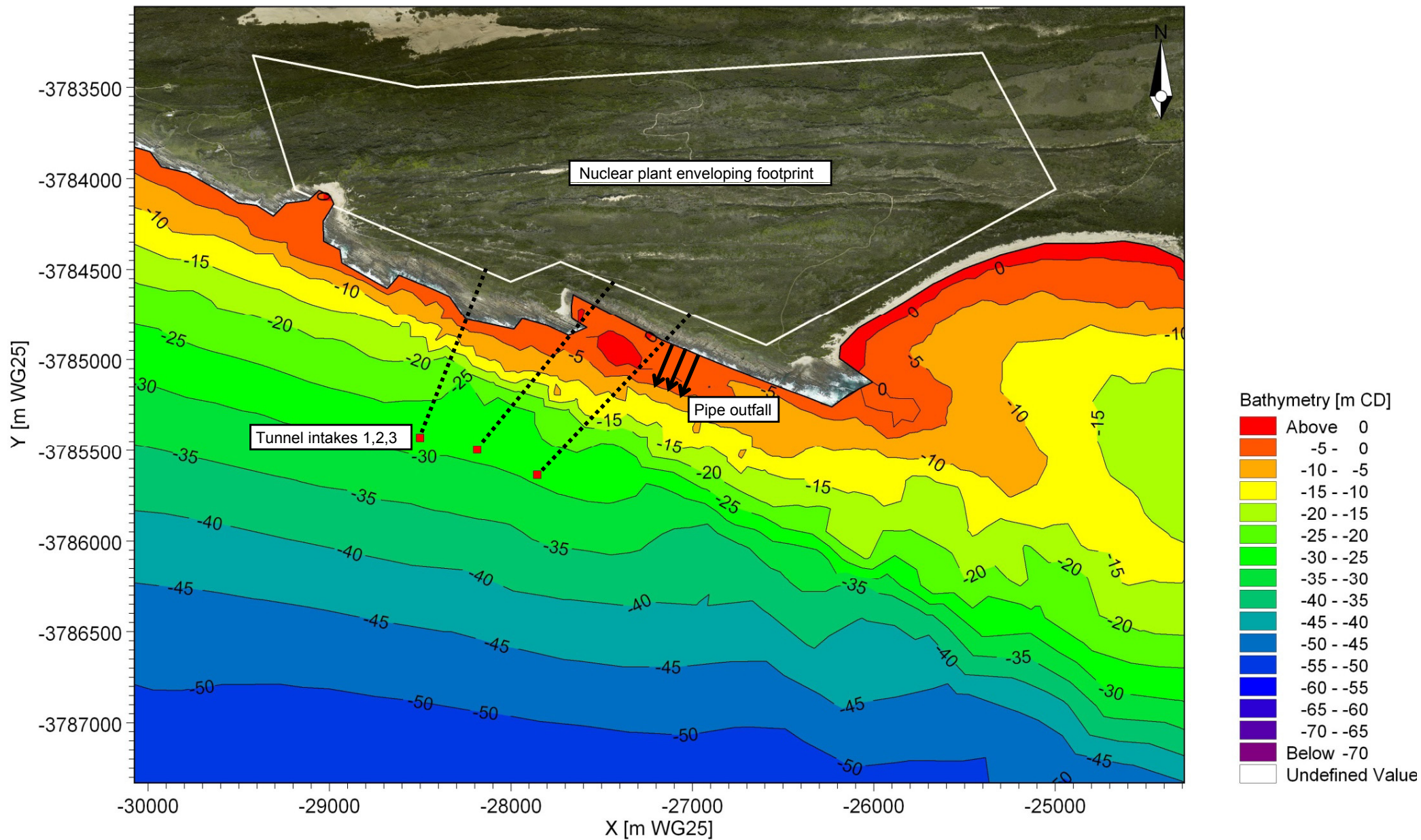


Title:

**Wave and wind time-series used in hydrodynamic and plume modelling.
14 day calm simulation period.**

Figure No.

7.12

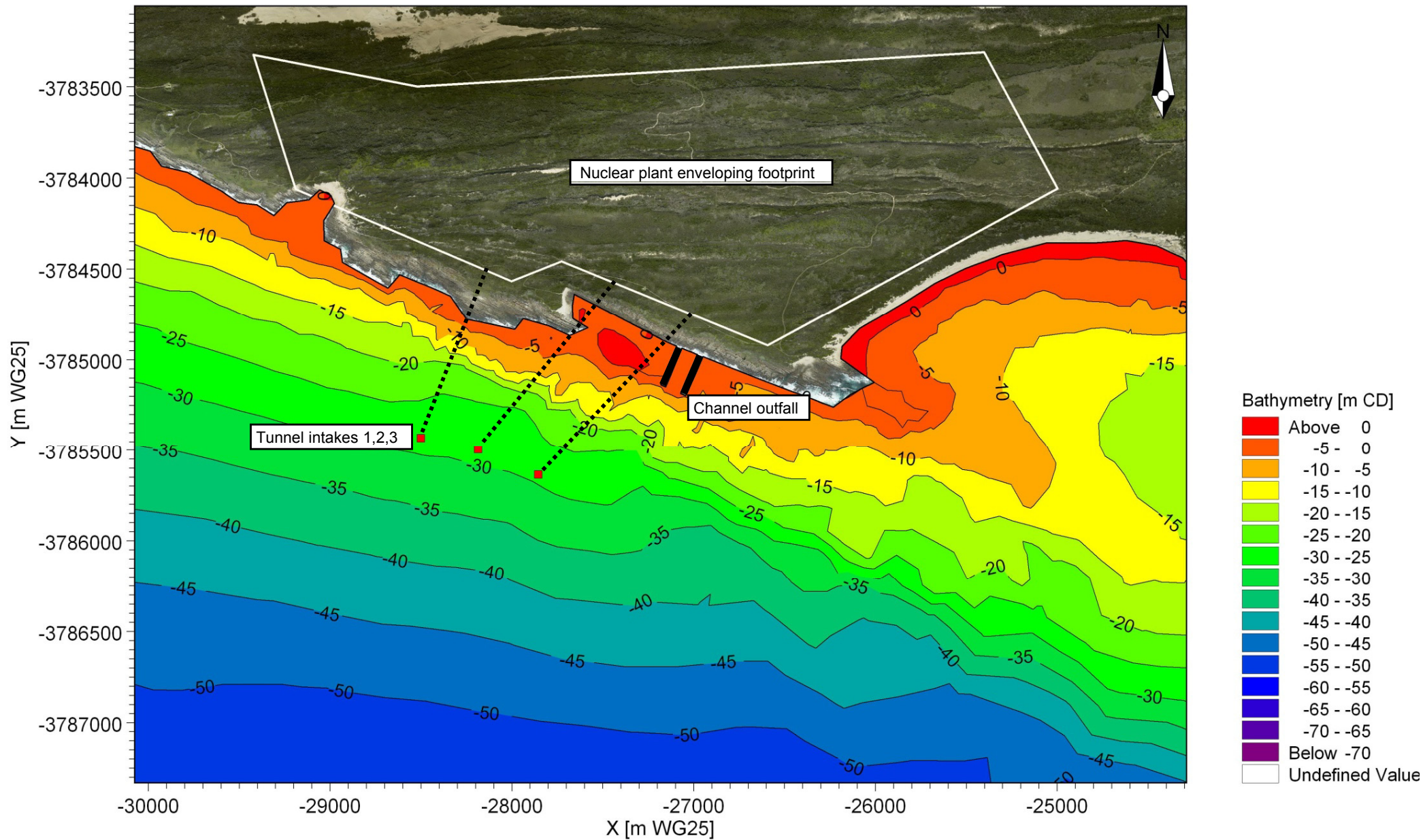


Title:

Layout 1: Offshore tunnel intake and nearshore pipeline outfall.

Figure No.

7.13

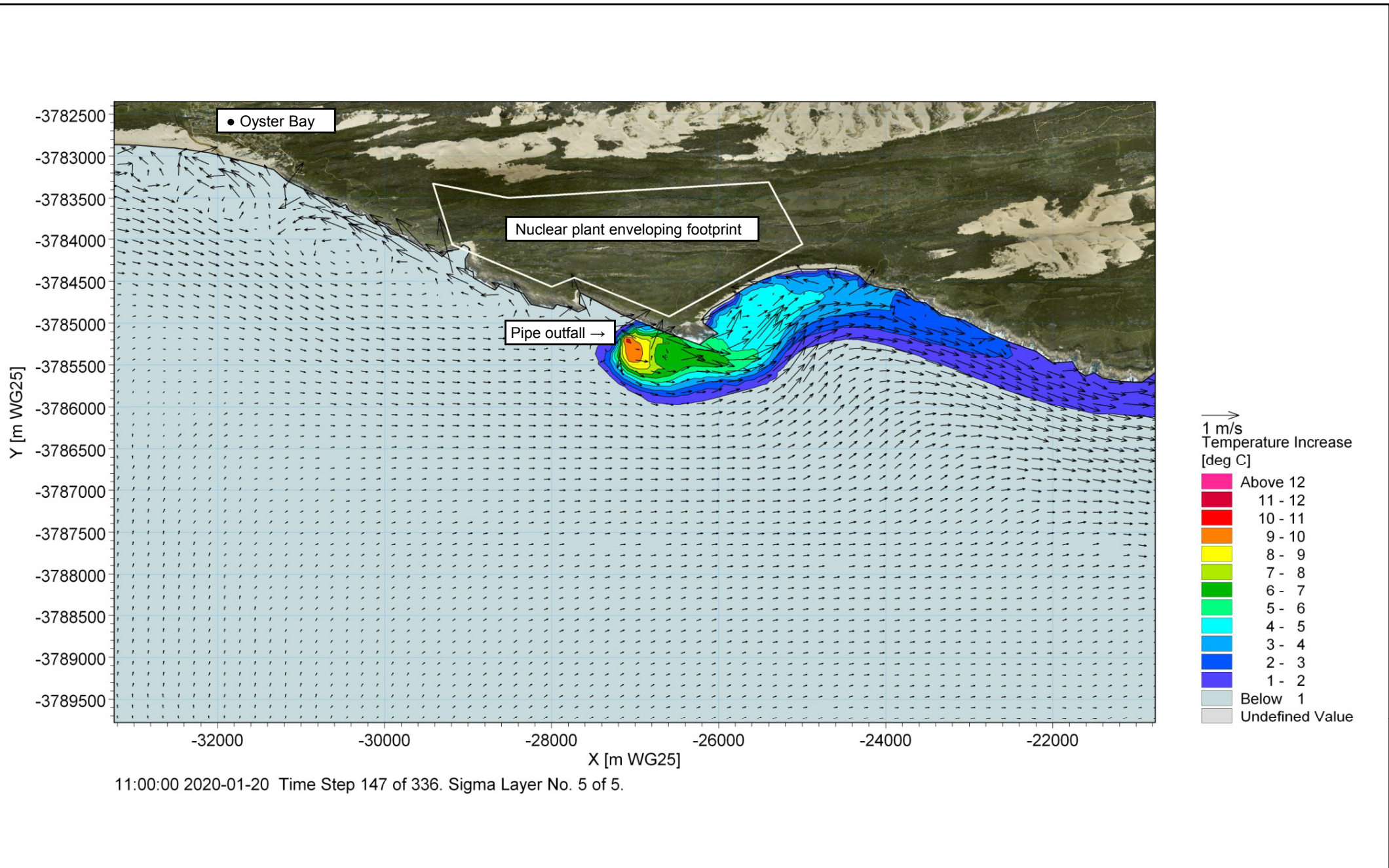


Title:

Layout 2: Offshore tunnel intake and nearshore channel outfall.

Figure No.

7.14

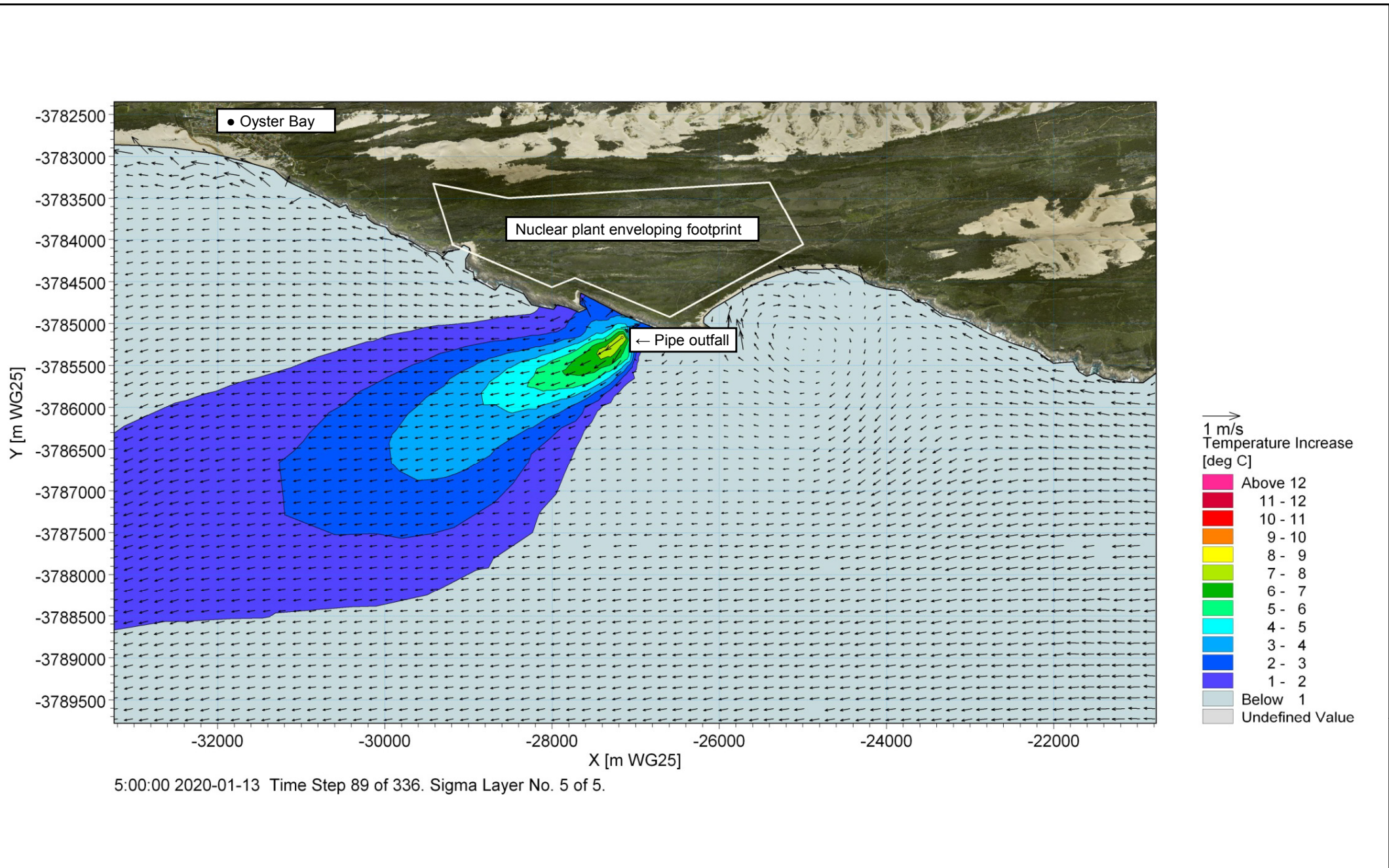


Title:

**Example of modelled currents and thermal plume near water surface at a time when the currents are predominantly wave-driven.
Power output: 10 000 MWe.**

Figure No.

7.15

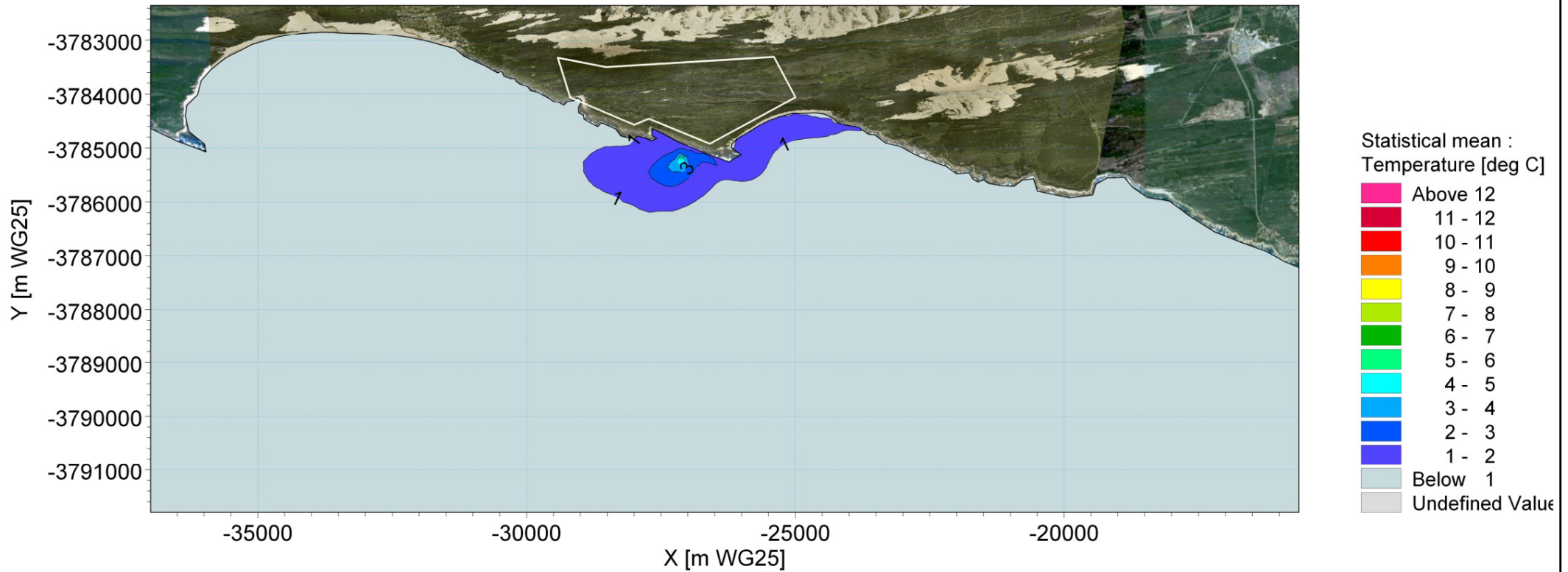


Title:

**Example of modelled currents and thermal plume near water surface at a time when the currents are predominantly wind-driven.
Power output: 10 000 MWe.**

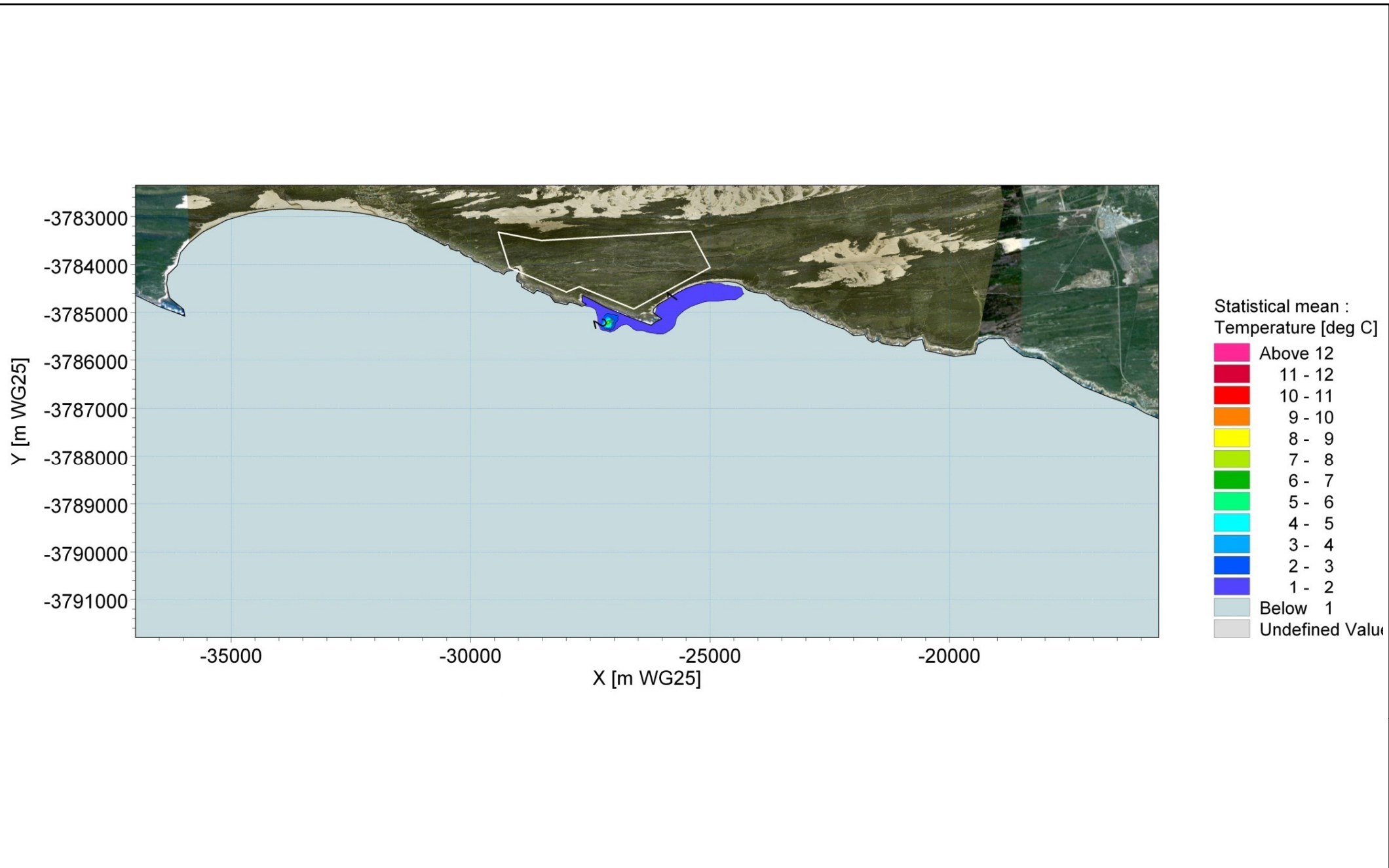
Figure No.

7.16



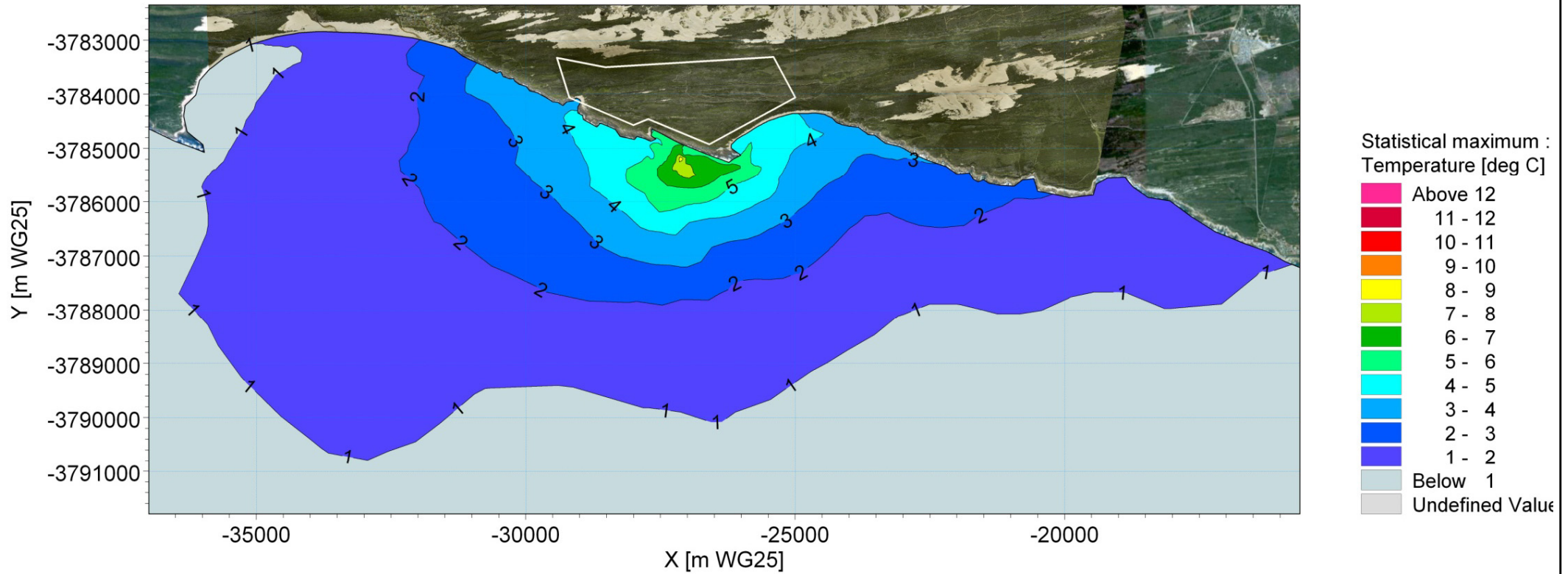
**Title: Thermal plume for Layout 1 (offshore tunnel intake, nearshore pipeline outfall).
 Mean increase in temperature near water surface.
 Power output: 4 000 MWe.**

**Figure No.
 7.17**

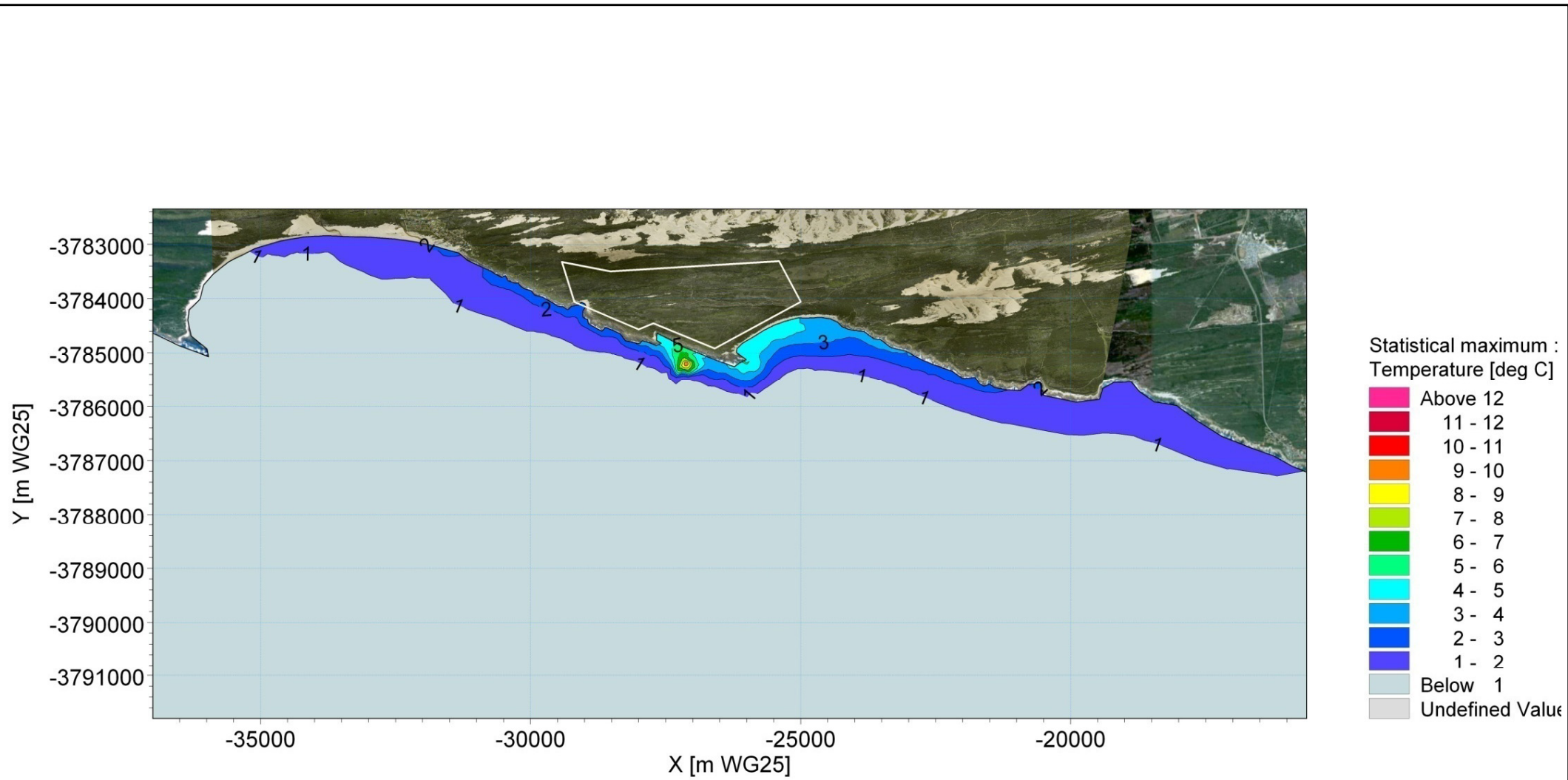


Title: Thermal plume for Layout 1 (offshore tunnel intake, nearshore pipeline outfall).
Mean increase in temperature near seabed.
Power output: 4 000 MWe.

Figure No.
7.18

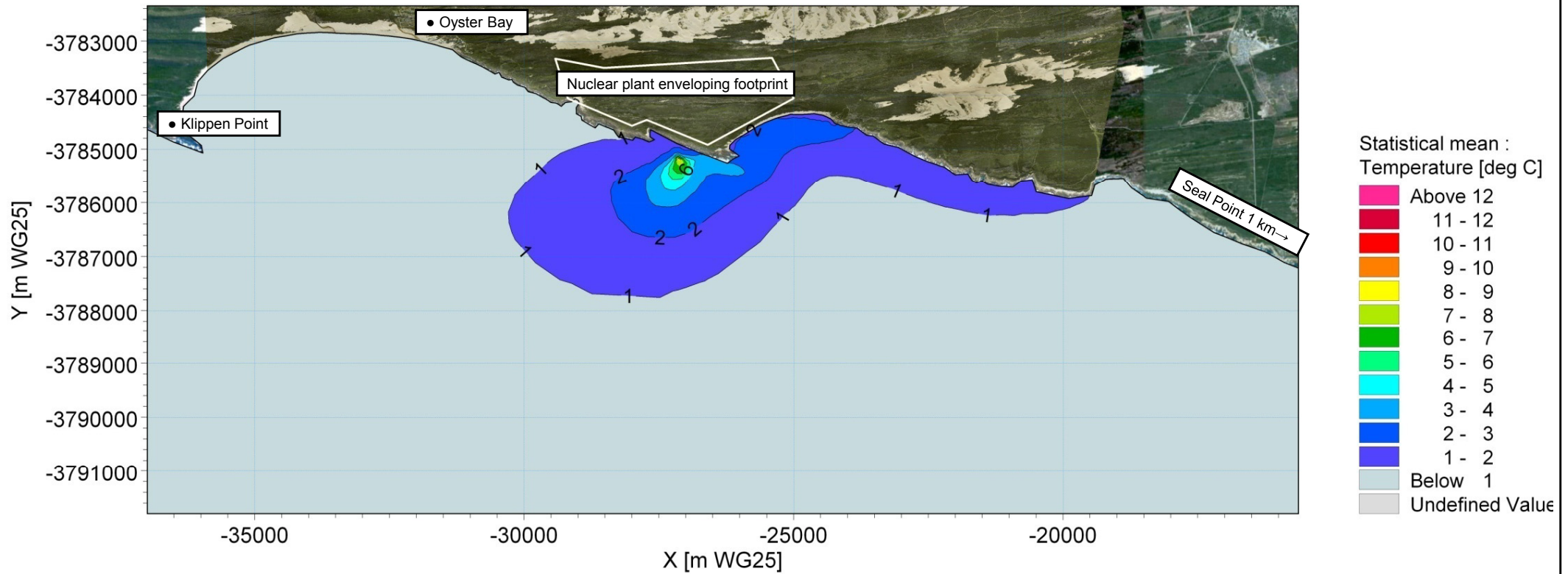


Title: Thermal plume for Layout 1 (offshore tunnel intake, nearshore pipeline outfall).
Maximum increase in temperature near surface.
Power output: 4 000 MWe.



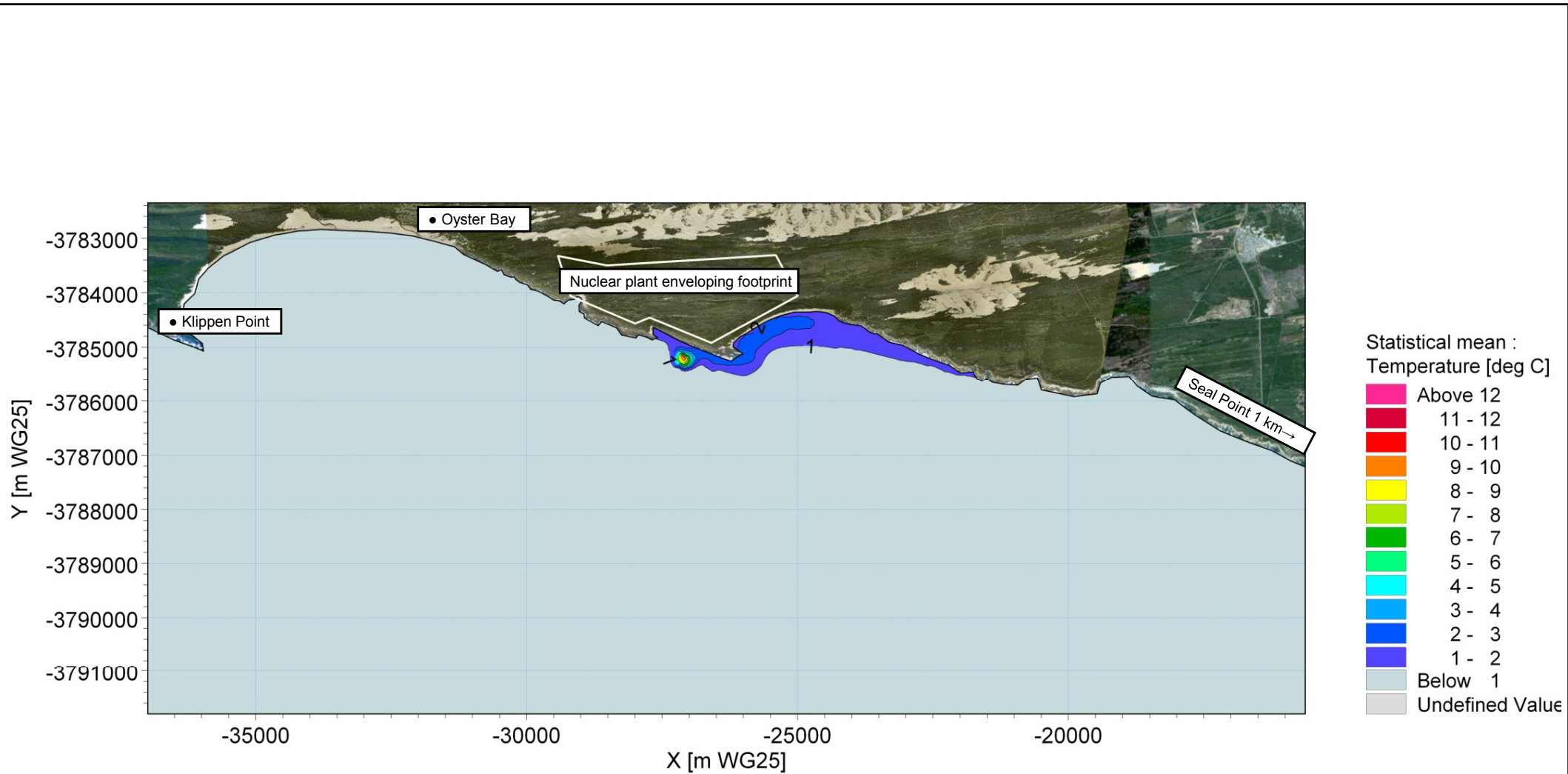
Title: Thermal plume for Layout 1 (offshore tunnel intake, nearshore pipeline outfall).
Maximum increase in temperature near seabed.
Power output: 4 000 MWe.

Figure No.
7.20



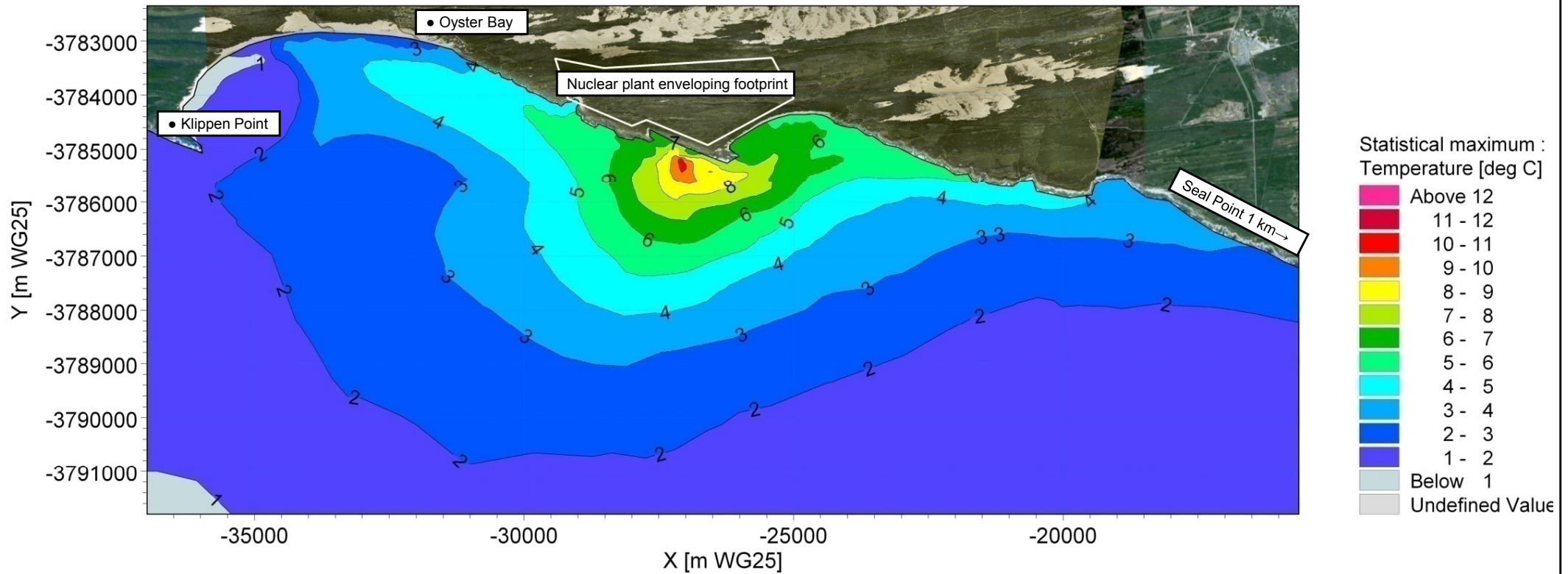
Title: Thermal plume for Layout 1 (offshore tunnel intake, nearshore pipeline outfall).
Mean increase in temperature near water surface.
Power output: 10 000 MWe.

Figure No.
7.21



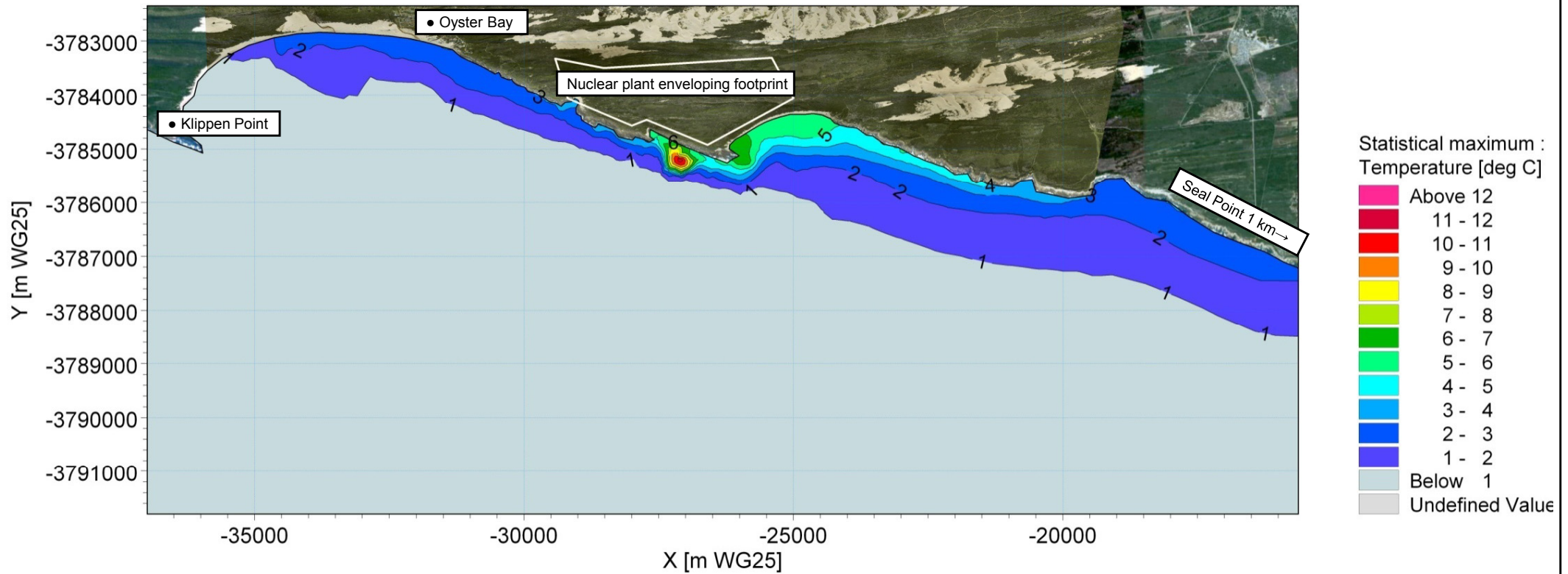
Title: Thermal plume for Layout 1 (offshore tunnel intake, nearshore pipeline outfall).
Mean increase in temperature near seabed.
Power output: 10 000 MWe.

Figure No.
7.22



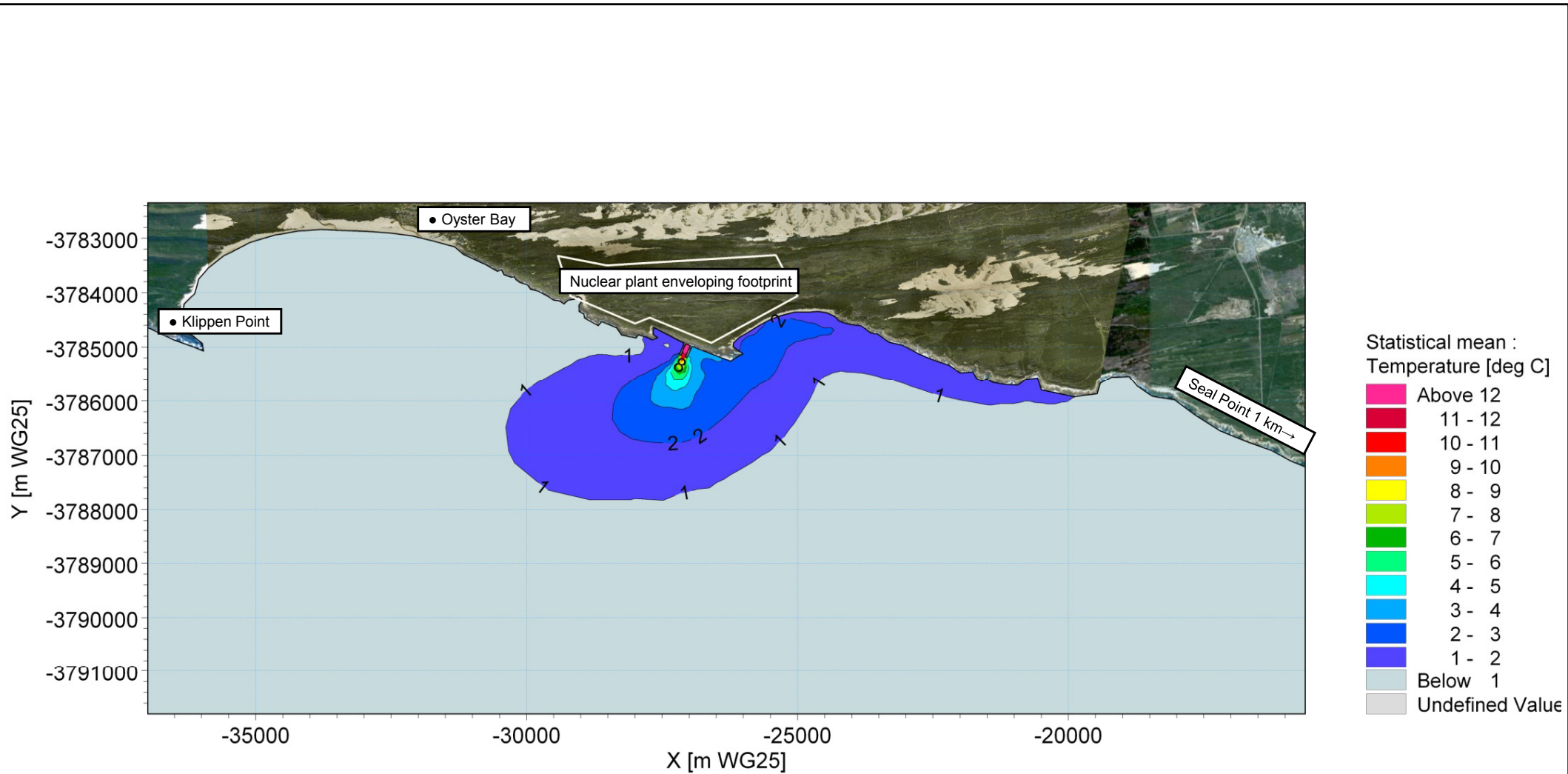
Title: Thermal plume for Layout 1 (offshore tunnel intake, nearshore pipeline outfall).
Maximum increase in temperature near surface.
Power output: 10 000 MWe.

Figure No.
7.23



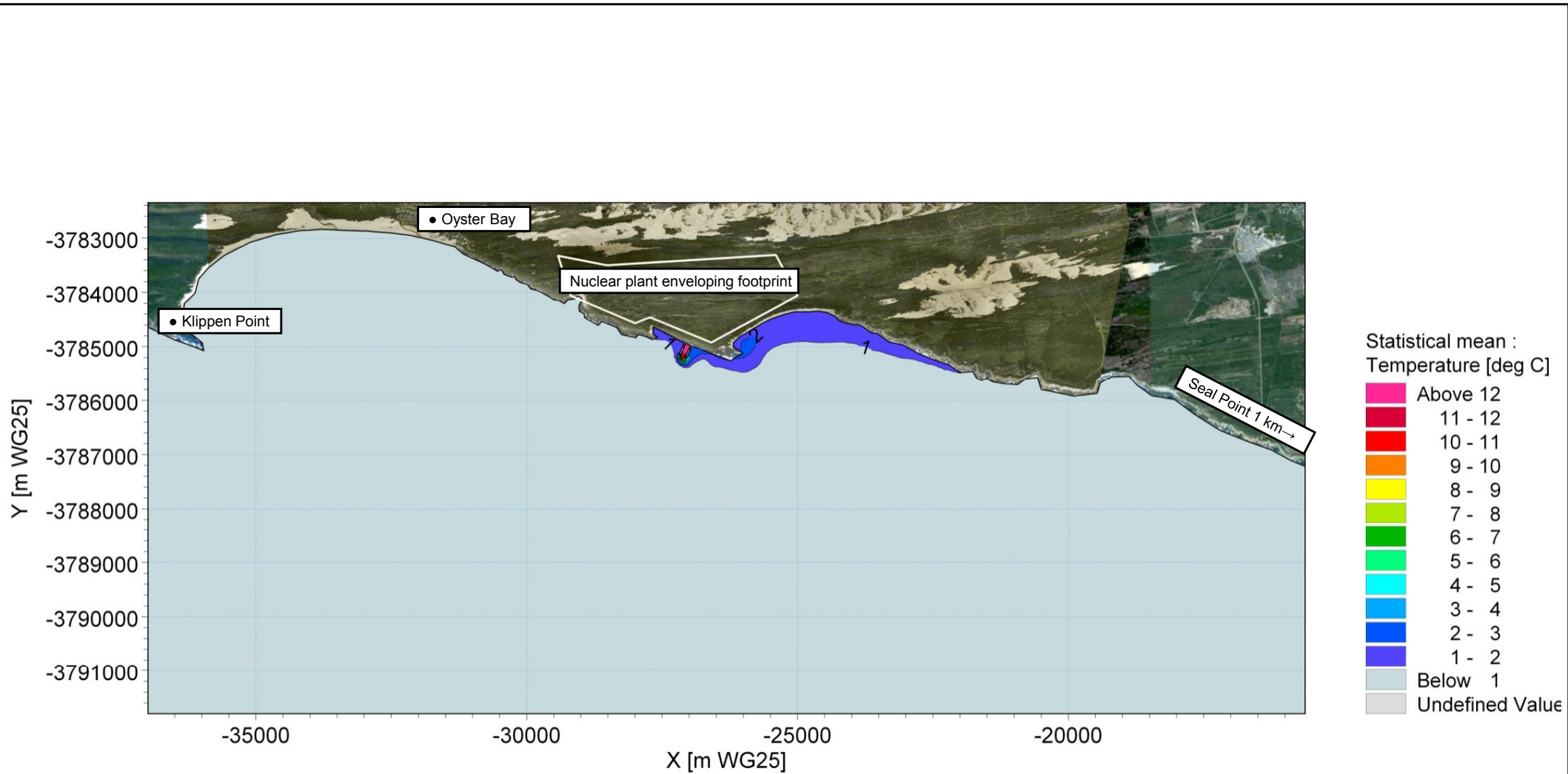
Title: Thermal plume for Layout 1 (offshore tunnel intake, nearshore pipeline outfall).
 Maximum increase in temperature near seabed.
 Power output: 10 000 MWe.

Figure No.
 7.24

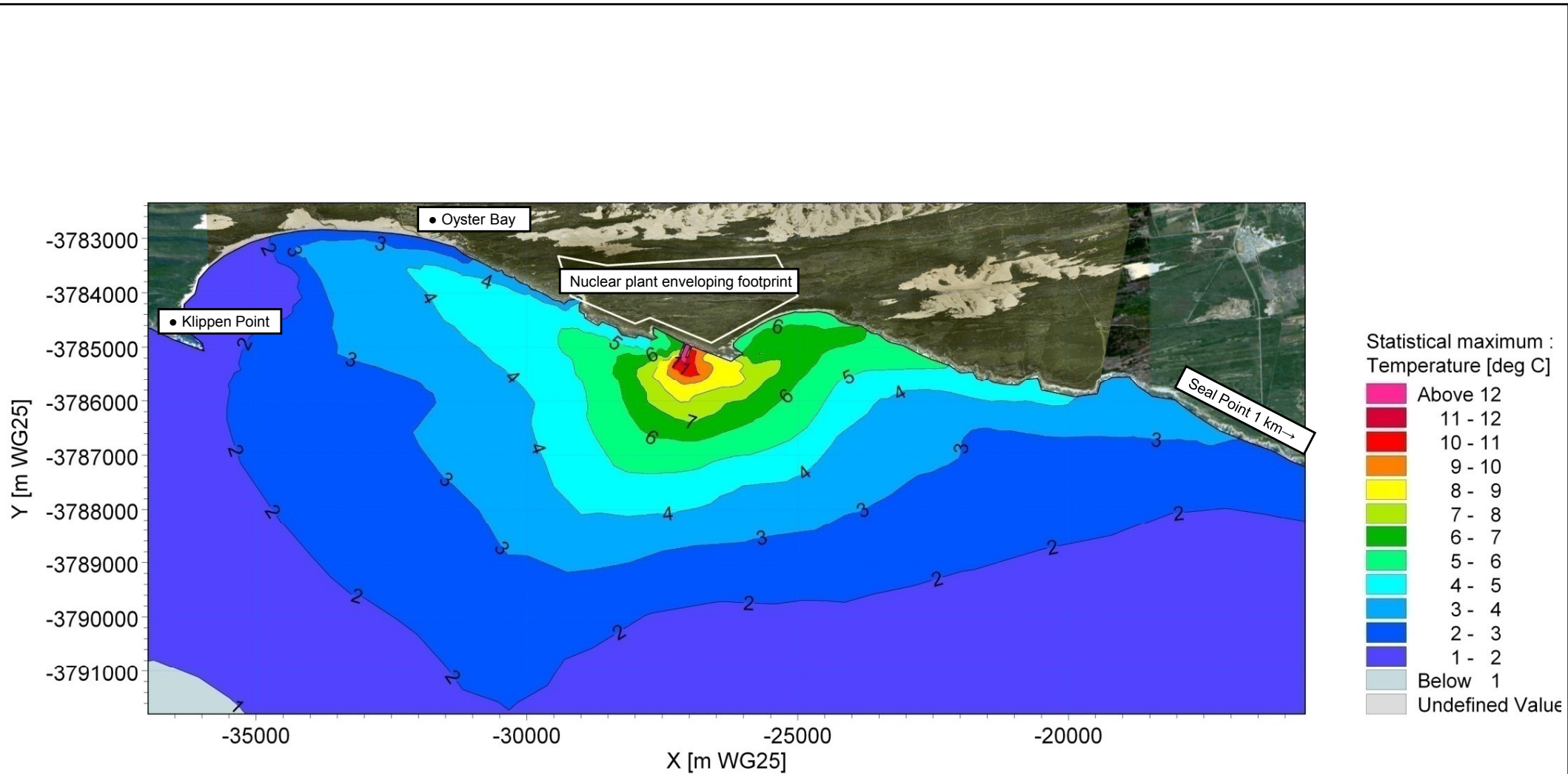


Title: Thermal plume for Layout 2 (offshore tunnel intake, nearshore channel outfall).
Mean increase in temperature near water surface.
Power output: 10 000 MWe.

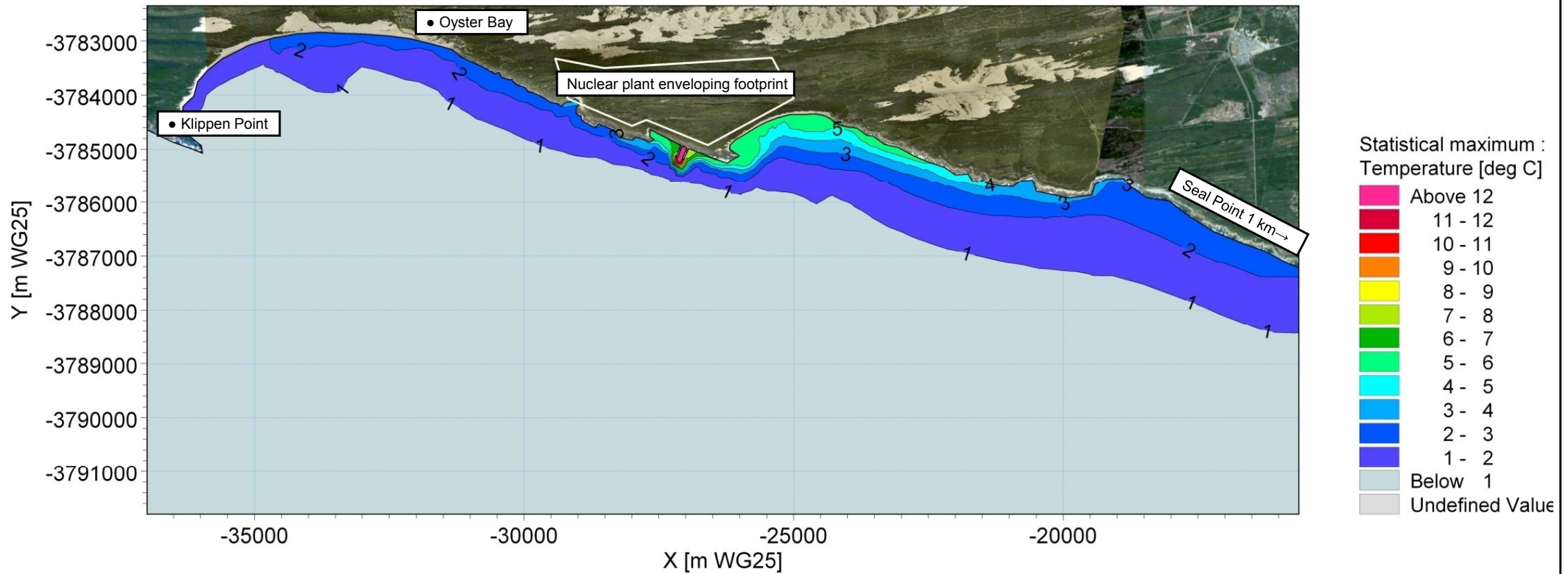
Figure No.
7.25



Title: Thermal plume for Layout 2 (offshore tunnel intake, nearshore channel outfall).
Mean increase in temperature near seabed.
Power output: 10 000 MWe.

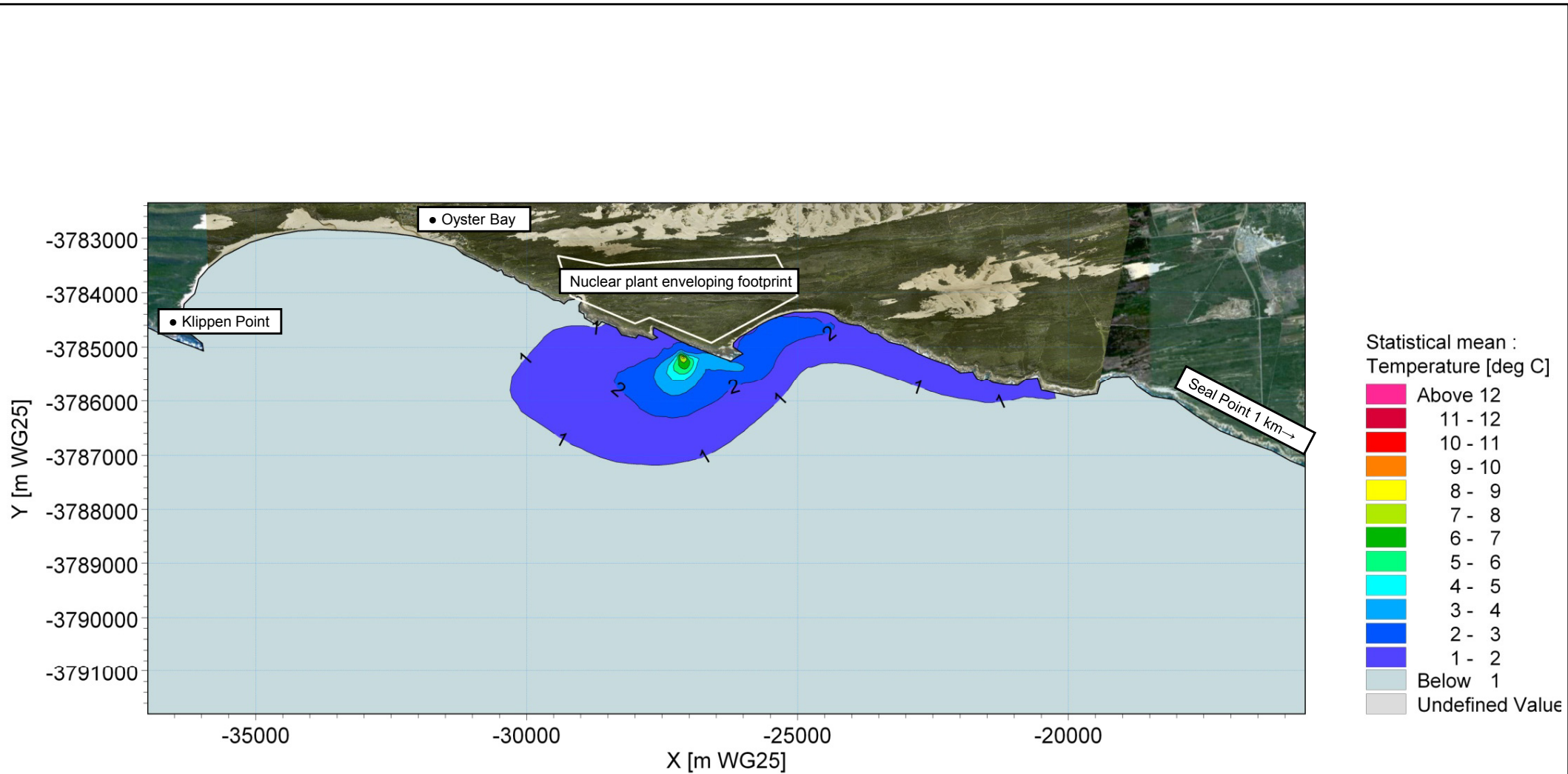


Title: Thermal plume for Layout 2 (offshore tunnel intake, nearshore channel outfall).
Maximum increase in temperature near surface.
Power output: 10 000 MWe.



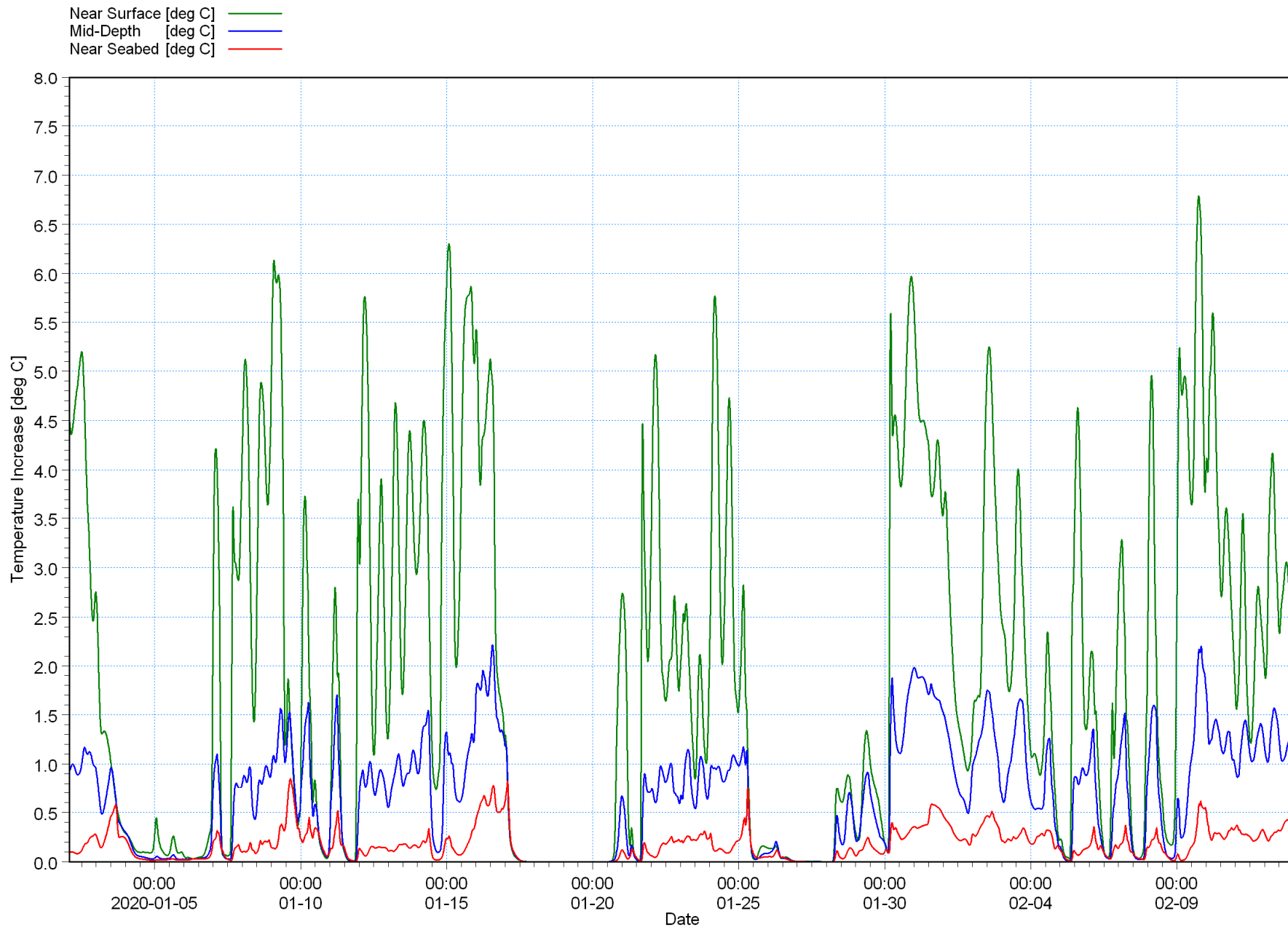
Title: Thermal plume for Layout 2 (offshore tunnel intake, nearshore channel outfall).
Maximum increase in temperature near seabed.
Power output: 10 000 MWe.

Figure No.
7.28



Title: Thermal plume for Layout 1 (offshore tunnel intake, nearshore pipeline outfall).
Mean increase in temperature near water surface. Power output: 10 000 MWe.
Sensitivity to climate change: wind speed increased 10% and wave height increased 17%.

Figure No.
7.29

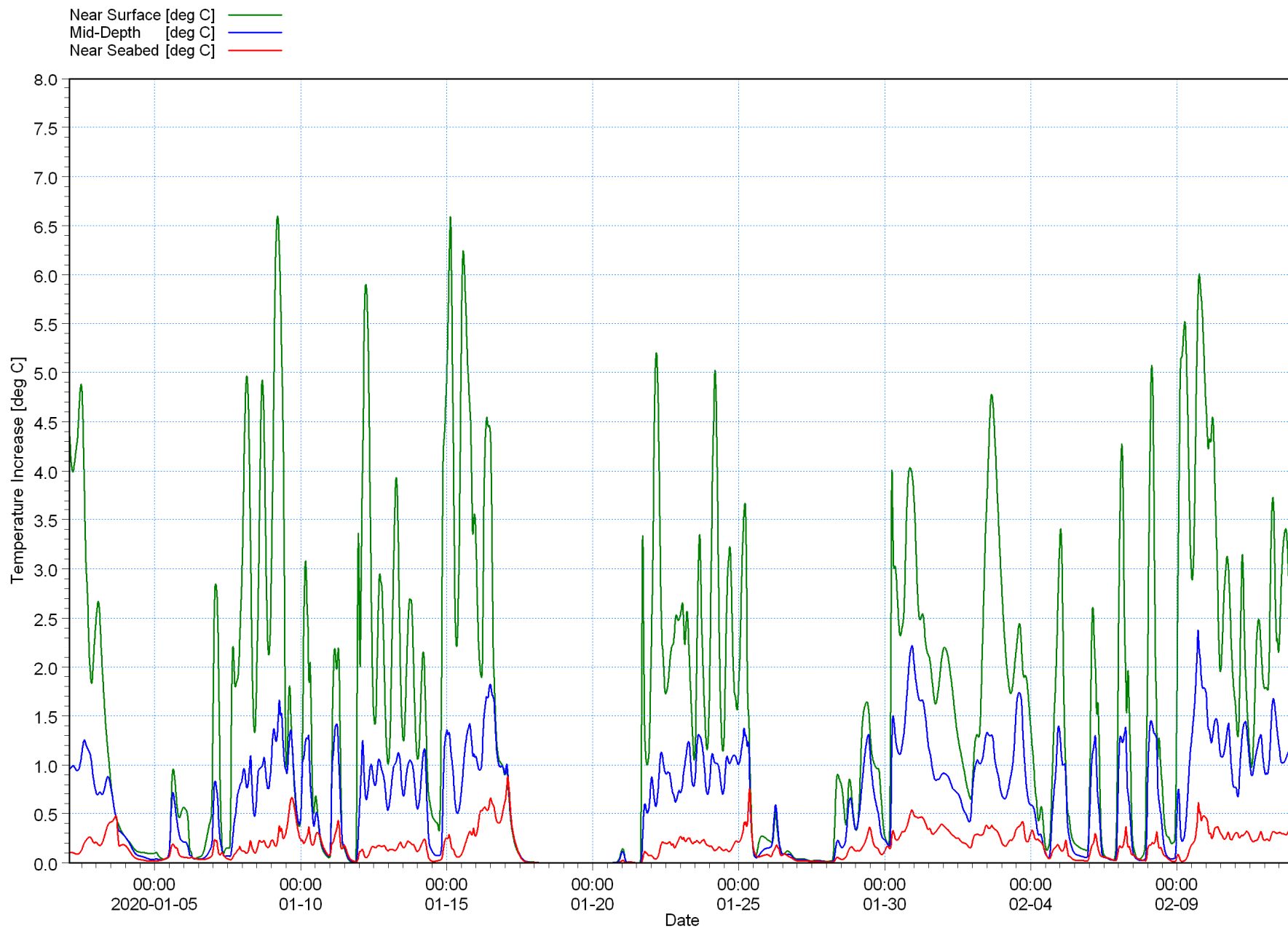


G:\Projects\1010_NuclearSites\Thyspunt\Models\Plume\11a\11b.m3fm - Result Files\3D_Point_Post.dfs0



**Title: Recirculation for Layout 1 (offshore tunnel intake, nearshore pipeline outfall).
 Temperature time-series at intake position. Note that intake will be located near the seabed.
 Power output: 10 000 MWe.**

**Figure No.
 7.30**

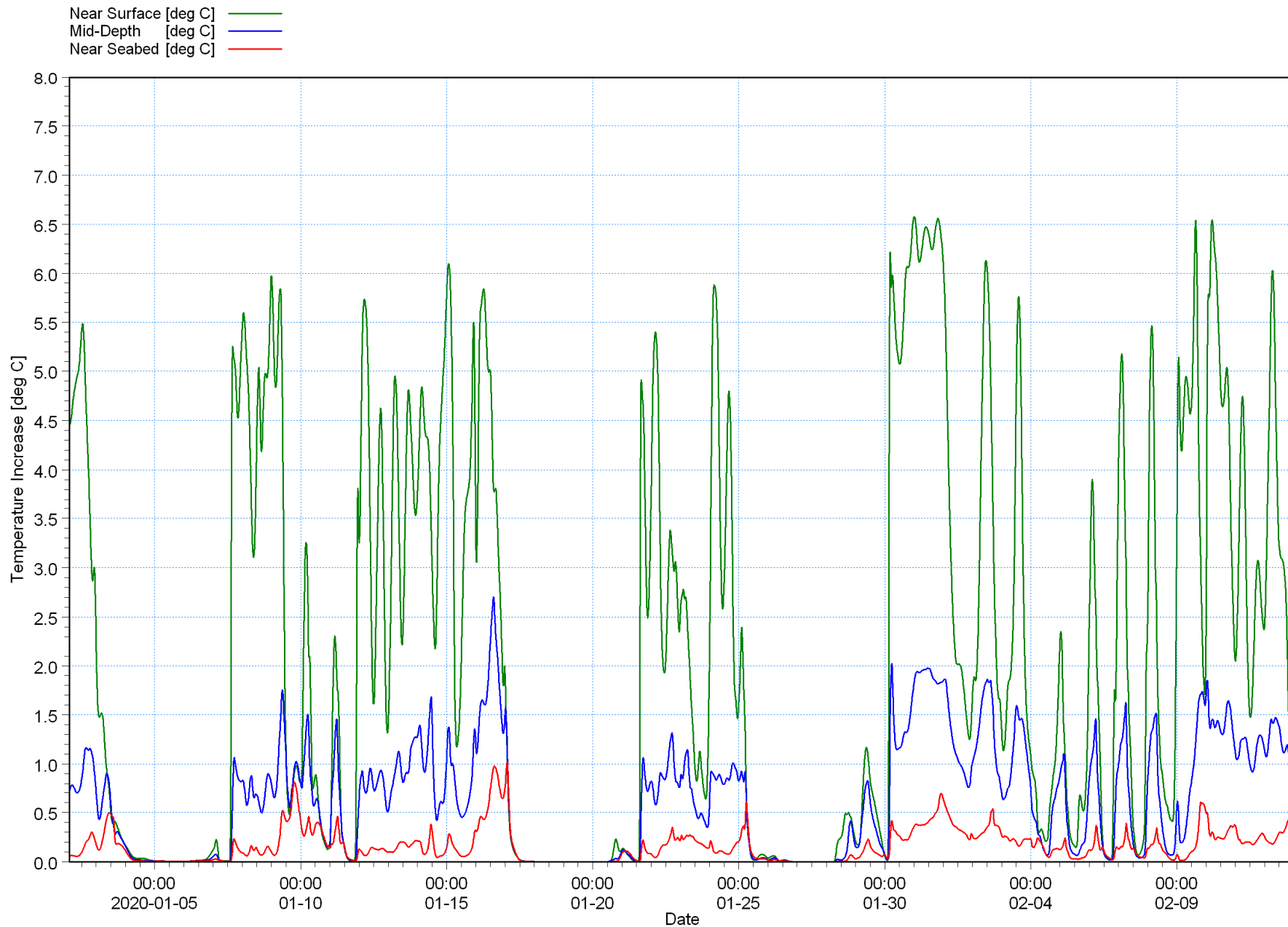


G:\Projects\1010_Nuclear\Sites\Thyspunt\Models\Plume\12a21b.m3fm - Result Files\3D_Point_Post.dfs0



Title: Recirculation for Layout 2 (offshore tunnel intake, nearshore channel outfall).
Temperature time-series at intake position. Note that intake will be located near the seabed.
Power output: 10 000 MWe.

Figure No.
7.31

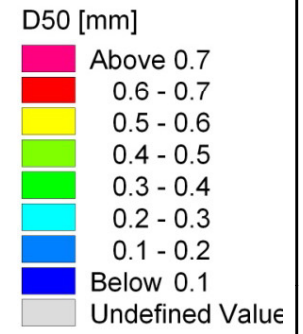
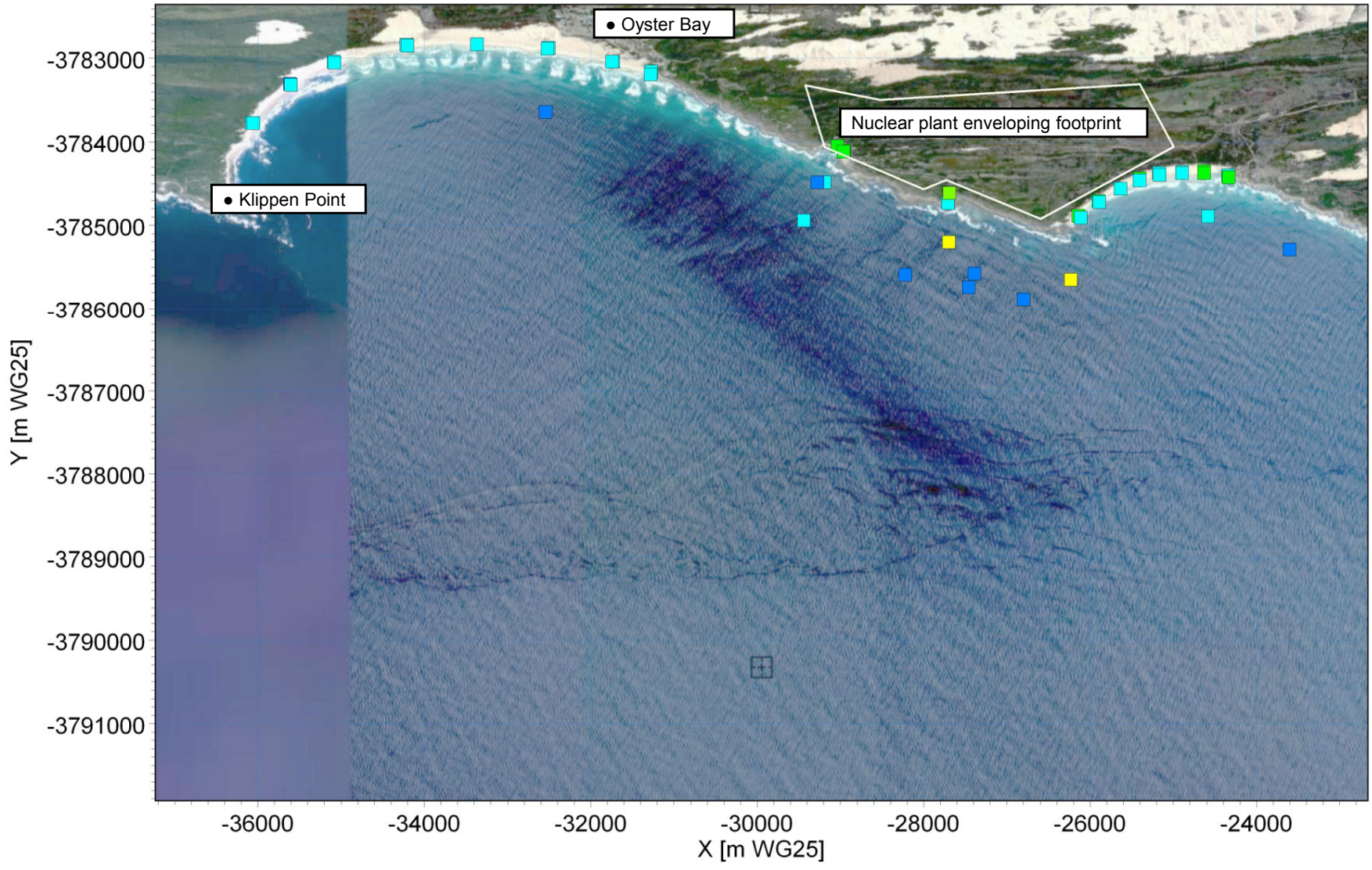


G:\Projects\1010_NuclearSites\Thyspunt\Models\Plume\21a11b.m3fm - Result Files\3D_Point_Post.dfs0



**Title: Recirculation for Layout 1 (offshore tunnel intake, nearshore pipeline outfall).
 Temperature time-series at intake position. Note that intake will be located near the seabed.
 Sensitivity to climate change: wind speed increased 10% and wave height increased 17%.**

**Figure No.
 7.32**

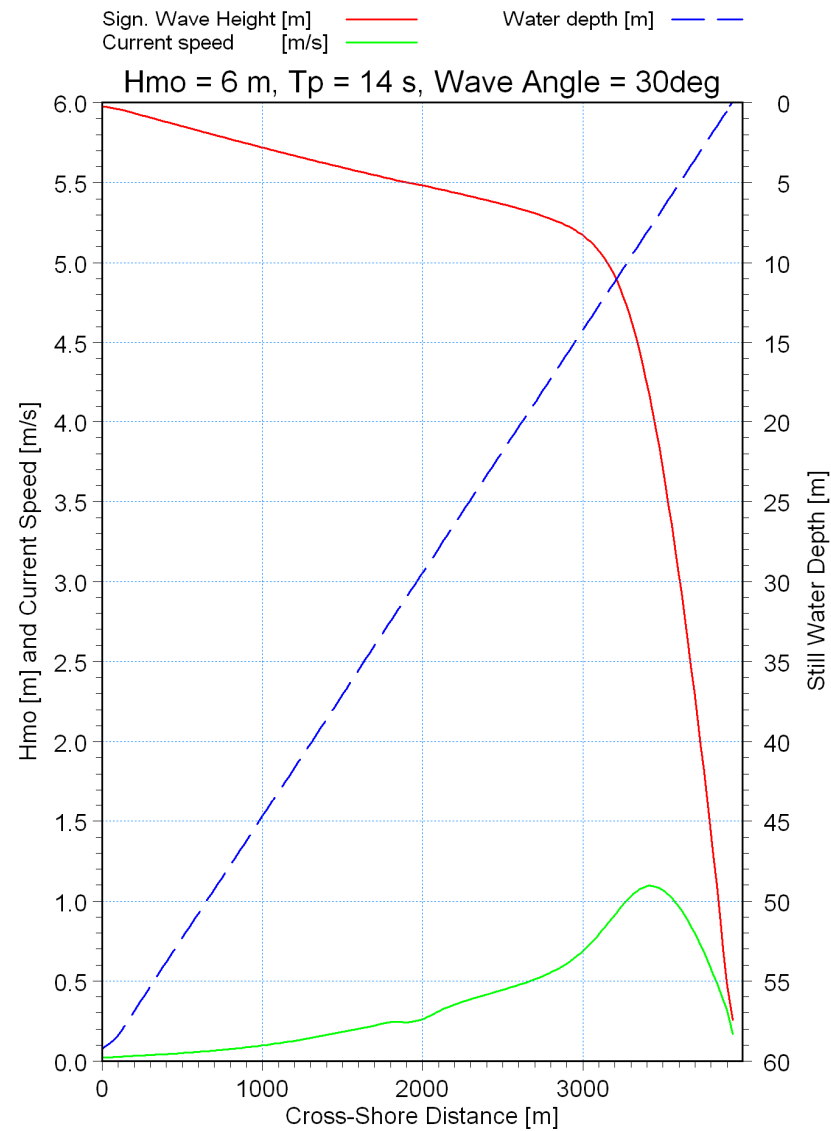
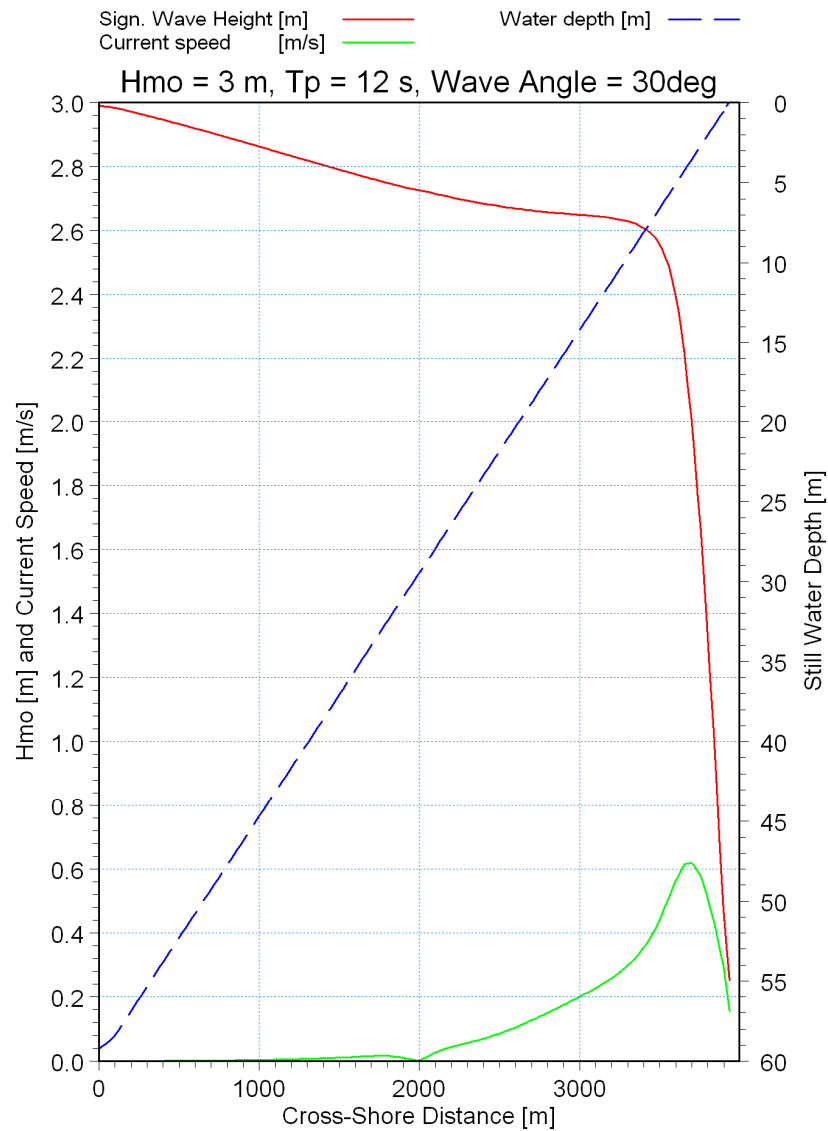


Title:

**Sediment transport modelling.
Measured D₅₀ grain size.**

Figure No.

8.1

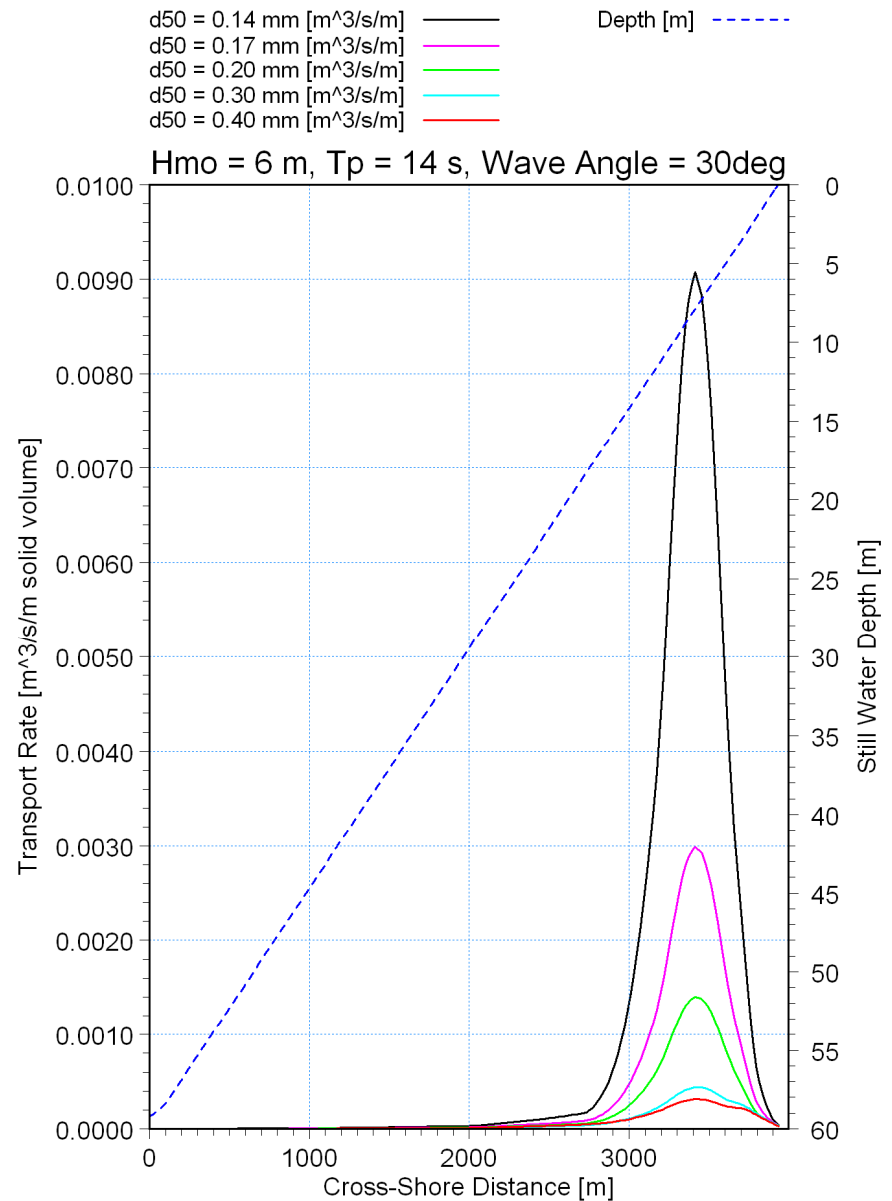
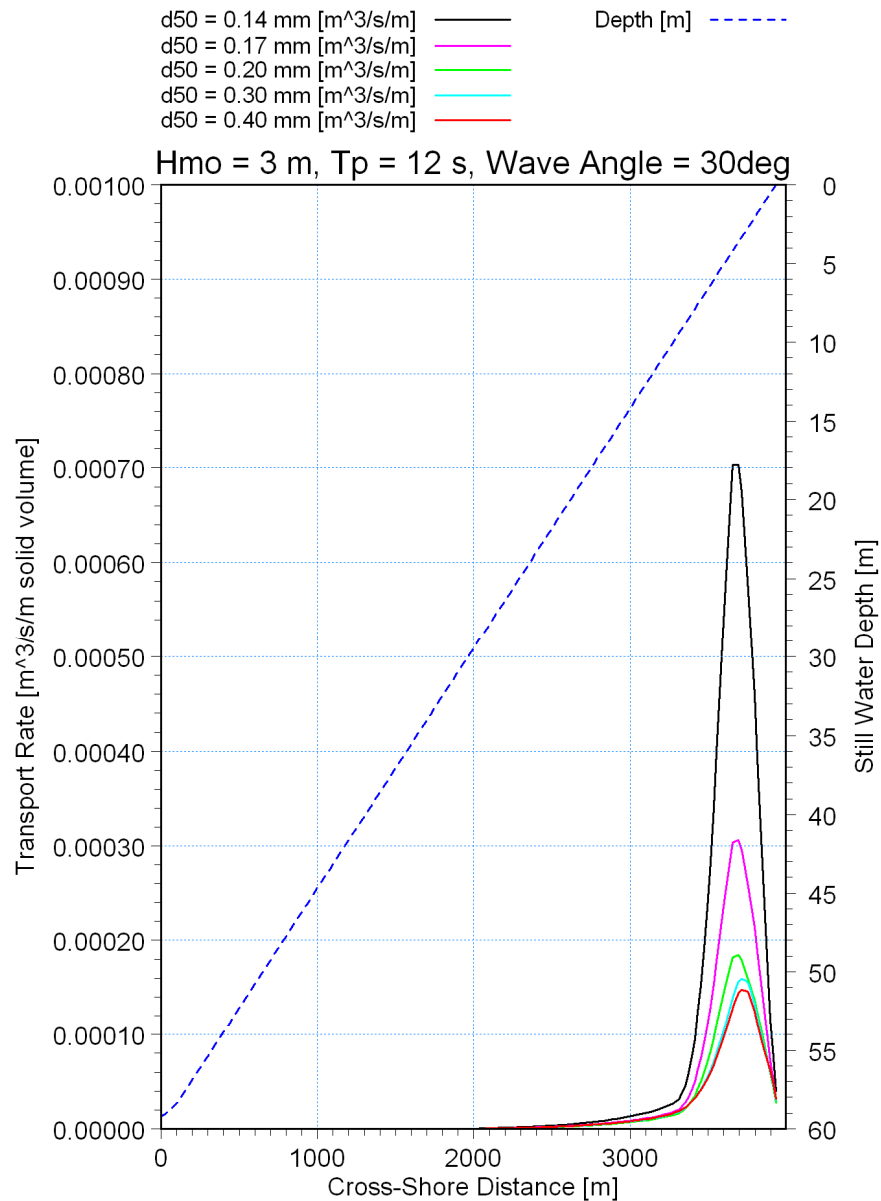


Title:

Sediment transport modelling.
Testing of wave and current modules in a simplified model comprising a uniform 1:67 beach slope with a wave approaching 30° from normal.

Figure No.

8.2

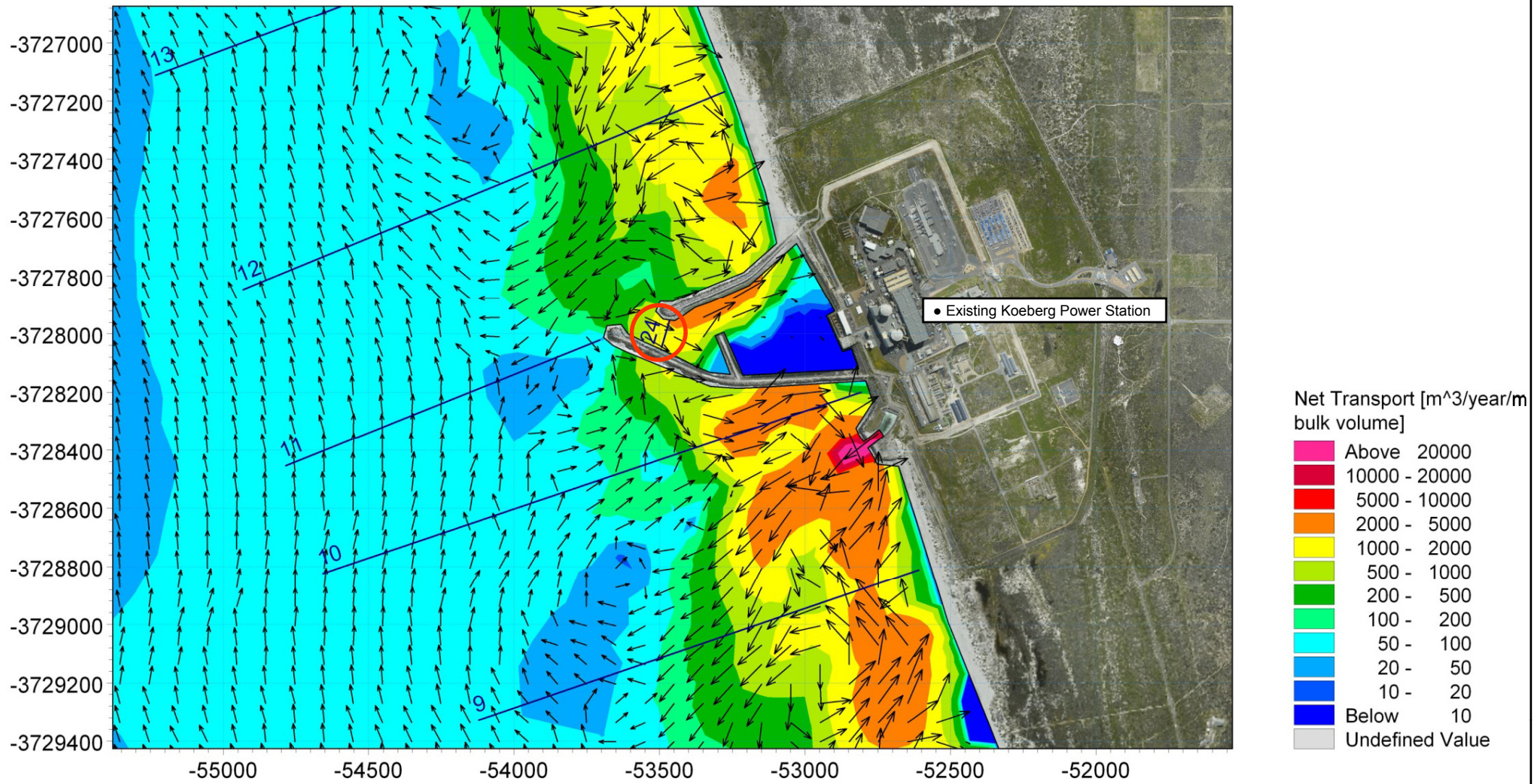


Title:

Sediment transport modelling.
Testing of the coupled wave, current and sediment transport model for a simplified case with a uniform 1:67 beach slope and a wave approaching 30° from normal.

Figure No.

8.3



Profile 24 is indicated inside the red circle.

Both the contour scale and vector length have a log scale

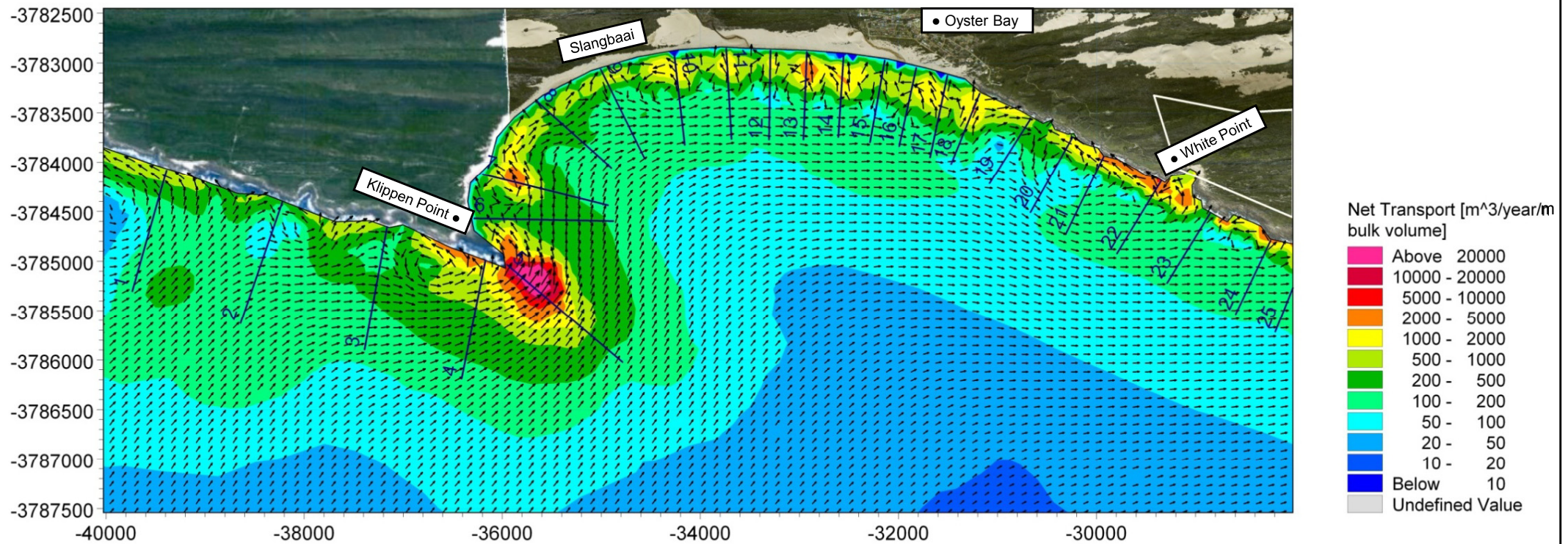


Title:

Sediment transport modelling.
Calibration of model based on sediment volume entering the existing Koeberg intake basin.
Modelled transport for Profile 24 = 140 000 m^3/year , measured transport = 132 000 m^3/year .

Figure No.

8.4



Both the contour scale and vector length have a log scale

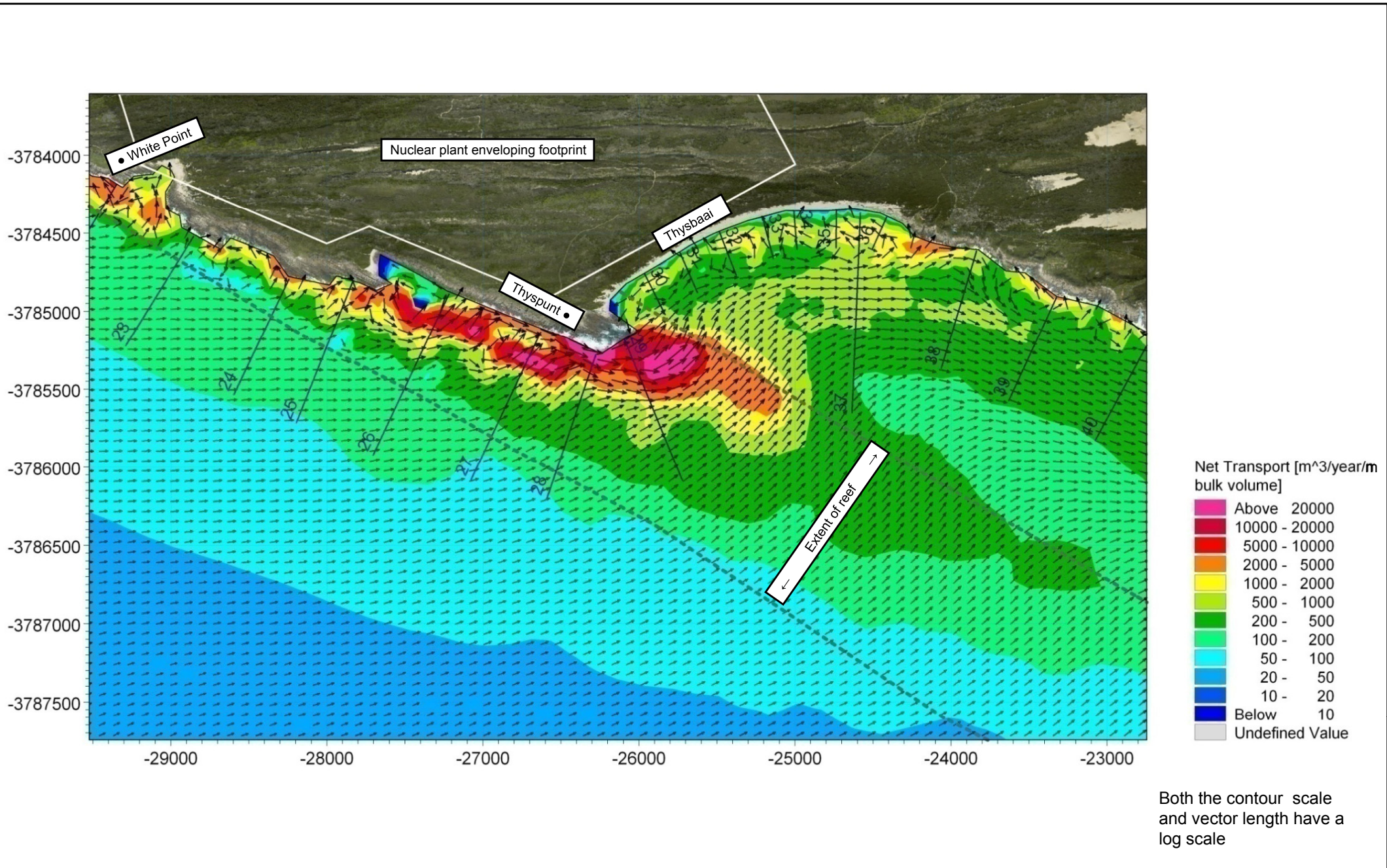


Title:

**Sediment transport modelling.
Potential net sediment transport to the west of Thyspunt, $D_{50} = 0.2$ mm.**

Figure No.

8.5

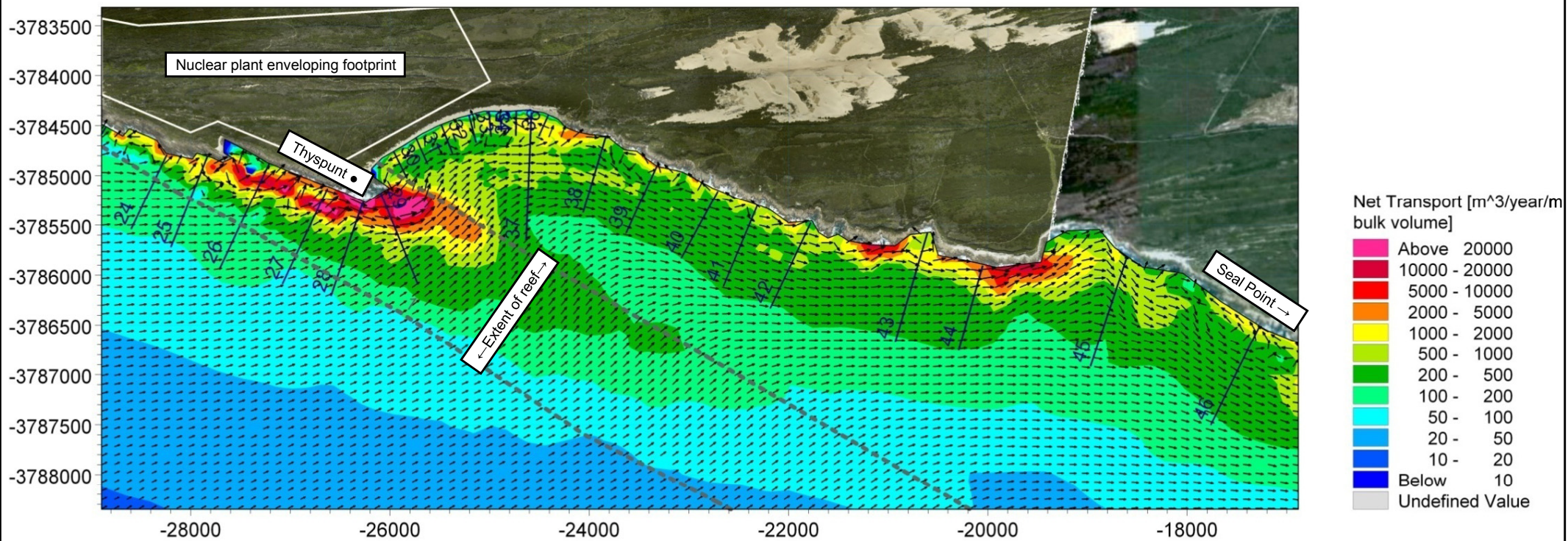


Title:

**Sediment transport modelling.
Potential net sediment transport at Thyspunt, $D_{50} = 0.2$ mm.**

Figure No.

8.6



Both the contour scale and vector length have a log scale

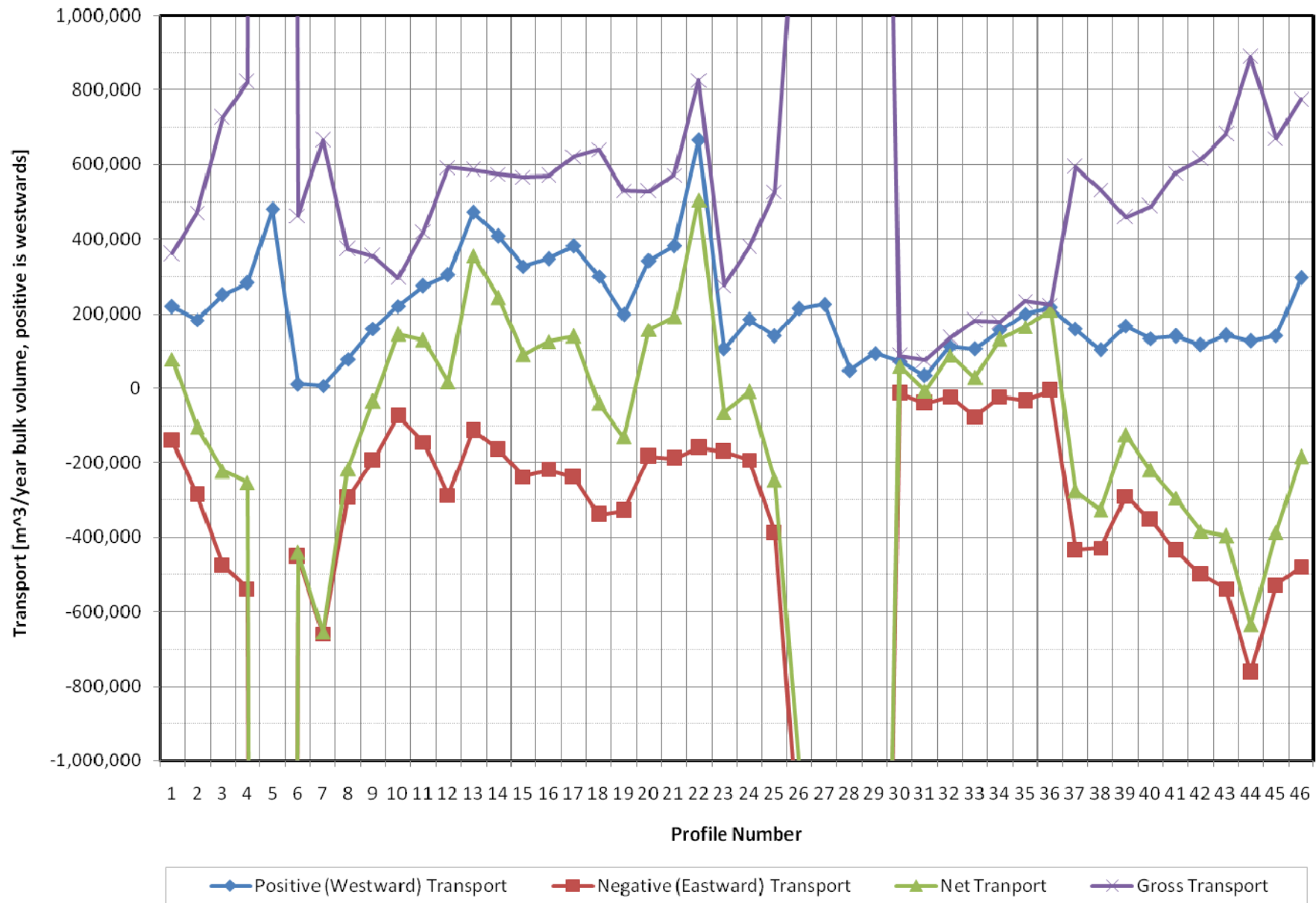


Title:

Sediment transport modelling.
Potential net sediment transport to the east of Thyspunt, $D_{50} = 0.2$ mm.

Figure No.

8.7

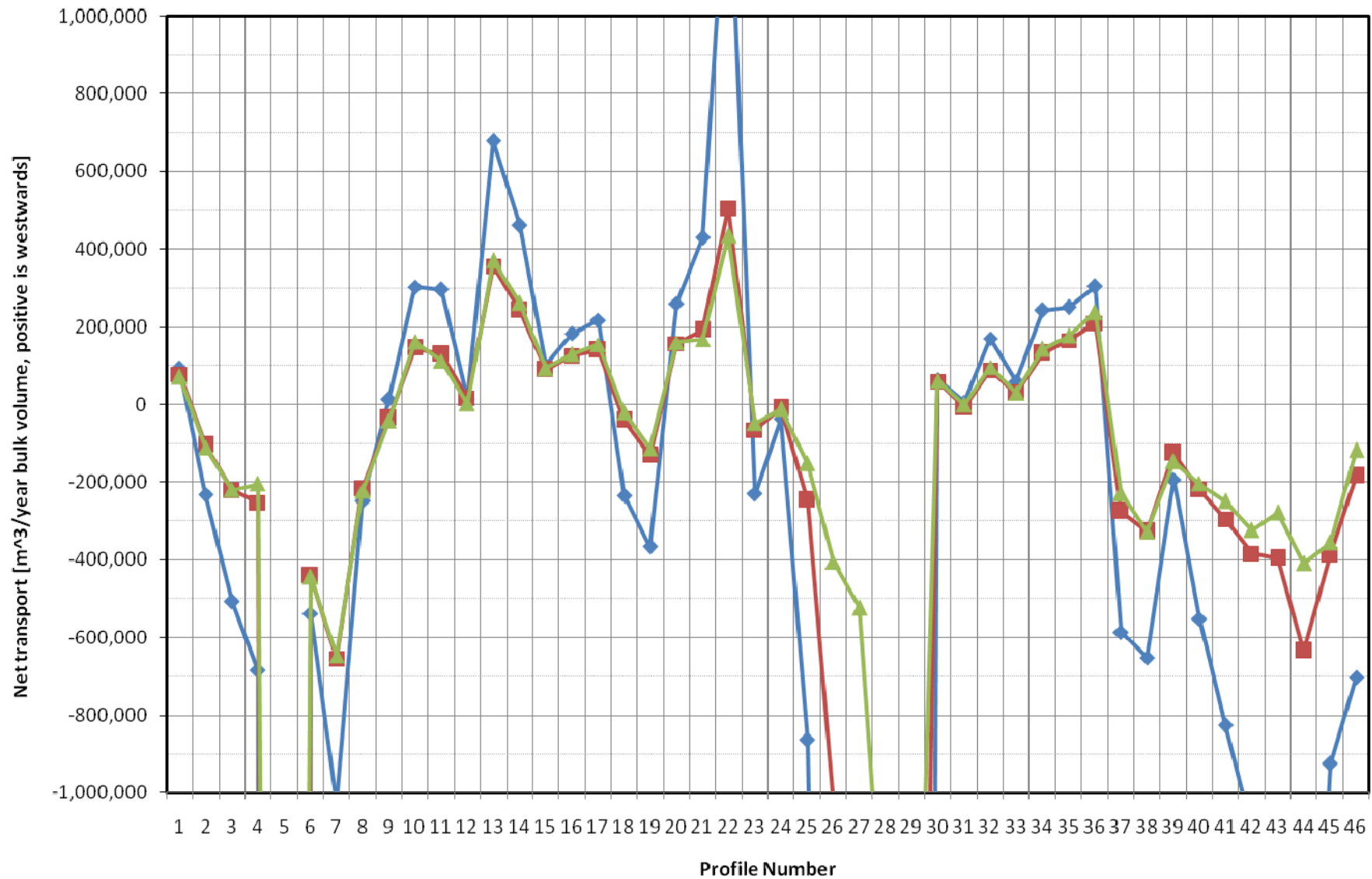


Title:

Sediment transport modelling.
Alongshore transport rates, $D_{50} = 0.2$ mm.
Refer to Figures 8.5 to 8.7 for profile locations.

Figure No.

8.8



◆ D50 = 0.15 mm
 ■ D50 = 0.2 mm
 ▲ D50 = 0.3 mm

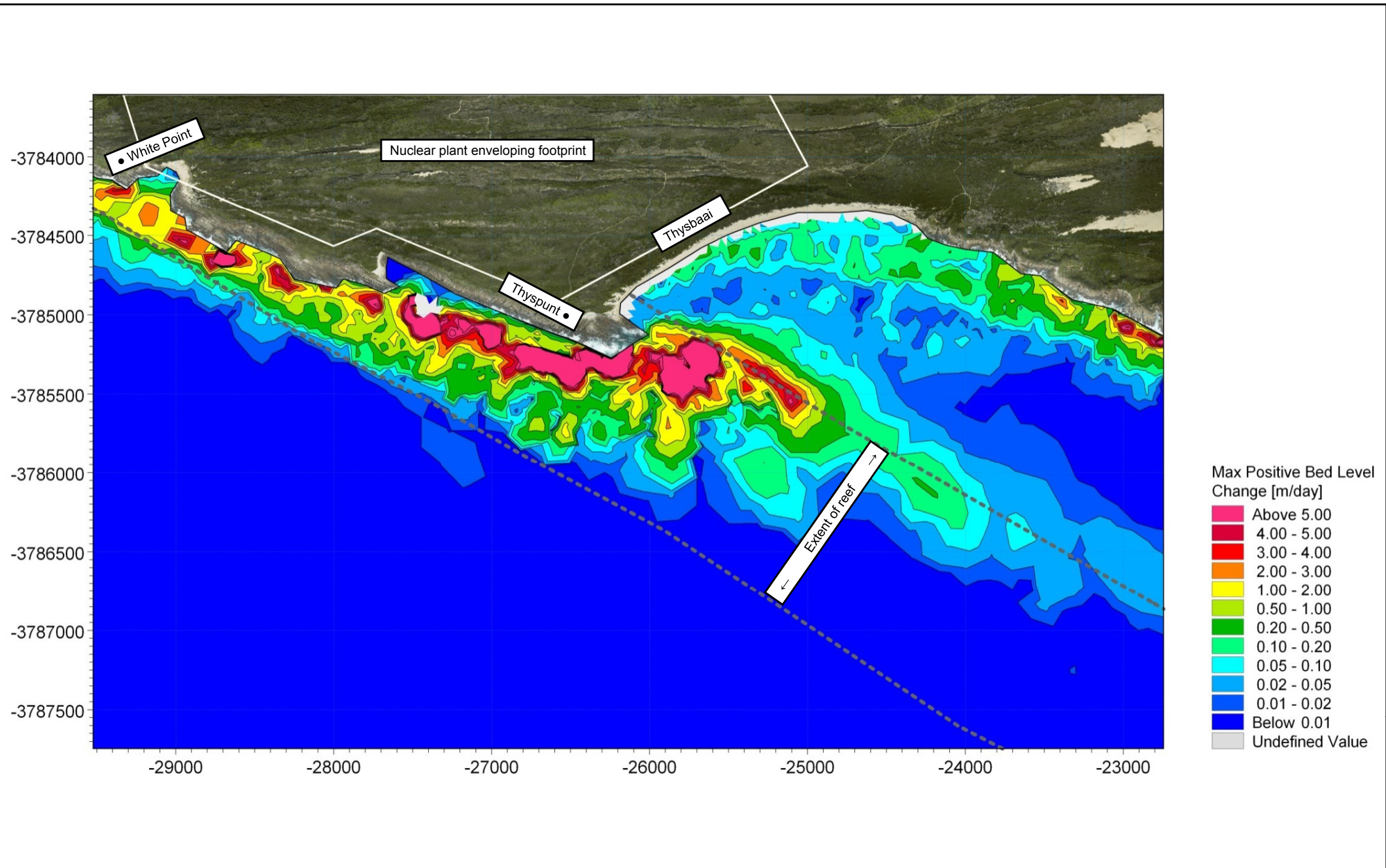


Title:

Sediment transport modelling.
Influence of grain size on net alongshore transport rates.
Refer to Figures 8.5 to 8.7 for profile locations.

Figure No.

8.9

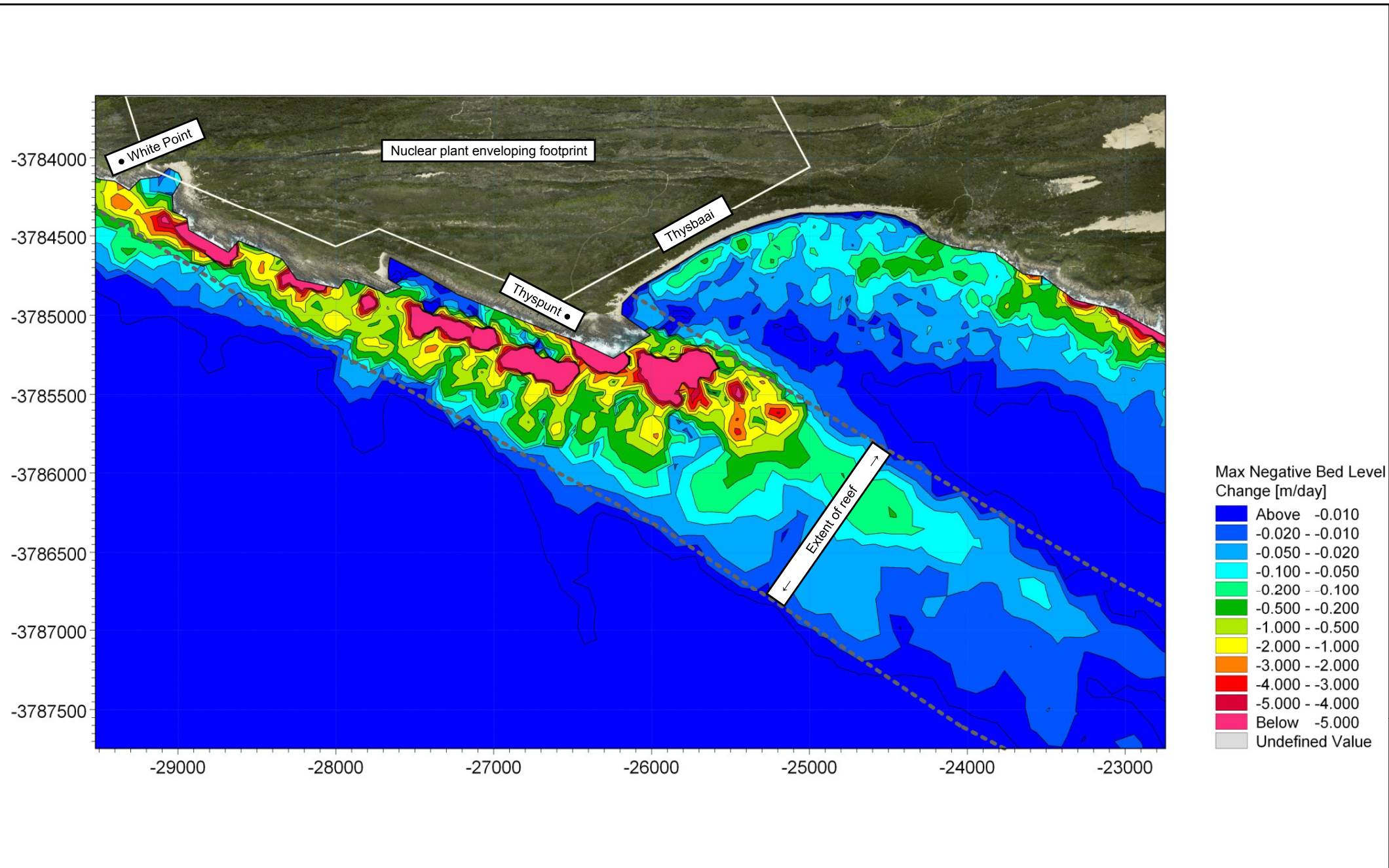


Title:

**Sediment transport modelling.
Maximum daily accretion rate.**

Figure No.

8.10

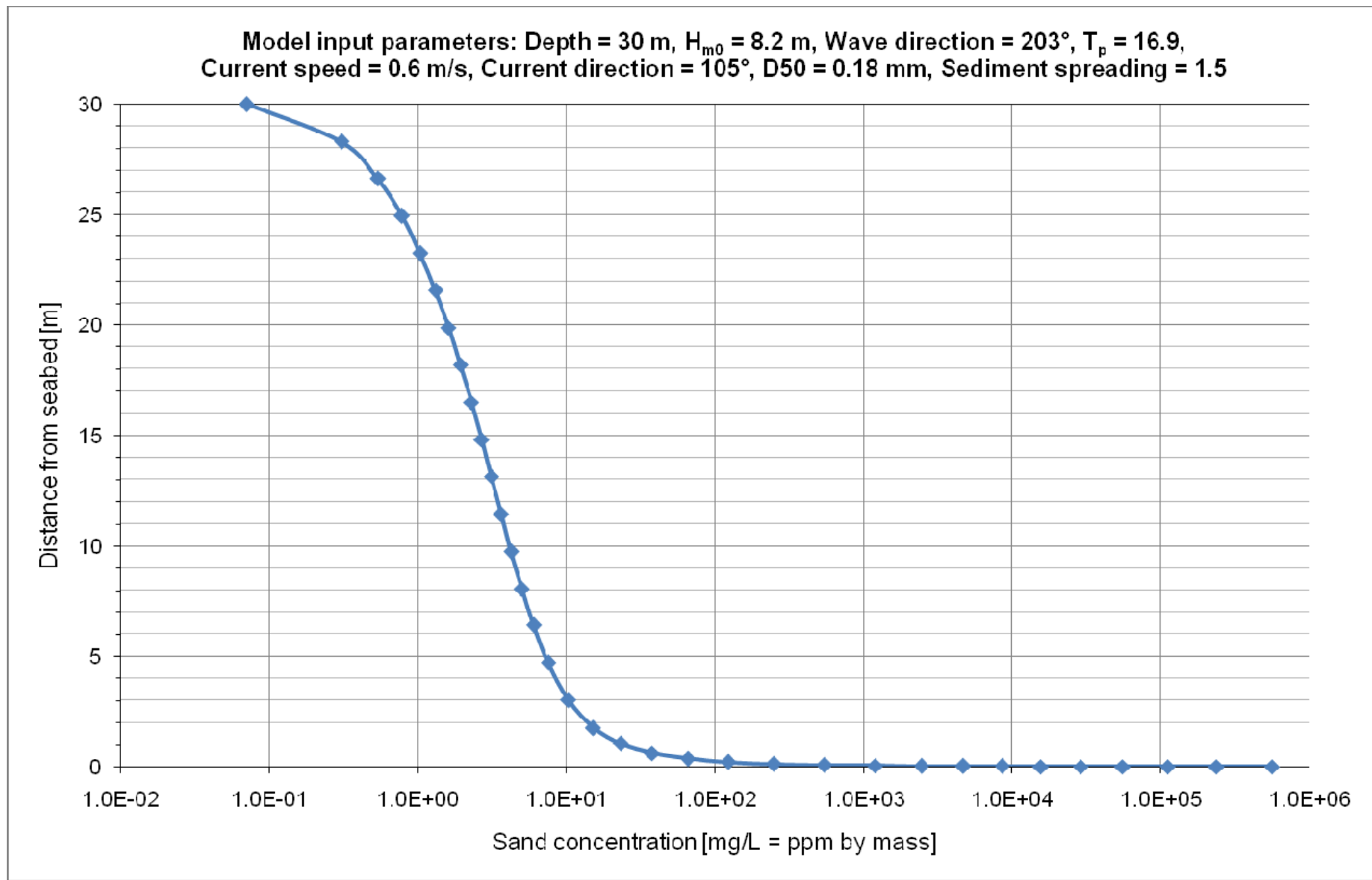


Title:

**Sediment transport modelling.
Maximum daily erosion rate.**

Figure No.

8.11



Title:

Example of modelled vertical profile of suspended sand concentration.

Figure No.

8.12